

ANALYTICA CHIMICA ACTA

An international journal devoted to all branches of analytical chemistry

EDITORS

HARRY L. PARDUE (West Lafayette, IN, U.S.A.)
ALAN TOWNSHEND (Hull, Great Britain)
J.T. CLERC (Berne, Switzerland)
WILLEM E. VAN DER LINDEN (Enschede, The Netherlands)
PAUL J. WORSFOLD (Plymouth, Great Britain)

Editorial Advisers

F.C. Adams, Antwerp
M. Aizawa, Yokohama
J.F. Alder, Manchester
C.M.G. van den Berg, Liverpool
A.M. Bond, Bundooera, Vic.
S.D. Brown, Newark, DE
J. Buffle, Geneva
P.R. Coulet, Lyon
S.R. Crouch, East Lansing, MI
R. Dams, Ghent
L. de Galan, Vlaardingen
M.L. Gross, Lincoln, NE
W. Heineman, Cincinnati, OH
G.M. Hieftje, Bloomington, IN
G. Horvai, Budapest
T. Imasaka, Fukuoka
D. Jagner, Gothenburg
G. Johansson, Lund
D.C. Johnson, Ames, IA
A.M.G. Macdonald, Birmingham
D.L. Massart, Brussels
P.C. Meier, Schaffhausen
M.E. Meyerhoff, Ann Arbor, MI

J.N. Miller, Loughborough
H.A. Mottola, Stillwater, OK
M.E. Munk, Tempe, AZ
M. Otto, Freiberg
D. Pérez-Bendito, Córdoba
C.F. Poole, Detroit, MI
S.C. Rutan, Richmond, VA
J. Ruzicka, Seattle, WA
A. Sanz-Medel, Oviedo
S. Sasaki, Toyohashi
T. Sawada, Tokyo
K. Schügerl, Hannover
M.R. Smyth, Dublin
M. Thompson, Toronto
G. Tölg, Dortmund
Y. Umezawa, Tokyo
E. Wang, Changchun
J. Wang, Las Cruces, NM
H.W. Werner, Eindhoven
O.S. Wolfbeis, Graz
Yu.A. Zolotov, Moscow
J. Zupan, Ljubljana

Author
Index

ANALYTICA CHIMICA ACTA

Scope. *Analytica Chimica Acta* publishes original papers, preliminary communications and reviews dealing with every aspect of modern analytical chemistry. Reviews are normally written by invitation of the editors, who welcome suggestions for subjects. Preliminary communications of important urgent work can be printed within four months of submission, if the authors are prepared to forego proofs.

Submission of Papers

Americas

Prof. Harry L. Pardue
Department of Chemistry
1393 BRWN Bldg, Purdue University
West Lafayette, IN 47907-1393
USA
Tel: (+1-317) 494 5320
Fax: (+1-317) 496 1200

Computer Techniques

Prof. J.T. Clerc
Universität Bern
Pharmazeutisches Institut
Baltzerstrasse 5, CH-3012 Bern
Switzerland
Tel: (+41-31) 654171
Fax: (+41-31) 654198

Other Papers

Prof. Alan Townshend
Department of Chemistry
The University
Hull HU6 7RX
Great Britain

Tel: (+44-482) 465027
Fax: (+44-482) 466410

Prof. Willem E. van der Linden
Laboratory for Chemical Analysis
Department of Chemical Technology
Twente University of Technology
P.O. Box 217, 7500 AE Enschede
The Netherlands

Tel: (+31-53) 892629
Fax: (+31-53) 356024

Prof. Paul Worsfold
Dept. of Environmental Sciences
University of Plymouth
Plymouth PL4 8AA
Great Britain

Tel: (+44-752) 233006
Fax: (+44-752) 233009

Submission of an article is understood to imply that the article is original and unpublished and is not being considered for publication elsewhere. *Anal. Chim. Acta* accepts papers in English only. There are no page charges. Manuscripts should conform in layout and style to the papers published in this issue. See inside back cover for "Information for Authors".

Publication. *Analytica Chimica Acta* appears in 14 volumes in 1993. The subscription price for 1993 (Vols. 267-280) is Dfl 4214.00 plus Dfl. 462.00 (p.p.h.) (total approx. US\$ 2597.75). *Vibrational Spectroscopy* appears in 2 volumes in 1993. The subscription price for *Vibrational Spectroscopy* (Vols. 4 and 5) is Dfl. 700.00 plus Dfl. 66.00 (p.p.h.) (total approx. US\$ 407.50). The price of a combined subscription (*Anal. Chim. Acta* and *Vib. Spectrosc.*) is Dfl. 4592.00 plus Dfl. 528.00 (p.p.h.) (total approx. US\$ 2844.50). All earlier volumes (Vols. 1-266) except Vols. 23 and 28 are available at Dfl. 259.50 (US 144.00), plus Dfl. 18.00 (US\$ 10.00) p.p.h., per volume. The Dutch guilder price is definitive. The U.S. dollar price is subject to exchange-rate fluctuations and is given only as a guide. Subscriptions are accepted on a prepaid basis only, unless different terms have been previously agreed upon.

Our p.p.h. (postage, packing and handling) charge includes surface delivery of all issues, except to subscribers in the U.S.A. Canada, Australia, New Zealand, China, India, Israel, South Africa, Malaysia, Thailand, Singapore, South Korea, Taiwan, Pakistan, Hong Kong, Brazil, Argentina and Mexico, who receive all issues by air delivery (S.A.L.—Surface Air Lifted) at no extra cost. For Japan, air delivery requires 25% additional charge of the normal postage and handling charge; for all other countries airmail and S.A.L. charges are available upon request.

Subscription orders. Subscription orders can be entered only by calendar year and should be sent to: Elsevier Science Publishers B.V., Journals Department, P.O. Box 211, 1000 AE Amsterdam, The Netherlands. Tel: (+31-20) 5803 642, Telex: 18582, Telefax: (+31-20) 5803598, to which requests for sample copies can also be sent. Claims for issues not received should be made within six months of publication of the issues. If not they cannot be honoured free of charge. Readers in the U.S.A. and Canada can contact the following address: Elsevier Science Publishing Co. Inc., Journal Information Center, 65 Avenue of the Americas, New York, NY 10010, U.S.A. Tel: (+1-212) 6333750, Telefax: (+1-212) 6333990, for further information, or a free sample copy of this or any other Elsevier Science Publishers journal.

Advertisements. Advertisement rates are available from the publisher on request.

Detailed "Instructions to Authors" for *Analytica Chimica Acta* was published in Volume 256, No. 2, pp. 373-376. Free reprints of the "Instructions to Authors" of *Analytica Chimica Acta* and *Vibrational Spectroscopy* are available from the Editor or from: Elsevier Science Publishers B.V., P.O. Box 330, 1000 AH Amsterdam, The Netherlands. Telefax: (+31-20) 5862845

US mailing notice – *Analytica Chimica Acta* (ISSN 0003-2670) is published biweekly by Elsevier Science Publisher (Molenwerf 1, Postbus 211, 1000 AE Amsterdam). Annual subscription price in the USA US\$ 2597.75 (subject to change), including air speed delivery. Second class postage paid at Jamaica, NY 11431. **USA Postmasters:** Send address changes to *Anal. Chim. Acta*, Publications Expediting, Inc., 200 Meacham Av., Elmont, NY 11003. Airfreight and mailing in the USA by Publication Expediting.

ANALYTICA CHIMICA ACTA

An international journal devoted to all branches of analytical chemistry

(Full texts are incorporated in *CJELSEVIER*, a file in the *Chemical Journals Online* database available on *STN International*; Abstracted, indexed in: *Aluminum Abstracts*; *Anal. Abstr.*; *Biol. Abstr.*; *BIOSIS*; *Chem. Abstr.*; *Curr. Contents Phys. Chem. Earth Sci.*; *Engineered Materials Abstracts*; *Excerpta Medica*; *Index Med.*; *Life Sci.*; *Mass Spectrom. Bull.*; *Material Business Alerts*; *Metals Abstracts*; *Sci. Citation Index*)

VOL. 279 NO. 2

CONTENTS

JULY 15, 1993

<i>Publisher's Note</i>	193
<i>Electroanalytical Chemistry and Sensors</i>	
Mechanically robust amine derivatized polystyrene for pH sensing based on polymer swelling S. Pan, V. Conway, Z. Shakhsher, S. Emerson, M. Bai, W.R. Seitz (Durham, NH, USA) and K.D. Legg (Wellesley, MA, USA)	195
Organic-phase biosensing of enzyme inhibitors J. Wang, E. Dempsey, A. Eremenko (Las Cruces, NM, USA) and M.R. Smyth (Dublin, Ireland)	203
Pulsed amperometric detection of proteins using antibody containing conducting polymers O.A. Sadik and G.G. Wallace (Wollongong, Australia)	209
Determination of the diffusion coefficient of oxygen in sodium chloride solutions with a transient pulse technique A.J. van Stroe and L.J.J. Janssen (Eindhoven, Netherlands)	213
Ion-selective electrode potentiometric studies on the complexation of copper(II) by soil-derived humic and fulvic acids R.M. Town and H.K.J. Powell (Christchurch, New Zealand)	221
Cholesterol sensor based on electrodeposition of catalytic palladium particles S. Dong, Q. Deng and G. Cheng (Changchun, China)	235
<i>Atomic Spectrometry</i>	
Direct graphite furnace atomic absorption spectrometric determination of metals in sea water: application of palladium modifiers and a fractal approach to their analytical support S. Sachsenberg, T. Klenke, W.E. Krumbein, H.J. Schellhuber and E. Zeeck (Oldenburg, Germany)	241
Halogen-assisted cleaning after-treatment in graphite furnace atomic absorption spectrometry for analysis of molybdenum-based materials B. Docekal and V. Krivan (Ulm, Germany)	253
End-on viewed inductively coupled plasma for the determination of trace impurities in high-purity scandium oxide by extraction chromatography X.-J. Yang and J.-S. Guan (Beijing, China)	261
Wet digestion of vegetable tissue using a domestic microwave oven M.-A. Mateo and S. Sabaté (Barcelona, Spain)	273
<i>Fluorimetry</i>	
Comparative study of Kalman filtering, synchronous excitation and numerical derivative techniques in fluorimetry J. Zhang, J. Yang, Y. Ren and Y. Zhang (Changchun, China)	281
<i>Flow-Injection Analysis</i>	
Fluorescence-based flow-injection determination of biotin and biotinylated compounds T. Smith-Palmer, M.S. Barbarakis, T. Cynkowski and L.G. Bachas (Lexington, KY, USA)	287
Spectrofluorimetric determination of emetine by flow injection using barium peroxide and UV derivatization C. Gómez Benito, T. García Sancho and J. Martínez Calatayud (Valencia, Spain)	293
Polypyrrole-dodecyl sulphate electrode as a microsensor for electroinactive cations in flow-injection analysis and ion chromatography R. Carabias Martínez, F. Becerro Domínguez, F. Martín González, J. Hernández Méndez (Salamanca, Spain) and R. Córdova Orellana (Valparaíso, Chile)	299

(Continued overleaf)

ห้องสมุดมหาวิทยาลัยศรีนครินทรวิโรฒ
29 ก.ค. 2536

Contents (continued)

Infrared Spectrometry

Ridge regression techniques for the optimization of piecewise linear discriminants: application to Fourier transform infrared remote sensing measurements
T.F. Kaltenbach and G.W. Small (Athens, OH, USA) 309

Chromatography

Assessment of the performance of various search systems for mass spectra files of steroids
M. Statheropoulos and C. Georgakopoulos (Athens, Greece) 323

Simultaneous preconcentration of chromium(III) and chromium(VI) prior to speciation analysis
G.-L. Ou-Yang and J.-F. Jen (Taichung, Taiwan) 329

Redox Equilibria

Effect of pH on the redox equilibria of immobilised 2,6-dichloroindophenol
G. Goodlet and R. Narayanaswamy (Manchester, UK) 335

Book Reviews 341

Author Index 345

Publisher's Note

We are pleased to announce that Professor Sarah Rutan of Virginia Commonwealth University, Richmond has accepted the invitation to join *Analytica Chimica Acta* as Associate Editor. Together with Prof. J.T. Clerc she will be responsible for the papers covering "Computer Techniques".

Professor Rutan's main research interests are in the application of computer methods in several areas of analytical chemistry, including the spectroscopic characterization of stationary phases in liquid chromatography, the development of kinetic-based detection methods for electrophoresis and thin-layer chromatography, and the development of multiwavelength fluorescence detection approaches in liquid chromatography. The chemometric methods used in these studies include Kalman filtering, rank annihilation, regression methods, and factor analysis. Her experience in different research areas will certainly be an asset to the journal and will serve the interests of its authors and readers.

We are sure you will all join us in welcoming Professor Rutan to this position, in which she will no doubt make a significant contribution to maintaining the continued high reputation of the journal.

Mechanically robust amine derivatized polystyrene for pH sensing based on polymer swelling

Sizhong Pan, Vicki Conway, Ziad Shakhsher, Susan Emerson, Mingqi Bai and W. Rudolf Seitz

Department of Chemistry, University of New Hampshire, Durham, NH 03824 (USA)

Kenneth D. Legg

Polysense, Inc., 29 Jefferson Road, Wellesley, MA 02181 (USA)

(Received 2nd November 1992; revised manuscript received 25th January 1993)

Abstract

Beads that change size as a function of pH have been prepared by suspension polymerization of vinylbenzyl chloride crosslinked with divinyl benzene followed by reaction with pure diethanolamine. Toluene is added to induce porosity, and Kraton G1652, a styrene–ethylene, butylene–styrene triblock copolymer, is included to increase mechanical robustness. The optimum formulation includes 48% toluene by volume and 2% (w/w) Kraton G1652. As the pH decreases, protonation of the amine puts a charge on the amine, causing the polymer to swell due to electrostatic repulsion between charged sites on the polymer. After the polymer is conditioned by exposure to acid, the ratio of the diameter in acid to the diameter in base is as high as 1.6 at an ionic strength of 0.10 M. The diameter ratio decreases with increasing ionic strength as predicted by theory. The diameter changes continuously from pH 6.0 to 8.0. This means that immobilization shifts the pK_a of the amine. The polymer beads undergo many swelling and shrinking cycles without degrading mechanically but are softer than desired for use in a pH sensor based on polymer swelling.

Keywords: Sensors; Polymerization; Polymer swelling; Polystyrene, amine derivatized

We are interested in developing fiber optic chemical sensors based on polymer swelling because they offer the prospect of improved robustness at low cost. In our devices, changes in polymer size are coupled to motion of a reflector that changes the intensity of light reflected into an optical fiber. We first demonstrated this concept using commercial ion exchange materials which shrink with increasing ionic strength [1]. Since then, we have significantly improved the design of the sensor so that it is more robust and easier to use. The new design has a diaphragm between the optical fibers and the polymer sensing ele-

ment so that the measurement is completely isolated from the optical properties of the sample [2].

We wish to further develop this concept by preparing polymer sensing elements that bind selected ions rather than responding to ionic strength. Because ion binding changes the charge on a polymer, it will cause either swelling or shrinking depending on whether ion binding causes an increase or decrease in the charge on the polymer [3]. Polymer size varies with the fraction of occupied ion binding sites. The overall response curve is similar to that for a conventional optical indicator where the signal is proportional to the fraction of indicator molecules combined with analyte [4].

Correspondence to: W.R. Seitz, Department of Chemistry, University of New Hampshire, Durham, NH 03824 (USA).

Polymers with the required properties for ion sensing are not available commercially. Therefore, we need to prepare our own materials. For our polymer substrate, we have chosen to work with polystyrene because it is thermally stable, mechanically strong and is amenable to a wide variety of derivatization chemistries [5]. Pores may be introduced by polymerizing styrene in the presence of an inert solvent, often called a porogen [6–8]. This improves analyte access to the interior of the polymer. The problem with polystyrene is that it has a glass transition temperature well above room temperature. Polystyrene based materials develop cracks and eventually fall apart when subjected to the stress of repetitive swelling and shrinking. We have found this to be a problem with commercial ion exchange materials, which are formulated for maximum mechanical robustness.

The “toughness” of polystyrene is greatly improved by the presence of small inclusions of an elastomer. High impact polystyrene, an important commercial material, is prepared by polymerizing styrene and butadiene under conditions such that the final product has elastic polybutadiene inclusions [9]. An alternate approach is to blend styrene–butadiene–styrene triblock copolymer with polystyrene [10]. The butadiene blocks form a separate elastic phase improving the toughness of the polystyrene. This approach has been used to prepare a mechanically robust sulfonated polystyrene membrane [11]. Toughness is also improved by polymerizing styrene in the presence of added triblock copolymer [12].

Here, we report the results of experiments to prepare toughened derivatized porous polystyrene beads by adding Kraton G1652, a commercially available styrene–ethylene, butylene–styrene triblock copolymer to otherwise conventional preparations of derivatized materials. The particular system chosen for this study was an amine derivatized polystyrene that swells upon protonation. It is prepared by copolymerizing vinylbenzyl chloride and divinyl benzene in the presence of toluene and Kraton G1652 and then reacting the resulting polymer beads with diethanolamine. Our results show that inclusion of Kraton G1652 in the polymer formulation enables us to prepare

beads that can undergo multiple swelling and shrinking cycles upon alternate exposure to acid and base without any observable mechanical deterioration.

EXPERIMENTAL

Reagents

Diethanolamine, diethylamine, toluene, ammonium chloride, hydrochloric acid, sodium acetate and sodium hydroxide were obtained from Fisher Scientific. Sodium chloride and ammonium hydroxide were from Baker. Hydroxybutyl methyl cellulose, benzoyl peroxide and xanthan gum were from Aldrich. Vinylbenzyl chloride (98% pure, 30% *para*/70% *meta*) was obtained from Dow Chemical. The divinyl benzene from Polysciences, contained 55% divinyl benzene (*meta* and *para*), 42% ethyl vinyl benzene and 3% other impurities. Kraton G1652, a styrene–ethylene, butylene–styrene triblock copolymer with a styrene/ethylene, butylene ratio of 29:71 was donated to us by Shell.

Apparatus

Suspension polymerization was carried out at 85°C in a 500-ml three-neck flask agitated by a paddle stirrer at 180 rpm. Bead diameters were measured with a Fisher stereomaster II microscope. An Orion 701A/digital ionalyzer was used to measure pH. A Perkin-Elmer 240B elemental analyzer was used to determine the percentages of carbon, hydrogen and nitrogen in polymer beads. Stress–strain curves were measured on a Model 1350 servohydraulic Instron.

Procedures

Polymerization was carried out by adding 50 ml of the solution of monomer, crosslinker and additives to 500 ml of water containing 0.040 g of xanthan gum and 0.028 g of hydroxybutyl methyl cellulose to stabilize the suspension [13]. In all experiments 1.5% benzoyl peroxide was included in the organic solution to initiate free radical polymerization. The mixture is stirred at 180 rpm for seven hours at 85°C. After polymerization, the beads are removed by filtration, washed with acetone and dried in air.

Amination was carried out by adding 20 ml of anhydrous diethanolamine to a flask containing poly(vinylbenzylchloride) beads. Usually, the polymer beads were preswollen in dioxane to shorten the rate of the amination reaction. The mixture was kept at room temperature for two days with intermittent shaking. Then, the product was treated with a dilute solution of acid three times followed by deionized water. The beads were then dried in the hood overnight.

Buffers were prepared so that the concentration of acid plus conjugate base was equal to 0.10 M. The measured pH was used to calculate the fractions of acid and base. This value was used to

calculate the amount of NaCl required to bring the ionic strength to 0.10 M.

Diameter ratios in toluene are reported as the ratio of the final diameter after exposure to toluene to the initial diameter before exposure to toluene. Acid–base diameter ratios are based on the ratio of the diameter of a bead in pH 4.0 acetate buffer with 0.10 M ionic strength to the diameter in pH 9.2 ammonia buffer with the same ionic strength. Volume swelling ratios were calculated by cubing the diameter ratio.

Cross-sections for examination by microscopy were prepared by embedding the bead in Polybed 812 epoxy from Polysciences followed by slicing

TABLE 1

Characteristics of poly(vinyl benzyl chloride) beads before and after derivatization

[%Nitrogen values for microporous beads are measured after drying by evaporation of toluene. They are in wt.-%. Divinyl benzene (DVB) values are in mol.-% (moles DVB/moles monomer \times 100). Kraton (Kra) values are in wt.-% (g Kraton/g monomer \times 100). Toluene (Tol) values are in vol.-% (ml toluene/ml monomer \times 100)]

Bead composition	Diameter ratio in toluene	Nitrogen (%)	Diameter ratio in acid–base
1.2% DVB, 0.0% Kra	1.550		Crack
2.3% DVB, 0.0% Kra	1.500	6.59	1.055
4.6% DVB, 0.0% Kra	1.350	7.26	1.097/Crack
6.8% DVB, 0.0% Kra	1.275	3.88	1.020/Crack
4.6% DVB, 0.8% Kra	1.300	6.52	1.022
4.6% DVB, 1.7% Kra	1.350	6.16	1.046
4.5% DVB, 3.2% Kra	1.375	6.41	1.069
4.4% DVB, 4.6% Kra	1.369	6.94	Crack
4.3% DVB, 6.3% Kra	Crack		
5.4% DVB, 0.0% Kra, 48.0% Tol	1.375	5.15	Crack
5.4% DVB, 0.4% Kra, 48.0% Tol	1.475	4.90	1.108
5.4% DVB, 0.8% Kra, 48.0% Tol	1.312	4.68	1.245 ^a
5.4% DVB, 0.8% Kra, 48.0% Tol	1.318		1.309 ^a
5.3% DVB, 1.2% Kra, 48.0% Tol	1.425	4.76	1.257
5.3% DVB, 1.6% Kra, 48.0% Tol	1.500	3.83	1.218
5.2% DVB, 4.0% Kra, 48.0% Tol	1.400	4.87	Crack
5.3% DVB, 1.6% Kra, 31.0% Tol	1.225	4.99	1.167
5.3% DVB, 1.6% Kra, 48.0% Tol	1.500	3.83	1.218
5.3% DVB, 1.6% Kra, 55.0% Tol	1.425	3.60	1.212
5.4% DVB, 0.8% Kra, 58.0% Tol	1.425	4.73	Crack
5.3% DVB, 1.6% Kra, 55.0% Tol	1.425	3.60	1.212
5.2% DVB, 3.2% Kra, 55.0% Tol	1.382	5.48	1.036

^a This formulation showed the largest acid–base swelling ratio and was selected for further work. To confirm this result two separate batches of beads with the same formulation were used.

with a glass knife. The cross-sections were between 0.5 and 1.0 μm thick.

The penetration modulus of selected swollen beads was determined by a published method [14].

RESULTS AND DISCUSSION

Choice of polymer

As noted in the introduction polystyrene is attractive as a polymer substrate because it is mechanically strong, thermally stable and amenable to a variety of derivatization strategies. One common approach is to chloromethylate styrene [5]. The chloromethyl group can then undergo a variety of further reactions. In this work, we planned to prepare a pH sensitive polymer by reacting chloromethylated polystyrene with a secondary amine to form a tertiary amine: $\text{P-CH}_2\text{Cl} + \text{NR}_1\text{R}_2\text{H} \rightarrow \text{P-CH}_2\text{NR}_1\text{R}_2 + \text{HCl}$

where P stands for the polystyrene substrate.

We performed preliminary experiments chloromethylating polystyrene by a published procedure [15]. We were successful in preparing beads that could be further reacted with diethanolamine. However, we were unable to observe any swelling at all when these beads were placed in pH 4.0 buffer. We attributed this, at least in part, to additional crosslinks introduced during chloromethylation [16]. Therefore we chose to prepare poly(vinylbenzyl chloride) directly so that a separate chloromethylation step was not required.

Effect of bead composition on swelling properties

Table 1 shows swelling properties for various bead formulations. The diameter ratio in toluene is measured before the beads are reacted with amine. The acid–base diameter ratio is measured after derivatization. The values shown in Table 1 were measured immediately after derivatization. It was subsequently found that the diameter ratio increases substantially if the derivatized beads are pretreated with acid.

Several conclusions may be drawn from the data in Table 1. The first two sets of experiments show that beads prepared in the absence of added

toluene swell significantly in toluene before derivatization. (Note that toluene is used both as a porogen *during* polymerization and as a solvent to test the degree of swelling *after* polymerization.) The degree of swelling is greater at lower cross linking levels as expected. However, after derivatization with diethanolamine, the acid–base swelling ratios are much smaller.

The inclusion of toluene in the polymer formulation leads to significantly larger diameter ratios both in toluene before derivatization and in acid–base after derivatization. The increase in diameter ratio before derivatization is consistent with literature results for polystyrene showing that the volume of solvent absorbed by a polymer bead is equal to volume of solvent initially present during bead preparation [6]. The results here indicate that swelling due to inclusion of a porogen is not greatly affected by polymer derivatization. This is not surprising since the effect of including a porogen that is a good solvent for both monomer and polymer is to form the polymer in a preswollen state which is less subject to chain entanglement.

When the percentage of toluene in the polymer formulation was reduced to 31%, the acid–base diameter ratio decreased. When the percentage of toluene was increased to 58%, the resulting beads were soft and tended to crack. Therefore, 48% toluene was chosen as the optimum concentration.

The addition of Kraton G1652 to various bead formulation did not significantly influence swelling properties. It did, however, have a pronounced effect on the mechanical properties. Beads without added Kraton tended to crack. This was observed at different cross linking levels as can be observed for the first set of experiments without added toluene. Cracking was also observed at 4% or more Kraton. This was observed not just for the three beads in Table 1 with the highest Kraton levels but also for a large number of other beads including both poly(vinylbenzyl chloride) and polystyrene. Typically, it was observed that the surface would crack and a layer would peel off.

Because the elastic inclusion content of toughened polystyrene is typically on the order of 10%

or more, several attempts were made to prepare beads with higher Kraton levels. However, these consistently resulted in misshapen flakes rather than the spherical beads required for sensing.

Since swelling in acid is primarily due to inclusion of a pore-forming solvent in the initial polymer formulation, cross linking does not seem to be a critical variable affecting swelling. Very low degrees, i.e. less than 2%, of crosslinking are unsatisfactory because they lead to fragile beads that deform readily and fall apart.

The theoretical nitrogen content assuming pure poly(vinylbenzyl chloride) is completely derivatized with diethanolamine is 6.8%. The presence of approximately 5% divinylbenzene will reduce this value to 6.5%. The % nitrogen data in Table 1 seem to indicate that derivatization is more complete for the beads prepared in the absence of toluene. However, we suspect that the nitrogen values are higher for these beads because, in the absence of pore-forming solvent, it is harder to completely wash out unreacted amine. One reason for this conclusion is the observation that two of the values in the table are significantly higher than the theoretical value.

Appearance, morphology and mechanical strength

Beads without added Kraton appear translucent, very similar to conventional commercially available ion exchange resins. Beads with added Kraton are opaque white, with the degree of opacity increasing with the level of Kraton. This confirms that this material is heterogeneous with inclusions that are comparable or greater in size than the wavelength of visible light. Swelling in toluene before derivatization or in acid after derivatization is accompanied by a noticeable decrease in opacity.

Cross-sections (thickness) of beads containing 2 and 4% Kraton were examined under a light microscope at a magnification of 20. The bead with 4% Kraton had a large cloudy center section surrounded by a layer which was completely clear (not unlike a yoke surrounded by the white in an egg). There was a line between the cloudy center and outer clear sections. This is consistent with the observed cracking behavior in which the outer

clear layer tended to peel off. In contrast, the cross-section of the bead with only 2% Kraton had tiny cloud specks more or less evenly dispersed in a clear background. This is the desired morphology when elastomer is added to a brittle material to improve toughness.

The morphology may be explained by considering what happens during polymerization. As polymer forms, the aliphatic middle blocks of Kraton separate out forming a distinct phase. At the higher Kraton levels, this apparently happens when the polymerizing bead is still sufficiently fluid for the Kraton to aggregate in the center of the bead. At lower Kraton levels, polymerization will proceed further before the point at which the aliphatic middle block phase separates is reached. At this point for the bead with 2% Kraton, the medium must be sufficiently viscous to locally trap the Kraton.

Unfortunately, the beads are quite soft compared to ion exchange resins. The penetration moduli for beads swollen in acid were less than 1 MPa. In the sensor arrangement that we have been using [2], the swelling force was similar in magnitude to the force generated by the diaphragm. The result is significant deformation of the bead in the sensor and failure to realize the full potential sensitivity to pH.

Swelling vs. pH

In early experiments, it was found that during the first few swelling and shrinking cycles, both the rate and the magnitude of swelling in acid increased for successive cycles, eventually reaching a steady state. Subsequently, it was realized that this steady state could be reached immediately by "conditioning" the bead in pH 4.0 buffer for a day. We postulate that the stresses accompanying bead swelling in acid cause crazing, i.e. the formation of a large number of microcracks. These cracks terminate at the elastic inclusions associated with Kraton. The presence of these cracks allows the bead to accommodate the stresses associated with swelling and shrinking without any further degradation. This is the commonly accepted mechanism for the toughening of polystyrene by elastic inclusions [10].

Figure 1 shows how the diameter of a typical

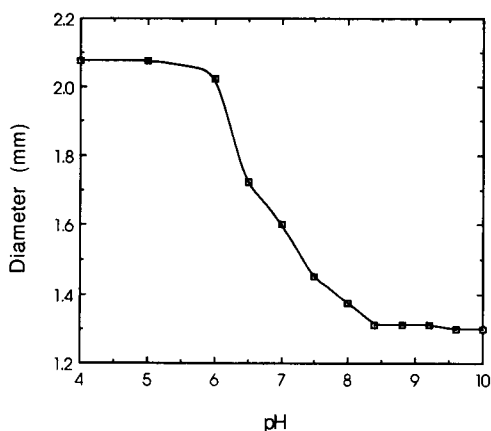


Fig. 1. Diameter vs. pH at an ionic strength of 0.10 M for an aminated bead prepared with 0.8% Kraton, 5.4% DVB and 48.0% toluene.

conditioned diethanolamine modified poly(vinylbenzyl chloride) bead varies with pH. The changes in diameter are substantial. After acid conditioning, the swelling ratio is close to 1.6, much larger than the initial diameter ratios shown in Table 1. The shape of the curve is similar to that observed for other types of indicators. However, according to theory, the volume swelling ratio to the 5/3 power (equal to the diameter ratio cubed) varies with the square of the charge on the polymer [3]. This means that diameter of the bead varies with the charge on the bead to the 2/5 power. This means that the pK_a is equal to the pH at the point where the diameter is equal to the minimum value plus 0.76 times the difference between the maximum and minimum values. Assuming this relationship holds for our beads, then

TABLE 2

Effect of ionic strength on the acid–base diameter ratio

	I.S. = 0.10 M		I.S. = 0.40 M		I.S. = 0.70 M	
	pH	Diam. (mm)	pH	Diam. (mm)	pH	Diam. (mm)
Bead 1	4.00	1.225	4.00	1.100	4.00	1.050
	9.20	0.750	9.20	0.800	9.20	0.800
Diameter ratio	1.633		1.375		1.313	
Bead 2	4.00	1.650	4.00	1.500	4.00	1.450
	9.20	1.100	9.20	1.125	9.20	1.150
Diameter ratio	1.500		1.333		1.261	

the pK_a of the immobilized diethanolamine is approximately 6.0.

The pK_a of diethanolamine immobilized on a polystyrene substrate is considerably lower than the solution value of 8.9. The hydrophobic polystyrene environment favors the uncharged form of the amine. One likely mechanism for the large shift is that the activity of water in the polymer is less than in solution. Hence, solvation by water is less effective at stabilizing the protonated form of the amine.

An experiment with diethylamine modified polystyrene was carried out to see if the observed pK_a shift was associated with the diethanolamine. It was found that the pK_a shift for diethylamine was very similar to that for diethanolamine.

Effect of ionic strength

Figure 2 shows diameter vs. pH for a bead at three different ionic strengths. As expected the total change in diameter decreases with increasing ionic strength.

According to theory the volume swelling ratio to the 5/3 power should vary inversely with ionic strength [3]. Table 2 presents data at three ionic strengths for two different beads. When volume ratio to the 5/3 power is plotted vs. ionic strength, the plot is linear with correlation coefficients of 1.000 for bead 1 and 0.980 for bead 2. This indicates that the swelling behavior is following theory so that the theoretical relationship may be used to correct for variations in ionic strength if necessary.

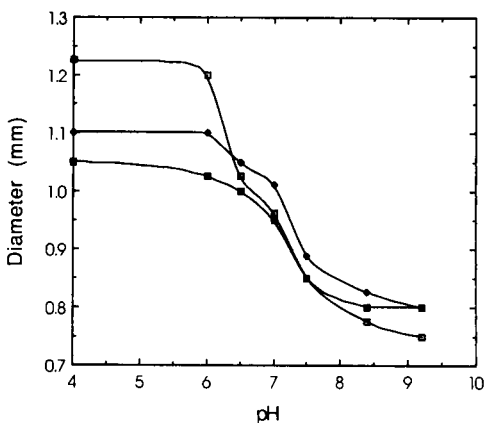


Fig. 2. Effect of ionic strength on the variation in diameter vs. pH for an aminated bead prepared with 0.8% Kraton, 5.4% DVB and 48.0% toluene. Key: □ = 0.10 M; ◆ = 0.40 M; ■ = 0.70 M.

Swelling rate

Figure 3 shows bead size vs. time after exposure to pH 4.0 buffer for three beads. These beads were conditioned in pH 4.0 buffer for 24 h and then equilibrated in pH 9.20 buffer before the rate of swelling was measured. The rate of shrinking is similar. As expected the rates of swelling and shrinking depend on bead diameter. However, for all diameters tested the rates are too slow for most sensing applications.

Late in this study, it was inadvertently discovered that addition of a few drops of concentrated

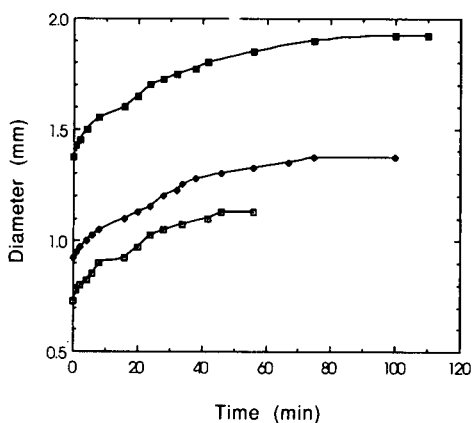


Fig. 3. Diameter vs. time after an bead is placed in pH 4.0 buffer. Data are shown for three beads with different diameters. The beads were prepared with 0.8% Kraton, 5.4% DVB and 48.0% toluene. Key: □ = bead 1; ◆ = bead 2; ■ = bead 3.

HCl to beads in 10 ml of pH 4.0 buffer led to faster response. Final volumes for 1 mm size beads were reached in 10 min. The addition of HCl was accompanied by leaching of a small amount of fluffy white powder from the polymer. We believe this to be Kraton G1652. The loss of this material may leave pores in the polymer allowing the hydrogen ion to diffuse more rapidly to the center of the polymer.

Effect of temperature

Bead diameter was measured as a function of temperature from 5 to 35°C at pH 9.20 and 4.00. At pH 9.20, the bead shrinks with increasing temperature. The temperature coefficient is $-0.37\%/^{\circ}\text{C}$. The reason that it shrinks rather expanding is that the driving force for swelling of an uncharged bead in a compatible solvent is primarily due to the entropy gain associated with solvation of the polymer chains. The effect is analogous to the well known shrinking of a rubber band with increasing temperature.

At pH 4.00, the bead increases in size with increasing temperature with an expansion coefficient of $0.2\%/^{\circ}\text{C}$. At this pH there is significant additional swelling due to charge on the polymer. This can be treated as an osmotic pressure effect [3]. The force causing solvent to enter the polymer is due to the difference in charge density in solution and on the polymer. Osmotic pressure is proportional to absolute temperature.

The temperature coefficient data can be used to estimate the effect of temperature on response of a sensor using one of these polymers. Interestingly, the fact that the temperature coefficient is negative for the uncharged polymer and positive for the charged polymer suggests that the temperature coefficient will be quite small in the optimum sensing region where the polymer is partially protonated.

Conclusions

The most significant result reported here is that derivatized porous polystyrene may be toughened by adding Kraton G1652. This suggests that it will be possible to develop robust longlasting ion sensors based on polymer swelling. However, the polymer beads reported here suffer from two serious deficiencies compared to the ion

exchange materials used previously [1,2]. Because they are relatively soft, the swelling forces are weak. In principle, this can be overcome by using a thin diaphragm with a low force constant in the sensor. In practice, however, thin diaphragms are a poor solution. They are more subject to rupture, more sensitive to environmental pressure fluctuations and less opaque to ambient light.

The authors thank Dow Chemical Co. and Shell Chemical Co. for providing samples of vinylbenzyl chloride and Kraton G1652, respectively. Todd Gross provided the instrumentation and expertise required to measure the penetration modulus of the beads. Partial financial support for this research was provided by a subcontract from Polysense, Inc. on DOE Grant DE-FG02-91ER81191.

REFERENCES

- 1 M.F. McCurley and W.R. Seitz, *Anal. Chim. Acta*, 249 (1991) 373.
- 2 M. Bai and W.R. Seitz, *Proc. SPIE*, Vol. 1796, in press.
- 3 P.J. Flory, *Principles of Polymer Chemistry*, Cornell University Press, Ithaca, NY, 1953.
- 4 W.R. Seitz, *J. Mol. Struct.*, 242 (1993) 105.
- 5 D.C. Sherrington and P. Hodge (Eds.), *Syntheses and Separations using Functional Polymers*, Wiley, New York, 1988.
- 6 J.R. Millar, D.G. Smith, W.E. Marr and T.R.E. Kressman, *J. Chem. Soc.*, (1963) 218.
- 7 W.L. Sederel and G.J. DeJong, *J. Appl. Polym. Sci.*, 17 (1973) 2835.
- 8 H. Galina, B.N. Kolarz, P.P. Wiczorek and M. Wojczynska, *Br. Polym. J.*, 17 (1985) 215.
- 9 J.L. Amos, *Polym. Eng. Sci.*, 14 (1974) 1.
- 10 G.F. Freeguard, *Br. Polym. J.*, 6 (197) 205.
- 11 F.P. Chlanda and R.S. Cooke, *U.S. Pat.*, 4,738,764 (1988).
- 12 K. Sardelis, H.J. Michels and G. Allen, *Polymer*, 28 (1987) 244.
- 13 P. Hodge and D.C. Sherrington (Eds.), *Polymer Supported Reactions in Organic Synthesis*, Wiley, New York, 1980, p. 469, Appendix.
- 14 P.P. Wiczorek, M. Ilavsky, B.N. Kolarz and K. Dusek, *J. Appl. Polym. Sci.*, 27 (1982) 277.
- 15 S. Itsuno, K. Uchikoshi and K. Ito, *J. Am. Chem. Soc.*, 112 (1990) 8187.
- 16 K.W. Pepper, H.M. Paisley and M.A. Young, *J. Chem. Soc.*, (1953) 4097.

Organic-phase biosensing of enzyme inhibitors

Joseph Wang, Eithne Dempsey¹ and Arkadi Eremenko²

Department of Chemistry, New Mexico State University, Las Cruces, NM 88003 (USA)

Malcolm R. Smyth

School of Chemical Sciences, Dublin City University, Dublin 9 (Ireland)

(Received 13th November 1992; revised manuscript received 18th January 1993)

Abstract

Organic-phase biosensors, suitable for monitoring low levels of enzyme inhibitors in non-aqueous media, are described. The inhibition of tyrosinase and horseradish peroxidase by thiourea, benzoic acid, diethyldithiocarbamate, hydroxylammonium sulphate and mercaptoethanol is exploited for highly sensitive amperometric measurements in organic media. Fast on-line monitoring of various inhibitors is illustrated in a flow-injection operation, with an enzyme inhibition based detector and an acetonitrile carrier solution. Repetitive injections of a 1×10^{-4} M diethyldithiocarbamate solution (at a rate of 60 samples per hour) yielded a relative standard deviation of 3.3%. Sensing advantages accrue from such operation, particularly applicability to inhibitors with poor water solubility and solvent-induced changes in the mechanism of inhibition, are discussed.

Keywords: Amperometry; Biosensors; Flow injection; Enzyme electrodes; Enzyme inhibition; Organic phase

The ability of enzymes to operate in non-aqueous environments [1] has led to the important development of organic-phase biosensors [2]. Such devices have an immense analytical potential, as they expand the scope of biosensors towards many important analytes (with poor water solubility) and towards many challenging hydrophobic sample matrices. Various organic-phase enzyme electrodes have thus been developed for monitoring phenols in olive oils [3] or in pharmaceutical formulations [4], cholesterol in butter and margarine [5], catechols in various alcohols [6] and for measuring hydrogen peroxide or organic peroxides [7,8].

The objective of the present study is to expand the concept of organic-phase biosensors toward measurements of important enzyme inhibitors. The modulation of enzymatic activity by inhibitors, such as pesticides or heavy metals, has been widely used for monitoring these inhibitors in aqueous solutions [e.g. 9,10]. In the following sections we report on analogous inhibitor measurements utilizing organic-phase biosensors. Such organic-phase assays of enzyme effectors should expand the scope of enzyme electrodes towards many important inhibitors that are not readily dissolved in aqueous solutions. In addition, the organic-phase operation may greatly effect the mechanism of inhibition. According to Zaks and Klibanov [11], the replacement of water with an organic solvent results with a reversal of the inhibitor selectivity of the enzyme (i.e., better enzyme inhibitors in water become poorer inhibitors in organic media, and vice versa). These changes, coupled with other improvements inher-

Correspondence to: J. Wang, Department of Chemistry, New Mexico State University, Las Cruces, NM 88003 (USA).

¹ Present address: School of Chemical Sciences, Dublin City University, Dublin 9 (Ireland).

² Present address: Research Center of Molecular Diagnostics and Therapy, Simpheropolsky Blvd. 8, 113149 Moscow (Russian Federation).

ent to biosensors in non-aqueous environments [2], should greatly enhance the power of enzyme inhibition based biosensors. These possibilities are demonstrated below utilizing the inhibition of horseradish peroxidase and tyrosinase, enzymes known for their biocatalytic activity in organic media [2–4,7,8].

EXPERIMENTAL

Apparatus

Experiments were carried out with a 10-ml electrochemical cell [Model CV-2, Bioanalytical Systems (BAS)]. The enzyme electrode, the Ag/AgCl reference electrode and platinum counter electrode joined the cell through holes in its PTFE cover. A 3-mm diameter glassy carbon disk (Model MF 2012, BAS) was used for preparing the enzyme electrode. The flow-injection system consisted of a 50-ml carrier reservoir, a syringe pump (Model 341B, Sage), a Rainin Model 5041 sample valve (20- μ l loop), interconnecting PTFE tubing (0.8 mm i.d.) and a glassy carbon thin-layer detector (Model TL-5 BAS). The reference electrode was placed in a downstream compartment.

Reagents

Horseradish peroxidase (EC 1.11.1.7, 100 U mg^{-1}), tyrosinase (EC 1.14.18.1, 2400 U mg^{-1}), benzoic acid, 2,4-dichlorophenoxyacetic acid (Sigma), phenol (Baker), acetonitrile, sodium, diethyldithiocarbamate, hydroxylammonium, dimethylmercury, 2-butanone peroxide, *o*-phenylenediamine (Aldrich), thiourea (Fisher), and tetraethylammonium *p*-toluenesulphonate (TEATS) (Fluka) were used as received. The poly(ester-sulphonic acid) polymer (Eastman AQ55D, Eastman Kodak) was obtained dissolved (28%, w/v) in water.

Procedure

For preparing the peroxidase sensor, a 20- μ l aliquot of the aqueous peroxidase solution (5 mg ml^{-1}) was first mixed with 20 μ l of the 2.8% Eastman AQ-55D polymer solution. The surface of the previously polished glassy carbon electrode

was covered by casting 20 μ l of the mixed enzyme-polymer solution. The film was dried for 30 min, using a heat gun ca. 50 cm away, to yield an enzyme surface loading of 5 U.

The preparation of the tyrosinase electrode (240 U per surface) was achieved by covering the electrode surface with a 10- μ l aliquot of the tyrosinase-polymer mixture (prepared by dissolving 2 mg of the enzyme in 200 μ l of 1.4% Eastman AQ polymer). Prior to use, the tyrosinase electrode was immersed in a 0.2 mM phenol solution in acetonitrile (0.1 M TEATS) for 10 min. This procedure allowed for rapid stabilization of the baseline upon use, as well as regeneration of the activity of the enzyme electrode after addition of reversible inhibitors.

All experiments were carried out at room temperature in acetonitrile solution [containing 2% (v/v) phosphate buffer and 0.1 M TEATS]. The amperometric response to 0.2 mM phenol and 1.0 mM 2-butanone peroxide was measured at -0.2 V (vs. Ag/AgCl), in order to allow detection of the liberated *o*-quinone and oxidized form of the *o*-phenylenediamine hydrogen-donor mediator (for tyrosinase and horseradish peroxidase, respectively). Batch experiments were carried out with a magnetic stirrer providing convective transport at 300 rpm. Flow analysis was carried out at 1.0 ml min^{-1} .

RESULTS AND DISCUSSION

The concept of organic-phase inhibitor biosensors is illustrated in the following sections for monitoring inhibitors of horseradish peroxidase and tyrosinase, in connection with the Eastman AQ-enzyme immobilization approach. Such immobilization scheme relies on the stability of Eastman AQ [poly(ester-sulphonic acid)] coatings in various organic solvents [12,13]. Figure 1 illustrates the suitability of the organic-phase peroxidase electrode for monitoring low levels of inhibitors in the presence of its organic peroxide substrate [14]. The steady-state response toward the 2-butanone peroxide (in acetonitrile media) rapidly decreases upon additions of the 2-mercaptoethanol (A) and hydroxylamine (B) in-

hibitors. The electrode responds very rapidly to these micromolar changes in the inhibitor concentrations with no need for an incubation period. Steady-state signals are achieved within 5–15 s. The decreased substrate response is proportional to the inhibitor concentration up to 1.5 mM (A) and 0.1 mM (B). The sensitivity (slope of the linear portion) corresponds to 649 (A) and 920 (B) nA mM⁻¹. The favorable signal-to-noise (*S/N*) characteristics offer detection limits of 10 (A) and 1.4 (B) μM (based on *S/N* = 3). No response was observed in controlled experiments involving additions of the solvent (dotted lines) or at the unmodified electrode.

The organic-phase tyrosinase electrode also offers convenient quantitation of enzyme inhibitors. Figure 2 shows the response of the tyrosinase electrode (in acetonitrile) to 0.2 mM phenol (S), followed by successive additions of 20 μM diethyldithiocarbamate (A, In) and 0.1 mM thiourea (B, In). A fast and sensitive response is

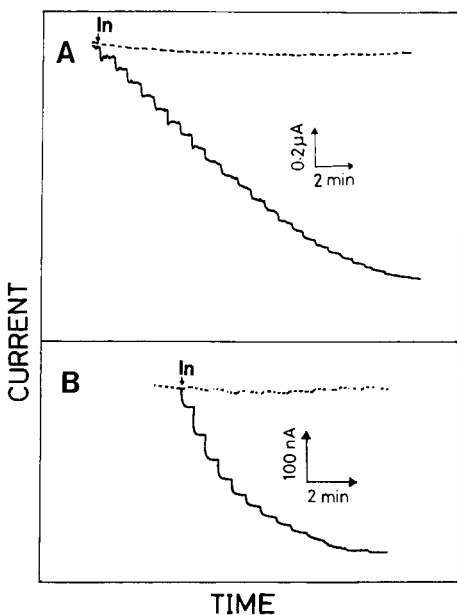


Fig. 1. Current-time recordings at the peroxidase electrode upon increasing the 2-mercaptoethanol (A) and hydroxylammonium sulphate (B) concentrations in 100 μM and 20 μM steps, respectively. Operating potential, -0.20 V; solution, acetonitrile-phosphate buffer (98:2, v/v), containing 0.1 M TEATS, 1 mM butanone peroxide and 0.2 mM *o*-phenylenediamine; stirring rate, 300 rpm.

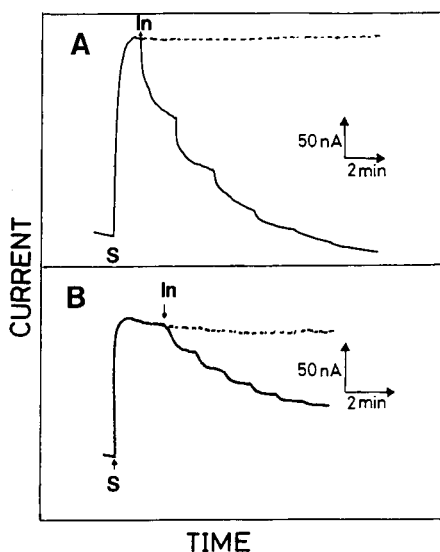


Fig. 2. Current-time recordings at the tyrosinase electrode upon increasing the diethyldithiocarbamate (A) and thiourea (B) concentrations in 20 μM and 100 μM steps, respectively. Conditions as in Fig. 1, but without *o*-phenylenediamine and butanone peroxide. S represents the initial response to the substrate addition (0.2 mM phenol).

observed for both inhibitors. Other compounds, exhibiting a slow inhibition (and hence response), can be determined by using different electrode surfaces. Examples of two such inhibitors are given in Fig. 3. These include the thiourea inhibition of peroxidase (A) and the dichlorophenoxyacetic acid inhibition of tyrosinase (B). Restoration of the enzyme activity (for retesting) could be accomplished by a short (5 min) incubation period in the presence of the substrate (1 mM).

Figure 4 displays calibration plots for several inhibitors, as obtained at the peroxidase (A) and tyrosinase (B) organic-phase electrodes. The different inhibition processes result in plots of different shapes. In most cases, the current rises linearly with the inhibitor concentration at first and then it starts to level off. One exception is the thiourea inhibition of peroxidase [A (a)] that yields a sigmoidal calibration graph (indicating a two-step mechanism, with a very slow inhibition at low concentrations and a faster one at higher levels). The linear range and the sensitivity differ from inhibitor to inhibitor. For example, for thiourea, mercaptoethanol and benzoic acid (at

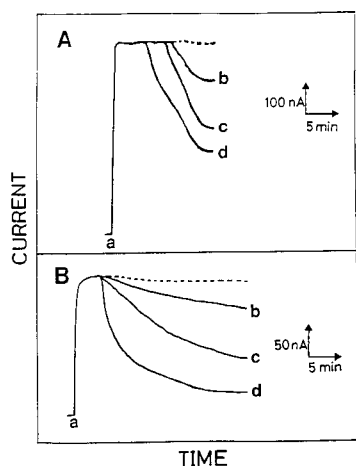


Fig. 3. Current–time recordings at the peroxidase (A) and tyrosinase (B) electrodes for increasing levels of thiourea and dichlorophenoxyacetic acid, respectively. Inhibitor concentrations: (A) 25 (b), 50 (c) and 100 (d) μM ; (B) 40 (b), 200 (c) and 1000 (d) μM ; (a) represents the substrate addition. Conditions as in Figs. 1 and 2, respectively, except that each curve was recorded after incubation in the substrate solution.

the tyrosinase electrode) linearity prevailed up to 0.15, 0.10, and 0.01 mM, respectively. For hydroxylammonium sulphate, mercaptoethanol and diethyldithiocarbamate (at the peroxidase electrode) linearity prevailed up to 0.10, 0.60, and 0.12 mM, respectively. Overall, the profiles shown in Fig. 4 reflect the kinetics and mechanism of the enzyme inactivation in the organic media.

The data of Figs. 1–4 have been used for calculating various kinetic parameters relevant to the inhibition process. For example, Table 1 displays values of $I_{0.5}$ (coefficient of 50% inhibition) and K_i (inhibition constant) for various inhibitors of tyrosinase. Benzoic acid exhibits the greatest degree of inhibition. The inhibition of tyrosinase appears to proceed through interaction with the active copper site [15]. It was suggested [11] that the organic media can affect the binding of inhibitors to the enzyme sites, and thus alters the kinetic parameters of the inhibition process. The fact that benzoic acid is the strongest inhibitor is indicative of such alteration. The data of Table 1 reflect these changes in the inhibition specificity and illustrate the utility of organic-phase enzyme electrodes for elucidating the inhibition process. Additional information on the inhibitory action

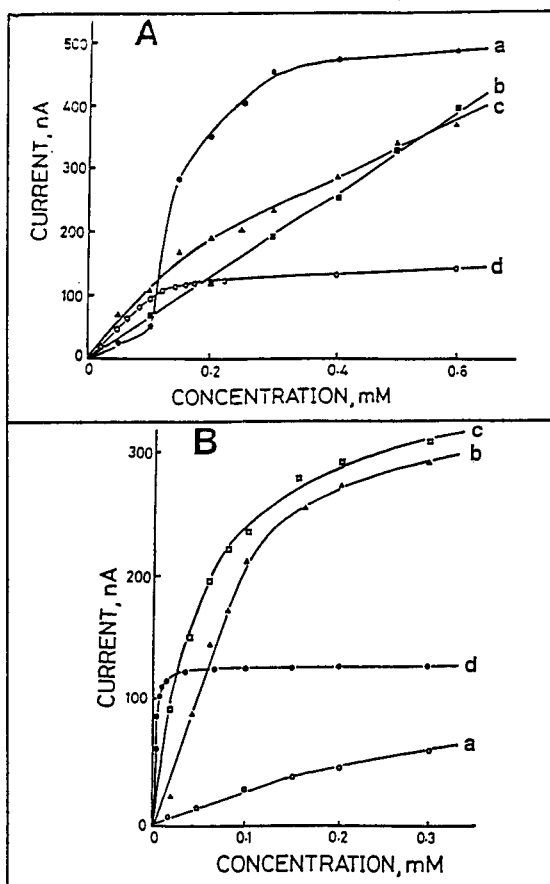


Fig. 4. Calibration curves for various inhibitors at the peroxidase (A) and tyrosinase (B) electrodes. (a) Thiourea, (b) 2-mercaptoethanol, (c) diethyldithiocarbamate, [A (d)] hydroxylammonium sulphate and [B (d)] benzoic acid. Conditions as in Figs. 1–3.

TABLE 1

Calculated $I_{0.5}$ and K_i values for inhibitors of tyrosinase ^a

Inhibitor	$I_{0.5}$ (mM) ^b	K_i (mM) ^c
Thiourea	0.325	1.723
Diethyldithiocarbamate	0.025	0.132
Benzoic acid	0.002	0.017
2-Mercaptoethanol	0.058	0.307
Dichlorophenoxyacetic acid	0.228	1.209
Dimethylmercury	1.200	6.362

^a Based on the calibration data of Fig. 4. ^b Concentration corresponding to 50% inhibition. ^c Concentration that doubles the slope of the $[1/\text{rate}]$ vs. $[\text{substrate}]$ plot.

can be achieved by examining the effect of the substrate concentration upon the response to the inhibitor. For example, the percent inhibition of diethyldithiocarbamate at the organic-phase tyrosinase electrode was not affected by the phenol concentration. Such behavior is consistent with a non-competitive inhibition process.

The attractive dynamic properties of the organic-phase inhibitor enzyme electrode can be exploited for on-line applications, as desired for continuous monitoring of flowing organic streams. An organic-phase flow detector for monitoring phenolic and peroxide substrates was developed recently in our laboratory [16]. Similarly, Fig. 5 illustrates flow-injection measurements of various inhibitors of tyrosinase [benzoic acid (B), thiourea (C) or diethyldithiocarbamate (D)] using an acetonitrile carrier solution. Such on-line monitoring relies on the decrease of the peak for the phenol substrate [vs. those observed without the inhibitor (A, E)]. The fast response to these changes in the inhibitor concentration permits an injection rate of 60 samples h^{-1} . The well-defined response to these 0.5 mM inhibitor solutions indicates convenient flow-injection quantitation of submillimolar and micromolar concentrations. Note also the complete renewal of the enzymatic activity, as indicated from comparison of the substrate peaks before (A) and after (E) this series.

Figure 6 displays the results of a flow-injection calibration experiment for diethyldithiocarbamate over the 0–400 μM range. The tyrosinase-based

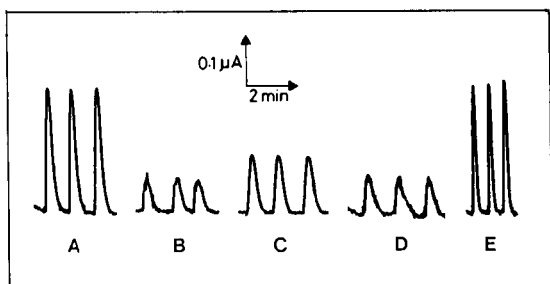


Fig. 5. Flow-injection peaks for 0.5 mM phenol solutions containing 0.5 mM benzoic acid (B), thiourea (C) and diethyldithiocarbamate (D), as well without inhibitor (A, E). Carrier solution, acetonitrile–phosphate buffer (98:2, v/v) containing 0.05 M TEATS and flowing at 1 ml min^{-1} . Potential, -0.2 V.

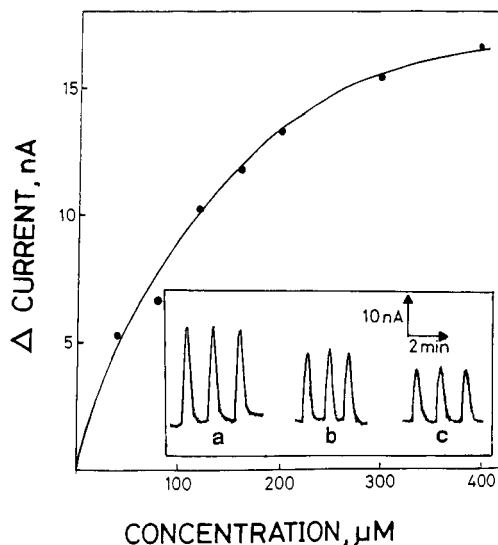


Fig. 6. Flow-injection calibration data for diethyldithiocarbamate at the organic-phase tyrosinase detector. Also shown (inset) are actual peaks for (a) 0, (b) 80, and (c) 160 μM inhibitor. Other conditions as in Fig. 5.

flow detector responds in a non-linear fashion to these changes in the dithiocarbamate concentration, with a rapid rise at first and then more slowly. Repetitive injections of the 100 μM diethyldithiocarbamate solution yielded a reproducible flow-injection response, with a relative standard deviation of 3.3%.

In conclusion, it has been demonstrated for the first time that organic-phase enzyme electrodes can be employed for monitoring inhibitors in non-aqueous environments. A new class of analytes has thus been added to those measured by organic-phase biosensors. The new devices extend the scope of inhibitor biosensors toward many inhibitors with poor water solubility, and offer useful insights into the inhibition action in organic solvents. Several of the inhibitors examined in this study (e.g., dichlorophenoxyacetic acid, thiourea, benzoic acid or dimethylmercury) are poorly soluble in water. Applicability to inhibitor measurements in previously inaccessible samples is also anticipated. The solvent-induced changes in the inhibitory action hold a great promise for manipulating the response (extended linearity of response or improved sensitivity) of inhibitor biosensors. While the concept is illus-

trated with inhibitors of peroxidase or tyrosinase, it could be extended to other enzymes and inhibitors. Analogous organic-phase measurements of enzyme activators should be accomplished in a similar manner.

E.D. acknowledges a Fulbright Award from the Institute of International Education.

REFERENCES

- 1 A.M. Klibanov, *CHEMTECH*, 16 (1986) 356.
- 2 S. Saini, G.F. Hall, M.E. Downs and A.P.F. Turner, *Anal. Chim. Acta*, 249 (1991) 1.
- 3 J. Wang, A.J. Reviejo and S. Mannino, *Anal. Lett.*, 25 (1992) 1399.
- 4 J. Wang and Y. Lin, *Analyst*, 118 (1993) 277.
- 5 G.F. Hall and A.P.F. Turner, *Anal. Lett.*, 24 (1991) 1375.
- 6 J. Wang, Y. Lin, A. Eremenko, A. Ghindilis and I. Kurochkin, *Anal. Lett.*, 26 (1993) 197.
- 7 F. Schubert, S. Saini and A.P.F. Turner, *Anal. Chim. Acta*, 245 (1992) 133.
- 8 J. Wang, B. Freiha, N. Naser, E. Romero, U. Wollenberger, M. Ozsoz and O. Evans, *Anal. Chim. Acta*, 251 (1991) 81.
- 9 A. Townshend and A. Vaughan, *Talanta*, 17 (1970) 289.
- 10 I. Dolmanova, T. Shekhovstova and V. Kutcheryaeva, *Talanta*, 34 (1987) 201.
- 11 A. Zaks and A.M. Klibanov, *J. Biol. Chem.*, 263 (1988) 3194.
- 12 J. Wang, Y. Lin and Q. Chen, *Electroanalysis*, 5 (1993) 23.
- 13 T. Gennett and W. Purdy, *Anal. Chem.*, 62 (1990) 2155.
- 14 J. Wang, B. Freiha, N. Naser, E. Romero, U. Wollenberger, M. Ozsoz and O. Evans, *Anal. Chim. Acta*, 254 (1991) 81.
- 15 K. Lerch, *Mol. Cell. Biochem.*, 5 (1983) 125.
- 16 J. Wang and Y. Lin, *Anal. Chim. Acta*, 271 (1993) 53.

Pulsed amperometric detection of proteins using antibody containing conducting polymers

O.A. Sadik and G.G. Wallace

Intelligent Polymer Research Laboratory, University of Wollongong, Chemistry Department, Northfields Avenue, Wollongong, NSW 2522 (Australia)

(Received 9th November 1992; revised manuscript received 1st February 1993)

Abstract

The use of pulsed potential waveforms to control antibody–antigen interactions on conducting polymer surfaces has been demonstrated. This enables detection of proteins at low levels and the use of antibody containing electrodes for multiple analyses.

Keywords: Amperometry; Antibodies; Polymers; Proteins

It has been recognised for some time now that the use of antibodies (Ab) in sensing technologies promises a degree of selectivity previously unattainable in electrochemical sensing [1–4]. The inherent molecular recognition capabilities of an Ab for the corresponding antigen (Ag) should prove extremely useful. However, some practical difficulties have mitigated against the realisation of this promise. In particular the generation of a sensitive, reproducible analytical signal due to the antibody–antigen interaction has proven difficult. These problems arise from the lack of a Faradaic (electron transfer) signal and from the irreversible nature of the Ab–Ag process.

In attempts to overcome these problems the use of potential measurements [5,6] or indirect amperometric immunoassay [6,7] has been addressed. Direct measurements enabling changes in the capacitive nature of the sensor surface (after the Ab–Ag interaction) to be determined

have also been employed. [8]. However, in all cases these procedures are time consuming due to the equilibrium times and/or the multistep procedures required.

Furthermore these approaches suffer from the fact that the Ab containing surface must be re-generated chemically to reverse the Ab–Ag interaction. It has been demonstrated previously that antibodies are readily incorporated into conducting polymers during synthesis [8,9] and that specific reactions of the corresponding Ag with the bound Ab are possible. In attempts to generate useful analytical signals alternating current (AC) voltammetry was employed previously. While sensitivity was adequate, reproducibility and the reusability aspects of this sensing system were not.

In this work we report for the first time the use of conducting polymer antibody containing electrodes with pulsed amperometric detection in a flow-injection analysis (FIA) system. The performances of this system with respect to electrical signal generation, reusability and reproducibility has been investigated. The polypyrrole antihuman serum albumin (AHSA) system has been used as a test case.

Correspondence to: G.G. Wallace, Intelligent Polymer Research Laboratory, University of Wollongong, Chemistry Department, Northfields Avenue, Wollongong, NSW 2522 (Australia).

EXPERIMENTAL

Reagents and standard solutions

All reagents were AR grade unless otherwise stated. LR grade pyrrole was obtained from Sigma. The pyrrole was distilled before use. Human serum albumin was obtained from Commonwealth Serum Laboratory (CSL), Melbourne (Batch No. 09801), anti-human albumin was obtained from Sigma.

Instrumentation

A homemade galvanostat, BAS 100A electrochemical analyser, a Dionex pulse amperometric detector (PAD-2), a Dionex analytical pump (APM-1) and ICI Instruments DP 600 chart recorder were employed. A platinum disk was used as the substrate on which the polymers were grown. A platinum gauze auxiliary electrode was used and the reference electrode was Ag/AgCl (3 M KCl). A thin-layer amperometric cell supplied by Dionex was used throughout this work. FIA was performed using a Dionex liquid chromatographic module (CMB-2). A 50- μ l sample loop was used for all experiments. The electrochemical cell was controlled by the Dionex pulsed amperometric detector and the current was recorded with the strip chart recorder.

Preparation of the antibody containing electrodes

Polypyrrole electrodes were prepared by galvanostatically electropolymerising pyrrole monomer (0.5 M) from aqueous solution containing 100 mg l⁻¹ AHSA solution onto a platinum substrate using a current density of 0.5 mA cm⁻². The working electrode was polished on a polishing cloth with alumina and then ultrasonicated prior to use. 0.5 M pyrrole was first mixed with water in a 25-ml standard flask, anti-HSA was added to the flask and mixed gently, it was gently deoxygenated for 10 min.

RESULTS AND DISCUSSION

Initially the preparation of antibody containing electrodes was considered. Antihuman serum al-

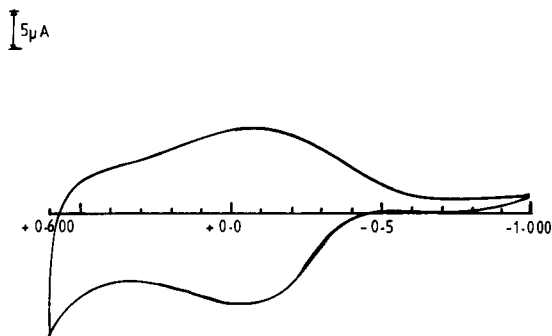


Fig. 1. Cyclic voltammogram obtained using polypyrrole (PP)-AHSA coated on platinum scanned in 0.1 M NaNO₃. Polymer was deposited using the conditions detailed in the experimental section. Scan rate = 100 mV s⁻¹.

bumin was incorporated into polypyrrole as described previously [8,9] and as detailed in the experimental section. The resultant polymer coated platinum electrode was mechanically stable and cyclic voltammetry (Fig. 1) revealed that the normal polymer oxidation/reduction processes did occur. As reported previously [8] no change in the cyclic voltammetry occurred when the Ab containing electrode was exposed to HSA.

This polymer was then coated on an electrode suitable for use in an FIA system. With a constant potential applied solutions containing the protein human serum albumin were injected. The hydrodynamic voltammograms obtained are shown in Fig. 2. An almost linear increase in the

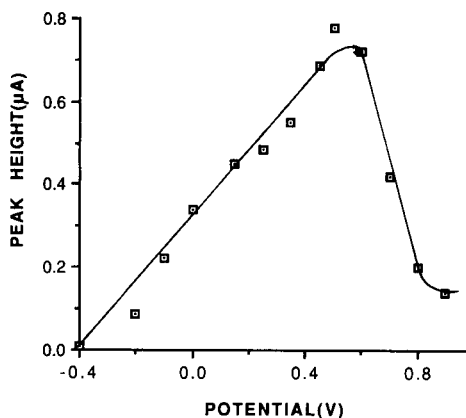


Fig. 2. Constant potential hydrodynamic voltammogram obtained using flow-injection analysis at a PP-AHSA coated electrode. Eluent was 0.1 M NaNO₃. Flow-rate = 1 ml min⁻¹. Concentration of HSA was 50 mg l⁻¹ (in 0.1 M NaNO₃).

current was observed as the potential was increased from 0.00 to +0.60 V. This signal may in part be due to changes in conductivity as the eluent passes through the cell [10], however, it is also known that the Ab–Ag₂ interaction is encouraged with more positive potentials applied [9]. The decrease in current at more positive potentials than +0.60 V was most likely due to over oxidation of the polymer at these potentials as reported previously [11]. This overoxidation reduces the conductivity of the polymer coating. With an applied potential of (+0.60 V) it was found that analytical responses could be obtained for injections of HSA. However their sensitivity was low and a detection limit of only 25 mg l⁻¹ was achieved. In addition the responses obtained suffered due to the fact that tailing peaks were obtained. This was presumably due to the irreversible nature of the antibody–antigen interaction with a constant applied potential.

The use of a pulsed electrochemical waveform to generate an analytical signal was subsequently investigated. Hughes and Johnson [12,13] have previously used pulsed amperometric detection to generate analytically useful signals as species interact with electrode surfaces. This knowledge combined with the fact that we have demonstrated the ability to modulate chemical interactions on conducting polymers electrochemically [9,14] suggested that the use of pulsed amperometric detection should prove useful for detection of proteins using Ab containing polymer electrodes.

A pulsed potential hydrodynamic voltammogram was then obtained using symmetric pulses with a pulse width of 120 ms. Keeping the initial potential (E_1) constant at +0.40 V, where Ab–Ag interactions are encouraged [9] the other potential (E_2) was varied between -0.40 and +0.90 V (Fig. 3). The current was always sampled at the end of E_2 . Pulsing to more positive potentials produced a small signal which did not increase with potential. However as the potential was pulsed negative the signal increased in magnitude at least down to 0.00 V. Increasing the negative potential limit further caused the response to decrease. Note also that as expected use of pulsed potentials markedly enhanced the magnitude of

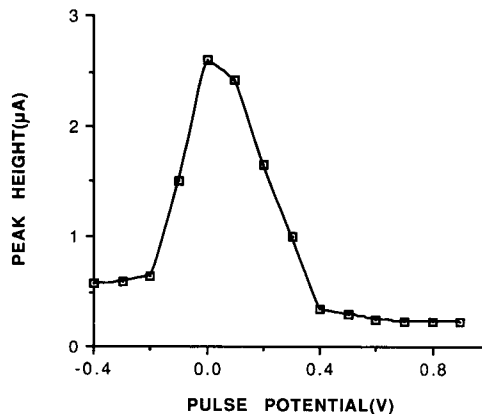


Fig. 3. Pulsed potential hydrodynamic voltammogram. Pulse width = 120 ms. The initial potential (E_1) was kept constant at +0.40 V. E_2 was varied recording to the value on the x-axis. Other conditions as in Fig. 2.

the responses obtained (compare y axes, Figs. 2 and 3). This amplification was due to increased capacitive currents obtained on pulsing and also presumably due to the multiple Ab–Ag interactions induced by pulsing.

Using these initial and final potential conditions the effect of pulse width on the response obtained was considered (Fig. 4). It was found that the sensitivity increased markedly as the pulse width was increased from 60 to 120 ms but increased only marginally with further increases. The variation in sensitivity (60–120 ms) highlights the role played by the kinetics of the Ab–Ag

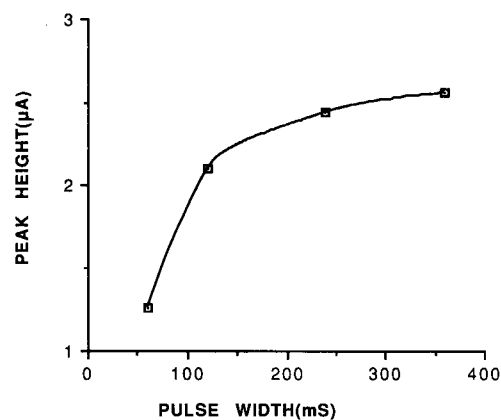


Fig. 4. Effect of pulse width on FIA responses obtained. Other conditions as in Fig. 3.

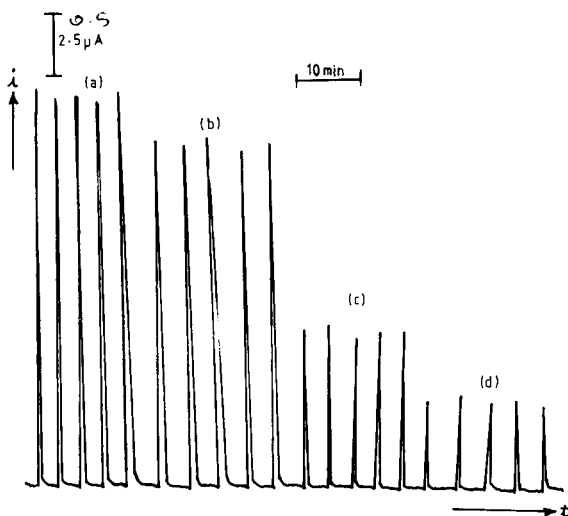


Fig. 5. Typical FIA responses obtained using conditions as in Fig. 2. Pulse width = 120 ms. HSA concentrations: (a) 50, (b) 25, (c) 15 and (d) 5 mg l⁻¹.

interaction in generating this signal. For practical purposes we decided to use a pulse width of 120 ms since it gives adequate sensitivity and adequate resolution for FIA.

Therefore using a pulsed wave form with the following conditions $E_1 = +0.40$ and $E_2 = 0.00$ V, $t_1 = 120$ ms and $t_2 = 120$ ms injections of HSA at various concentrations was then considered. Typical responses are shown in Fig. 5 and calibration curves are shown in Fig. 6. Blank calibration curves on platinum and polypyrrole-NO₃ were

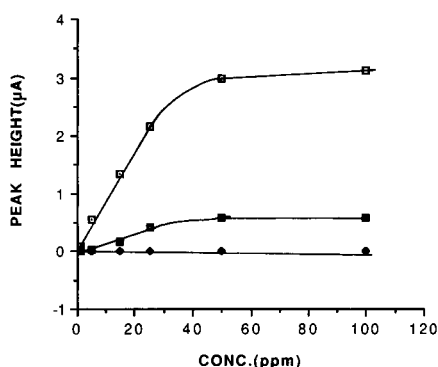


Fig. 6. Calibration curves obtained using conditions as in Fig. 5. □ = PP-AHSA; ♦ = bare platinum; ■ = PP-NO₃.

also obtained to verify that the signal was in fact due to Ab–Ag interactions.

The reproducibility of the responses obtained was adequate ($\pm 5\%$ over 10 injections) in the range 5 to 50 ppm protein and detection limits of less than 1 mg l⁻¹ were estimated.

Conclusions

A rapid, sensitive and reproducible detection method for HSA based on the use of polypyrrole-HSA with pulsed amperometric detection in an FIA mode has been developed. This approach overcomes many of the practical problems previously associated with direct electrochemical immunoassay. The approach should prove extremely useful for other Ab–Ag systems.

Prof. G.G. Wallace acknowledges the financial support of the Australian Research Council. The authors are indebted to Melinda John for discussions held in the early part of this work.

REFERENCES

- 1 J.R. North, Trends. Biotechnol. 7 (1985) 180.
- 2 M.A. Arnold and M.E. Meyerhoff, Crit. Rev. Anal. Chem., 20 (1988) 149.
- 3 C.R. Lowe, Philos. Trans. Roy. Soc., London, B324 (1989) 487.
- 4 G. Nagy and E. Pungor, Bioelectrochem. Bioenerg., 20 (1988) 1.
- 5 D.L. Bush and G.A. Rechnitz, Anal. Lett., 20 (1987) 1781.
- 6 M.J. Green, Philos. Trans. Roy. Soc., London, B316 (1987) 135.
- 7 D. Monroe, Crit. Rev. Clin. Sci. 28 (1990) 1.
- 8 R. John, M.J. Spencer, M.R. Smyth and G.G. Wallace, Anal. Chim. Acta, 249 (1991) 381.
- 9 A.J. Hodgson, T.W. Lewis, K. Maxwell, M.J. Spencer and G.G. Wallace, J. Liquid Chromatogr., 13 (1990) 3091.
- 10 O. Sadik and G.G. Wallace, Electroanalysis, in press.
- 11 A. Witkowski, M.S. Freund, A. Brajter-Toth, Anal. Chem. 63 (1991) 622.
- 12 S. Hughes and D.C. Johnson, Anal. Chim. Acta, 149 (1983) 1.
- 13 S. Hughes and D.C. Johnson, Anal. Chim. Acta, 132 (1981) 11.
- 14 W.E. Price, G.G. Wallace and H. Zhao, J. Electroanal. Chem. 334 (1992) 111.

Determination of the diffusion coefficient of oxygen in sodium chloride solutions with a transient pulse technique

A.J. van Stroe and L.J.J. Janssen

Department of Instrumental Analysis, Faculty of Chemical Engineering, Eindhoven University of Technology, P.O. Box 513, 5600 MB Eindhoven (Netherlands)

(Received 18th November 1992; revised manuscript received 5th February 1993)

Abstract

An accurate and rapid method for determining the diffusion coefficients of electrochemically active gases in electrolytes is described. The technique is based on chronoamperometry where transient currents are measured and interpreted with a Cottrell-related equation. The diffusion coefficients of oxygen were determined for NaCl solutions varying from 0.085 to 0.846 M within the temperature range 20–40°C. A relationship for the diffusion coefficient of oxygen as a function of temperature is given for the several NaCl concentrations.

Keywords: Amperometry; Sensors; Chronoamperometry; Diffusion coefficient; Oxygen; Transient pulse technique

The diffusivity of oxygen as a function of the NaCl concentration and temperature is of great importance for chemical engineers in the design of oxygen measurement devices, especially in physiological and medical studies. This holds in particular for oxygen sensors built in accordance with the Clark principle [1]. NaCl solution in a Clark cell is used as a reference electrolyte, which is separated from the test solution by a membrane. The oxygen concentration in the NaCl solution is in equilibrium with the concentration in the test solution. If in such a device a reducing potential step is applied and the corresponding transient current is followed, it is possible to measure the oxygen concentration by knowing the diffusion coefficient of oxygen in the NaCl solution at that specific temperature. It is for this reason that the diffusion coefficient has to be determined in NaCl solutions with a known oxy-

gen concentration, using a convenient and accurate method.

Electrochemical methods that make use of data obtained from the measurement of the diffusion-controlled current are the most reliable. A valuable equation in this instance is the Cottrell equation [2], which requires a knowledge of the solubility of gases in electrolytes. The solubility of oxygen in NaCl solutions is well known as a function of temperature [3–5].

The purpose of this work was to develop a rapid method for measuring oxygen diffusion coefficients in electrolyte solutions with a simple, commercially available disc electrode. The methodology is general and can be extended to gases other than oxygen.

THEORY

When an electrochemical system is taken from its equilibrium position into the transport-controlled region by means of an applied potential

Correspondence to: A.J. van Stroe, Department of Instrumental Analysis, Faculty of Engineering, Eindhoven University of Technology, P.O. Box 513, 5600 MB Eindhoven (Netherlands).

step (potentiostatic condition) and the current variation with time is observed, it is known that the electrochemical system shows time-dependent characteristics. The applied potential in this instance has to be sufficiently high to achieve a surface concentration of the electro-active species of virtually zero. We consider the general reaction $\text{Ox} + n e^- \rightarrow \text{Red}$.

For a flat surface electrode (e.g., a platinum disc) in an unstirred solution, the diffusion is initially linear and essentially one-dimensional. This holds true as long as the extension of the concentration gradient is small compared with the diameter of the electrode surface. This linear diffusion can be described mathematically; a rigorous development was given by Kolthoff and Lingane [6]. The diffusion-controlled Faradaic current $[i_F(t)]$ due to the reduction of the electroactive species can be written as

$$i_F(t) = nFA_e C_\infty (D/\pi t)^{1/2} \quad (1)$$

where n = number of electrons involved in the electrode reaction, F = the Faraday (charge on 1 mol of electrons) (C), A_e = electrode area (m^2), D = diffusion coefficient ($\text{m}^2 \text{s}^{-1}$), C_∞ = concentration of the electroactive species in the bulk solution (mol m^{-3}) and t = time (s). This current–time equation of chronoamperometry is known as the Cottrell equation [2]. Its validity was verified in detail by the classical experiments of Laitinen and Kolthoff [7,8].

However, when a potential step is applied, the measured current, i_{tot} , consists of both the Faradaic current (i_F), which is described by the Cottrell equation, and the capacitive current (i_c) [9]:

$$i_{\text{tot}} = i_F + i_c = nFA_e C_\infty (D/\pi t)^{1/2} + (\Delta E/R_s) \exp(-t/R_s C_{\text{dl}}) \quad (2)$$

where ΔE = magnitude of the applied potential step (V), R_s = solution resistance (Ω) and C_{dl} = double-layer capacitance (F). For very small times, just after applying the potential step, the capacitive current predominates over the Faradaic current. As the capacitive current decays exponentially with a time constant ($R_s C_{\text{dl}}$), its contribution will diminish and eventually i_F will prevail.

Because of the non-Faradaic current that flows just after the onset of the potential step and which at the beginning contributes to the total measured current, the current $i_F(t)$ cannot be related to an absolute value of time (t). What is certain are absolute values of $i_F(t)$, measured during a certain time interval (Δt). Therefore, it is necessary to rewrite Eqn. 1 as a function of time:

$$\frac{1}{[i_F(t)]^2} = \frac{\pi}{(nFA_e C_\infty)^2} \times \frac{1}{D} \times t \quad (3)$$

Hence, if the inverse square of $i_F(t)$ is plotted against t , a linear plot is obtained, of which the slope $h = \Delta\{1/[i_F(t)]^2\}/\Delta t$ gives information about the diffusion coefficient of the electroactive species:

$$D = \frac{\Delta t}{\Delta \left\{ \frac{1}{[i_F(t)]^2} \right\}} \times \frac{\pi}{(nFA_e C_\infty)^2} \quad (4)$$

In this way, the diffusion coefficient of oxygen can be determined electrochemically. The same effect is achieved if the slope (h) is plotted against time. By plotting this slope as a function of time, one should obtain a horizontal line, the absolute value of which is proportional to the reciprocal diffusion coefficient of the electroactive species. If this line is not horizontal, this is an indication that another effect is playing an important role (e.g., charging of the electrical double layer, non-uniform distribution of the concentration of electroactive species at the moment of applying the potential pulse, non-linear diffusion and/or convective disruption of the diffusion layer).

EXPERIMENTAL

Instrumentation

A platinum rotating disc electrode (RDE) equipped with a Motomatic E-550-M stirring motor was used as the working electrode for the reduction of oxygen. For these experiments a Wenking POS 73 potentiostat was used, provided with a digital multimeter (Fluke 8600A). Temper-

ature control of the one-compartment cell was effected with a circulation water-bath (Colora NB-32981). For the potential step a Model 3300A function generator (Hewlett-Packard) was used. The current was measured instantly with the pulse application, therefore the measurement had to be made with a storage oscilloscope or another fast recording device. A Tekronix Type 2430A storage digital oscilloscope was used to record the transient currents. The resulting signal was available for display/printing and computation via a connector (IEEE) on the back of the chassis.

Procedures

For these experiments a three-electrode system was used in an electrolysis cell (glass vessel) with a capacity of 160 cm³. A polished platinum disc electrode (RDE) was used as the working electrode ($A_e = 0.5013 \times 10^{-4}$ m²), together with a platinum counter electrode with a surface area of 5×10^{-4} m² and a saturated calomel reference electrode (SCE) with Luggin capillary. A circulating water-bath was used to keep the temperature constant ($\pm 0.1^\circ\text{C}$). The solutions were prepared in distilled, demineralized water with the purest commercially available sodium chloride (Pro Analysi grade) purchased from Merck. Seven solutions were prepared, varying in NaCl concentration from 0.085 to 0.846 M and with a pH between 6.6 and 6.8. The NaCl solutions were saturated with oxygen (purchased from Hoek Loos, Netherlands) for at least 30 min at the prevailing atmospheric pressure. This was accomplished by bubbling the oxygen through the vessel before measurement and by guiding the gas above the electrolyte solution during the measurement. The solution was allowed to become quiescent for a period of at least 1 min before pulsation. The potential was stepped from +300 to -690 mV (vs. SCE). In this way the potential was changed from a value where no Faradaic processes occur to a value where diffusion is the sole mechanism of mass transport of oxygen to the electrode surface.

This procedure consisted in applying a very brief single-potential pulse (1 s at -690 mV), measurement of the response current and evaluation of the data. Before a duplicate measurement

was made, the working electrode was rotated with a rotation speed of at least 40 s⁻¹ to obtain reproducible results. Owing to the force convection of this rotation, the oxygen concentration near the electrode was equilibrated and at the same time the reaction products were dissipated.

RESULTS AND DISCUSSION

By working out the measured transient currents as described in the theory, is it possible to determine the diffusion coefficients, but first all the parameters needed in order to apply Eqn. 3 must be known. An important factor needed for using this equation is the number of electrons (n) involved in the reduction of oxygen. A bipotentiostat (Type Bi-pad) from Tacussel was used together with a rotating ring disc electrode (RRDE) in separate experiments to determine the number of electrons needed for the reduction of oxygen. It was found that $n = 3.94$.

Equation 3 requires also the solubility of the electroactive species in the electrolyte. For the solubility of oxygen in NaCl solutions, the following equation is used [3]:

$$10^3\alpha = \exp\left\{\left(-7.424 + \frac{4417}{T} - 2.927 \ln T + 4.238 \times 10^{-2}T\right) - [m_{\text{Cl}}]\left(-0.1288 + \frac{53.44}{T} - 4.442 \times 10^{-2} \ln T + 7.145 \times 10^{-4}\right)\right\} \quad (5)$$

where α = Bunsen absorption coefficient, i.e., the volume of gas ($T = 0^\circ\text{C}$ and 760 Torr) dissolved in a volume of the solvent when the partial pressure of the gas is 760 Torr [10], $[m_{\text{Cl}}]$ = amount of chloride in grams per 1000 g of solution and T = temperature (K). It gives the dependence of oxygen solubility on temperature and salt concentration. The coefficients for this equation are based on measurements for $273.16 \leq T$ (K) ≤ 308.16 and $0 \leq [m_{\text{Cl}}] \leq 3\%$ and agree to better than $\pm 1\%$ with values from the literature [4,5].

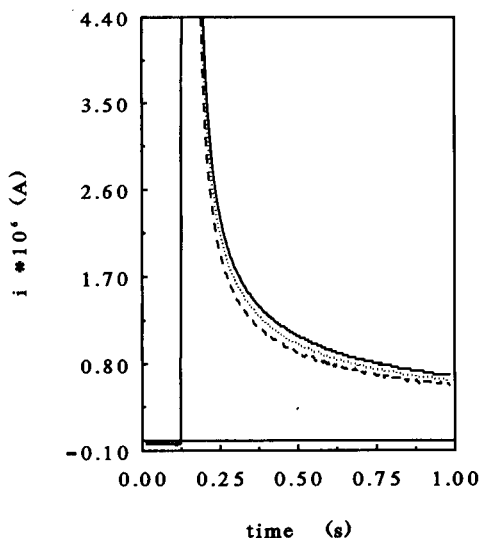


Fig. 1. Transient curves in 0.154 M NaCl solution for various temperatures (solid line, 20°C; dotted line, 30°C; dashed line, 40°C). A potential step of +300 to -690 mV vs. SCE is applied to the cathode (RDE). The initial spike at the onset of the pulse is a charging effect at the cathode surface; the remainder of the trace is a result of the reduction of oxygen.

Figure 1 shows some measured transient curves in a 0.154 M NaCl solution (physiological salt concentration) for various temperatures. In Figure 2 the inverse square of $i_F(t)$ is plotted against time. This plot is linear, so its derivative plotted as a function of time (Fig. 3) is horizontal. In Fig. 3 time zero corresponds to the beginning of the potential step ($t = 0.125$ in Figs. 1 and 2). The advantage of plotting the differential quotient of Eqn 2 as a function of time lies in the fact that sometimes the slope of $1/[i_F(t)]^2$ vs. t looks almost straight, but will not give a horizontal line if the derivative of the plot is plotted. In this instance the measured current is being perturbed by other factors, e.g., changing properties of the electrode and/or convective interference. The experimental diffusion coefficients for oxygen (D_{O_2}) in NaCl solutions as a function of temperature over the concentration range 0.085–0.846 M are given in Table 1. These values are compared with the diffusion coefficient of oxygen in pure water. Unfortunately, literature values of the oxygen diffusion coefficient vary considerably even under the same conditions. For example, at 25°C,

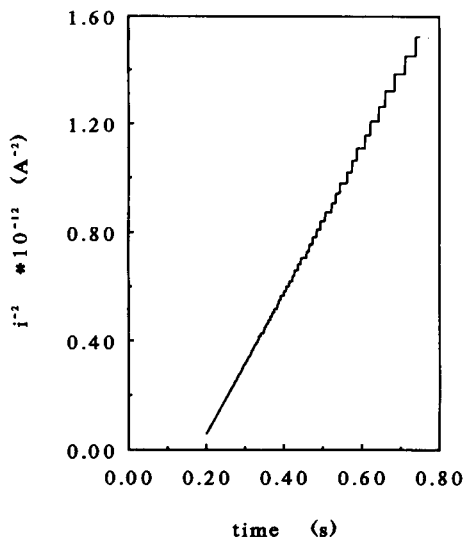


Fig. 2. Plot of $1/[i_F(t)]^2$ versus time for 0.154 M NaCl solution at 20°C.

its values range from 1.87×10^{-9} to 2.60×10^{-9} $m^2 s^{-1}$ [11]. Despite this, the tabulated values show close agreement with the values reported by Ferrel and Himmelblau [12].

For all NaCl concentrations, D_{O_2} increases as a function of temperature. Maintaining the temperature constant is very important as the solubility of oxygen is strongly influenced by it. A fluctuation of ± 0.5 K will give an average deviation of

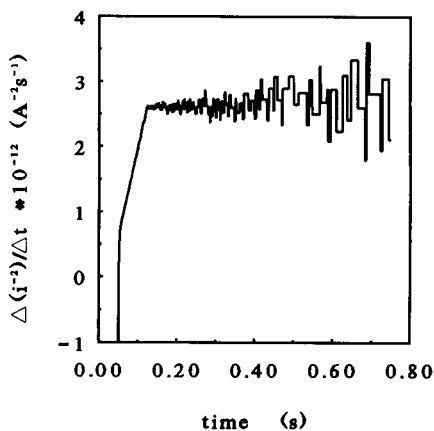


Fig. 3. The derivative of Fig. 2: plot of $\Delta\{1/[i_F(t)]^2\}/\Delta t$ versus time for 0.154 M NaCl solution at 20°C and with $\Delta t = 0.1$.

$\pm 0.8\%$ in oxygen concentration in this specific temperature range, which will give a deviation in D_{O_2} of $\pm 1.6\%$.

In general, the presence of ions results in a decrease in D_{O_2} . However, in the study presented here, this effect of increasing the NaCl concentration in the range 0.085–0.846 M on D_{O_2} is negligible. These results are inconsistent with the results reported by Ju and Ho [13]. They determined the diffusion coefficient for oxygen with steady-state concentration measurements of dissolved oxygen with a commercially available polarographic oxygen electrode, where they found a rapid decrease in the D_{O_2} values for the same NaCl concentration range. On the other hand, in better agreement with our measurements is the work of Akita [14]. He predicted with an empirical relationship, for which the diffusion in pure water and the densities of the solutions must be known, only a slight decrease in the diffusivity of oxygen as a function of NaCl concentration.

According to the Eyring theory of rate processes [15], the temperature variation of D_{O_2} can be expressed in the form

$$D_{O_2} = A_2 \exp(-E_a/RT) \quad (6)$$

where A_2 is a constant [frequency factor ($m^2 s^{-1}$)], E_a is the activation energy ($J mol^{-1}$) for the diffusion process and R is the gas constant ($J mol^{-1} K^{-1}$). By taking the natural logarithm of D_{O_2} and plotting it against $1/T$, for each NaCl concentration an Arrhenius plot (Fig. 4) is ob-

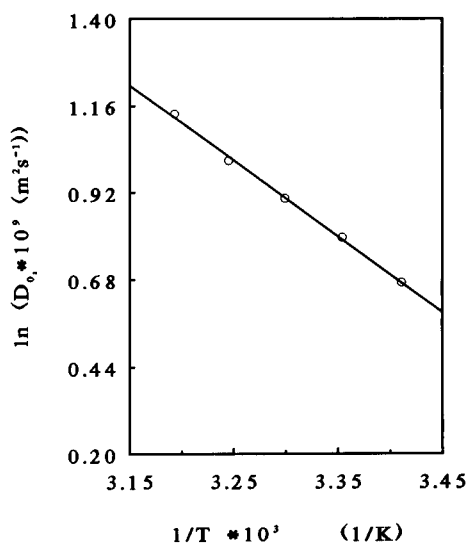


Fig. 4. Arrhenius plot for 0.154 M NaCl solution. The calculated diffusion coefficients give a straight line for the Arrhenius plot, showing a good fit to Eqn. 6.

tained. These Arrhenius plots give straight lines with a slope of $-E_a/R$ and an intercept of $\ln A_2$. Equation 6 proves to be a good fit to the values in Table 1, as shown in Fig. 4. The value of E_a for the various NaCl concentrations could be calculated accurately using this Arrhenius plot. The activation energy seemed to be independent of the NaCl concentration in the observed range of 0.085–0.846 M NaCl (Fig. 5). For E_a an average value of $1.79 \times 10^4 J mol^{-1}$ was found with a relative standard deviation of 3.8%. However, the intercept ($\ln A_2$) is greatly dependent on the devi-

TABLE 1

Measured diffusion coefficients for oxygen ($10^{-9} m s^{-1}$) as a function of temperature and NaCl concentration

Temperature (°C)	NaCl concentration (M)							
	0.0 ^a (0.0) ^{a,b}	0.0846 (3) ^b	0.154 (5.46) ^b	0.282 (10) ^b	0.4231 (15) ^b	0.5642 (20) ^b	0.7052 (25) ^b	0.8463 (30) ^b
20	1.98 ^a	1.94	1.96	1.95	1.93	1.91	1.96	1.97
25	2.26 ^a	2.20	2.22	2.21	2.12	2.17	2.25	2.24
30	2.56 ^a	2.5	2.47	2.48	2.38	2.47	2.55	2.51
35	2.90 ^a	2.80	2.74	2.71	2.69	2.78	2.88	2.81
40	3.26 ^a	3.15	3.12	3.14	3.00	3.12	3.23	3.13

^a Values for D_{O_2} in pure water according to Ferrel and Himmelblau [12]. ^b Values in parentheses are $[m_{Cl}]$ = amount of chloride in grams per 1000 g of solution (Eqn. 5).

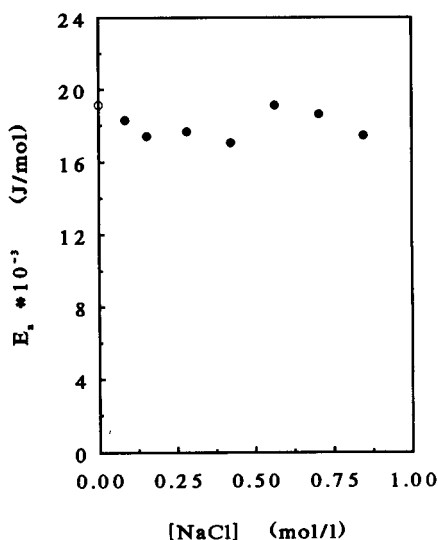


Fig. 5. Activation energy as a function of NaCl concentration. ● = This work; ○ = from [12].

ation of the fitted slope of the Arrhenius plot, and so in this way it is not possible to determine A_2 with high precision. For example, if the estimated value of the activation energy varies by 4%, the predicted value of the frequency factor can vary by ca. 30%. Because of this sensitivity of A_2 to the value of the E_a in the Arrhenius plot, secondary plots were made of D_{O_2} as a function

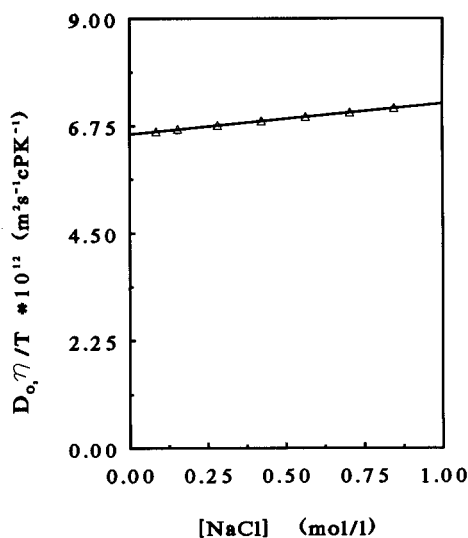


Fig. 6. Plot of $D_{O_2} \eta / T$ versus NaCl concentration.

of $\exp(-E_a/RT)$ while using the average E_a calculated from the primary Arrhenius plot. This was carried out for the various NaCl concentrations and straight lines were obtained with a slope of A_2 . The pre-exponential factor also seemed to be independent of the NaCl concentration in the observed range. For A_2 an average value of $3.051 \times 10^{-6} \text{ m}^2 \text{ s}^{-1}$ could be calculated with a relative standard deviation of 4.96%.

Because of the agreement between Eqn. 6 and the experimentally determined temperature dependence of the diffusivity for all NaCl concentrations, the possibility of interpreting D_{O_2} in terms of temperature-independent properties was examined. This was carried out with a Stokes–Einstein type of relationship, where $D_{O_2} \eta / T$ is constant over a certain temperature range [16] [η is the viscosity of the solution (cP)]. Within the NaCl concentration range 0.085–0.846 M, $D_{O_2} \eta / T$ is independent of temperature for the present system and thus in agreement with the Stokes–Einstein relationship. $D_{O_2} \eta / T$ seems to increase slightly and linearly as a function of NaCl concentration (Fig. 6) within this concentration range.

It is concluded that the method presented is very rapid and simple in terms of operation and precision.

This work was supported by StiPT (Stimulating Project Team Technology Policy), Ministry of Economic Affairs, Netherlands, project number MTR 90039.

REFERENCES

- 1 L.C. Clark, US Pat., 2913 386 (1959).
- 2 A. Cottrell, Z. Phys. Chem., 42 (1947) 365.
- 3 E.J. Green and D.E. Carrit, J. Mar. Res., 25 (1967) 140.
- 4 J.H. Carpenter, Limnol. Oceanogr., 11 (1966) 264.
- 5 W. Gilbert, W. Pawley and K. Park, Carpenter's Oxygen Solubility Tables and Nomograph for Sea-Water as a Function of Temperature and Salinity, Data Report No. 29, U.S. Office of Naval Research, 1968.
- 6 I.M. Kolthoff and J.L. Lingane, Polarography, Interscience, New York, 1952.
- 7 H.A. Laitinen and I.M. Kolthoff, J. Am. Chem. Soc., 62 (1939) 3344.
- 8 H.A. Laitinen, Trans. Electrochem. Soc., 82 (1924) 289.

- 9 A.J. Bard and L.R. Faulkner, *Electrochemical Methods: Fundamentals and Applications*, Wiley, New York, 1980.
- 10 S. Glasstone, *Thermodynamics for Chemists*, Van Nostrand, New York, 1947.
- 11 D.M. Himmelblau, *Chem. Rev.*, 64 (1964) 527.
- 12 R.T. Ferrel and D.M. Himmelblau, *J. Chem. Eng. Data*, 12 (1967) 111.
- 13 L.K. Ju and C.S. Ho, *Biotechnol. Bioeng.*, 27 (1985) 1495.
- 14 K. Akita, *Ind. Eng. Chem. Fundam.*, 20 (1981) 89.
- 15 S. Glasstone, K.J. Laidler and H. Eyring, *The Theory of Rate Processes*, McGraw-Hill, New York, 1941.
- 16 C.R. Wilke, *Chem. Eng. Prog.*, 49 (1949) 218.

Ion-selective electrode potentiometric studies on the complexation of copper(II) by soil-derived humic and fulvic acids

Raewyn M. Town and H. Kipton J. Powell

Department of Chemistry, University of Canterbury, Private Bag, Christchurch (New Zealand)

(Received 18th September 1992; revised manuscript received 18th January 1993)

Abstract

Ion-selective electrode potentiometry was used to probe the Cu(II) complexation capacity of soil-derived humic acids (HAs) and fulvic acids (FAs) at pH 5.0, 6.3, and 7.0. The relative stabilities of these complexes at pH 2.5–7.5 were determined. For FAs at pH 5.0, 6.3 and 7.0, complexation capacity measurements indicated that 15–18%, 28–33% and 40–50% of carboxyl groups, respectively, may be involved in strong Cu(II) binding (assuming bidentate coordination). For HAs the proportions were 21–27%, 57–67% and 75–95%, respectively, indicating a more “efficient” distribution of the fewer chelating moieties. Normalized to carboxyl content, HAs were a much stronger Cu(II) complexant than FAs. Also, the colloidal/particulate HA molecules were stronger complexants than were the smaller (soluble) HA moieties. The apparent stability of Cu(II)–humic complexes decreased with increasing metal-to-ligand ratio and with increasing ionic strength. The presence of other weakly complexing metal ions, such as Mg(II), at relatively high concentrations inhibited Cu(II) complexation; Al(III) was bound in preference to copper(II) in the pH range 3.5–5.5. By comparison with binding by discrete ligands, aliphatic carboxyl moieties, e.g., malonate and citrate, were established as appropriate models for humic substance chelating groups; salicylate and phthalate complexed Cu(II) far too weakly to be considered as significant complexants in weakly acidic to near-neutral solutions.

Keywords: Ion selective electrodes; Potentiometry; Complexation; Copper; Fulvic acids; Humic acids; Soils

Most models for metal complexation by humic substances involve the calculation of conditional stability constants by least-squares fitting at one pH (e.g., [1,2]). Interpretation of data over a pH range is difficult. Indeed, the effects of pH and ionic strength on the extent of complexation of a single metal ion cannot be quantitatively described and multi-metal binding cannot be modelled at all [3].

Correspondence to: R.M. Town, Department of Analytical Chemistry, University of Geneva, Sciences II, 30 Quai E.-Ansermet, CH-1211 Geneva 4 (Switzerland) (present address).

Further, it is not certain whether 1:1 and 1:2 metal-to-ligand complexes are formed. The assumption that both species are formed may improve the least-squares fit for the humic substance data [4], but other models postulating multiple sites or site interactions and only 1:1 stoichiometry may fit the data equally well [5].

Metal complexation by humic substances may involve donor groups other than those which deprotonate at lowest pH (as assumed by Young and Bache [6]), or which are numerically dominant (as assumed by Murray and Linder [7]). Further, the presence of different functional

groups in humic substances with different protonation constants means that the coordination mode will vary with pH, ionic strength and metal-to-ligand ratio [3]. The variation of the conditional stability constant with metal-to-ligand ratio has been cited as evidence for two types of binding sites in humic substances [8–11]. This may be erroneous; there may in fact be an almost infinite spectrum.

In addition to “simple” complexation, other reactions may occur. For example, formation of colloidal precipitates, aggregation and adsorption on other colloidal matter and formation of mixed ligand complexes have been proposed for the water-soluble fulvic acid fraction [4,11,12].

Many of the attempts to model metal binding properties of humic substances have not accommodated the inherent complexity of these heterogeneous macromolecules. For humic substances neither the free ligand concentration, the nature of the binding sites nor their respective protonation constants are known. Therefore, quantitative analysis of metal ion–humic equilibria is inappropriate. Our approach to understanding the nature and strength of donor sites in humic substances involves direct comparison of experimental complexation curves with those measured or calculated for finite mixtures of model ligands [13,14]. In contrast to studies involving variation of metal concentration at constant pH, we varied the pH and interpreted the change in coordination site with pH.

EXPERIMENTAL

Standard solutions

Water purified using a Milli-Q system (Millipore) (resistance 18 M Ω) was used to prepare all solutions.

A stock standard Cu(II) solution was prepared by dissolution of $\text{Cu}(\text{NO}_3)_2 \cdot 3\text{H}_2\text{O}$ (BDH, AnalaR) in 8.96×10^{-4} mol l $^{-1}$ HCl. Its concentration (0.1036 mol l $^{-1}$) was determined gravimetrically as the benzoin- α -oximate and electrolytically by deposition on a platinum cathode [15]. Working standard Cu(II) solutions (10^{-2} – 10^{-6} mol l $^{-1}$) were prepared by accurate dilution

of the stock standard solution with 0.10 mol l $^{-1}$ KNO_3 (pH 4).

Stock standard HNO_3 solutions (ca. 1 mol l $^{-1}$) were prepared by dilution of concentrated HNO_3 (BDH, AnalaR) and were standardized by titration against weighed amounts of Tris (Fluka, puriss p.a.).

KOH (BDH, AnalaR) solutions were prepared in carbonate free Milli-Q-purified water.

A stock standard solution of KNO_3 (1.00 mol l $^{-1}$) was prepared by dissolution of the appropriate weight of this dried salt (Riedel-de Haën, für Analyse).

Humic substances

Fulvic acid (FA) was the sample FA4, extracted from International Humic Substances Society (IHSS) peat by the acid pyrophosphate–XAD-7 method [16]. The ash content was 0.2%; the carboxyl equivalent weight (the weight per mole of titratable carboxyl acidity) was 139. FA solutions were prepared by dissolving the appropriate weight in Milli-Q-purified water.

Humic acid (HA) was the IHSS reference soil Summit Hill humic acid. The ash content was 1.15%; the carboxyl equivalent weight was 287. To effect complete dissolution, the HA was initially “predissolved” in ca. 0.8 mol l $^{-1}$ KOH, allowed to stand for ca. 1 h, then diluted to the appropriate volume and the pH adjusted to ca. 7 by addition of Aristar HNO_3 . The solution resulting after membrane filtration (0.025 μm) of the pH 7 solution is referred to as “filtered HA”.

Electrodes

Each electrode pair was connected to a Radiometer PHM 64 pH meter. Calomel electrodes (Radiometer K401) were encased in glass jackets containing 0.10 mol l $^{-1}$ KNO_3 (Vycor junction) to minimize chloride interference on the copper ion-selective electrode (ISE). The pH was measured with a glass (Beckman)–calomel electrode pair.

The concentration of free Cu(II) was measured with a Radiometer Selectrode–calomel electrode pair. The ion-selective electrode (ISE) was conditioned for 12 h in 0.1 mol l $^{-1}$ EDTA after application of electroactive Cu(II) Selec-

trode powder (S42015). When not in use the ISE was stored in Milli-Q-purified water. Experiments were performed under constant light conditions because a Cu(II) ISE is photosensitive [17].

Copper(II) titrations

Titrations were performed in a double-walled Pyrex cell (capacity 60–100 ml) fitted with an air-tight lid containing ground-glass Quickfit entry ports for insertion of electrodes, a nitrogen bubbler and burette tips.

Gilmont micrometer syringes fitted with 2.5-ml glass burette tips were used to dispense alkali, acid and metal titrants.

Initial oxygen removal from the test solutions was effected by purging for 30 min with oxygen-free nitrogen (saturated with water vapour at 25°C); during each titration a positive nitrogen pressure was maintained over the solution.

Before and after every titration the glass-calomel electrode pair was standardized against three NBS buffers, viz., 0.05 molal potassium hydrogenphthalate ($\text{pH}_{\text{NBS}} = 4.006$), 0.025 molal disodium hydrogenphosphate–0.025 molal potassium dihydrogenorthophosphate ($\text{pH}_{\text{NBS}} = 6.863$) and 0.01 molal sodium tetraborate decahydrate ($\text{pH}_{\text{NBS}} = 9.180$).

Cu(II) binding as a function of metal:ligand ratio, “the complexation capacity (*CC*) curve”, was measured by incremental addition of standard Cu(II) solutions to humic substance solutions (0.017 mg ml^{-1}) at pH 5.0, 6.3 and 7.0 ($I = 0.10 \text{ mol l}^{-1} \text{ KNO}_3$) to generate total Cu(II) concentrations in the range $0.0\text{--}1.5 \times 10^{-4} \text{ mol l}^{-1}$. At each datum point pCu was determined and the total “free” (non-complexed) metal concentration was calculated: $[\text{free metal}] = [\text{Cu(II)}] + [\text{Cu(OH)}^+] (\log *K = -7.71) + [\text{Cu}^2(\text{OH})_2^{2+}] (\log *\beta = -10.99)$ [18]. The pH was maintained constant by addition of standard KOH to neutralize protons released in the coordination reaction and those added via the acidic Cu(II) solution. From an inflection in the plot of free metal versus total added metal, followed by a linear portion with slope approximately equal to 1.0, it was inferred that the *CC* had been reached. The *CC* was obtained by extrapolation of the linear

portion of the curve to the abscissa. Titration of discrete ligands, such as citrate, established the validity of this technique (as opposed to use of the intersection of the tangents of the “two linear sections of the graph” [19]). At least two separate titrations were performed for each humic substance sample at each pH.

At the end of each titration, the solution was back-titrated with standard HNO_3 (to pH 2.5–2.8); the ISE was then calibrated in situ by addition of aliquots of standard Cu(II). Separate titrations using Cu(II)–citrate buffers had established linearity in the range pCu 2–7.5.

Metal binding as a function of pH, the “metal binding curve”, was determined by titrating an acidic Cu(II)–humic substance solution ($I = 0.10 \text{ mol l}^{-1} \text{ KNO}_3$) with standard KOH in the pH range 2.5–7.5. pCu was determined at each datum point and the total free metal concentration was calculated. The weight of humic substance used was such as to give a carboxyl group concentration of $1.8 \times 10^{-4} \text{ mol l}^{-1}$ (unless stated otherwise). Thus, for a 1:4.5 metal-to-ligand (COOH) ratio the concentration of Cu(II) used was $4.0 \times 10^{-5} \text{ mol l}^{-1}$, whereas for a 1:20 ratio it was $9.0 \times 10^{-6} \text{ mol l}^{-1}$.

Simulation of binding curves

Metal binding as a function of pH and of metal-to-ligand ratio at fixed pH was calculated for model ligands using FORTRAN computer programs. These programs calculated the percentage of each species present at each pH, or each total Cu(II) concentration, from the metal–ligand stoichiometry and the known protonation constants. Stability constants measured at 25°C and $I = 0.1 \text{ mol l}^{-1}$ were chosen whenever possible [20].

Experimental determination of the binding curves for model ligands for which disparate equilibrium models have been published indicated that the equilibrium Cu(II) binding model for citrate proposed by Ramamoorthy et al. [21] provided a better fit to the experimental data than that of Field et al. [22], whereas for tartrate the model of Bottari et al. [23] was superior to that of Rajan and Martell [24]. The calculated “free

Cu(II) concentration” included hydrolysis products (see above).

RESULTS

Calibration of the Cu(II) ion-selective electrode

The Nernstian slope of the Cu(II) ISE in the presence of humic and fulvic acids was 30.2 mV, in good agreement with the theoretical value of 29.6 mV. Although this slope remained constant during the course of this work, a continual small drift in the intercept of the plot of e.m.f. versus pCu (to more positive e.m.f. values) was observed. Although it is reported that humic substances are not significantly adsorbed on ISEs [4], the electrode calibration was performed in the presence of ligand at pCu \approx 3.5, 4.0 and 5.0 at pH 2.5–2.8 after each ISE titration (measurable complexation of Cu(II) occurs at pH > 3.0).

The apparent concentration of free Cu(II) was enhanced if the ISE was calibrated at pH < 2.5. In this pH region the electrode also responds to hydrogen ions [25].

Copper(II) complexation capacity curves

Typical CC curves for HA at pH 5.0 and 7.0 are shown in Fig. 1; the linear portion of these curves was established to 1.6×10^{-4} mol l⁻¹

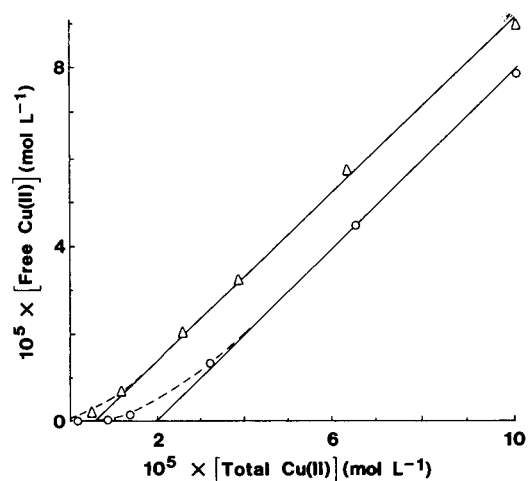


Fig. 1. Complexation capacity curves for humic acid determined by Cu(II) ISE at (Δ) pH 5.0 and (\circ) pH 7.0. Humic acid = 17.0 mg l⁻¹; $I = 0.10$ mol l⁻¹ KNO₃.

Cu(II). Similar curves were obtained for FA (not shown).

The Cu(II) CC of FA at pH 5.0 (expressed per mg FA) was not altered by a threefold change in the concentration of FA, nor by an increase in ionic strength from 0.10 to 0.60 mol l⁻¹ KNO₃.

Assuming bidentate coordination (i.e., two carboxyl groups in each polydentate coordination site, as in citrate and malonate) then, for FA at pH 5.0, 6.3 and 7.0, the CC was equivalent to ca. 15–18%, 28–33% and 40–50% of carboxyl groups involved in complexation, respectively. For HA (either unfiltered or filtered in alkaline solution) the proportions were 21–27%, 57–67% and 75–95%, respectively. The correction for Cu(II) hydrolysis was very large at pH 7.0, hence these data are less precise, although stable e.m.f. readings were obtained. It is probable that a metastable system existed. The “free Cu(II) concentration” was greater than that predicted from the solubility quotient for Cu(OH)₂, which Ganelina [26] reported as $10^{-19.36}$ mol³ l⁻³.

For HA suspended in solution at pH 5.0 (and not filtered), the CC was the same as that for HA predissolved in KOH. In contrast, for an HA solution prepared and then filtered (0.025 μ m) at pH 5.0, but adjusted to the same final carboxyl group concentration, the CC was 2.5 times less than that of the whole sample on the basis of carboxyl groups involved in complexing at pH 5.0 and on the basis of the weight of material present.

Copper(II) binding curves

Plots of percentage of free Cu(II) versus pH at fixed Cu(II)-to-ligand (COOH) ratios $\{[\text{Cu(II)}] = 4.0 \times 10^{-5}$ and 9.0×10^{-6} mol l^{-1} $\}$ were constructed for FA and HA (Fig. 2). Figure 2 includes the binding curve for HA measured at the same concentration by weight (mg ml⁻¹) as for FA $\{[\text{Cu(II)}] = 4.0 \times 10^{-5}$ mol l^{-1} $\}$. Also shown is the boundary calculated for precipitation of Cu(OH)₂ from a solution containing Cu(II) and its hydrolysis products.}}

Binding of HA to Cu(II) was measured as a function of pH using unfiltered HA and filtered HA (for which 0.025- μ m filtration was effected at pH 12 or 5.0). The binding curves for the whole

sample and that filtered at alkaline pH were the same, whereas that for the pH 5.0 filtrate was displaced to higher pH (weaker binding): by 0.19 at 50% free Cu (d_{50}) and 0.33 pH at d_{10} .

Comparison of the binding curves for HA with those for FA indicated that the binding strength of these substances is similar on a weight (mg ml⁻¹) basis (FA, [COOH] = 1.8×10^{-4} mol l⁻¹; HA, [COOH] = 8.5×10^{-5} mol l⁻¹). Thus, at the same carboxyl group concentration the HA curves were displaced markedly to lower pH, indicating stronger binding. For a 1:4.5 Cu(II)-to-COOH ratio $\{[Cu(II)] = 4.0 \times 10^{-5}$ mol l^{-1} the pH displacement between the HA and FA curves was 0.53 at d_{50} and 0.63 at d_{10} ; for a 1:20 ratio $\{[Cu(II)] = 9.0 \times 10^{-6}$ mol l^{-1} the displacement was 0.65 and 1.0, respectively.}}

Effect of competing ions on Cu(II) binding curves

In 0.60 mol l⁻¹ K(I), the Cu(II) binding curve for FA (●, 1:20 ratio) was displaced to higher pH (weaker binding) relative to 0.10 mol l⁻¹ K(I) (○) (Fig. 3). The displacement was 0.25 at d_{50} and 0.50 at d_{10} . For an HA binding curve (at the same concentration by weight as FA) the pH displacement

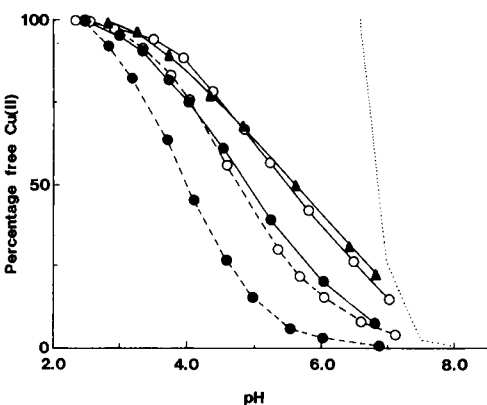


Fig. 2. Copper (II) binding curves for (●) humic acid and (○) fulvic acid at fixed Cu(II)-to-ligand (COOH) ratios. [Ligand-COOH] = 1.8×10^{-4} mol l⁻¹; [Cu(II)] = (solid lines) 4.0×10^{-5} or (dashed lines) 9.0×10^{-6} mol l⁻¹; $I = 0.10$ mol l⁻¹ KNO₃. The curve (▲ —▲) is for humic acid at the same concentration by weight (mg l⁻¹) as fulvic acid; [Cu(II)] = 4.0×10^{-5} mol l⁻¹. Dotted line, boundary calculated for Cu(OH)₂ precipitation.

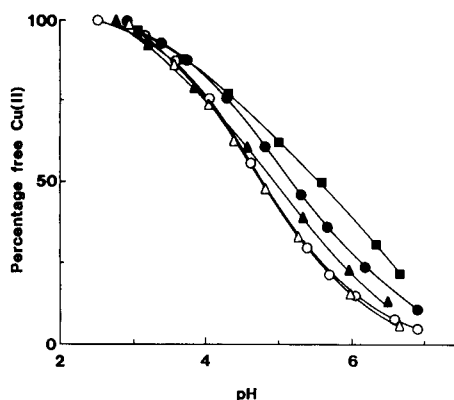


Fig. 3. Copper(II) binding curves for humic and fulvic acids showing the effect of Mg(II) and K(I). [Ligand-COOH] = 1.8×10^{-4} mol l⁻¹ (except Δ); [Cu(II)] = 9.0×10^{-6} mol l⁻¹. Fulvic acid in (○) 0.10 mol l⁻¹ KNO₃, (●) 0.60 mol l⁻¹ KNO₃ and (■) 0.06 mol l⁻¹ Mg(II). (▲) Humic acid in 0.60 mol l⁻¹ KNO₃ and (Δ) humic acid at the same weight concentration as FA, [COOH] = 8.7×10^{-5} mol l⁻¹, in 0.10 mol l⁻¹ KNO₃.

ment was less, being 0.0 at pH 4.0, 0.19 at d_{50} and 0.38 at d_{10} [0.10 mol l⁻¹ K(I), curve not shown].

The binding curve for FA at a 1:20 ratio was measured in the presence of 0.06 mol l⁻¹ Mg(II) (a concentration equivalent to the sum of divalent ions in sea water). The curve (■) was displaced significantly to higher pH, by 0.38 at d_{50} and 1.0 at d_{10} (Fig. 3).

Binding curves for FA at a 1:4.5 ratio $\{[COOH] = 1.8 \times 10^{-4}$ mol l⁻¹, [Cu(II)] = 4.0×10^{-5} mol l^{-1} were measured in the presence of Al(III) (1.0×10^{-5} and 4.0×10^{-5} mol l⁻¹; added as the nitrate salt). The curves were displaced to higher pH in the pH range 3.5–6.5 (Fig. 4). In the presence of 1.0×10^{-5} mol l⁻¹ Al(III) the pH displacement was 0.25 at d_{50} and 0.38 at d_{10} ; for 4.0×10^{-5} mol l⁻¹ Al(III) the displacement was 0.38 and 0.51, respectively.}

Cu(II) binding curves were calculated in the presence of Al(III) (via the equilibrium program SIAS [27]) for the discrete ligands salicylate and malonate $\{[COOH] = 1.8 \times 10^{-4}$ mol l⁻¹, [Cu(II)] = 4.0×10^{-5} mol l⁻¹, [Al(III)] = 4.0×10^{-5} mol l⁻¹. For malonic acid, Al(III) displaced the Cu(II) binding curve to higher pH, by 0.25 at d_{50} and 0.5 at d_{10} . The species distribution diagram (not shown) indicated that in the pH range

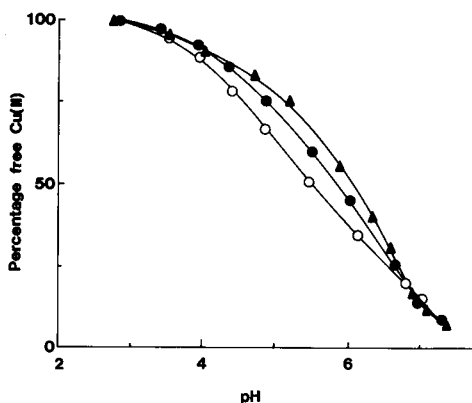


Fig. 4. Effect of Al(III) on Cu(II)–fulvic acid binding curves. [Ligand-COOH] = 1.8×10^{-4} mol l⁻¹; [Cu(II)] = 4.5×10^{-5} mol l⁻¹. [Al(III)] = (○) 0.0, (●) 1.0×10^{-5} and (▲) 4.0×10^{-5} mol l⁻¹.

3.5–6.0 a greater percentage (by 30–35%) of the total Al(III) concentration was complexed by malonate than was Cu(II), but at pH > 6.5, Al(OH)₄⁻ became the predominant Al(III) species, while most of the Cu(II) remained complexed with malonate to pH > 8.0. At a lower ligand concentration ([COOH] = 2.7×10^{-5} mol l⁻¹), but the same Al(III) and Cu(II) concentrations (4.0×10^{-5} mol l⁻¹), Cu(II)–malonate complexation was almost completely suppressed by Al(III) binding to malonate (pH 4.0–5.8), with significant formation occurring only above pH 6.0 [where Al(III) is hydrolysed].

DISCUSSION

Two types of experiments were performed, viz., metal binding curves [plots of percentage of free Cu(II) versus pH] and complexation capacity curves [plots of free Cu(II) versus total added Cu(II)]. In the titrations involving HA a solid phase was present. Precipitation could also occur on complexation of Cu(II) by fulvic acid [28–30].

The curves for FA were compared with those for HA (both unfiltered and 0.025- μ m membrane filtered) on the basis of both the carboxyl group content and the weight of material. For the same

weight concentration of humic substance, the carboxyl group content of HA was approximately half that of FA.

Copper(II) complexation capacity curves

Compared with HA, FA has a lower proportion of carboxyl groups involved in strong bonding with Cu(II) (less than half of the total at pH 7.0 assuming bidentate carboxyl coordination). This is consistent with a high proportion of structurally isolated carboxyl groups (non-chelating moieties), stereochemically inaccessible carboxyl groups or groups that are weak complexants with Cu(II) below pH 7.0 (e.g., salicylate).

For HA the proportion of carboxyl groups involved in strong Cu(II) binding was ca. 1.5 times greater than that for FA at pH 5.0 and ca. 2.0 times greater at pH 6.3 and 7.0. This observation is consistent with HA carboxyl groups having more favourable configuration for Cu(II) complexation than those of FA. It could also be inferred that HA contains a greater proportion of more basic moieties which deprotonate and complex in the higher pH range (e.g., salicylate); alternatively, the HA moieties may undergo some conformational change over this pH range which generates more effective coordination sites [31,32].

On a weight basis, the CC for HA (unfiltered or filtered in alkaline solution) was similar to that for FA, ca. 1.0×10^{-3} and 1.2×10^{-3} mol Cu(II) g⁻¹ humic substance at pH 6.3 and 7.0, respectively. Complexation capacities are reported to be typically 0.3×10^{-3} – 3.0×10^{-3} mol Cu(II) g⁻¹ humic substance [33].

The CC for an HA sample that was filtered in alkaline solution was the same as that for an unfiltered solution. This implies that the moieties that are insoluble at pH 12 do not contribute significantly to the CC [34].

The CC for an HA sample that had been equilibrated then 0.025- μ m membrane filtered at pH 5.0 was less than half that for the unfiltered sample on the basis of both the carboxyl group content and the weight of material present. This indicates that the solid humic acid phase does contribute significantly to the Cu(II) CC under these experimental conditions. At pH 5.0

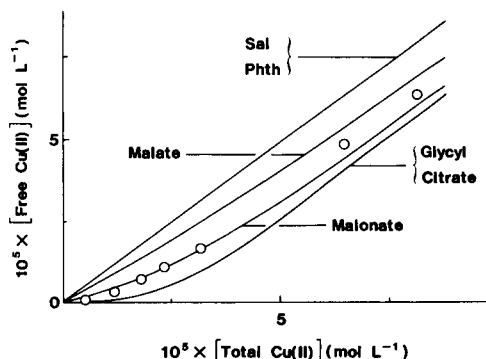


Fig. 5. (○) Complexation capacity curves measured for humic acid by Cu(II) ISE and calculated curves for model ligands; pH = 6.3. For humic acid, $[\text{COOH}] = 5.58 \times 10^{-5} \text{ mol l}^{-1}$; for model ligands, $[\text{ligand}] = 2.47 \times 10^{-5} \text{ mol l}^{-1}$. $I = 0.10 \text{ mol l}^{-1} \text{ KNO}_3$. Sal = salicylic acid; Phth = phthalic acid; Glycyl = glycylaspartic acid.

molecules with lower molecular weight dominate in the soluble fraction [35].

To facilitate comparisons between filtered and unfiltered HA samples, it was assumed that these fractions had the same carboxyl equivalent weight. However, there is evidence that the larger molecules may have a lower carboxylate content [36–38].

Modelling of Cu(II) complexation capacity curves

Previous work [13] established that at pH 5.0 citric acid was a good model for FA CC curves. This was also observed for HA in the present work. The CC curves for humic acid at pH 6.3 ($[\text{COOH}] = 5.58 \times 10^{-5} \text{ mol l}^{-1}$) are compared with those for model ligands in Fig. 5. The total concentration of model ligands used for these simulations ($2.47 \times 10^{-5} \text{ mol l}^{-1}$) was chosen to be equivalent to the measured CC for the humic substance at pH 6.3 ($[\text{COOH}] = \text{CC}$). At this pH the more weakly binding malonic acid is an appropriate model for both the FA (not shown) and HA curves. Although the total carboxyl concentration for the HA and FA solutions was the same in these experiments, the proportion of carboxyl groups involved in complexation was not equivalent (as determined by the CC measurements).

Comparison of Cu(II) binding by humic and fulvic acids

The Cu(II) binding curves for all humic substances were displaced to higher pH (weaker complexing) at the higher Cu(II) concentration ($4.0 \times 10^{-5} \text{ mol l}^{-1}$), indicating the heterogeneity of available chelation sites (Fig. 2).

On the basis of carboxyl group content the binding curves for HA (1:4.5 and 1:20 ratio) were displaced significantly to lower pH compared with those for FA, indicating stronger binding (Fig. 2). This again indicates that the carboxyl groups in HA have more favourable configurations for strong Cu(II) complexation and/or that HA contains functional groups, other than carboxyl, which strongly complex Cu(II).

Compared with the result for unfiltered HA which had been equilibrated at pH 5.0, the binding curve for an HA sample equilibrated and $0.025\text{-}\mu\text{m}$ membrane filtered at this pH (then adjusted to the same weight composition) was displaced to higher pH (not shown). This indicates that the larger HA molecules are stronger complexants for Cu(II) than are those of lower molecular weight. This experimental observation has been predicted theoretically [39].

Reversibility of binding curves

The reversibility of the binding curves was measured at a 1:20 Cu(II)-to-COOH ratio. Addition of HNO_3 to a Cu(II)-FA solution that had stood at pH 7 overnight generated the same binding curve as was obtained for addition of KOH to an acidic solution of Cu(II) and FA.

In contrast, for a Cu(II)-HA solution that had stood at pH 7 overnight, the e.m.f. values obtained for the reverse titration were more positive. At pH 3 the difference was 2.6 mV relative to the original acidic solution; for a solution immediately acidified, the e.m.f. was 1.2 mV more positive. A more positive e.m.f. value indicates a lower free Cu(II) concentration. This result may arise from the formation of non-labile Cu(II)-HA species that do not dissociate on acidification. Many studies on the equilibration of metals with humic acids have indicated that a significant proportion of the metal is not recoverable by acidification or by ligand exchange [40–42]. Very stable

metal species may be associated with solid humic phases [43].

Slowly reacting sites could also explain this phenomenon [44], e.g., Cu(II) complexation by cyclic porphyrin structures [45]. Evidence has been presented for copper(II) porphyrin-type complexes persisting in humic (but not fulvic) acids treated with strong acid [46–48].

Simulation of binding curves

It has been assumed that the functional groups in humic substances which are numerically dominant (salicylate and phthalate) will control metal complexing [7,49]. This is probably erroneous as it has been demonstrated that humic substances complex Cu(II) much more strongly than do these moieties [4,11,17,50]. The binding curves for FA and HA are compared with those for discrete model ligands in Figs. 6 and 7, respectively. The concentration of model ligands used for these simulations was chosen such that their *CC* was equivalent to that for a humic substance solution at pH 6.3. The much weaker complexation by salicylate is clearly demonstrated. Malonate is the best model for FA binding at both metal-to-ligand ratios; however, it provides a poor fit to the data above pH \approx 5 where more basic moieties may then contribute to complexing. This is illustrated by glycylaspartate and 5-methoxy-*N*-(2-hydroxybenzyl)sarcosine (MHBS). For HA, complexation

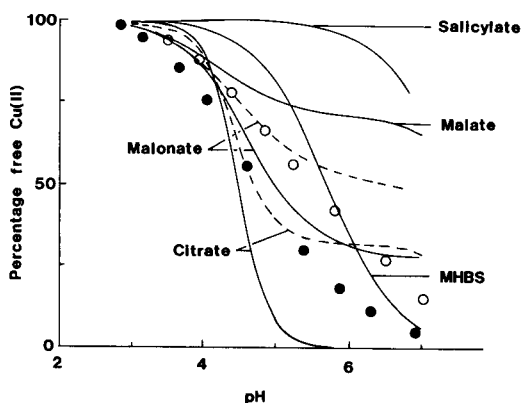


Fig. 6. Copper(II) binding curves for fulvic acid at $[\text{COOH}] = 1.8 \times 10^{-4} \text{ mol l}^{-1}$ and $[\text{Cu(II)}] = (\circ) 4.0 \times 10^{-5}$ and $(\bullet) 9.0 \times 10^{-6} \text{ mol l}^{-1}$. Calculated curves for model ligands at $[\text{ligand-COOH}] = 2.7 \times 10^{-5} \text{ mol l}^{-1}$ (see text) and $[\text{Cu(II)}] = (\text{dashed lines}) 4.0 \times 10^{-5}$ or $(\text{solid lines}) 9.0 \times 10^{-6} \text{ mol l}^{-1}$.

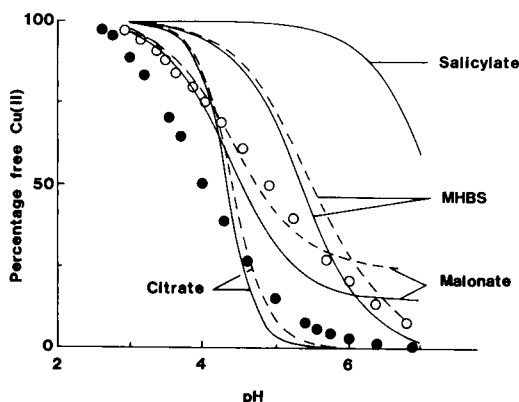


Fig. 7. Copper(II) binding curves for humic acid at $[\text{COOH}] = 1.8 \times 10^{-4} \text{ mol l}^{-1}$ and $[\text{Cu(II)}] = (\circ) 4.0 \times 10^{-5}$ or $(\bullet) 9.0 \times 10^{-6} \text{ mol l}^{-1}$. Calculated curves for model ligands at $[\text{ligand-COOH}] = 5.58 \times 10^{-5} \text{ mol l}^{-1}$ (see text) and $[\text{Cu(II)}] = (\text{dashed lines}) 4.0 \times 10^{-5}$ or $(\text{solid lines}) 9.0 \times 10^{-6} \text{ mol l}^{-1}$.

at $9.0 \times 10^{-6} \text{ mol l}^{-1} \text{ Cu(II)}$ and $\text{pH} < 4.5$ (strongest binding sites utilized) is much stronger than for any of the model ligands considered (Fig. 7). At the higher Cu(II) concentration the HA binding curve is reasonably well modelled by malonate up to $\text{pH} \approx 6$.

The heterogeneous nature of humic substances means that the coordination mode may change with pH and with metal-to-ligand ratio. The observation that different discrete ligands more closely model sections of the humic substance curves at different pH values supports this hypothesis. Hence, a more realistic model would involve several ligand moieties competing for available metal ions.

Models for Cu(II) complexation in which the choice of model ligands was based on the fulvic acid $\text{p}K_a$ spectrum [13,14] have been reported. However, this work has established, on the basis of complexation capacity measurements, that comparison of Cu(II) binding curves for humic substances and model ligands should consider carboxyl group concentrations significantly below the total humic substance carboxyl content. Further, the Cu(II) *CC* of humic substances increased as the pH increased (from ca. 8% of the total carboxyl group concentration at pH 5.0 to 22% at pH 7.0 for FA and from ca. 12% to 42%, respectively, for HA). These factors should be

included in models used to simulate binding curves via mixtures of discrete model ligands.

The ligand model mixture used in this work consisted of citric acid 0.72×10^{-5} , tricarballic acid 1.44×10^{-5} , malic acid 1.44×10^{-5} , salicylic acid 7.20×10^{-5} , acetylacetone 1.60×10^{-5} and MHBS $0.80 \times 10^{-5} \text{ mol l}^{-1}$. The concentration of amino acid moieties was 100% of the typical characterized amino acid content of FAs; this contrasts with 30% assumed in previous work [13,14]. This change in the concentration of nitrogen-containing moieties had a dramatic effect on the calculated curve (the fit to the FA data was greatly improved at $\text{pH} > 5.5$; not shown), indicating the critical role that these chelating groups may have in determining metal coordination by humic substances.

The contribution from “cascade binding” was also considered. The model ligand (L) MHBS (I) was included to illustrate this $\{\log K (\text{Cu} + \text{L} \rightleftharpoons \text{CuL}) = 7.05, \log K (\text{Cu} + \text{L} \rightleftharpoons \text{CuH}_{-1}\text{L} + \text{H}^+) = 3.07$ [51]]. The proximity of a phenolic hydroxyl group (in itself weakly binding) to a strongly coordinating amino acid moiety promotes the formation of a more stable complex (via a six-membered chelate ring). That is, in a humic substance, isolated weakly complexing groups such as phenolic or aliphatic hydroxyl, may contribute to binding, even via less favoured seven- or eight-mem-

bered chelate rings, if the ligand is strongly anchored to the metal via a five- or six-membered chelate ring. Fluorescence quenching measurements support this concept [13,14]. These can be explained by either polydentate fluorescent moieties being involved in Cu(II) complexation, or by the fluorescent centres (predominantly substituted aromatics [52]) being within one or two carbon atoms of the primary binding sites. A structural unit consistent with the latter interpretation is II, where the primary binding site is a “citrate-like” moiety. Cascade binding incorporating the phenolic group may contribute to strong Cu(II) complexation above $\text{pH} 5.5$. Complexing by polycarboxylate ligands is essentially complete below this pH and additional binding at $\text{pH} > 5.5$, as observed for HA and FA, must involve groups with low acidity, such as phenols or amino acid nitrogen.

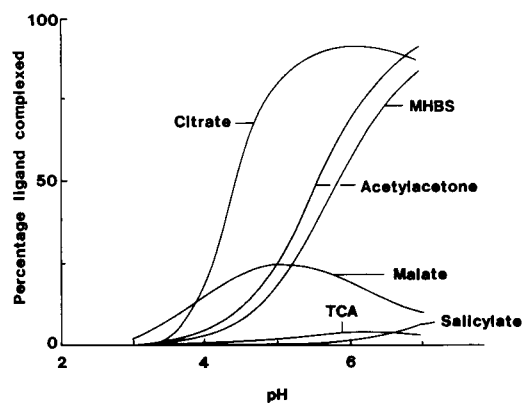
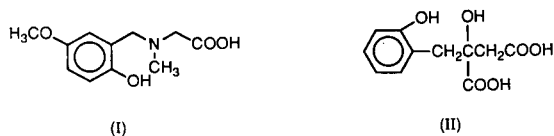


Fig. 8. pH dependence of Cu(II) binding to model ligands in a mixture representing possible chelating moieties in a humic sample [1:4.5 Cu(II)-to-COOH ratio, $[\text{Cu(II)}] = 4.0 \times 10^{-5} \text{ mol l}^{-1}$]; for ligand composition, see text. TCA = tricarballic acid.

The limited nitrogen content of humic substances restricts the concentration of amino acid ligands that can be included in the model. Cascade binding in Cu(II)–MHBS is effective at relatively low pH ; however, for a ligand which forms a seven- or eight-membered chelate ring with Cu(II) the stability constant will be lower, i.e., the reaction will occur at higher pH . Hence the inclusion of such moieties at significant concentrations could have a measurable impact on the calculated Cu(II) binding curves. Substitution of MHBS for glycylaspartic acid had no effect on the calculated binding curve.

The percentage of carboxyl groups and of each binding moiety involved in Cu(II) complexation in the mixed model ligand solutions was pH dependent (Fig. 8). This illustrates that in a mixture of discrete ligands, having different metal–ligand stability constants, the proportion of each donor group involved in complexing will change with pH . For the model ligand composition used in Fig. 8 (given above), 15% of the total carboxyl groups were involved in complexing at $\text{pH} 5.0$ and 18% were utilized at $\text{pH} 6.3$. For fulvic acid the

proportions were 15–18% and 28–33%, respectively. However, the maximum proportion of carboxyl groups which participate in Cu(II) complexation at a given pH is determined by measurement of the *CC* (which is measured in the presence of excess metal ion). Further, the proportion of each moiety involved in complexing will vary with metal-to-ligand ratio, as modelled by the selected discrete ligands.

For HA there was a greater discrepancy between the measured *CC* and that calculated for complexation in the mixture of discrete ligands (at pH 6.3 the *CC* for HA was greater by a factor of 1.7). This indicates that there are some functional groups in humic acids which are not adequately modelled by the discrete ligands. Alternatively, “cascade binding” (see above) of carboxyl groups may occur in humic acids, and/or the humic molecules could undergo some conformational changes as the pH increases.

Therefore, to simulate the HA binding curves the concentration of ligand moieties included in the model was 1.7 times greater than that for FA. The model consisted of citric acid 1.224×10^{-5} , tricarballic acid 2.448×10^{-5} , salicylic acid 1.224×10^{-4} , malic acid 2.448×10^{-5} , acetylacetone 2.72×10^{-5} and MHBS, $1.6 \times 10^{-5} \text{ mol l}^{-1}$ (equivalent to 100% of the assumed amino acid content). The calculated curves are given in Fig.

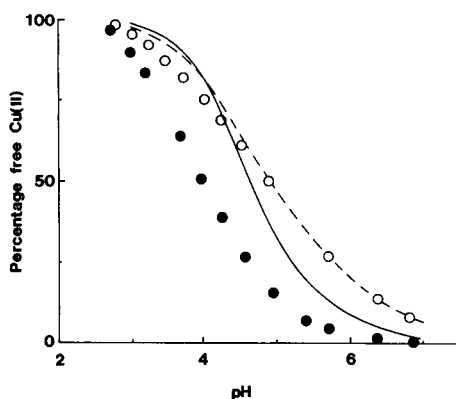


Fig. 9. Copper(II) binding curves measured for humic acid $[\text{COOH}] = 1.8 \times 10^{-4} \text{ mol l}^{-1}$ and $[\text{Cu(II)}] = (\circ) 4.0 \times 10^{-5}$ or $(\bullet) 9.0 \times 10^{-6} \text{ mol l}^{-1}$ and calculated for a mixture of model ligands representing possible chelating moieties in a humic sample with $[\text{Cu(II)}] = (\text{dashed line}) 4.0 \times 10^{-5}$, or $(\text{solid line}) 9.0 \times 10^{-6} \text{ mol l}^{-1}$. For ligand composition, see text.

9. A lower concentration of acetylacetone resulted in a poorer fit to the HA data.

Although the models provide a reasonable fit to the HA data at a Cu(II)-to-COOH ratio of 1:4.5, Fig. 9 indicates that insufficient very strong Cu(II) complexants are included in the simulations.

Unlike FA, the models did not provide an adequate fit to the HA data at the lower Cu(II) concentration (Fig. 9). It is noted that if other factors such as “cascade binding” of carboxyl groups do indeed contribute to complexation then a simple increase in the concentration of model ligand carboxyl groups cannot simulate this effect.

Effect of competing metal ions on Cu(II) binding curves

Although increasing the concentration of potassium (KNO_3) from 0.10 to 0.60 mol l^{-1} had no effect on the Cu(II) complexation capacity of FA, the metal binding curves for both humic and fulvic acids were displaced to higher pH (Fig. 3). The conformation of humic molecules may be altered at the higher ionic strength [53], thus affecting their ability to bind Cu(II). Alternatively, the high concentration of potassium [10 000–60 000 times that of Cu(II)] may allow it to ion pair with anionic donors in competition with Cu(II) complexation. Indeed, calculation of the Cu(II) binding curve for malonic acid in the presence of 0.10 and 0.60 mol l^{-1} K(I) ($\log K = 0.68$ [54]) indicated that potassium ions can compete for Cu(II) complexation sites under these experimental conditions with $1.8 \times 10^{-4} \text{ mol l}^{-1}$ COOH and $9.0 \times 10^{-6} \text{ mol l}^{-1}$ Cu(II).

This decrease in stability of copper(II) humic complexes with increasing ionic strength is important for speciation predictions in natural systems. Extrapolation of ISE (and anodic stripping voltammetry) results (both of which utilize high background electrolyte concentrations) to low ionic strength freshwater conditions may greatly overestimate the expected activity of copper(II) in the environment.

The Cu(II) binding curve for FA was displaced to higher pH in the presence of 0.06 mol l^{-1} Mg(II) (Fig. 3). To provide a comparison, the

effect of Mg(II) and Ca(II) on Cu(II) complexation by citric acid was calculated from published stability constants. The species considered were CuL ($\log \beta = 6.03$), CuL_2 (10.43) [21], MgL (3.40), MgHL (7.52), MgH_2L (5.19), CaL (3.55), CaHL (7.78) and CaH_2L (5.40) [20]. In a solution $1.8 \times 10^{-4} \text{ mol l}^{-1}$ in carboxyl groups and $9.0 \times 10^{-6} \text{ mol l}^{-1}$ in Cu(II), the amount of Cu(II) bound to citrate was 54%, 98% and 100% at pH 4.0, 5.0 and 6.0, respectively. In the presence of 0.053 mol l^{-1} Mg(II) and 0.01 mol l^{-1} Ca(II) (sea water composition), these were reduced to 26%, 50% and 53% respectively. This indicates that Ca(II) and Mg(II), when present in relatively high concentration, can compete effectively for even the strongest Cu(II) complexation sites.

Other workers have reported minimal effects of Ca(II) (up to 0.01 mol l^{-1}) on the Cu(II) complexation capacity of HA [55,56] or FA [57]. However, measurement of the complexation capacity involves titration of humic substances with a metal ion to concentrations in large excess over the ligand.

The Cu(II) binding curve for FA (1:4.5 ratio) measured in the presence of Al(III) was displaced to higher pH in the pH range 3.5–6.5, indicating competitive complexation by Al(III) (Fig. 4). A greater effect was observed for the higher concentration of Al(III). In contrast to Mg(II) or K(I), each curve became coincident with that in the absence of competing metal at pH > 6.5. At pH > 6.5 Cu(II) may displace fulvic-bound Al(III), which is hydrolysed to $\text{Al}(\text{OH})_4^-$, or Al(III) may be redistributed to different binding sites [which do not compete with Cu(II)].

The coordination of Cu(II) in the presence of Al(III) was further probed by calculating binding curves for discrete model ligands. On the basis of the results for malonic acid it seems likely that Al(III) would not remain bound to humic substances above pH 6 (see Results). Because of the very low stability of the Cu(II)–salicylate complex, compared with Al(III)–salicylate, complexation by such moieties could not account for the Al(III)–induced change in Cu(II) binding [Al(III)–salicylate binding could, however, lower the affinity of an adjacent complexation site for Cu(II)].

Environmental levels of Al(III) are significantly greater than those of Cu(II). Typical concentrations of Al(III) are 5×10^{-6} – $1 \times 10^{-4} \text{ mol l}^{-1}$ in soil interstitial waters and 7.4×10^{-7} – $1.8 \times 10^{-6} \text{ mol l}^{-1}$ in acidic lake waters. In contrast, the typical Cu(II) concentration in freshwaters is $4.7 \times 10^{-8} \text{ mol l}^{-1}$ and that in soil interstitial waters is 1.5×10^{-7} – $9.5 \times 10^{-7} \text{ mol l}^{-1}$ [58]. Hence Al(III) could have a significant impact on Cu(II) speciation in the pH range 3.5–5.5 typical of natural humic waters and Podzolic soils.

Because of hydrolysis, $\text{Al}(\text{OH})_4^-$ becomes the major Al(III) species at pH > 6 in the presence of carboxylate ligands, whereas ions such as K(I) and Mg(II) remain complexed to the organic ligand. Humic substances may have sufficient capacity to coordinate both Cu(II) and other metal ions in solution, but may not compete strongly against metal hydrolysis.

Conclusions

On the basis of carboxyl group content, humic acid has a greater complexation capacity and a greater binding strength than does fulvic acid. This indicates that the fewer carboxyl groups in HA are distributed more “efficiently” in terms of metal binding than those in FA. The HA carboxyl groups could also be in close proximity to other coordination sites which facilitate strong Cu(II) complexation.

The colloidal/particulate HA molecules exhibited both a greater complexation capacity and a greater binding strength than did the smaller soluble molecules. Hence the colloidal/particulate humic phase may play an important role in environmental processes. It may be the predominant sink for metal ions, moderate their toxicity to biota and provide a buffer to influxes of metal contaminants into soils and natural waters.

Measurements performed in the presence of competing metal ions indicated that studies on the coordination of isolated humic substances to single metal ions cannot be used directly to estimate the speciation of metal ions in the environment. Further detailed studies on the competitive complexation of metal ions by humic substances will be important in understanding their role in

determining the speciation of trace metals in soils and natural waters.

The binding curves for both fulvic and humic acids could be modelled by mixtures of simple aliphatic carboxylate moieties. The types of moieties likely to dominate Cu(II) complexation by humic substances in weakly acidic and neutral solutions are citrate and malonate; salicylate moieties are unlikely to be involved except in alkaline media. Calculations including the model ligands glycyloaspatic acid and MHBS indicated that nitrogen-containing species (even when present in very low concentration) have a significant impact on the Cu(II) binding curve.

The present approach provides a useful basis for identifying the types of moieties which are most (and least) likely to be involved in Cu(II) complexation. Further, it facilitates an understanding of the effects of various parameters (e.g., pH, ionic strength, metal-to-ligand ratio and presence of competing metal ions) on metal sequestration by a complicated system.

Any realistic model of metal ion complexation by humic and fulvic acids must take into account the heterogeneity of these substances as classes of ligands, their ability to form species other than simple 1:1 complexes and the presence of more than one phase.

REFERENCES

- 1 F.J. Stevenson, *Soil Sci.*, 123 (1977) 10.
- 2 D.R. Turner, M.S. Varney, M. Whitfield, R.F.C. Mantoura and J.P. Riley, *Geochim. Cosmochim. Acta*, 50 (1986) 289.
- 3 E.M. Perdue, in I.H. Suffet and P. MacCarthy (Eds.), *Aquatic Humic Substances. Influence on Fate and Treatment of Pollutants*, American Chemical Society, Washington, DC, 1989, pp. 281–295.
- 4 J. Buffle, F.-L. Greter and W. Haerdi, *Anal. Chem.*, 49 (1977) 216.
- 5 S.E. Cabaniss, M.S. Shuman and B.J. Collins, in C.J.M. Kramer and J.C. Duinker (Eds.), *Complexation of Trace Metals in Natural Waters*, Martinus Nijhoff/Dr. W. Junk, The Hague, 1984, pp. 165–179.
- 6 S.D. Young and B.W. Bache, *J. Soil Sci.*, 36 (1985) 261.
- 7 K. Murray and P.W. Linder, *J. Soil Sci.*, 34 (1983) 511.
- 8 R.D. Guy and C.L. Chakrabarti, *Can. J. Chem.*, 54 (1976) 2600.
- 9 R.A. Saar and J.H. Weber, *Environ. Sci. Technol.*, 16 (1982) 510A.
- 10 M.S. Varney, D.R. Turner, M. Whitfield and R.F.C. Mantoura, in C.J.M. Kramer and J.C. Duinker (Eds.), *Complexation of Trace Metals in Natural Waters*, Martinus Nijhoff/Dr. W. Junk, The Hague, 1984, pp. 33–46.
- 11 T. Midorikawa, E. Tanoue and Y. Sugimura, *Anal. Chem.*, 62 (1990) 1737.
- 12 D.P. Rainville and J.H. Weber, *Can. J. Chem.*, 60 (1982) 1.
- 13 J.E. Gregor, H.K.J. Powell and R.M. Town, *J. Soil Sci.*, 40 (1989) 661.
- 14 J.E. Gregor, H.K.J. Powell and R.M. Town, *Sci. Total Environ.*, 81/82 (1989) 597.
- 15 A.I. Vogel, *Textbook of Quantitative Inorganic Analysis*, Longman, London, 1974.
- 16 J.E. Gregor and H.K.J. Powell, *J. Soil Sci.*, 37 (1986) 577.
- 17 V. Cheam, *Can. J. Soil Sci.*, 53 (1973) 377.
- 18 R.N. Sylva and M.R. Davidson, *J. Chem. Soc., Dalton Trans.*, (1979) 232.
- 19 T.M. Florence, *Analyst*, 111 (1986) 489.
- 20 D.D. Perrin, *Stability Constants of Metal-Ion Complexes*, Pergamon, Oxford, 1979.
- 21 S. Ramamoorthy, P.G. Manning and C. Guarnaschelli, *J. Inorg. Nucl. Chem.*, 34 (1972) 3443.
- 22 T.B. Field, J.L. McCourt and W.A.E. McBryde, *Can. J. Chem.*, 52 (1974) 3119.
- 23 E. Bottari, A. Liberti and A. Rufolo, *Inorg. Chim. Acta*, 3 (1969) 201.
- 24 K.S. Rajan and A.E. Martell, *J. Inorg. Nucl. Chem.*, 29 (1967) 463.
- 25 J. Buffle, P. Deladoey, F.-L. Greter and W. Haerdi, *Anal. Chim. Acta*, 116 (1980) 255.
- 26 E.Sh. Ganelina, *Zh. Prikl. Khim.*, 37 (1964) 1358.
- 27 J.J. Fardy and R.N. Sylva, *Rep. Aust. Energy Comm., AAEC/E445* (1978) 1.
- 28 M. Schnitzer and H. Kerndorff, *Water Air Soil Pollut.*, 15 (1981) 97.
- 29 A. Piccolo and F.J. Stevenson, *Geoderma*, 27 (1982) 195.
- 30 D.S. Gamble, C.H. Langford and A.W. Underdown, *Org. Geochem.*, 8 (1985) 35.
- 31 W.T. Bresnahan, C.L. Grant and J.H. Weber, *Anal. Chem.*, 50 (1978) 1675.
- 32 R. Bonnett and R.P.C. Cousins, *Org. Geochem.*, 11 (1987) 497.
- 33 J. Buffle, A. Tessier and W. Haerdi, in C.J.M. Kramer and J.C. Duinker (Eds.), *Complexation of Trace Metals in Natural Waters*, Martinus Nijhoff/Dr. W. Junk, The Hague, 1984, pp. 301–316.
- 34 L.E. Sojo, D.S. Gamble, C.H. Langford and R.H. Zienius, *J. Environ. Sci. Health*, B24 (1989) 619.
- 35 H.K.J. Powell and R.M. Town, *Anal. Chim. Acta*, 267 (1992) 47.
- 36 M.R. Collins, G.L. Amy and C. Steelink, *Environ. Sci. Technol.*, 20 (1986) 1028.
- 37 J.I. Kim, G. Buckau, G.H. Li, H. Duschner and N. Psarros, *Fresenius' J. Anal. Chem.*, 338 (1990) 245.
- 38 G. Dell'Agnola and G. Ferrari, *J. Soil Sci.*, 22 (1971) 342.
- 39 B. Bartschat, S.E. Cabaniss and F.M.M. Morel, *Environ. Sci. Technol.*, 26 (1992) 284.

- 40 P. Sequi, G. Guidi and G. Petruzelli, *Geoderma*, 13 (1975) 153.
- 41 J. Slavek, J. Wold and W.F. Pickering, *Talanta*, 29 (1982) 743.
- 42 M.K.S. Mak and C.H. Langford, *Can. J. Chem.*, 60 (1982) 2023.
- 43 W.R. Fischer, *Z. Pflanzenernähr. Bodenkd.*, 149 (1986) 382.
- 44 J.A. Lavigne, C.H. Langford and M.K.S. Mak, *Anal. Chem.*, 59 (1987) 2616.
- 45 D.K. Cabbiness and D.W. Margerum, *J. Am. Chem. Soc.*, 92 (1970) 2151.
- 46 B.A. Goodman and M.V. Cheshire, *Nature (London)*, 244 (1973) 158.
- 47 B.A. Goodman and M.V. Cheshire, *J. Soil Sci.*, 27 (1976) 337.
- 48 M.V. Cheshire, M.L. Berrow, B.A. Goodman and C.M. Mundie, *Geochim. Cosmochim. Acta*, 41 (1977) 1131.
- 49 M.L.S. Goncalves and A.M. Mota, *Talanta*, 34 (1987) 839.
- 50 V. Cheam and D.S. Gamble, *Can. J. Soil Sci.*, 54 (1974) 413.
- 51 R.M. Town, PhD Thesis, University of Canterbury, New Zealand, 1991.
- 52 R.A. Saar and J.H. Weber, *Environ. Sci. Technol.*, 16 (1982) 510A.
- 53 K. Ghosh and M. Schnitzer, *Soil Sci.*, 129 (1980) 266.
- 54 P.G. Daniele, A. De Robertis, C. De Stefano, S. Sammartano and C. Rigano, *J. Chem. Soc., Dalton Trans.*, (1985) 2353.
- 55 J.G. Hering and F.M.M. Morel, *Environ. Sci. Technol.*, 22 (1988) 1234.
- 56 J.G. Hering and F.M.M. Morel, *Environ. Sci. Technol.*, 22 (1988) 1469.
- 57 D.M. McKnight and R.L. Wershaw, in R.C. Averett, J.A. Leenheer, D.M. McKnight and K.A. Thorn (Eds.), *Humic Substances in the Suwannee River, Georgia: Interactions, Properties and Proposed Structures*, U.S. Geol. Survey Open File Report, No. 87-557, 1989, pp. 59–79.
- 58 J. Buffle, *Complexation Reactions in Aquatic Systems*, Horwood, Chichester, 1988.

Cholesterol sensor based on electrodeposition of catalytic palladium particles

Shaojun Dong, Qing Deng and Guangjin Cheng

Changchun Institute of Applied Chemistry, Chinese Academy of Sciences, Changchun, Jilin 130022 (China)

(Received 30th November 1992; revised manuscript received 25th January 1993)

Abstract

A layer of palladium particles was electrodeposited on a glassy carbon electrode. The dispersed Pd particles resulted in a large decrease in overvoltage for the electrochemical oxidation of H_2O_2 down to +0.4 V vs. Ag/AgCl, based on which a new kind of cholesterol sensor was fabricated. Cholesterol oxidase was immobilized on the Pd-dispersed electrode by cross-linking with glutaraldehyde and a layer of poly(*o*-phenylenediamine) (PPD) film was electropolymerized on the enzyme layer. The sensor shows a linear response in the concentration range 0.05–4.50 mmol l^{-1} with a rapid response of less than 20 s. The polymer film can prevent interference from uric acid and ascorbic acid and also increases the thermal stability of the sensor. The sensor can be used for 200 assays without an obvious decrease in activity.

Keywords: Amperometry; Biosensors; Cholesterol; Enzyme electrodes; Palladium

The determination of cholesterol in human serum is important in clinical analysis, as it is related directly to the diagnosis of various kinds of disease such as heart disease and arteriosclerosis. Various methods have been described for this purpose, such as spectrophotometry [1], fluorimetry [2], potentiometry [3], amperometry [4–8] and coulometry [9]. Spectrophotometry has been widely used in medicine, but it is usually time consuming, with tedious procedures. An amperometric enzymatic method based on a combination of enzyme and electrochemical reactions is especially attractive because of the use of small sample volumes, the improvements in selectivity, accuracy and precision and the ease of handling.

In this work, a new kind of cholesterol sensor was fabricated, based on electrodeposition of palladium on a glassy carbon electrode. Cholesterol

oxidase is immobilized on the electrode by cross-linking with glutaraldehyde. The H_2O_2 produced is monitored by measuring the current of H_2O_2 oxidation electrocatalysed by dispersed palladium particles. Interferences and the loss of enzyme are avoided by a poly(*o*-phenylenediamine) (PPD) film electropolymerized on the enzyme layer. The polymer film also improves the thermal stability of the sensor.

EXPERIMENTAL

Reagents and apparatus

All electrochemical experiments were carried out with a PAR 370 electrochemical system. The temperature was controlled by a thermostated circulating water bath. The pH values were measured on a Beckman Φ -60 pH meter.

Cholesterol oxidase (EC 1.1.3.6, 27 U mg^{-1}) (CHO), cholesterol (Sigma), PdCl_2 , *o*-phenylenediamine and bovine serum albumin (BSA) were

Correspondence to: Shaojun Dong, Changchun Institute of Applied Chemistry, Chinese Academy of Sciences, Changchun, Jilin 130022 (China).

of analytical-reagent grade. Solutions were prepared using doubly distilled water. Britton–Robinson buffer solution was used.

Preparation of enzyme electrode

Electrodeposition of palladium. A glassy carbon (GC) electrode (diameter 3 mm) was polished with diamond paper and then with α -alumina powder, and finally cleaned with distilled water in an ultrasonic bath. The GC electrode was immersed in a solution containing 5 mmol l^{-1} $PdCl_2$, the layer was electrodeposited by cyclic potential scanning between -0.4 and 1.0 V vs. Ag/AgCl at 50 $mV s^{-1}$ for 10 min, then the electrode was washed with distilled water and dried in air. The loading levels of Pd on the electrode were 40 – 60 $\mu g cm^{-2}$, which were calculated from the changes consumed on successive repeated scans assuming that the coulombic efficiency is unity under the potential scan.

Fabrication of enzyme electrode. A 2-mg amount of CHO and 15 mg of BSA were dissolved in 0.2 ml of phosphate buffer (0.05 mmol l^{-1} , pH 7.0) and 10 μl of this enzyme solution, consisting of 220 U ml^{-1} CHO and 7.5% BSA, and 3 μl of 2.5% glutaraldehyde solution were mixed thoroughly. A 1- μl volume of the matrix solution was placed on the palladium-dispersed electrode with a microsyringe, allowed to dry and cross-linked at room temperature, and then kept in a refrigerator for 1 h. Finally, the electrode was washed by immersion in buffer (pH 7.0) to remove excess of glutaraldehyde. The electropolymerization of the PPD film was carried out by potential scanning of two cycles between 0 and 1.0 V vs. Ag/AgCl at 5 $mV s^{-1}$ in a fresh solution (pH 7.0) containing 5 mmol l^{-1} of *o*-phenylenediamine [10,11]. The enzyme electrode was thoroughly washed after preparation and stored in buffer solution (pH 7.0) at $4^\circ C$ when not in use.

Measuring procedure

Preparation of substrate solution. Cholesterol was insoluble in aqueous solution, so an emulgent was needed. Triton X-100 may play an important role in the activity of enzymes. Karube et al. [4] found that the response current was highest when

the concentration of the emulgent was 5–10%. In this work, a substrate solution composed of isoamyl alcohol–isopropyl alcohol–Triton X-100–buffer (4 : 10 : 5 : 81) was prepared.

Measurement of steady-state currents. A standard three-electrode, one-compartment electrochemical cell was used for all electrochemical experiments. The enzyme electrode was used as the working electrode, a silver/silver chloride electrode as the reference electrode and a platinum wire as the counter electrode. The temperature of solution was maintained at $37 \pm 0.5^\circ C$. The potential was kept at $+0.5$ V vs. Ag/AgCl. Solutions were stirred with a magnetic stirrer.

RESULTS AND DISCUSSION

Catalysis of the modified electrode

All electrodes covered with sputtered metal particles were much more efficient than the corresponding pure solid metal even when careful electrochemical pretreatment was applied [12]. It was found that the deposition of sputtered Pd or Pt or a mixture of sputtered Pd–Au on a carbon electrode resulted in a decrease by several hundred millivolts of the large overvoltages for the electrochemical oxidation of H_2O_2 [13]. However, appropriate apparatus is not available electrodeposition is convenient. Many workers have used solutions containing hexachloroplatinate to obtain a catalytic Pt layer on carbon electrodes [14–16]. However, electrodeposited Pt cannot decrease the overvoltage [17]. It was found that electrodeposition of palladium on a carbon electrode can decrease the overvoltage for the electrochemical oxidation of H_2O_2 to $+0.4$ V [18]. The palladium particles were electrodeposited in a fresh buffer solution (pH 5) containing 5 mmol l^{-1} $PdCl_2$ in order to prevent the deactivation of the enzyme layer. Figure 1 shows the cyclic voltammograms of the electrodeposition of Pd and Pt in pH 5 buffer. Figure 2 shows the current responses of Pd- and Pt-dispersed electrodes to 2 mmol l^{-1} H_2O_2 . The current was high enough from $+0.4$ on the Pd-dispersed electrode and from $+0.6$ V on the Pt-dispersed electrode, and the Pt-dispersed electrode was more susceptible

to interference with the electrochemical conversion of H_2O_2 . Therefore, the Pd-dispersed electrode was adopted in subsequent work.

Immobilizing enzyme and avoiding interferences

The immobilization of enzymes is one of the most important procedures with biosensors. Cholesterol oxidase can be entrapped on a polypyrrole film [5,8], but the cost of using large amounts of the enzyme is high, and the current responses are small because the enzyme is only slightly doped into the polymer film. We immobilized the enzyme by cross-linking with glutaraldehyde, but could not avoid the loss of enzyme and interferences. Keeping the potential at +0.5 V, ascorbic acid can influence to the extent of 100% and uric acid to 170%. Nafion and Eastman-AQ are fairly efficient at preventing the interference of anions. Many reports have been published [19,20], but Nafion is easily dissolved and an AQ membrane easily thickens in the substrate solution which contains isoamyl alcohol and isopropyl alcohol. Electropolymerization of *o*-phenylenediamine was adopted. The individual standard concentrations of ascorbic acid, uric acid and cholesterol are 0.06, 0.3 and 1.0–1.4 mmol l^{-1} in human serum samples [21]. Figure 3 shows that there were virtually no interferences with the response.

Current response

The hydrodynamic current–potential profile at the enzyme electrode in a 1 mmol l^{-1} cholesterol solution in pH 7 buffer is shown in Fig. 4. The current response reaches a plateau from +0.45 to +0.6 V vs. Ag/AgCl. On this basis, a working potential of +0.5 V was chosen for studying the electrode response.

Figure 5 shows the effect of the solution pH on the current response. The optimum pH was 7–8 for the free enzymes, 6–8 for enzymes immobilized by cross-linking only and 6.5–10.5 for enzymes immobilized by cross-linking combined with poly(*o*-phenylenediamine). Hence the polymer extends the pH range of the enzyme electrode. There have been few reports on the mechanism of action and structure of PPD. As a possible unit

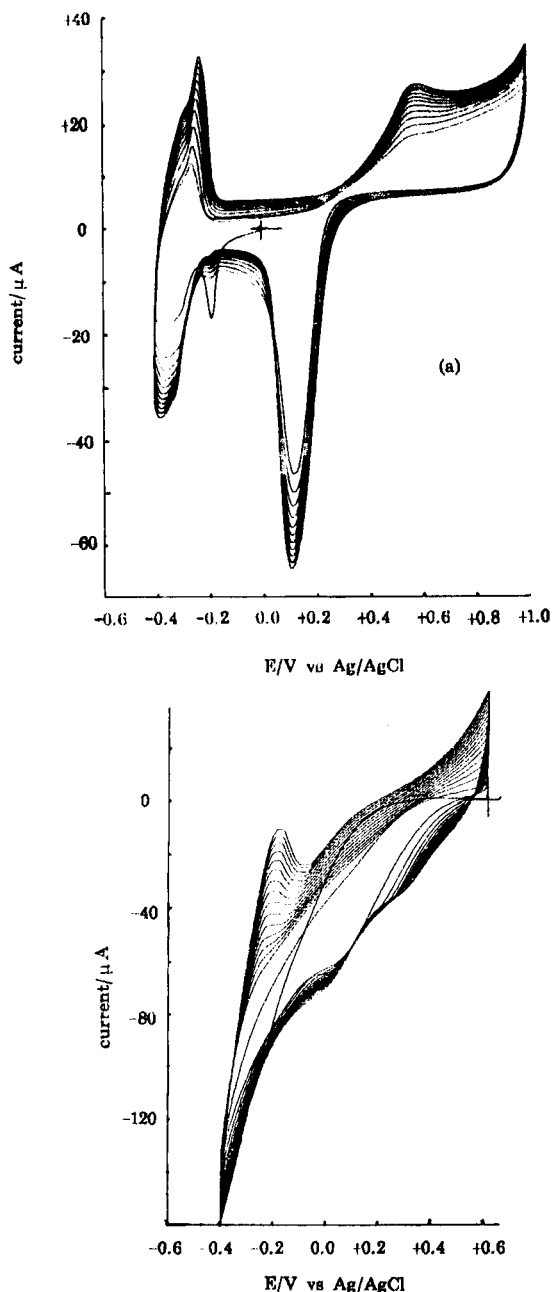


Fig. 1. Cyclic voltammograms recorded continuously at a bare GC electrode in a solution of (a) 5 mmol l^{-1} PdCl_2 and (b) 5 mmol l^{-1} PtCl_6^{2-} in pH 5 buffer. Scan rate, 50 mV s^{-1} ; time, 10 min.

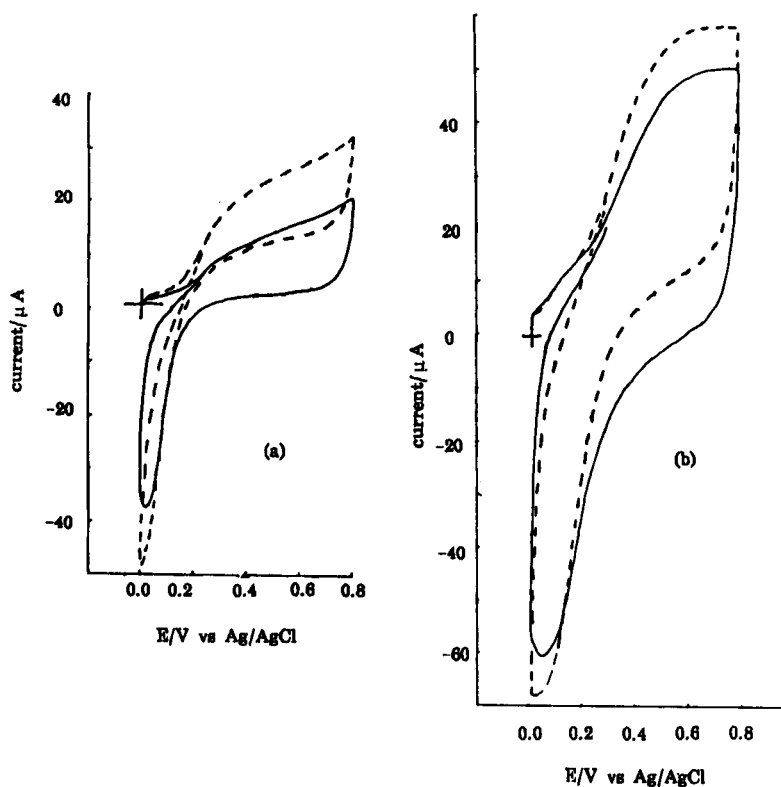
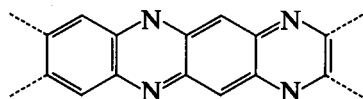


Fig. 2. Cyclic voltammograms for the electrocatalytic oxidation of $2 \text{ mmol l}^{-1} \text{ H}_2\text{O}_2$ in buffer (pH 7.0) at (a) a Pd- and (b) Pt-dispersed GC electrode. Scan rate 50 mV s^{-1} . Solid line, buffer solution; dashed line, $2 \text{ mmol l}^{-1} \text{ H}_2\text{O}_2$.

structure of the PPD, an asymmetric "quinoid" structure



was proposed by Chiba et al. [11]. The protonation of amine linkages might be attributed to acidification of the environment around the immobilized enzymes. Thus the sensor prepared

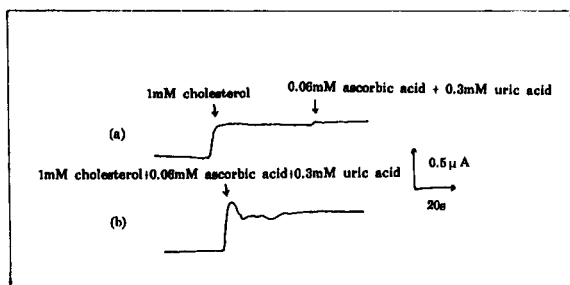


Fig. 3. Steady-state current response of the cholesterol sensor in the (a) absence and (b) presence of some interferences. Potential, $+0.5 \text{ V}$.

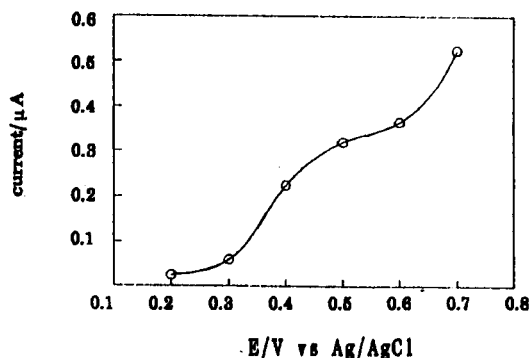


Fig. 4. Hydrodynamic voltammogram obtained at the enzyme electrode for 1 mmol l^{-1} cholesterol.

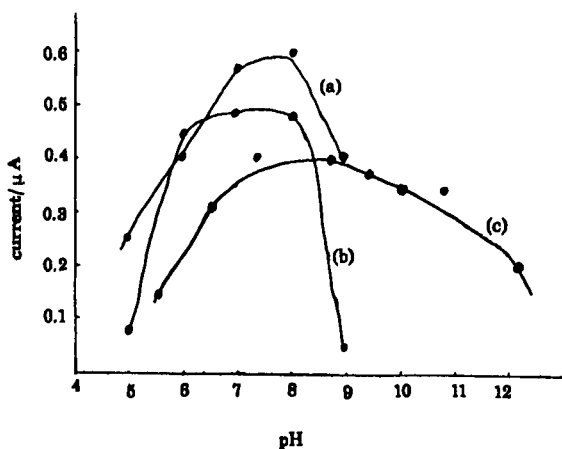


Fig. 5. Dependence of current response to cholesterol (1 mmol l^{-1}) on the solution pH. Potential, $+0.5 \text{ V}$ vs. Ag/AgCl . (a) Free enzyme; (b) cross-linking; (c) enzyme immobilized by cross-linking and PPD film.

shows a good response even in pH 10.5 buffer solution.

The effect of temperature is shown in Fig. 6. It can be concluded that the immobilization used improves the thermal stability of the enzyme. When the temperature reaches 50°C the film becomes unstable. Considering the lifetime of the sensor, the optimum temperature was chosen as 37°C .

Figure 7 shows the typical steady-state current response of the sensor determined under the optimum conditions discussed above. The detection limit of the enzyme electrode was $5 \mu\text{mol l}^{-1}$ according with a signal-to-noise ratio > 2 . Figure

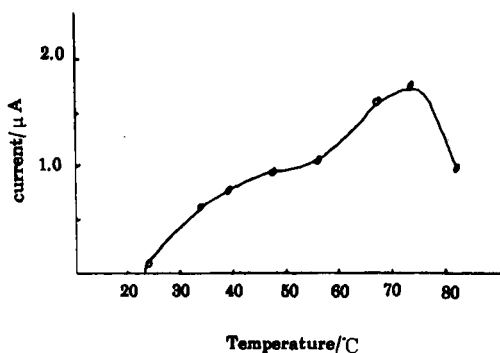


Fig. 6. Dependence of current response to cholesterol (1 mmol l^{-1}) on temperature.

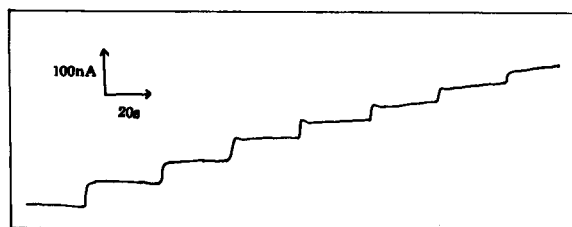


Fig. 7. Typical steady-state current response of the enzyme electrode on increasing the concentration of cholesterol in 0.1 mmol l^{-1} steps. Potential, $+0.5 \text{ V}$; temperature, 37°C ; electrolyte, pH 7.0 buffer.

8 shows a typical calibration graph of experimental steady-state current vs. cholesterol concentration. A linear relationship was obtained in the range $0.05\text{--}4.50 \text{ mmol l}^{-1}$. As human serum contains $0.7\text{--}1.8 \text{ mmol l}^{-1}$ of free cholesterol, the enzyme electrode can meet the requirement for such a determination. The response time determined by single potential step chronoamperometry was less than 20 s. The enzyme electrode shows good reproducibility: for seven replicate determinations of $125 \mu\text{mol l}^{-1}$ cholesterol in pH 7 buffer, the response was 85, 82, 80, 85, 80, 83 and 82 nA; the relative deviation was less than 2%. Table 1 shows the results obtained using six equivalently prepared electrodes for the determination of 0.20, 0.38, 0.55 and 0.71 mmol l^{-1} ,

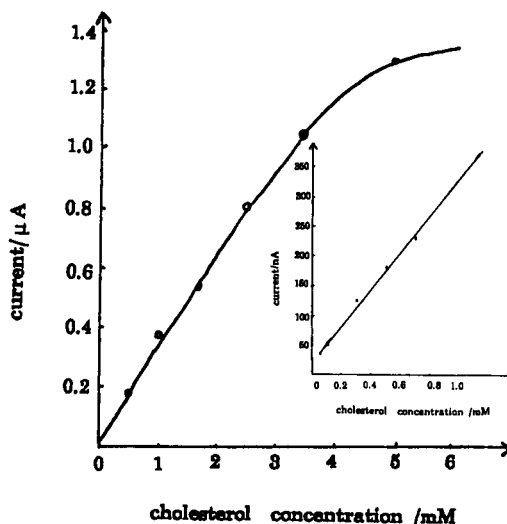


Fig. 8. Calibration graph for the enzyme electrode. Experimental parameters as in Fig. 7.

TABLE 1

Current responses for the detection of cholesterol using six equivalently prepared electrodes (A–F) with experimental parameters as in Fig. 7

Concentration (mmol l ⁻¹)	Response (nA)					
	A	B	C	D	E	F
0.20	225	150	175	200	200	225
0.38	500	450	450	450	500	600
0.55	750	700	700	850	750	750
0.71	950	950	925	950	1000	1000

cholesterol. The relative standard deviations were less than 10%.

The enzyme electrode showed good stability for prolonged use. No appreciable decrease in activity was observed after 200 assays. Over 70% of the activity of the immobilized enzyme was retained after at least 2.5 months at 4°C.

It is concluded that the reported electrode is a simple, convenient, sensitive and stable tool for the determination of cholesterol.

This project was supported by the National Natural Science Foundation of China.

REFERENCES

- 1 A. Zeatris and B. Zak, *Anal. Chem.*, 29 (1969) 143.
- 2 H. Huang, J.W. Kuan and G.G. Guilbault, *Clin. Chem.*, 21 (1975) 1605.
- 3 D.S. Papastathopoulos and G.A. Rechnitz, *Anal. Chem.*, 47 (1975) 1972.
- 4 I. Karube, K. Hara and S. Suzuki, *Anal. Chim. Acta*, 139 (1982) 127.
- 5 Y. Kajiya, R. Tsuda and H. Yoneyama, *Denki Kagaku*, 12 (1990) 1213.
- 6 U. Wollenberger, F. Scheller and M. Janchen, *Bioelectrochem. Bioeng.*, 11 (1983) 307.
- 7 N. Oyama, S. Ikeda and T. Ohsaka, *Electroanalysis*, 3 (1991) 665.
- 8 Y.-H. Luo, D.-S. Zheng and R.-K. Zhang, *Gao Deng Xue Xiao Hua Xue Xue Bao*, 10 (1991) 1320.
- 9 S. Uchiyama, S. Kato and S. Suzuki, *Electroanalysis*, 2 (1990) 59.
- 10 S.V. Sasso, R.J. Pierce, R. Walla and A.M. Yacynych, *Anal. Chem.*, 62 (1990) 1111.
- 11 K. Chiba, T. Ohsaka, Y. Ohnuki and N. Oyama, *J. Electroanal. Chem.*, 219 (1987) 117.
- 12 J.J. Lingane and P.J. Lingane, *J. Electroanal. Chem.*, 5 (1963) 411.
- 13 L. Gorton and T. Svensson, *J. Mol. Catal.*, 38 (1986) 49.
- 14 K. Hajizadeh, H.B. Halsall and W.R. Heineman, *Talanta*, 38 (1991) 37.
- 15 J. Wang, R. Li and M.-S. Lin, *Electroanalysis*, 1 (1989) 151.
- 16 Y. Ikariyama, S. Yamauchi and H. Ushioda, *Anal. Lett.*, 20 (1987) 1791.
- 17 L. Gorton, E. Cdogregi and E. Dominguez, *Anal. Chim. Acta*, 250 (1991) 203.
- 18 Q. Chi and S. Dong, *Anal. Chim. Acta*, 278 (1993) 17.
- 19 S. Dong, B. Wang and B. Liu, *Biosensors Bioelectron.*, 7 (1991) 215.
- 20 G. Fortier, R. Beliveau and D. Belanger, *Anal. Lett.*, 23 (1990) 1607.
- 21 C. Bertrand, P.R. Coulet and D.C. Gautheron, *Anal. Lett.*, 12 (1979) 1477.

Direct graphite furnace atomic absorption spectrometric determination of metals in sea water: application of palladium modifiers and a fractal approach to their analytical support

Stefan Sachsenberg, Thomas Klenke, Wolfgang E. Krumbein, Hans J. Schellnhuber and Erich Zeeck

*Institute for Chemistry and Biology of the Marine Environment (ICBM), Carl von Ossietzky University of Oldenburg,
P.O. Box 2503 W-2900 Oldenburg (Germany)*

(Received 25th September 1992; revised manuscript received 12th January 1993)

Abstract

Sea water, like other high-salinity matrices, causes severe interferences in the direct determination of metals by graphite furnace atomic absorption spectrometry (GFAAS), even when Zeeman-effect background correction is applied. A method for eliminating these interferences by the application of mixed modifier system of ammonium oxalate and tetraamminepalladium(II) chloride is presented. In particular these modifiers optimize the direct GFAAS determination of lead and manganese. For cadmium, however, only ammonium oxalate should be used as a modifier. The geometry of the microdistribution of palladium on the palladium-conditioned graphite platform was investigated in order to elucidate possible stabilizing effects of palladium on the analytes which were observed with the different modifiers. Fractal characteristics of the palladium elemental distribution were ascertained by a scanning electron microscope–energy-dispersive x-ray spectrometer image box-counting analysis. The fractal dimension [$D_B(0) = 1.77 \pm 0.04$ and 1.81 ± 0.04] and electron microscopic investigations indicated differences in the structure of palladium deposits on the platform. These variations in the palladium geometry affect the analytes to a certain extent.

Keywords: Atomic absorption spectrometry; Cadmium; Fractals; Lead; Manganese; Palladium modifier; Sea water; Waters

Alkali and alkaline earth element halides cause interferences in the direct determination of metals by graphite furnace atomic absorption spectrometry (GFAAS). The mechanism of these interferences has been extensively studied [1,2]. Halides in the gas phase suppress the formation of the atom population during atomization [1]. In addition, an interference by non-atomic absorption in the fine-structured line spectrum of the

alkali metal halides [3,4] has been observed. Interferences also occur owing to light scattering by sodium chloride particles. This is almost always the case when metals have to be determined in the presence of a sea-water matrix [5–7].

To overcome these problems, many chemical modifiers have been developed and applied in order to separate the halides using, e.g., ammonium nitrate and nitric acid [8–10], or by matrix matching with EDTA [11] or ascorbic acid [12].

Earlier studies on the concentration of certain heavy metals in seawater and marine interstitial water did not give satisfactory results when using these modifiers. When applying our equipment it

Correspondence to: T. Klenke, Institute for Chemistry and Biology of the Marine Environment (ICBM), Carl von Ossietzky University of Oldenburg, P.O. Box 2503, W-2900 Oldenburg (Germany).

was observed that especially with lead the common modifiers did not work when a sea-water matrix with a salinity of 3.4% was present.

There is evidence, however, that the presence of platinum-group metals makes it possible to increase the ashing temperature significantly, which, in turn, helps to separate the matrix from the analyte [13–15]. Palladium was used preferentially because of its low price and relatively good stability in aqueous solutions [16].

The stabilizing effects of palladium on several metals such as lead and manganese are probably due to the reduction and simultaneous formation of intermetallic bonds [2,17–19]. The dominant physical and chemical process involved in the stabilization is the formation of compounds or solid solutions of the analytes with palladium; atomization occurs by dissociative adsorption of these associates [18,19].

One way of elucidating these stabilizing effects is a geometrical approach to the distribution of the palladium domains. Surface reaction effects depend strongly on the geometrical conditions of the support [20], because the shape and the local density of the reactive domains determine the rates of the mediated processes. It has recently been realised that the fractal analysis of geometrical properties may help in understanding various natural processes on different scales [21,22]. Focusing on physico-chemical processes it could in particular be shown that both chemical and physical surface reactions depend on the supporting fractal geometry [20,22,23], which is usually analysed by box-counting techniques [21,24,25].

This paper presents a method for eliminating sea-water interferences with the determination of metals in seawater by adding a new mixed modifier system of ammonium oxalate and tetraamminepalladium(II) chloride. Lead was chosen in order to study and verify the effects of palladium modifiers, as lead is the element that suffers most from interferences with halide matrices. The described mixed modifier system may also be useful for the determination of other metals in the presence of sea water. A second, complementary aspect of the investigation is a fractal approach to the surface geometry of the palladium-conditioned graphite platform in order to detect possi-

TABLE 1

Instrumental parameters

Parameter	Lead	Manganese	Cadmium
Lamp current (mA)	4	5	4
Slit width (nm)	1.0	0.2	0.5
Slit height	Normal	Reduced	Normal
Wavelength (nm)	217.0	279.5	228.8
Zeeman-effect background correction	On	On	On

ble stabilizing effects of palladium on the analytes.

EXPERIMENTAL

Equipment

A Varian SpectrAA 30-Z graphite furnace atomic absorption spectrometer with a Zeeman-effect background compensation and a separate signal/background recording system and hollow-cathode lamps were used. The operational conditions are given in Tables 1 and 2. In general the work was carried out with L'vov platforms and the gas-stop mode during the atomization phase. Nitrogen with a purity of 99.999% was used as an inert gas.

The L'vov platforms used were examined under a Cambridge Instruments S 180 scanning electron microscope (SEM) equipped with a Link Ortec 6230 energy-dispersive x-ray spectrometer (EDX).

TABLE 2

General furnace parameters

Step	Parameters
Drying	350°C, ramp 5 s, hold 25 s, gas flow 3 l min ⁻¹
Ashing	Temperature variable, ramp 5 s, hold variable gas flow 3 l min ⁻¹ (for variable parameters see Table 3)
Atomization	Pb: 2500°C, ramp 1 s, hold 2.5 s Mn: 2500°C, ramp 1 s, hold 2.5 s Cd: 1900°C, ramp 0.8 s, hold 1 s Gas flow (all cases) 0.01 min ⁻¹

The image analysis as well as the determination of fractal dimensions by box-counting analysis were carried out by applying the technique introduced by Block and co-workers [24,25].

Reagents

Ultrapure water was prepared by using a Milli-Q system (Millipore) and further purification was achieved by means of a Chelex-100 ion-exchange column (column length, 200 mm; grain size, 200–400 mesh; ammonium form) (Bio-Rad).

Palladium solutions were prepared by dissolving tetraamminepalladium(II) chloride (99.999% pure, Aldrich) in ultrapure water. Ammonium oxalate (Merck) was purified by extraction with ammoniumtetramethylenedithiocarbamate and 2,7-dimethylpentanone. Standard solutions were prepared by diluting 1000 mg l^{-1} standard solutions (Merck). Ultrapure acids were used (Suprapur, Merck).

Procedure

All laboratory ware was cleaned according to common standards in ultratrace analysis. To obtain a suitable blank, metals were removed from the sea water prior to spiking. The sea water was pretreated by filtering it through activated carbon and by further purifying it by means of a Chelex-

100 ion-exchange column (column length, 200 mm; grain size, 200–400 mesh; ammonium form). Blank values, determined by direct measurements, expressed as relative absorption, were lead 0.001, manganese 0.004 and cadmium 0.003. The analyte matrix samples were spiked to lead concentrations of 20 and $50 \mu\text{g l}^{-1}$.

Sample and modifier volumes were injected separately with an autosampler system. Generally, the injection volume was set to 20 and $10 \mu\text{l}$, respectively. Each sample was dried for 25 s at 350°C (lead and manganese) or 300°C (cadmium). The temperature chosen depended on the set of instruments used. However, the real temperature of the L'vov platform and the sample droplet may be lower.

Various ash temperatures, modifier volumes and salinities were applied in order to study possible concentration-related effects (Table 2).

All measurements were made by means of the peak-area mode.

RESULTS

Chemical modifiers

Two different modifiers were investigated. M-1 is a 0.1% (w/v) solution of tetraamminepalla-

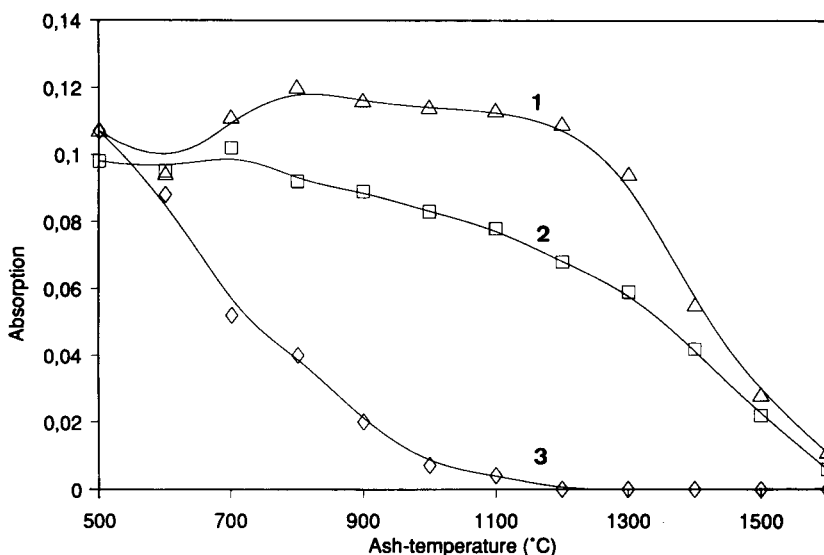


Fig. 1. Influence of ashing temperature and modifier composition on signal ($20 \mu\text{l}$ of a $20 \mu\text{g Pb l}^{-1}$ solution in 1% HCl matrix). 1 = With modifier M-2; 2 = with modifier M-1; 3 = without modifier.

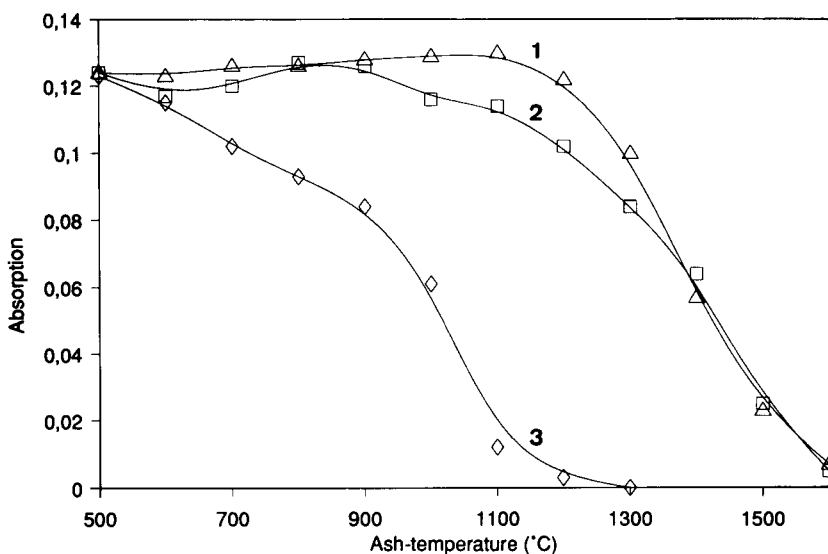


Fig. 2. Influence of ashing temperature and modifier composition on signal ($20 \mu\text{l}$ of a $20 \mu\text{g Pb l}^{-1}$ solution in 1% HNO_3 matrix). 1 = With modifier M-2; 2 = with modifier M-1; 3 = without modifier.

dium(II) chloride in ultrapure water. This palladium compound was chosen first because its contamination by other metals is very low and second because of its high solubility and stability in water. M-2 is a novel composition of tetraammine-palladium(II) chloride and ammonium oxalate

with concentrations of 0.1% and 1% (w/v), respectively. It should be noted that this composite (M-2) only remains stable ca. 2 h. Therefore, the mixture should be always freshly prepared. A mixture of palladium(II) chloride and ammonium oxalate is more stable and is expected be equally

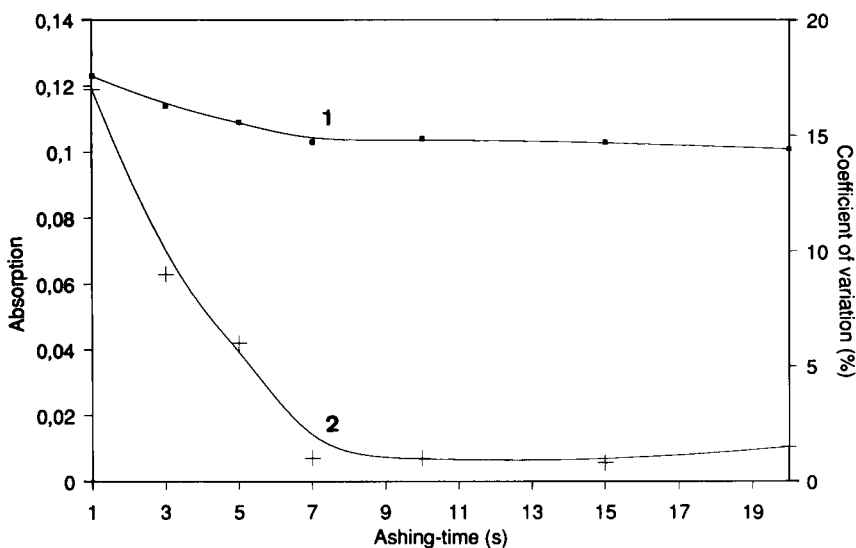


Fig. 3. Influence of ashing time on the signal and the reproducibility ($20 \mu\text{g Pb}$ in 1% HCl matrix + $2 \mu\text{l}$ modifier M-2, $20\text{-}\mu\text{l}$ sample volume). 1 = Relative-signal; 2 = coefficient of variation (relative standard deviation).

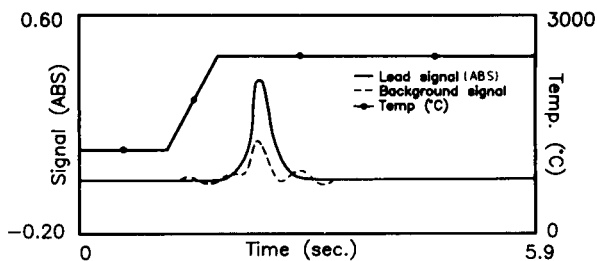


Fig. 4. Atomization/background signals of a sea-water sample spiked to a final concentration of $50 \mu\text{g Pb l}^{-1}$ solution ($10\text{-}\mu\text{l}$ sample and $5 \mu\text{l}$ of modifier M-2 added).

suitable. However, contamination levels of trace elements are higher in commercially available palladium chloride reagent [Aldrich, 99.995% palladium(II) chloride].

Conditions

Figures 1 and 2 show the dependence of the ashing temperature on the signal absorbance of lead in the presence of chloride and nitrate matrices. When no modifier was applied, a striking decrease in the sensitivity was observed at ashing temperatures $> 500^\circ\text{C}$. When modifier M-1 was used, a gradual decrease in sensitivity at temperatures $> 800^\circ\text{C}$ could be detected. In contrast modifier M-2 gave no significant decrease in sen-

sitivity up to 1200°C . This is important, because the ashing temperature is necessary to separate the bulk of sodium chloride from the platform. The possibility of increasing the ashing temperature to levels up to 1200°C without a significant decrease in sensitivity by applying the palladium modifiers, has been clearly demonstrated. When M-2 was used in the presence of the chloride matrix (1% HCl), a relative increase in sensitivity of 40% could be observed, which clearly contrasts with the findings obtained with M-1 at an ashing temperature of 1200°C . Also, a relative increase of 20% was observed at an ashing temperature of 1200°C when a nitrate matrix (1% HNO_3) was present (Fig. 2).

Figure 3 illustrates that the optimum ashing time is 10–15 s when M-2 is used at 900°C . Ashing periods of less than 7 s under the same conditions decrease the reproducibility (precision) dramatically. Probably a minimum reaction time is necessary to establish a uniform palladium–metal association and to remove the interfering matrix compounds from the graphite tube.

Figure 4 shows the signal-to-background relationship for a real sea-water sample with a salinity of 3.4% spiked with $50 \mu\text{g Pb l}^{-1}$. A significant depression of the background and a symmetrical peak shape were observed when M-2 was

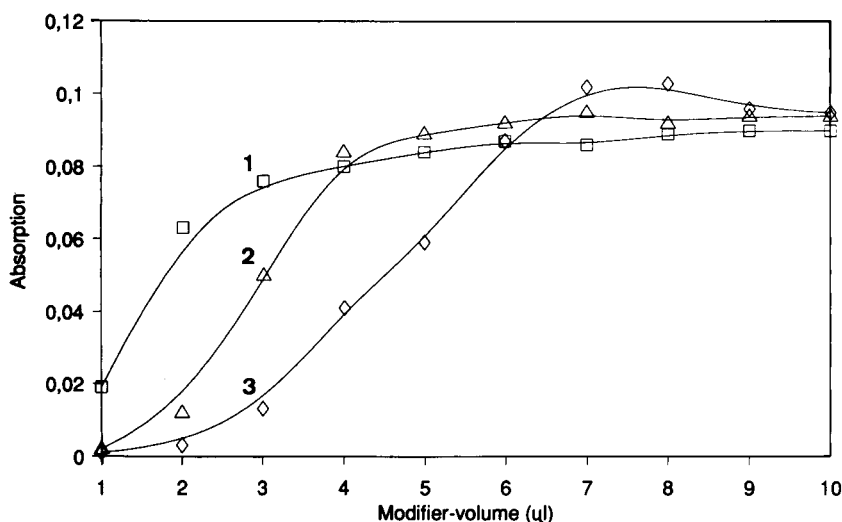


Fig. 5. Influence of modifier volume on the signal ($10\text{-}\mu\text{l}$ samples of different salinities spiked with $50 \mu\text{g Pb l}^{-1}$; modifier M-2). Salinity: 1 = 1.0%; 2 = 2.0%; 3 = 3.4%.

used. In general, a higher salinity requires a larger amount of modifier, as shown in Fig. 5. When the salinity is 3.4% (coastal sea-water salinity of the German Bight), the optimum for background suppression is 7 μl for a 10- μl sample volume, based on the composition of M-2.

The M-2 modifier also yields good results with the determination of other metals in sea water. Figure 6 shows the dependence of signal absorption on the ashing temperature for cadmium when modifiers M-1 and M-2 were applied. It could be shown that also for cadmium the M-2 modifier yields the best results and also provides the possibility of increasing the ashing temperature to ca. 800°C without a significant decrease in sensitivity. However, for the direct determination of cadmium, the palladium-based modifiers did not work in a satisfactory way when a sea-water matrix was present, because cadmium could not be stabilized up to a temperature of 1200°C, which is necessary to separate the sodium chloride matrix. For cadmium a 2% ammonium oxalate modifier would be more suitable [26,27], as this type of modifier permits the atomization of cadmium before the bulk salt matrix evaporates into the gas phase.

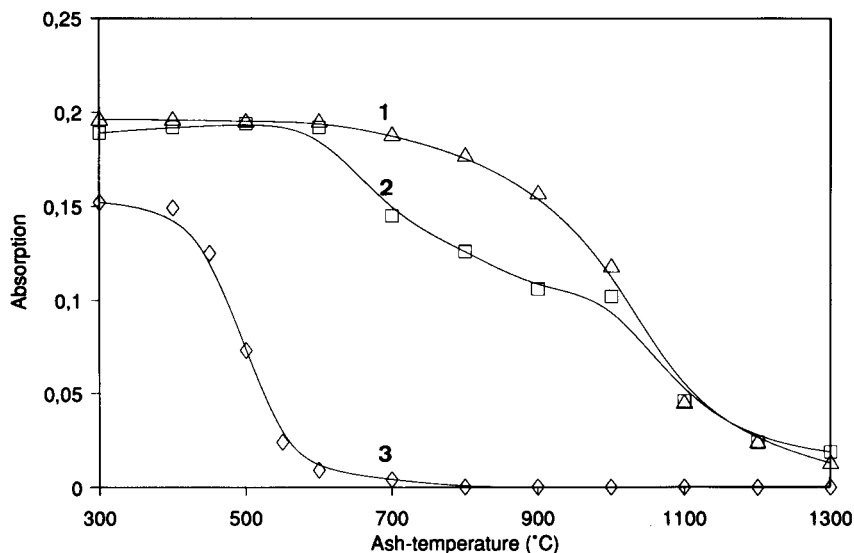


Fig. 6. Influence of ashing temperature and modifier composition on signal (20 μl of a 2 $\mu\text{g Cd l}^{-1}$ solution in 1% HCl matrix). 1 = With modifier M-2; 2 = with modifier M-1; 3 = without modifier.

TABLE 3

Optimized analytical parameters for lead, manganese and cadmium in a sea-water matrix (3.4% salinity)

Metal	Ashing temperature (°C)	Ashing time (s)	Sample volume (μl)	Modifier volume (μl)	Detection limit ^a
Lead	1200	20	10	6–7	0.4 $\mu\text{g l}^{-1}$
Manganese	1400	20	20	5–10	0.1 $\mu\text{g l}^{-1}$
Cadmium	350	10	10	5	5 ng l^{-1}

^a The detection limit is twice the standard deviation.

Table 3 gives the detection limits for lead and manganese when the M-2 modifier is used with a 10- μl injection volume and also the detection limits for cadmium when a 2% ammonium oxalate modifier is applied.

Table 4 gives the results obtained from the analyses of different sea-water samples. For comparison, aliquots of the sea-water samples were analysed not only directly but also after extraction; the procedure is described elsewhere [27]. The results from both methods were comparable. In general, the concentrations of lead and manganese in unpolluted sea areas are very low and exceed the detection limit of the direct GFAAS

TABLE 4

Results for analyses of sea-water samples ^a

Sample	Pb ($\mu\text{g l}^{-1}$)	Mn ($\mu\text{g l}^{-1}$)	Cd (ng l^{-1})
(A) Nearshore sea water from East Frisian Isles/Wadden Sea	0.8 \pm 0.3 ^b 0.88 \pm 0.06 ^c	8.7 \pm 0.6 –	290 \pm 15 309 \pm 10
(B) Sea water from German Bight	1.0 \pm 0.5 ^b 0.78 \pm 0.04 ^c	8.6 \pm 0.6 –	980 \pm 10 1000 \pm 30
(C) Reference standard CASS II ^d	< Detection limit ^b 0.026 \pm 0.005 ^c 0.019 \pm 0.006 ^e	2.1 \pm 0.2 – 1.99 \pm 0.15	28 \pm 10 19 \pm 4 19 \pm 4

^a Means \pm standard deviations ($n=10$). ^b Direct measurement. ^c Extracted; for extraction method, see [27]; unpublished results. ^d Obtained from the National Research Council of Canada. ^e Certified values.

method, even though there are no matrix interferences. Sea-water samples A and B, however, show remarkable amounts of lead and manganese, which are due to local circumstances. The

concentrations in these samples are within the range of the direct method detection limit. However, at a concentration of $1 \mu\text{g l}^{-1}$, which is close to the detection limit of the proposed method, the precision is relatively low, which is acceptable with an injection volume of $10 \mu\text{l}$.

Palladium geometry and stabilizing effects

In the above it was demonstrated that palladium modifiers in different mixtures stabilize certain metals in a specific way. However, the stabilizing mechanisms of the modifiers in the analytical procedure are still a matter of speculation. The observed effects of these palladium modifiers on optimizing the GFAAS determination of certain metals in high-salinity matrices needs to be further elucidated by means of investigations on the physical and chemical processes prevailing in the graphite cuvette during the analytical steps. As catalytic effects are the focus of investigation, it should be mentioned that the geometry of the catalyst domains, especially shape, size and local



Fig. 7. SEM image of palladium domains on a L'vov platform using $20 \mu\text{l}$ of 0.1% tetraaminepalladium(II) chloride solution (modifier M-1). Dried and ashed until atomization step (Table 1). Area ca. $35 \times 25 \mu\text{m}$.

density, governs the mechanisms of stabilizing or catalytic effects. Thus, a fractal analysis of the geometric properties on the palladium-conditioned graphite platform may be useful in order to elucidate the mediated processes.

SEM–EDX studies were done to evaluate the surface conditions of a palladium-conditioned L'vov platform and the distribution, shape and size of the palladium deposits. The surface topography of the platform is characterized by large-scale imbrication and small-scale crater features. At palladium concentrations and modifier volumes which are favourable for the proposed analytical conditions, the scanning electron micrographs exhibit a different deposition behaviour for the two modifiers in question. The deposition of palladium from an M-1 solution results in distinct palladium domains with a slightly concentric internal structure and with locally high palladium concentrations (Fig. 7). The presence of ammonium oxalate (modifier M-2) promotes the depositon of palladium on the platform in a finely

dispersed form (Fig. 8). Enrichment domains of palladium droplets are scarce.

Optical and analytical information on the palladium distribution may additionally be achieved with the SEM–EDX mode. On the basis of box-counting analysis of SEM–EDX images it was found that the palladium distribution exhibits a fractal behaviour (Figs. 9–12). The effect of ammonium oxalate (modifier M-2) is the promotion of a more dispersed palladium distribution. This is indicated by a slightly higher fractal dimension [$D_B(0) = 1.81 \pm 0.04$] in comparison with the fractal dimension observed during the application of modifier M-1 [$D_B(0) = 1.77 \pm 0.04$]. However, a statistically significant difference between the two dimensions could not be observed.

The fractal dimensions of palladium on the platform correspond to the fractal dimensions obtained from mathematically ideal, deterministic fractals (Mandelbrot–Given curve or Sierpinski carpet) and from related, statistically random, similar structures. Additionally, they may be ob-

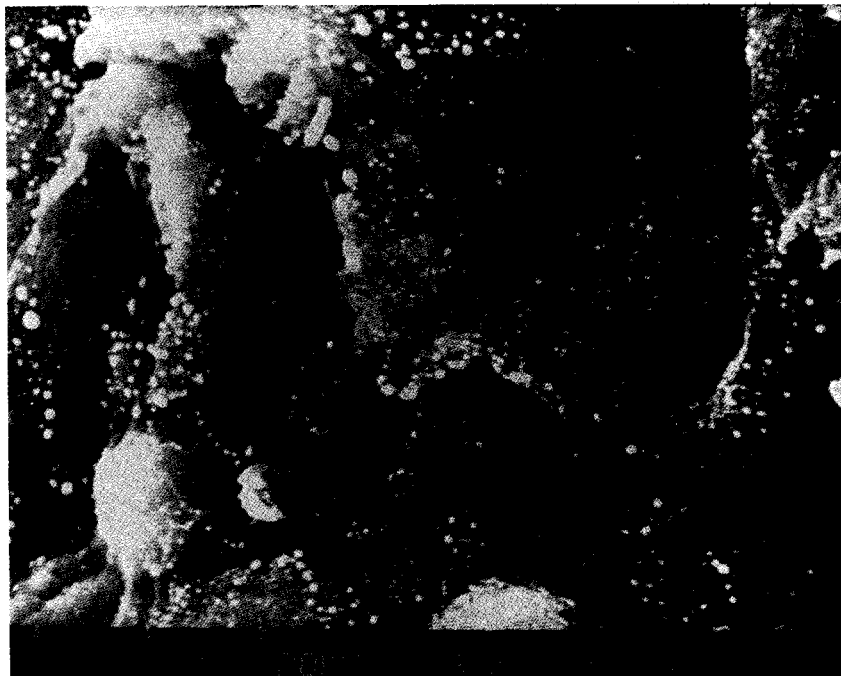


Fig. 8. SEM image of palladium domains on a L'vov platform using 20 μl of a composition of tetraamminepalladium(II) chloride and ammonium oxalate with concentrations of 0.1% and 1%, respectively (modifier M-2). Dried and ashed until atomization step (Table 1). Area ca. $25 \times 16 \mu\text{m}$.

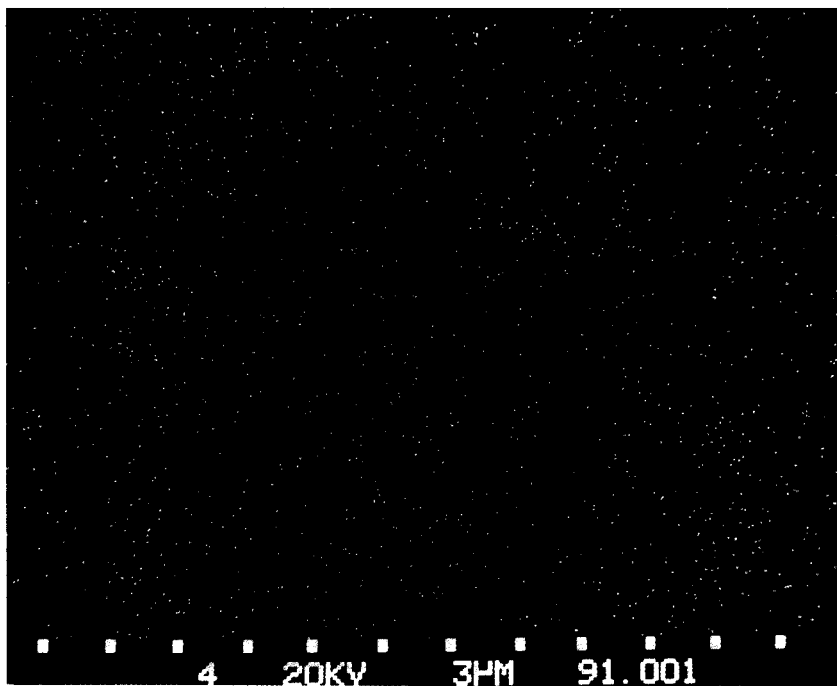


Fig. 9. SEM-EDX palladium distribution pattern corresponding to Fig. 7.

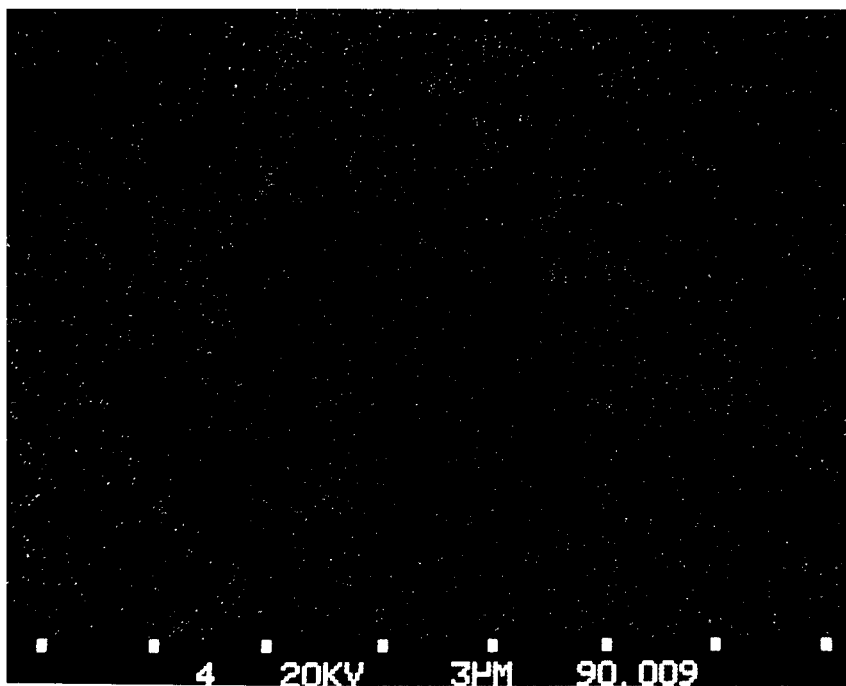


Fig. 10. SEM-EDX palladium distribution pattern corresponding to Fig. 8.

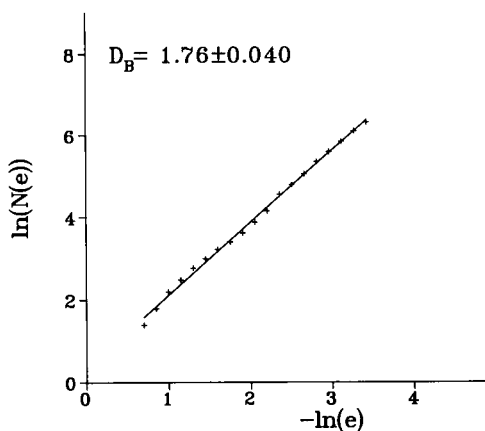


Fig. 11. Fractal dimension [$D_B(0)$] of palladium distribution for M-1 (cf., Figs. 7 and 9). $N(e)$ = number of boxes, e = number of occupied boxes in the course of a box counting analysis.

tained from natural structures of percolation clusters [21] in a Euclidian two-dimensional space. Fractal dimensions close to $D_B(0) = 1.90$ have also recently been detected during rapid phase transitions [23] and with reactants on catalytically active surfaces [20]. This value is higher and differs significantly from those resulting from slower aggregation processes like diffusion-limited aggregation (DLA) or cluster-cluster aggregation (CCA) [22]. In this study, these slower DLA or

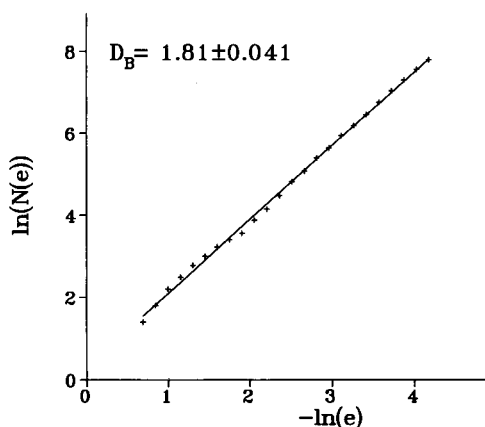


Fig. 12. Fractal dimension [$D_B(0)$] of the palladium distribution for M-2 (cf., Figs. 8 and 10); $N(e)$ = number of boxes; e = number of occupied boxes in the course of a box counting analysis.

CCA processes were suppressed by the short drying phase at relatively high temperatures. Prolongation of this step, however, may promote the slower aggregation processes and yield more extensive palladium domains with smaller surface areas, which is indicated by smaller fractal dimensions.

It is still unclear in what way palladium interacts with the analytes, e.g., by promoting the reduction of the analytes and their deposition on the platform or by a reduction with a simultaneous formation of palladium-analyte associates (see [2,18] for other scenarios). The latter, however, must be favoured, as retardation of the analyte atomization occurs when palladium modifiers are applied. This may be due to intermetallic bonds in palladium-analyte associates [2,17].

Under the analytical conditions suggested for sea-water samples, the sensitivity of the SEM-EDX technique is too low for further investigation of these associates. This might have been helpful for obtaining some ideas on the stabilizing mechanisms. For this reason it is still unknown if and in what way the fractal palladium distribution is affected by factors such as the surface fractal of the graphite platform, sorption phenomena or processes occurring during the solute-solid-phase transition.

Thus, taking into account the sensitivity of the SEM and SEM-EDX techniques, the distribution of palladium is a microscopic dispersion. Especially in the presence of ammonium oxalate this results in a large surface-to-volume ratio of palladium for stabilizing effects, and additionally it ensures the rapid thermal dissociation of palladium-analyte associates. However, at present no further statement can be made regarding other physico-chemical properties of this stabilizing system as discussed by Welz et al. [2] and Styris and co-workers [18,19]. In particular, this applies to the mechanisms involved and the activity of these reactions.

Conclusion

The proposed palladium-based chemical modifiers contribute to both the precision and the accuracy of direct GFAAS determinations of metals in high-salinity matrices such as sea water.

Although the metal concentrations in open sea waters are often too low for a direct determination, the described modifier system is useful for the analysis of sea water in polluted areas or matrices with a high salinity and also for the determination of interstitial water concentrations in marine sediments.

Fractal analysis of the microstructure and microcomposition of catalytically active surfaces yields valuable information on the genesis, geometry and possible properties of the reactants or catalyst distribution in question. Further investigations along these lines, including tunnelling microscopy, are needed in order to obtain a clear picture of the stabilizing effects of palladium during GFAAS operation. In particular, multifractal analysis of the palladium domains measure should be performed. Computer simulations of the sorption/desorption on surfaces with fractal patchiness will also permit a better insight into the pertinent mechanisms.

Financial support of this work by the Federal Ministry of Science and Technology (BMFT grant, MFU 05798) is gratefully acknowledged.

REFERENCES

- 1 J.M. Shekiri, Jr., R.K. Skogerboe and H.E. Taylor, *Anal. Chem.*, 60 (1988) 2578.
- 2 B. Welz, G. Schlemmer and J.R. Mudokavi, *Anal. Chem.*, 60 (1988) 2567.
- 3 B.V. L'vov, *Spectrochim. Acta, Part B*, 33 (1987) 153.
- 4 M.J. Adams, G.F. Kirkbright and P. Rienvatana, *At. Absorpt. Newsl.*, 5 (1975) 105.
- 5 D.A. Segar and J.G. Gonzalez, *Anal. Chim. Acta*, 58 (1978) 7.
- 6 I. Havezov and E. Ivanova, *Fresenius' Z. Anal. Chem.*, 315 (1983) 26.
- 7 R.E. Sturgeon, *Spectrochim. Acta, Part B*, 44 (1989) 1209.
- 8 R.D. Ediger, G.E. Peterson and J.D. Kerber, *At. Absorpt. Newsl.*, 14 (1975) 127.
- 9 A. Le Bihan and J. Courtot-Coupetz, *Analisis*, 3 (1975) 59.
- 10 R.E. Sturgeon, S.S. Berman, A. Desaulniers and D.S. Russel, *Anal. Chem.*, 51 (1979) 2364.
- 11 R. Guevremont, *Anal. Chem.*, 52 (1980) 1574.
- 12 M. Tominaga, K. Bansho and Y. Umezaki, *Anal. Chim. Acta*, 169 (1985) 171.
- 13 X.Q. Shan, Z.M. Ni and Z. Li, *Talanta*, 31 (1984) 150.
- 14 Z.M. Ni and X.Q. Shan, *Spectrochim. Acta, Part B*, 42 (1978) 937.
- 15 G. Schlemmer and B. Welz, *Spectrochim. Acta, Part B*, 41 (1986) 1157.
- 16 L. Ping, K. Fuwa and K. Matsumoto, *Anal. Chim. Acta*, 171 (1985) 279.
- 17 X.Q. Shan and D.X. Wang, *Anal. Chim. Acta*, 173 (1985) 315.
- 18 D.L. Styris, L.J. Prell and D.A. Redfield, *Anal. Chem.*, 63 (1991) 503.
- 19 D.L. Styris, L.J. Prell, D.A. Redfield, J.A. Holcombe, D.A. Bass and V. Majidi, *Anal. Chem.*, 63 (1991) 508.
- 20 R.M. Ziff and K. Fichthorn, *Phys. Rev. B*, 34 (1986) 2038.
- 21 J. Feder, *Fractals*, Plenum, New York London, 1988, p. 283.
- 22 D. Avnir (Ed.), *The Fractal Approach to Heterogeneous Chemistry*, Wiley, Chichester, 1989, p. 441.
- 23 J.M. Gordon, A.M. Goldman, J. Maps, D. Costello, R. Tiberio and B. Whitehead, *Phys. Rev. Lett.*, 56 (1986) 2280.
- 24 A. Block, W. v. Bloh, Th. Klenke and H.J. Schellnhuber, *J. Geophys. Res.*, 96B (1991) 16223.
- 25 A. Block, W. v. Bloh and H.J. Schellnhuber, *Phys. Rev. A*, 42 (1990) 1869.
- 26 M. Kowles and B. Pohl, *GIT, Suppl.*, 1 (1987) 40.
- 27 S. Sachsenberg, Th. Klenke, W.E. Krumbein and E. Zeeck, *Fresenius' J. Anal. Chem.*, 342 (1992) 163.

Halogen-assisted cleaning after-treatment in graphite furnace atomic absorption spectrometry for analysis of molybdenum-based materials

B. Docekal¹ and V. Krivan

Sektion Analytik und Höchstreinigung, Universität Ulm, Albert-Einstein-Allee 11, W-7900 Ulm (Germany)

(Received 3rd November 1992; revised manuscript received 1st February 1993)

Abstract

Carbon tetrachloride and carbon tetrafluoride were tested as possible halogen precursors in the cleaning after-treatment stage in graphite furnace atomic absorption spectrometry for the removal of the interfering molybdenum matrix. The results show that applying sample masses up to 0.1 mg of molybdenum introduced as metal, oxide and silicide, the matrix can be effectively volatilized. Interference effects caused by residual halogenated pyrolytic products retained in the atomizer after the carbon tetrafluoride treatment can be effectively eliminated by using a mixture of hydrogen and argon as a purge gas in the atomization stage. By this gas-phase modification procedure, the signals of Co, Cr, Cu, Fe, Mg, Mn and Ni can be recovered to the original level. The procedure improves the analytical lifetime of the graphite atomizer to up to 200–300 replicate runs.

Keywords: Atomic absorption spectrometry; Chlorination; Fluorination; Halogen-assisted cleaning; Molybdenum matrix

High-purity molybdenum oxide is an intermediate material in the production of molybdenum and molybdenum silicide used as gate and interconnect materials in very large-scale integration (VLSI) technology. Graphite furnace atomic absorption spectrometry (GFAAS) is a very sensitive method for the determination of metallic trace impurities in these materials [1]. Compound methods based on sample decomposition and matrix/trace separations are limited by the introduction of a blank in these stages [2]. Therefore, in principle, methods involving minimized sample

handling are to be preferred [3]. However, analysis of materials based on refractory carbide-forming elements by GFAAS without matrix separation is, as a rule, accompanied by the accumulation of refractory residue in the atomizer. In spite of the enhancement of analytical characteristics due to matrix modification by molybdate and due to carbide coating of tubes and platforms, reported for several elements [4], experience indicates [3] that multiple introduction of a refractory matrix into the graphite atomizer often leads to the formation of an irreproducible coating on the graphite surface causing interference in the determinations.

Alternate “active” gases have been introduced as chemical modifiers during a certain stage of the heating programme in order to prevent the formation of carbides of the analyte elements [4]. Direct injection of chlorine into the carbon tube

Correspondence to: V. Krivan, Sektion Analytik und Höchstreinigung, Universität Ulm, Albert-Einstein-Allee 11, D-W-7900 Ulm (Germany).

¹ Permanent address: Czech Academy of Sciences, Institute of Analytical Chemistry, Veverí 97, CS-61142 Brno (Czech Republic).

atomizer during thermal pretreatment has been utilized for the removal of chromium and vanadium carbides [5]. However, using common AAS instrumentation, handling with elemental halogens is very difficult. Nevertheless, some halogenated organic compounds can be introduced into the graphite furnace as precursors for the in situ production of halogens. Carbon tetrachloride [6,7] trifluoromethane (Freon 23) [7–10] and PTFE powders [11,12] have been used in halogen-assisted atomization and volatilization of refractory carbide-forming analyte elements.

Considering the thermal stability of the halogenated compounds, free halogens can be produced by pyrolysis of these compounds at different temperatures. For instance, the reaction gas mixture formed by pyrolysis of carbon tetrachloride at 600°C [13] contains, in addition to approximately 30 mol% of free chlorine, a variety of chlorinated compounds. No build-up of pyrolytic carbon has been observed at this temperature. Carbon tetrafluoride (Freon 14) decomposes in a graphite furnace at temperatures above 1200°C. Approximately 50 mol% of free fluorine is formed in the gas phase at 1900°C; at higher temperatures, the reactive gases start to attack the graphite.

The paper reports results of investigations of cleaning halogenation after-treatment using carbon tetrachloride and carbon tetrafluoride as chlorine and fluorine precursor agents for the removal of the matrix during the GFAAS procedure for the analysis of high-purity molybdenum-based materials.

EXPERIMENTAL

Reagents and samples

Guaranteed reagent (GR) carbon tetrachloride (Merck, Darmstadt) and 2.8-purity grade carbon tetrafluoride (R 14) (Linde, Unterschleissheim) were used as halogenation agents. A gas mixture containing 6.5% (v/v) hydrogen in spectroscopic-grade argon, supplied by Linde, was used for gas-phase modification during the preatomization and atomization stages.

Powdered ultra-high-purity molybdenum metal, molybdenum trioxide and molybdenum silicide were supplied by Metallwerk Plansee (Reutte, Austria). Ammonium molybdate solution was prepared by dissolution of molybdenum trioxide in a stoichiometric amount of Suprapur grade ammonia solution (Merck). Doubly dis-

TABLE 1

Temperature programme for experiments with alternate gases

Exp. parameter	Stage								
	1 Drying	2 Charring	3 Atomiza- tion	4 Clean- out	5 Cool- down	6 After- treatment	7 Blow- out ^a	8 Clean- out	9 Cool- down
Temperature (°C) ^b	240	300 ^c	variable ^d	2700	20	variable	variable	2600	20
Ramp time (s)	5	10	0	1	1	1	1	1	1
Hold time (s)	35	15	6	2	4	40	30	5	10
Internal gas flow-rate (ml min ⁻¹)	300	300 ^{h,i}	20 ^h	300	300	variable ^j	300 ^h	300	300

^a Puffing off the alternate gas present in the tubing and furnace by argon or argon–hydrogen mixture. ^b Nominal values. ^c Variable values in determination of optimum temperature (charring curve). ^d Atomization temperature 2600°C for Ca, 2500°C for Co, Cr, Cu, Fe and Ni, 2200°C for Mn and 2000°C for Mg. ^e Nominal tube after-treatment temperature 900°C for CCl₄ and 1900°C for R14. ^f Maximum power heating. ^g Read command ON; 3 s before start of atomization stage magnet ON. ^h Argon or 6.5% (v/v) mixture of hydrogen in argon. ⁱ Filling the tubing between the programmer and the furnace prior to atomization. ^j Either R 14-gas (100 ml min⁻¹) or tetrachloromethane-saturated vapour (300 ml min⁻¹) was admixed into an internal argon flow (20 ml min⁻¹).

tilled water was used for the preparation of slurries and solutions.

Apparatus

In all experiments, a Perkin-Elmer 5000 Zeeman-effect corrected atomic absorption spectrometer, equipped with an HGA-500 graphite furnace atomizer, an AS-40 autosampler and a Model 3600 Data Station, and pyrolytic graphite-coated tubes with inserted fork-shaped platforms (Part No. BO 505057) were used.

Scanning electron micrographs of the platform surface were obtained with a Zeiss DSM 962 microscope applying magnification in the range 12–5000 \times at an accelerating voltage of 25 kV.

The microscope was also equipped with a Philips EDAX 9800 microprobe system for element-specific surface analysis.

Procedure

The preparation, homogenization and dispensing of the slurries were described in detail in a previous paper [3]. The spectrometric measurements were performed at the recommended analytical lines. At a certain stage in the programme, vapours of the halocarbons were introduced as an internal purge gas into the atomizer (see Table 1). A lower internal argon flow-rate was mixed with a stream of these gaseous modifiers in a Perkin-Elmer dual-channel accessory (Part No.

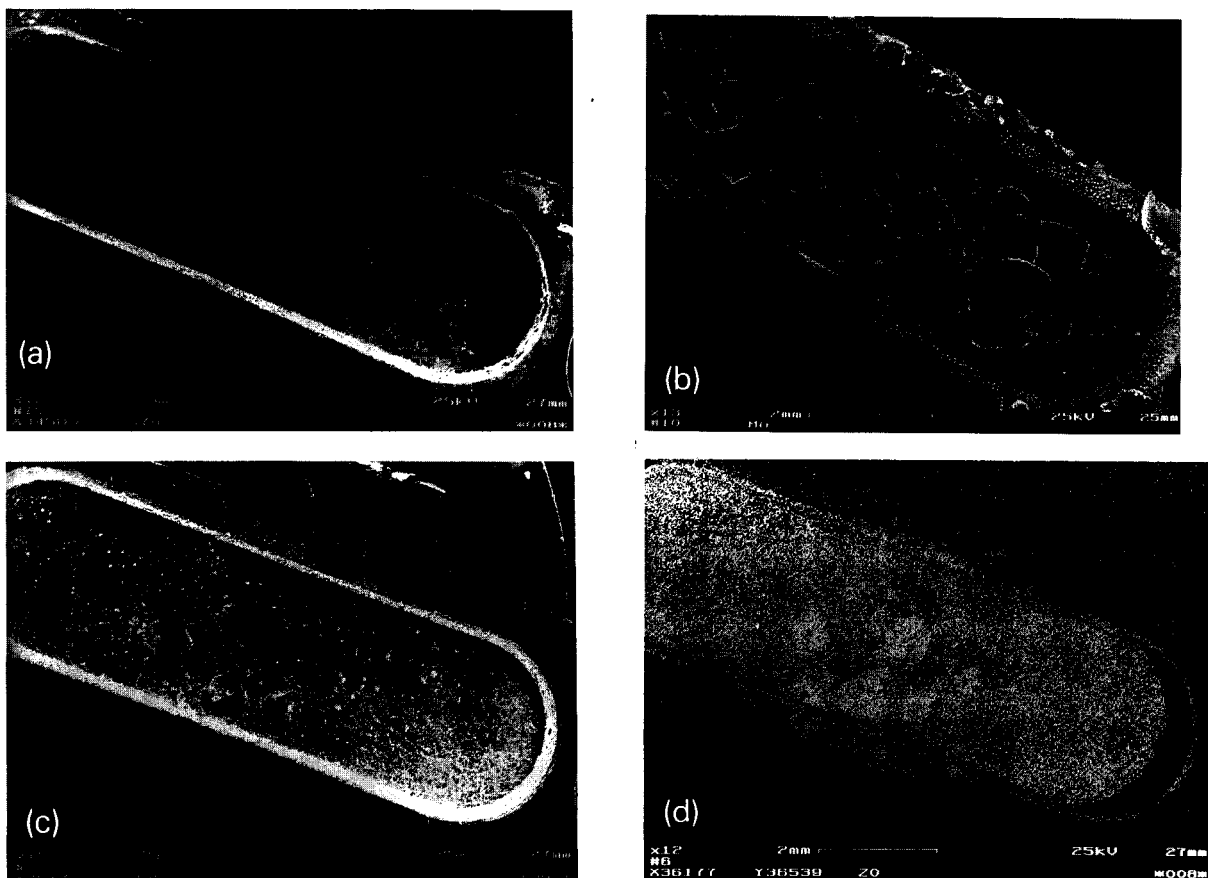


Fig. 1. Scanning electron micrographs of the platform surface after (a) 92 replicate atomizations of 0.2 mg of ammonium molybdate applied as a solution, (b) 120 replicates of 0.2 mg of molybdenum oxide supplied as a slurry, (c) 23 replicates of 0.2 mg of molybdenum silicide applied as a slurry and (d) complementary EDAX micrograph to (c).

290-0383) originally constructed for the introduction of the methane–argon mixture in the pyrolytic coating procedure. Analogously to the original purpose, the accessory was connected to the internal gas supply lines between the HGA controller and the furnace. The vapour of carbon tetrachloride was obtained by passing the argon through the liquid carbon tetrachloride contained in a wash-bottle. The mass flow-rate of this halocarbon was determined at room temperature by measuring the mass loss of the liquid phase and it was in good agreement with reported data [14] for the partial pressure of carbon tetrachloride (12 and 18 kPa at 20 and 30°C, respectively). The flow-rate was controlled by the pressure regulator of the argon cylinder and checked by a flow meter. Freon 14 was introduced into the dual-channel accessory directly from the steel cylinder. The flow-rate was controlled and measured in the same way as described for carbon tetrachloride.

For the gas-phase modification during the atomization stage, argon containing 6.5% (v/v) hydrogen was introduced by means of the HGA programmer.

RESULTS AND DISCUSSION

Build-up of refractory residue

In preliminary experiments in absence of halogenated gas modifiers (see Table 1; stages 6–9 were not involved), it was found that replicate executions of the procedure with solutions and with slurries of molybdenum-based materials (0.05–0.1 mg of Mo contained in aliquots of 20 μ l) resulted in the accumulation of the refractory matrix forming an inhomogeneous coating on the surface of the platform (see Fig. 1). This observation is in agreement with the reported macro behaviour of metallic molybdenum present or formed in a graphite oven [15]: it carburizes above 1100°C and it smelts above 2000°C with the formation of refractory molybdenum carbides. It was observed that the structure of the residue depended on the position of the sample on the platform, on the particle size and on the amount of the material introduced. A shiny surface was formed when molybdate solution was repeatedly

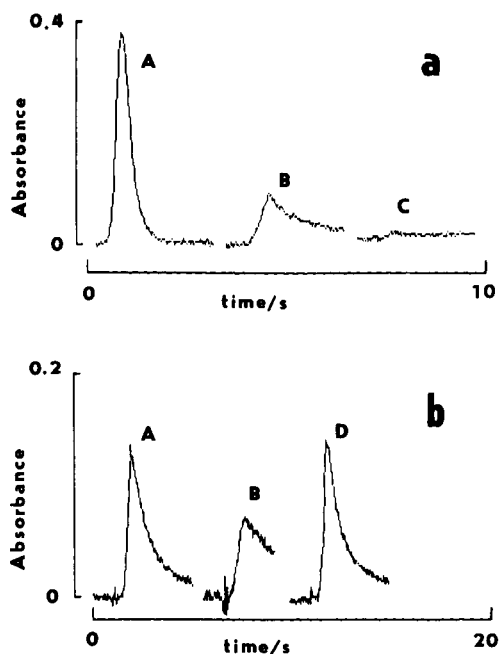


Fig. 2. Influence of replicate slurry introduction of molybdenum trioxide (0.2 mg) on the signal of (a) 0.2 ng of iron and (b) 0.5 ng of cobalt: (A) before any slurry injection; (B) and (C) after 34 and 120 runs, respectively; (D) signal trace obtained after 75 runs applying R14-assisted after-treatment.

processed. However, a cracked layer occurred at more than 80 replicates with molybdate solution or slurries of fine powders of molybdenum trioxide (mean particle size 3.7 μ m [3]). After twenty atomizations, a blistered structure appeared with powdered molybdenum silicide and molybdenum metal both having an average particle size of 40–50 μ m.

The formation of the refractory residue affected the properties of the atomizer resulting especially in a decrease of its lifetime (down to approximately 20 runs). For Co, Cr, Cu, Fe, Mn and Ni, progressive signal depressions, enhanced signal tailings and even signal distortions were observed. On the other hand, the signals of the alkali metals were not influenced. Some examples for the above-discussed interferences are given in Fig. 2. In addition, the sample aliquots could not be reproducibly positioned on the platform, owing to the formation of massive cracked layers

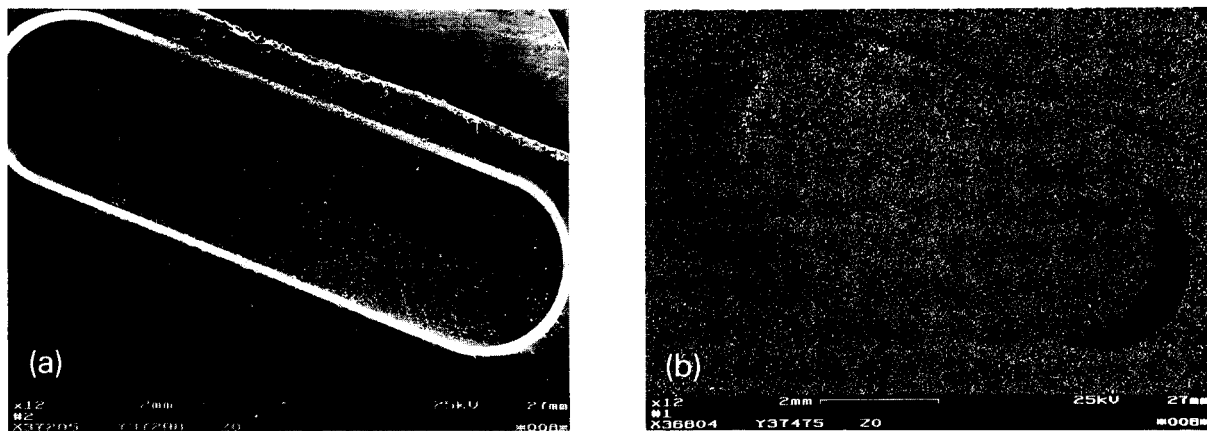


Fig. 3. (a) Scanning electron micrograph and (b) EDAX micrograph of platform surface after 61 replicate atomizations of 0.2 mg of molybdenum silicide dispensed as a slurry involving carbon tetrachloride-assisted after-treatment.

and of 'bridges' connecting the tube wall and the platform in the region of the sampling hole.

Halocarbon-assisted clean-out after-treatment

To avoid the interferences mentioned above, the residual refractory matrix components have to be removed from the tube. For this purpose, halogen-assisted volatilization may be considered as a suitable approach. Volatile molybdenum halides can be produced by reactions of molybdenum metal and molybdenum carbide with halogens and halocarbons at high temperatures [16,17].

Applying this principle, the removal of the molybdenum matrix (typically 0.1 mg of the matrix element) is only meaningful in the after-treatment stage, because the introduction of the reactive gas would cause considerable pre-atomization losses of many analyte elements by co-volatilization during the pretreatment stage and, in addition, it would give rise to interference, decreasing the atomization efficiency of the analyte elements [8,9,18]. This assumption was also demonstrated experimentally.

In the clean-out after-treatment, several temperature-dependent parameters affecting the effi-

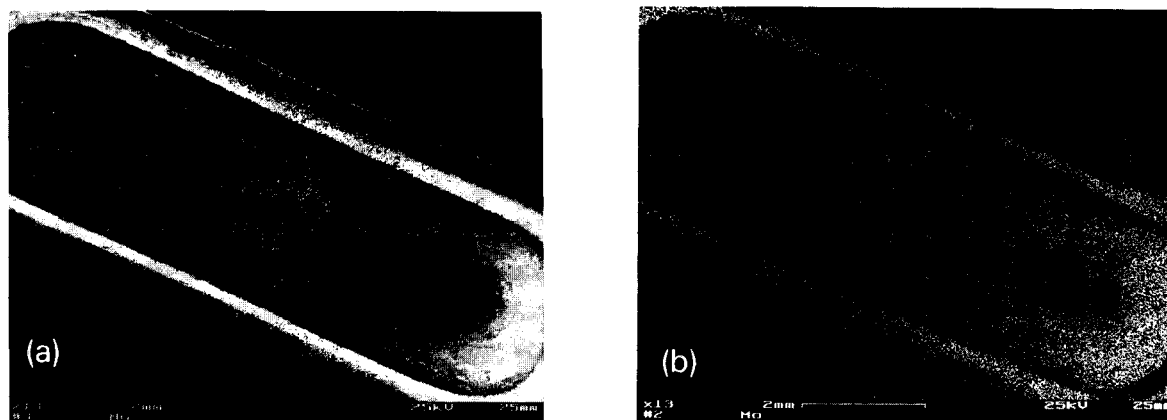


Fig. 4. (a) Scanning electron micrograph and (b) EDAX micrograph of platform surface after 76 replicate atomizations of 0.2 mg of molybdenum trioxide dispensed as a slurry involving carbon tetrafluoride-assisted after-treatment.

ciency of molybdenum removal must be considered. These parameters include the composition of pyrolytic products [13] (especially with respect to free halogens and pyrolytic carbon), thermal stability of molybdenum halides [19] and probability of reaction of halogens with the molybdenum matrix [17,19,20]. On the basis of the published data on these opposite temperature effects, compromise experimental conditions (given in Table 1, footnote j) were chosen for the halocarbons tested. The optimum after-treatment pyrolysis temperature should allow the achievement of as high as possible halogen yields and thermal stability of molybdenum halides and as low as possible pyrolytic carbon build-up. The amount of halocarbons required (given by the flow-rate and duration of introduction) was derived from the amount of sample to be dispensed (0.1 mg of molybdenum) and from the approximate reported reaction probability of 1/100.

Applying these conditions, the clean-out after-treatment procedure was successfully used for both halocarbons tested (see Figs. 3 and 4). Molybdenum-specific EDAX micrographs showed that there was almost no molybdenum on the surface of the after-treated platforms even if more molybdenum-based material was repeatedly dispensed, in contrast to the untreated platforms (compare Figs. 1d and Fig. 3b). Only negligible residue was observed at the cooler ends of the

platform cavity (see Fig. 4b) where the halogenation reaction took place slowly, probably owing to longitudinal temperature differences existing in this type of atomizer. If the sample mass was increased to 0.3 mg of molybdenum (0.5 mg of molybdenum oxide), a slight accumulation of the matrix residue was observed.

Influence of halocarbons on sensitivity

The signals of the analyte elements may be depressed by halogens [8,9,18] retained in form of pyrolytic products in the graphite furnace from a previous clean-out treatment. The analyte element can be lost in molecular form without being atomized, thus causing signal depression. Therefore, the effect of using halocarbons on the absorption signals of the analyte elements was investigated in more detail.

As expected, considerable depression of the signals was observed in the halocarbon-assisted experiments (see Table 1; stage 8 was not involved in the programme, hydrogen was not admixed in stages 2, 3 and 7). The extent of this interference was progressive with increasing number of after-treatments applied up to 4–5 runs, and with further increase in the number of runs it did not change significantly. The results for signal recoveries based on the evaluation of integrated absorbances of the depressed and original signals are given in Table 2. Further, it was observed that

TABLE 2

Recoveries of absorption signals obtained by halocarbon-assisted after-treatment in absence and presence of 6.5% (v/v) hydrogen in argon internal gas during the atomization stage

Element	Wave-length (nm)	Element mass (ng)	Sensitivity (pg per 1% absorbance) ^a	Signal recovery ^b			
				CCl ₄		CF ₄	
				No hydrogen	With hydrogen	No hydrogen	With hydrogen
Ca	422.7	0.02	–	–	–	< 0.1	0.42 ± 0.05
Co	242.5	0.5	14	< 0.1	0.85 ± 0.02	0.99 ± 0.03	1.00 ± 0.02
Cr	357.9	0.25	6.0	< 0.1	0.99 ± 0.03	0.11 ± 0.02	0.99 ± 0.04
Cu	324.8	0.5	18	0.24 ± 0.02	1.01 ± 0.04	0.80 ± 0.03	0.97 ± 0.02
Fe	248.3	0.2	7.7	–	–	0.72 ± 0.14	0.97 ± 0.03
Mg	285.2	0.01	0.36	< 0.1	0.22 ± 0.02	0.17 ± 0.03	0.99 ± 0.02
Mn	279.5	0.1	4.4	< 0.1	0.19 ± 0.05	0.56 ± 0.06	0.95 ± 0.02
Ni	232.0	1	24	–	–	0.09 ± 0.03	1.00 ± 0.02

^a Applying a 20- μ l aliquot of 1% (w/v) molybdenum oxide aqueous slurry and assuming 100% signal recovery. ^b Expressed as integrated absorbance ratio of the signal recorded after the preceding after-treatment and the original signal recorded prior to the after-treatment \pm standard deviation ($n = 5$).

the wettability of the platform surface decreased with the number of runs, probably owing to retained pyrolytic products. The acceptable charring temperature was also decreased down to approximately 300°C. This behaviour was not changed either by a prolonged blow-out stage (stage 7) or by involving an additional clean-out stage (stage 8). The original properties of the atomizer were restored after about 10–15 replicate runs without application of halocarbons (stages 6–9 were not involved). By separate experiments, it was demonstrated that no memory effects due to halocarbons in the tubing occurred.

Addition of hydrogen to argon during the charring stage has been reported as an effective modification for elimination of the interference caused by chlorides [21–24]. However, applying this procedure in the blow-out stage (stage 7) did not remove the retained halogens and, consequently, did not achieve the recovery of the signals. Nevertheless, as stated by L'vov [25], hydrogen forms relatively stable molecules with halogens and, via this process, equilibria can be shifted, causing a decrease in the concentration of free halogens in the gas phase during the atomization. The introduction of hydrogen into the argon (6.5%, v/v) during the atomization (stages 2 and 3) improved the signals considerably (see Table 2), especially if carbon tetrafluoride was used; except for calcium, the original signals were restored (for an example, see traces A and D in Fig. 2b). When using carbon tetrachloride, however, the gas-phase modification was not as efficient as in carbon tetrafluoride (see Table 2), probably owing to the more pronounced retention of chlorinated pyrolytic products in the atomizer.

Conclusion

In the analysis of molybdenum-based sample materials, a carbon tetrafluoride-assisted clean-out after-treatment has proved to be an effective tool for the removal of the residual molybdenum matrix from the graphite furnace. Including this additional stage, the analytical lifetime of the graphite furnace atomizer can be extended up to 200–300 runs, whereas without the after-treatment, signal depression takes place in a progres-

sive manner from the first runs. The introduction of carbon tetrafluoride as an alternate gas and its flow control is easy, also using conventional instrumentation. However, the internal gas must contain hydrogen during the atomization stage in order to reduce sufficiently interferences caused by adsorbed halogenated products on the graphite atomizer. The results obtained in this study suggest that the combined technique based on Freon-assisted after-treatment and hydrogen-assisted atomization is promising approach for the analysis of sample materials containing refractory carbide-forming matrix elements that form volatile halides. The applicability of this technique to further Freons–matrix combinations is under investigation.

Mr. W.H. Fritz, Sektion Elektronenmikroskopie, University of Ulm, is acknowledged for the scanning electron and EDAX micrographs. This work was supported by the Bundesministerium für Forschung und Technologie, Bonn, Germany.

REFERENCES

- 1 H.M. Ortner, W. Blödorn, G. Friedbacher, M. Grassbauer, V. Krivan, A. Virag, P. Wilhartitz and G. Wünsch, *Mikrochim. Acta*, 1 (1987) 233.
- 2 H.M. Ortner, *Fresenius' J. Anal. Chem.*, 343 (1992) 695.
- 3 B. Docekal and V. Krivan, *J. Anal. At. Spectrom.*, 8 (1993) in press.
- 4 D.L. Tsalev, V.I. Slaveykova and P.B. Mandjukov, *Spectrochim. Acta Rev.*, 13 (1990) 225.
- 5 J.P. Matousek and H.K.J. Powell, *Spectrochim. Acta*, Part B, 41 (1986) 1347.
- 6 G. Záray, T. Kántor, G. Wolff, Z. Zadegorska and H. Nickel, *Mikrochim. Acta*, 107 (1992) 345.
- 7 G.F. Kirkbright and R.D. Snook, *Anal. Chem.*, 51 (1979) 1938.
- 8 U. Hamm and K. Bächmann, *Fresenius' J. Anal. Chem.*, 315 (1983), 591.
- 9 B. Welz and G. Schlemmer, *At. Spectrosc.*, 9 (1988) 81.
- 10 G.F. Kirkbright and L.-X. Zhang, *Analyst*, 107 (1982) 617.
- 11 M. Huang, Z. Jiang and Y. Zeng, *J. Anal. At. Spectrom.*, 6 (1991) 221.
- 12 B. Hu, Z. Jiang and Y. Zeng, *Fresenius' J. Anal. Chem.*, 340 (1991) 435.
- 13 *Gmelin' Handbook of Inorganic Chemistry, Carbon, System No. 14, Part D2*, Springer, Berlin, 1974, pp. 92, 219, 355.
- 14 *Gmelin' Handbook of Inorganic Chemistry, Carbon, System No. 14, Part D2*, Springer, Berlin, 1974, p. 174.

- 15 Gmelin' Handbook of Inorganic Chemistry, Molybdenum, System No. 53, Vol. A3, Springer, Berlin, 1983, pp. 79–80.
- 16 Gmelin' Handbook of Inorganic Chemistry, Molybdenum, System No. 53, Verlag Chemie, Berlin, 1935, p. 196.
- 17 Gmelin' Handbook of Inorganic Chemistry, Molybdenum, System No. 53, Vol. A3, Springer, Berlin, 1983, pp. 60–63, 224.
- 18 W. Frech, E. Lundberg and A. Cedergren, *Prog. Anal. At. Spectrosc.*, 8 (1985) 257.
- 19 Gmelin' Handbook of Inorganic Chemistry, Molybdenum, System No. 53, Suppl. B5, Springer, Berlin, 1990, pp. 68, 245.
- 20 D.E. Rosner and H.D. Allendorf, *J. Phys. Chem.*, 69 (1965) 4290.
- 21 B. Welz, G. Schlemmer and J.R. Mudakavi, *Anal. Chem.*, 60 (1988) 2567.
- 22 G.F.R. Gilchrist, C.L. Chakrabarti, J.P. Byrne and M. Lamoureux, *J. Anal. At. Spectrom.*, 5 (1990) 175.
- 23 W. Frech and A. Cedergren, *Anal. Chim. Acta*, 82 (1976) 83.
- 24 W. Frech and A. Cedergren, *Anal. Chim. Acta*, 82 (1976) 93.
- 25 B.V. L'vov, *Spectrochim. Acta, Part B*, 33 (1978) 153.

End-on viewed inductively coupled plasma for the determination of trace impurities in high-purity scandium oxide by extraction chromatography

Xiao-Jin Yang and Jing-Su Guan

Analytical Chemistry Laboratory, Institute of Atomic Energy, P.O. Box 275 (88), Beijing 102413 (China)

(Received 21st April 1992; revised manuscript received 22nd January 1993)

Abstract

A sensitive method is described for the simultaneous determination of eighteen trace impurities in high-purity scandium oxide using an end-on viewed inductively coupled plasma (ICP) combined with an aerosol desolvation apparatus after the separation and preconcentration of the impurities. The operating conditions of the end-on viewed ICP were optimized and possible interferences caused by the matrix scandium in the end-on viewed plasma were studied. The chromatographic separation of trace amounts of impurities from large amounts of scandium, prior to the ICP atomic emission spectrometric (AES) measurements, using a trioctylphosphine oxide–Levextrel resin column was investigated. Satisfactory recoveries were obtained for impurities added to Specpure-grade scandium oxide, with average recoveries of 94–111% and precisions of better than 10% for most of the elements. The practical limits for determination were 0.08 (Mn)–4 $\mu\text{g g}^{-1}$ (Zn) for 0.1 g of sample. The results obtained for a high-purity scandium oxide sample by the proposed method agreed very well with those obtained by other techniques. The proposed separation procedure and the end-on viewed ICP-AES method are shown to have several advantages.

Keywords: Atomic emission spectrometry; Inductively coupled plasma spectrometry; Liquid chromatography; Extraction; Scandium oxide; Trace impurities

In recent years, scandium has become a material of scientific and technological significance, and has found important applications in the electronics industry and in atomic energy and laser techniques, etc. [1]. The levels of trace impurities in high-purity scandium oxide are important because of stringent quality control specifications, particularly in 99.99% scandium oxide used in laser rods ($\text{Gd}_3\text{Sc}_2\text{Ga}_3\text{O}_{12}$). For example, it is necessary to determine accurately 35 trace impurities in scandium oxide used for laser crystals in which the total content of the 35 impurities must

be less than 10 $\mu\text{g g}^{-1}$. However, few methods for the analysis of high-purity scandium oxide have been published.

Inductively coupled plasma atomic emission spectrometry (ICP-AES) has been widely applied to the determination of trace elements owing to its potential advantages of low detection limits, good precision and wide dynamic ranges of calibration. The direct determination of impurities in scandium oxide by ICP-AES has been reported [2]; however, the method is not suitable for high-purity scandium oxide of 99.99% purity because of the extremely low contents of the trace impurities and spectral and other physical interferences. Therefore, the separation of matrix scandium and preconcentration of the impurities are essential

Correspondence to: Xiao-Jin Yang, Analytical Chemistry Laboratory, Institute of Atomic Energy, P.O. Box 275 (88), Beijing 102413 (China).

in order to avoid such interferences and to improve the detectability. Ion-exchange systems have been applied for the separation of scandium from aluminium, iron, titanium, calcium and other cations [3–5], in which ion-exchange resins were used the column stationary phase and chelating organic reagents or salts such as NH_4SCN , $\text{CH}_3\text{COONH}_4$ and NH_4NO_3 as selective mobile phases. If ICP-AES is applied with these systems, large amounts of organic reagents or salts in the mobile phase cause clogging of the ICP torch and spectral interferences due to molecular bands such as CO, CN, OH, NH or SN [6]. In addition, concentrated salt solutions tend to influence the nebulization efficiency owing to their high viscosity. A liquid–liquid extraction method with tributyl phosphate (TBP) [7] was investigated, but the acidity of extraction was too high (13 M HNO_3) and the separation efficiency, expressed as enrichment factor, was only about 30.

Triethylphosphine oxide (TOPO) is a neutral organophosphorus extractant, that extracts scandium effectively and has been used for the extraction chromatographic separation of various cations [8–10] and of rare earth elements from scandium oxide [11]. Levextrel resin [12,13], which is a styrene–divinylbenzene-based copolymer combined with an organic extractant, has been extensively applied in extraction chromatography owing to its high separation efficiency [14–16]. In this work, the chromatographic behaviour of a

TOPO–Levextrel resin column with trace impurities and large amounts of scandium was investigated for separation purposes.

As it has been reported that an end-on (axially) viewed ICP gives lower detection limits than a conventional side-on viewed ICP [17–19] and that ICP coupled with aerosol desolvation further improves the detection limits for simultaneous multi-element analysis compared with that with no desolvation owing to the decreased background emission [20–22], an end-on viewed ICP set-up in conjunction with an aerosol desolvation apparatus (Fig. 1) was employed in this work.

EXPERIMENTAL

Apparatus

The experimental facilities used are outlined in Table 1. The end-on viewed ICP source in conjunction with the aerosol desolvation system is shown schematically in Fig. 1. The ICP torch was mounted on an X–Y–Z translator so that the central orifice of the torch pointed directly towards the entrance slit of the spectrometer. Optical observations were made through the exhaust hole of the plasma discharge. Radiation from the plasma was focused as a 1:1 image to the entrance slit of the spectrograph. An air cut-off stream was positioned below the plasma torch to

TABLE 1
Components of the experimental set-up

Component	Description
Spectrograph	Model W-100, 1-m plane grating spectrograph (Suzhou Optics), grating with 1200 grooves mm^{-1} , reciprocal linear dispersion 0.83 nm mm^{-1} , imaging with unit magnification on slit using a single condensing lens ($f = 75 \text{ mm}$), entrance slit width $12 \mu\text{m}$, height 1 mm, central wavelength 290.0 nm
r.f. generator	Quartz-controlled 27.12 MHz, 2.5 kW
Plasma torch	Fassel-type torch, positioned horizontally with axis coincident with optical axis (see Fig. 1)
Load coil	Two-turn copper tubing 6 mm diameter
Nebulizer	Pneumatic, concentric-type glass nebulizer
Air cut-off stream system	Glass device with slot-shaped orifice ($25 \times 0.5 \text{ mm}$); air cut-off stream pressure 0.55 kg cm^{-2} , flow-rate 60 l min^{-1}
Aerosol desolvation system	Temperature of heated spray chamber 180°C ; double-walled condenser cooled with tap water
Photographic plate	UV III and UV I type (Tianjin)
Microphotometer	Model M ϕ -2; S scale

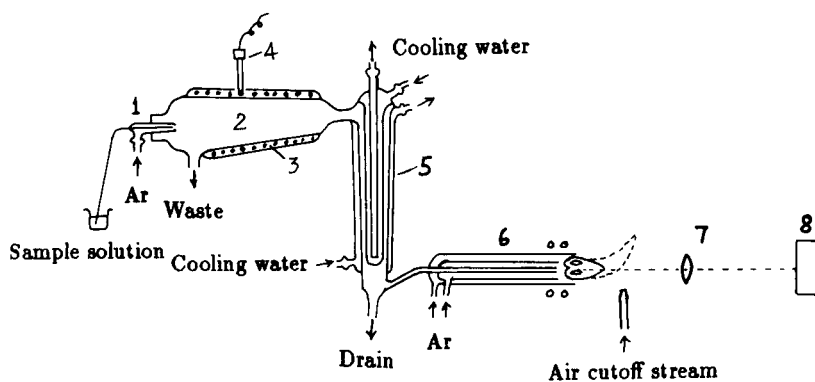


Fig. 1. Schematic diagram of the end-on viewed plasma set-up in conjunction with the aerosol desolvation system. 1 = Pneumatic, concentric nebulizer; 2 = heater spray chamber; 3 = heating coil; 4 = thermocouple; 5 = double-wall condenser; 6 = plasma torch; 7 = lens; 8 = spectrograph.

protect the focusing optics from thermal damage and to remove cooler absorbing atoms in the tail plume of the plasma which might cause self-absorption. The distance (22–25 mm) between the air cut-off stream and plasma torch was such that there was no discernible effect on the plasma tail flame. The sample introduction into the plasma was effected via pneumatic, concentric-type glass nebulizer combined with a streamline spray chamber (50 mm o.d. (big end) \times 25 mm o.d. (small end) \times 150 mm length quartz tube). The chamber was progressively wound with resistance wires (0.41 mm o.d., $30 \Omega \text{ m}^{-1}$). The temperature of the heated spray chamber was measured as a fixed position outside by a thermocouple and controlled by a temperature controller (temperature range 100–300°C). A double-walled glass condenser cooled with tap water was used to remove the water in the hot aerosol. UV III- and UV I-type photographic plates were used for recording spectra in the ranges 210–250 and 250–350 nm, respectively.

Reagents

Deionized water and guaranteed-reagent grade nitric acid (Beijing Chemicals) were further purified in a sub-boiling distillation quartz apparatus. Stock standard solutions of 1 mg ml^{-1} of individual elements were prepared from high-purity or Specpure metals or salts. The series of working standard solutions used for ICP-AES calibration were prepared by suitable dilution of the stock

standard solutions with 1 M nitric acid; the concentrations of the analytes are listed in Table 2.

The TOPO–Levextrel resin [TOPO loading 60% (w/w); 75–120 mesh] was supplied by Beijing Research Institute of Chemical Engineering and Metallurgy.

Specpure scandium oxide, obtained from Johnson Matthey Chemicals, was used as a base matrix for the study of elution behaviour and for recovery tests.

Preparation of chromatographic column

A 10-g amount of TOPO–Levextrel resin was packed into a borosilicate glass column (20 \times 1 cm i.d.) as a suspension in water. Before using the column, the resin was rinsed with 50 ml of water, 50–100 ml of 1 M HNO_3 and 30 ml of water (1 ml min^{-1}) in order to remove any metallic impurities. Before loading, the resin column was pre-equilibrated with 30 ml of 1 M HNO_3 .

TABLE 2

Concentrations of analytes in standard solutions used for ICP-AES calibration

Element	Concentration ($\mu\text{g ml}^{-1}$)							
	0.1	0.2	0.5	1	2	5	10	
Sn, Zn	0.1	0.2	0.5	1	2	5	10	
Ca, Al, Co, Fe,								
V, Cr, Ba	0.01	0.02	0.05	0.1	0.2	0.5	1	
Pb, Ni, Mg, Cd	0.02	0.04	0.1	0.2	0.4	1	2	
Cu, Mn, Ti, Sr, Be	0.002	0.004	0.01	0.02	0.04	0.1	0.2	

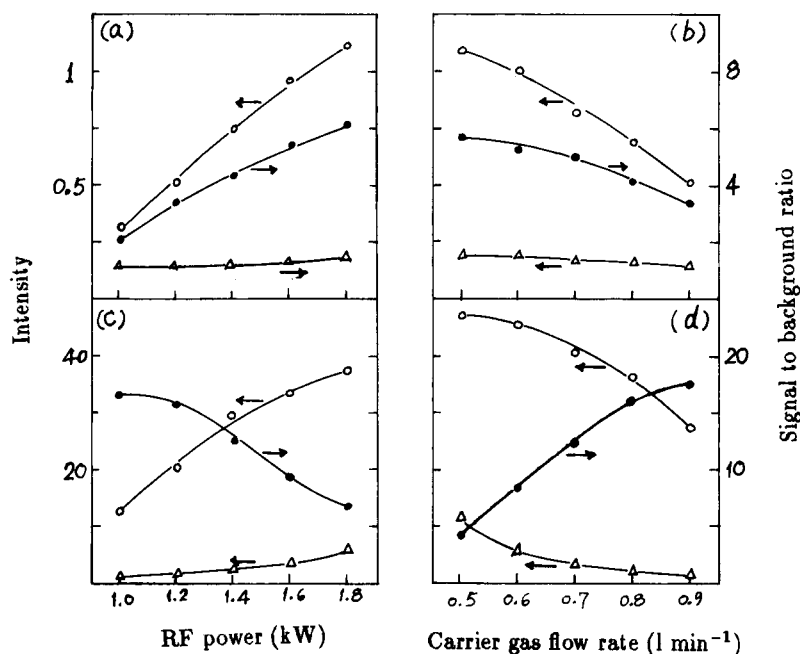


Fig. 2. Effect of r.f. power and carrier gas flow-rate on signal intensities, background levels and signal to background ratios. (a, b), Ni II 231.6-nm line; (c, d), Cu I 324.7-nm line. ○ = Signal intensity; △ = background intensity; ● = signal-to-background ratio.

Procedure for investigation of chromatographic separation

A typical procedure was as follows. An aliquot of solution (3 ml) containing 5–10 μg of each metal and 0.1 g of scandium oxide was poured on to the top of the resin and eluted with dilute nitric acid. Scandium was extracted by TOPO in the stationary phase and the metallic impurities were eluted with dilute nitric acid. The effluent was fractionated into 3-ml portions and the con-

centration of impurity elements was determined by ICP-AES. Subsequently, the extracted scandium was stripped with oxalic acid solution. Ten 10-ml fractions were collected and the scandium content in each fraction was determined by EDTA titrimetry [23] after eliminating the oxalic acid by evaporation with addition of 0.5 ml of concentrated perchloric acid to decompose the oxalic acid.

Wavelengths of analyte lines

The wavelengths of the analyte lines selected are given in Table 3.

TABLE 3

Analyte emission lines used for analysis

Element	Wavelength (nm)	Element	Wavelength (nm)
Zn I	213.8	Mg II	279.0
Cd II	226.5	Pb I	283.3
Co II	228.6	Sn I	286.3
Ba II	230.4	Al I	308.2
Be I	234.8	V II	311.0
Ni II	231.6	Ca II	317.9
Fe II	238.2	Ti II	323.4
Mn II	257.6	Cu I	324.7
Cr II	267.7	Sr II	346.4

RESULTS AND DISCUSSION

Optimization of operating conditions

The influence of desolvation temperature was investigated. On raising the temperature of the heated spray chamber from 120 to 250°C stepwise, the intensities of the analytes increased gradually from 120 to 160°C and remained constant in the range 160–200°C. In this work, the

temperature of the heated spray chamber was fixed at 180°C.

When viewing the plasma in the conventional side-on configuration, the analytical performance is affected by the parameters of coolant, auxiliary and carrier gas flow-rates, r.f. power and observation height above the load coil, and the control of these parameters is important because of the spatial dependence [24,25] that elements exhibit. For the same reason, the effect of these parameters, except observation height, on an end-on viewed plasma is also important. Therefore, the effect of plasma operating parameters was studied with the present end-on viewed plasma coupled with an aerosol desolvation system. Figure 2 shows the effect of r.f. power and carrier gas flow-rate on signal intensities, background levels and signal-to-background ratios (S/B) of the Ni II 231.6- and Cu I 324.7-nm lines. The signal intensity increased with increase in r.f. power and decreased significantly with increase in carrier gas flow-rate. The background level for the Ni II 231.6-nm line remains approximately constant over a wide range of ICP operating conditions (1.0–1.8 kW powers and 0.5–0.9 l min⁻¹ carrier gas flow-rates), whereas, the background intensity for the Cu I 324.7-nm line is strongly dependent on the power and carrier gas flow-rate, especially above 1.6 kW power and below 0.7 l min⁻¹ carrier gas flow-rate. Very similar results for the background level have been observed for the 200–250 nm and 300–350 nm region, respectively. This different behaviour of background level had a significant influence on S/B ratios, namely, the S/B ratio of the Ni II 231.6-nm line changed similarly with the signal intensity and that of the Cu I 324.7-nm line very differently to the Ni II 231.6-nm line. The S/B ratio behaviours similar to those of the Ni II 231.6-nm and Cu I 324.7-nm lines were observed for the Zn I 231.8-nm to Mn II 257.6-nm lines and for the Mg II 279.0-nm to Sr II 346.4-nm lines, respectively, listed in Table 3. Thus, the analytical lines in the region above 260 nm require a relatively high carrier gas flow-rate and low r.f. power for the best detection limits, whereas for those below 260 nm the best detection limits are attained at a lower carrier gas flow-rate and greater r.f. power. This trend with

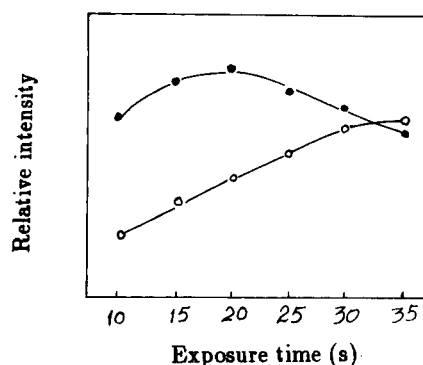


Fig. 3. Effect of exposure time on the line intensity. ○ = Ni II 231.6-nm line; ● = Cu I 324.7-nm line.

end-on viewing was the same with the side-on viewing. It was found from univariate studies that the flow-rates of coolant and auxiliary gas have no significant effect on the analytical signals. On the basis of previous experience, with 1.6- and 1.2-kW r.f. power, the coolant and auxiliary gas flow-rates remained at 16 and 1 and at 14 and 0.8 l min⁻¹, respectively. The effect of exposure time on the line intensity is shown in Fig. 3. The results of this multivariate optimization are given in Table 4. For the routine analysis of samples, a set of reasonable compromise parameters of r.f. power 1.3 kW, coolant, auxiliary and carrier gas flow-rates of 14, 0.8 and 0.75 l min⁻¹, respectively, and exposure time 20 s were used for simultaneous multi-element determinations.

Because the effect of the plasma parameters could be interdependent, it has been suggested

TABLE 4

Optimized parameters for simultaneous multi-element determination

Parameter	Wavelength (nm)	
	210–250	250–350
R.f. power (kW)	1.6	1.2
Argon gas flow-rate (l min ⁻¹):		
Coolant gas	16	14
Auxiliary gas	1	0.8
Carrier gas	0.6	0.8
Exposure time (s)	30	20

that the plasma parameters should be optimized simultaneously by the simplex method [26,27]. The values obtained were found to be similar to those from the univariate study.

The observation height above the load coil in the conventional side-on viewed plasma is another important parameter for simultaneous multi-element determination. When using an end-on viewing orientation, spectrum viewing was effected through the entire length of the central channel of the plasma discharge, so the plasma background emission was lower in magnitude owing to masking of the outer argon torus at the entrance slit, which, in turn, resulted in higher signal-to-background ratios and lower detection limits for most elements by factors of three to ten or even more. The above two advantages of the end-on over the conventional side-on viewed plasma have been emphasized previously [17,18]. Although the concept of observation height has no meaning in the end-on viewed configuration, the relationship between the entrance slit height of the spectrometer and the central tube orifice diameter of the ICP torch, which is shown schematically in Fig. 4, should be considered. This relationship has not previously been discussed in the literature [17,18]. In this experiment a central tube orifice diameter of 1.8 mm, rather than 1.2–1.5 mm of the conventional torch, was used for analytical purposes, because it created a larger diameter “hole” in the plasma discharge. Figure 5 shows the effect of the entrance slit height on the contribution of the Mn II 257.61-nm line intensity. It can be seen that a 3-mm entrance slit height resulted in an increased plasma background, probably owing to the entrance of surrounding bright torus. Hence the limited slit height was suitable for the end-on

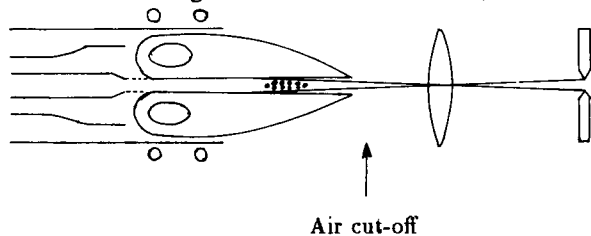


Fig. 4. Schematic diagram of the central tube orifice diameter of the plasma torch, the central channel diameter of plasma discharge and the entrance slit height.

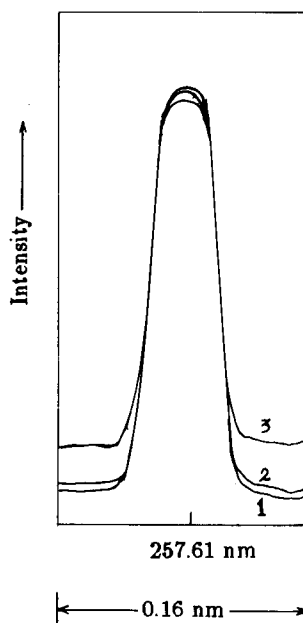


Fig. 5. Spectral profiles of Mn II 257.6-nm line with different entrance slit heights: (1) 1; (2) 2; (3) 3 mm.

construction, because the analyte emission, which was restricted in the narrow centre zone of the plasma discharge, could be selected from the surrounding bright torus-shaped background emission by the narrow slit height. In Kato et al.'s work [28], the slit height was limited to 500 μm . In this work, the entrance slit height was fixed at 1 mm for convenience.

Matrix effects on emission intensity

Another important factor when considering the emission intensity of an analyte signal is its susceptibility to inference. Demers [17] investigated the effects of $\text{Ca}_3(\text{PO}_4)_2$, Ca–Al and Na–K matrices in the end-on viewed plasma. Davies et al. [18] investigated the effect of phosphate on calcium in the end-on viewed plasma. Their results showed that the effects of the matrix in the end-on viewed plasma are greater than those in the side-on viewed plasma. In this work, the effect of scandium as the matrix on the analytes in the end-on viewed plasma was investigated. Figure 6 depicts the effect of different scandium concentrations in the range 0–100 $\mu\text{g ml}^{-1}$ on the emission intensities of 1 $\mu\text{g ml}^{-1}$ solutions of

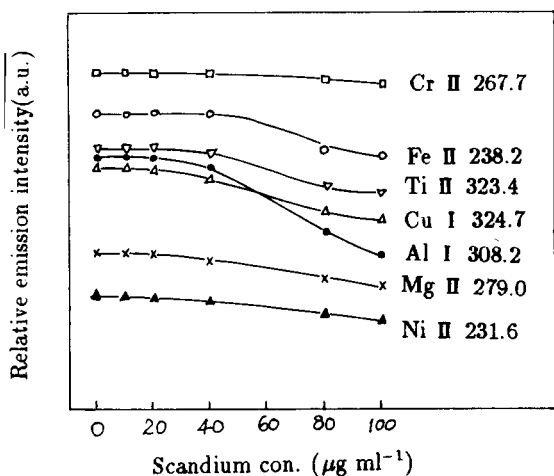


Fig. 6. Effect of scandium concentration on analyte emission intensities.

analyte ions (Ti and Cu $0.1 \mu\text{g ml}^{-1}$). Figure 7 shows the effect of r.f. power and carrier gas flow-rate on the emission intensities using $1 \mu\text{g ml}^{-1}$ analyte and $0\text{--}100 \mu\text{g ml}^{-1}$ scandium solutions. It can be seen that the lower the scandium

concentration, the more intense is the emission signal, with little effect on emission signal intensity between scandium concentrations of 10 and $40 \mu\text{g ml}^{-1}$, and the maximum signal intensities occurring for the analytes only. The intensities at the background positions show a considerable increase with increasing matrix concentration, which causes a larger decrease in net intensity with increasing matrix concentration. In particular, the line emission was completely annihilated by background emission caused by the matrix when the flow-rate of carrier gas was $< 0.6 \text{ l min}^{-1}$ and/or the r.f. power was $> 1.6 \text{ kW}$ in the presence of $100 \mu\text{g Sc ml}^{-1}$. Hence, when the end-on viewed plasma was used for simultaneous multi-element analysis, the matrix should be separated as completely as possible from the analytes so as to improve the detectability.

Chromatographic separation

A previous study [10] showed that scandium was effectively extracted with TOPO in the range $0.5\text{--}9 \text{ M}$ nitric acid, and with TBP at a concentra-

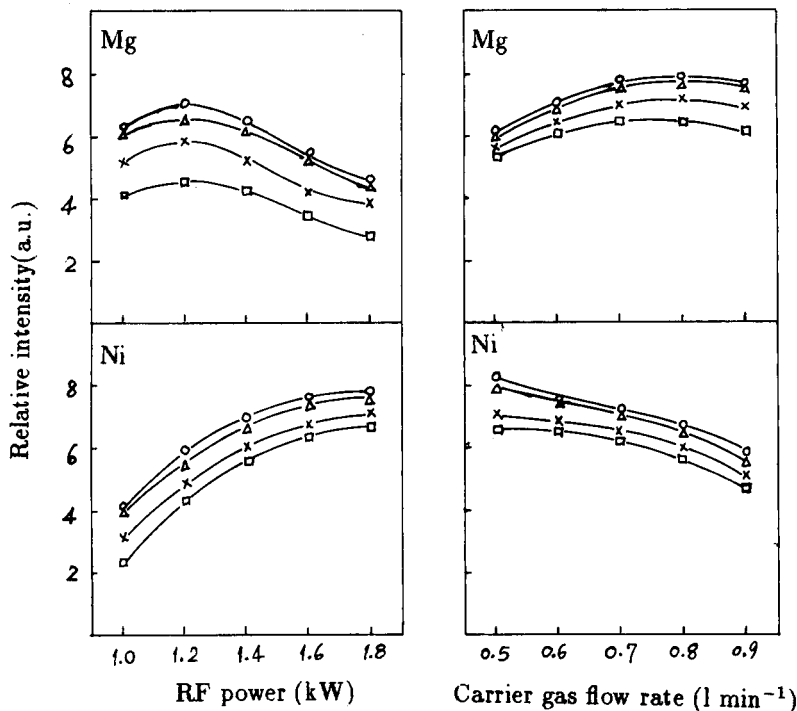


Fig. 7. Matrix effect on analytes as a function of the r.f. power and carrier gas flow-rate. Analyte concentration (Mg and Ni): $1 \mu\text{g ml}^{-1}$. Matrix scandium concentration: $\circ = 0$; $\Delta = 10$; $\times = 40$; $\square = 100 \mu\text{g ml}^{-1}$.

tion of > 9 M nitric acid. It has also been reported [7] that the extraction of scandium with TBP should be carried out in 13 M HNO_3 medium. Vijayalakshimi et al. [29] indicated that in 1 M HNO_3 , TOPO could quantitatively extract uranium leaving Al, Ba, Cd, Co, Cu, Mn, Ni, Pb, Sr, Ti, V, et c., in the aqueous phase. Therefore, in this work, TOPO was adopted for its higher extractability at lower acid concentrations. The chromatographic behaviour of the TOPO–Levextrel resin column was investigated as follows.

Different resin bed heights (10, 15 and 20 cm) were tested. The results showed that for 0.1 g of scandium oxide the scandium was not completely retained with 10- and 15-cm resin bed heights, but was completely complexed with a 20-cm bed height with no scandium being detected in the 50 ml of effluent (0.5–3 M HNO_3). Therefore, a 20-cm resin height was used in subsequent studies.

The effect of the concentration of nitric acid in the range 0.5–3 M as eluent was investigated. The results showed that scandium was quantitatively retained on the column and 30 ml of 1–3 M nitric acid were sufficient to eluate all the elements studied. The elution profiles for Al, Co, Cr, Fe and Ti with 1 M HNO_3 as eluent are shown in Fig. 8. Ba, Be, Ca, Cd, Cu, Mg, Mn, Ni, Sr and Zn showed the similar elution behaviours to Co

and Pb, and Sn and V similar to those for Cr, Fe and Ti. A similar elution behaviour with 2 and 3 M HNO_3 was observed. From Fig. 8 it can be seen that Al, Fe and Ti gave larger elution peak widths compared with Co. The elution peaks of all the elements studied with 1–3 M HNO_3 were sharp, but long tails with 0.5 M HNO_3 were observed for Ti and Cr. Hence 1 M HNO_3 was used for the elution of the impurities in subsequent experiments.

The effects of stripping agents on scandium were examined. Neither of the mineral acids studied (HCl and HNO_3) was effective for stripping the adsorbed scandium. Owing to the strong complexation of Sc^{3+} with $\text{C}_2\text{O}_4^{2-}$, oxalic acid was used as the stripping agent. The desorption curve for scandium with 0.5 M oxalic acid is shown in Fig. 8, which indicates that 80 ml of 0.5 M oxalic acid sufficient for desorption. The scandium eluates were collected for the recovery of scandium oxide, which is very expensive. The recovery of scandium oxide was over 99%. If an oxalic acid–ammonium oxalate mixture is used, the efficiency of stripping should be more satisfactory.

The effect of flow-rate was also examined. The flow-rate was varied from 0.5 to 1.5 ml min^{-1} . It was found that flow-rates of 1 M nitric acid up to 1 ml min^{-1} did not affect the retention of scandium and a stripping agent flow-rate of 0.5 ml min^{-1}

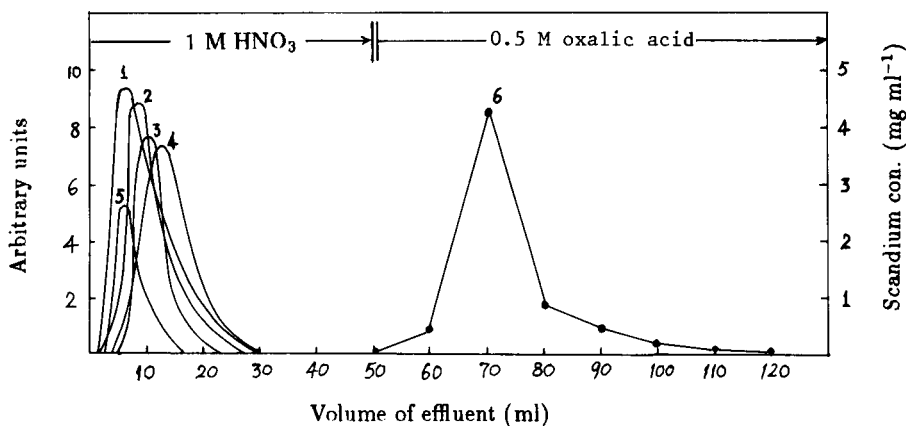


Fig. 8. Separation of impurities from scandium oxide with a TOPO–Levextrel resin column (20×1 cm i.d.). 1 = Cr; 2 = Fe; 3 = Al; 4 = Ti; 5 = Co; 6 = Sc. Loading, 5 μg of impurities and 0.1 g of scandium oxide; flow-rate, 1 ml min^{-1} for 1 M HNO_3 and 0.5 ml min^{-1} for 0.5 M oxalic acid.

min⁻¹ remained suitable. The total time required for separation is about 90 min.

The resins in the column could be regenerated by passing 40 ml of water through the column after elution with acid. It was found that the TOPO–Levextrel resin was stable and the separation procedure was carried out fifteen times using the same column with no decrease in of separation efficiency.

The eluate was analysed for scandium. The scandium concentration in the eluate was found to be < 0.1 $\mu\text{g ml}^{-1}$ for a freshly prepared column and < 1 $\mu\text{g ml}^{-1}$ for a regenerated column. In terms of the effect of the matrix on the analytes studied as above, it is seen that this low concentration of scandium will not interfere with the determination of the impurity elements by end-on viewed ICP-AES and the proposed separation conditions are satisfactory.

Analytical calibration

The linear regression calibration data for the determination of impurities by end-on viewed ICP-AES combined with aerosol desolvation under the conditions defined in Table 4 are presented in Table 5. The calibration data measured on different days were reproducible.

Final analytical procedure

A sample (0.1 g) was accurately weighed into a quartz beaker and dissolved in 1.5 ml of purified concentrated nitric acid by gentle warming on a hot-plate until the scandium oxide was completely dissolved. The solution was then evaporated nearly to dryness to remove excess acids and the residue was dissolved in 3 ml of 1 M HNO₃. The solution was passed through a chromatographic column previously pre-equilibrated with 1 M HNO₃. Scandium was extracted by TOPO in the stationary phase and the impurities were eluted with 30 ml of 1 M HNO₃ at a flow-rate of 1 ml min⁻¹. The 30 ml of effluent containing the analytes were collected in a PTFE beaker and concentrated to 2 ml in 1 M HNO₃. This 2 ml of solution was then analysed by the proposed ICP-AES method using the analyte lines selected in Table 3 under the operating condi-

TABLE 5

Linear regression of calibration data for the determination of impurities by ICP-AES

Element	Calibration range ($\mu\text{g ml}^{-1}$)	Slope ($\text{ml } \mu\text{g}^{-1}$)	Intercept	Standard deviation ($\mu\text{g ml}^{-1}$)	Correlation coefficient
Al	0.02–1	0.820	1.538	4.4×10^{-3}	0.9988
Ba	0.01–1	1.089	1.604	4.0×10^{-3}	0.9997
Be	0.002–0.2	1.136	2.406	6.1×10^{-4}	0.9993
Ca	0.01–1	1.186	1.390	1.8×10^{-2}	0.9921
Cd	0.04–2	1.078	1.129	6.2×10^{-3}	0.9993
Co	0.02–1	1.061	1.014	4.7×10^{-3}	0.9984
Cr	0.01–1	1.111	2.287	3.1×10^{-3}	0.9994
Cu	0.002–2	1.053	3.006	9.1×10^{-4}	0.9995
Fe	0.02–1	1.026	1.493	6.3×10^{-3}	0.9988
Mg	0.02–2	1.167	1.285	6.0×10^{-3}	0.9992
Mn	0.002–0.2	1.048	3.038	5.8×10^{-4}	0.9994
Ni	0.04–2	1.059	0.975	5.4×10^{-3}	0.9994
Pb	0.04–2	1.003	0.796	5.3×10^{-3}	0.9996
Sn	0.2–10	1.061	1.362	3.9×10^{-2}	0.9989
Sr	0.004–0.2	1.185	2.473	5.9×10^{-4}	0.9979
Ti	0.002–0.2	1.006	2.864	9.8×10^{-4}	0.9985
V	0.01–1	1.024	2.554	3.8×10^{-3}	0.9990
Zn	0.2–10	1.369	0.453	2.9×10^{-2}	0.9990

tions defined in Table 4. Experimental blanks were prepared similarly.

Blank and limit of detection

In order to evaluate the blank contamination and the detection limits, six replicate blank procedures were carried out. For each metal, no sample solution was loaded on the column during the separation and preconcentration sequence, but all the other steps were the same. The blanks means “total blank”, including the resin blank, the dissolution acid blank, the elution blank and the contamination during the concentration procedure. The experimental blank values obtained were equivalent to 0.15 $\mu\text{g ml}^{-1}$ for Ca, 0.1 $\mu\text{g ml}^{-1}$ for Fe and 0.04 $\mu\text{g ml}^{-1}$ for Al, which are often subject to contamination from the laboratory environment, and were negligibly small for the other elements. The detection limits, defined as three times the standard deviation of the blank, are given in Table 6. In order to provide a realistic estimate of the lower levels of detectability, we employed the lowest quantitatively determinable concentration (LQD) calculated from the blank

TABLE 6

Detection limits, lowest quantitative determinable concentration (LQD) of impurities in high-purity scandium oxide after separation and preconcentration and the specification values for high-purity scandium oxide

Element	Detection limit ($\mu\text{g ml}^{-1}$)	LQD ^a ($\mu\text{g g}^{-1}$)	Specification value ^b ($\mu\text{g g}^{-1}$)	
			99.99% ^c	99.9995% ^c
Al	0.04	0.8	10	2
Ba	0.007	0.4		
Be	0.0004	0.08		
Ca	0.15	2.9	50	5
Cd	0.005	0.8		
Co	0.006	0.4	5	1
Cr	0.002	0.4	5	1
Cu	0.0008	0.1	5	1
Fe	0.1	2	10	3
Mg	0.004	0.8	5	2
Mn	0.0004	0.08	5	1
Ni	0.006	0.8	5	1
Pb	0.008	5	5	2
Sn	0.05	4	5	1
Sr	0.0008	0.08		
Ti	0.0006	0.08	10	1
V	0.001	0.4	10	2
Zn	0.06	4	5	3

^a Calculated for 0.1 g of sample in final 2-ml volume. ^b Presented by Human Research Institute of Rare Earth Metal Material. ^c Relative purity of scandium oxide ($\text{Sc}_2\text{O}_3/\text{rare earth oxides}$).

value and the concentration of the lowest point on the linear calibration graphs. The LQDs, expressed as $\mu\text{g g}^{-1}$ with respect to the mass of scandium oxide, together with the specification values for high-purity scandium oxide, are given in Table 6. It can be seen that the LQDs are well below the specification values for impurities in high-purity scandium oxide with 99.99–99.9995% purity, so the present detection power in real sample analyses is effective. Owing to the influence of the blank values, the LQD values for Ca, Fe and Al were relatively high. Therefore, to improve the LQD values, it is important that the blank values be reduced. It should be pointed out that an increase in the mass of the sample taken and the length of the resin of the column can further decrease the LQD values.

Accuracy and precision

First, the proposed method was applied to the analysis of Specpure scandium oxide and the results are given in Table 7. Synthetic sample solutions were then prepared from the analysed Specpure scandium oxide, and the accuracy and precision of the proposed procedure were assessed by measuring the recoveries and relative standard deviations for these synthetic sample solutions. Six Specpure scandium oxide samples (0.1 g) were dissolved in 1.5 ml of concentrated nitric acid, to which impurity solutions (containing 0.02–2.5 μg of metals) were added. The subsequent procedure was as described above. The analytical data and recoveries for the six experiments are given in Table 7. For the six experiments, the average recoveries of impurities are in range 94–111% and the precision, expressed as the relative standard deviation (R.S.D.), is better than 10% for most of the elements.

Because of the lack of a certified standard reference material for trace metals in scandium oxide, the accuracy was also estimated by com-

TABLE 7

Recoveries of impurities added Specpure scandium oxide and relative standard deviation ^a

Element	Impurities ($\mu\text{g g}^{-1}$)			Recovery (%)	R.S.D. (%)
	Initial	Added	Found		
Al	2.05	4.0	6.25	106	11
Ba	0.44	2.0	2.5	103	4
Be	< 0.08	0.20	0.20	100	5
Ca	19.6	25.0	47.1	110	13
Cd	< 0.8	2.0	2.05	103	5
Co	< 0.4	1.0	1.01	101	7
Cr	0.46	1.0	1.50	104	4
Cu	0.53	2.0	2.47	97	8
Fe	17.9	25.0	43.3	102	11
Mg	< 0.8	2.0	2.20	110	7
Mn	0.42	2.0	2.56	107	5
Ni	4.76	20.0	26.8	110	3
Pb	0.86	2.0	3.06	110	5
Sn	< 4	10.0	11.1	111	4
Sr	< 0.08	0.2	0.19	95	7
Ti	0.50	2.0	2.52	101	9
V	< 0.4	1.0	1.02	102	14
Zn	5.13	10.0	15.5	104	4

^a Mean results and R.S.D. for $n = 6$.

TABLE 8

Comparison of analytical results ($\mu\text{g g}^{-1}$) for a high-purity scandium oxide sample obtained by the proposed method and by other methods

Element	This work ^a	TBP–AES ^b	TBP–AAS ^c	SSMS ^d
Al	4.46 ± 0.05	4.65	4.79	
Ba	0.47 ± 0.04			
Be	< 0.08			
Ca	34.5 ± 4.7	33.2	31.4	
Cd	< 0.8			
Co	0.59 ± 0.02	0.62	0.56	< 1.0
Cr	2.56 ± 0.10	2.80	2.88	
Cu	0.34 ± 0.03	0.35	0.31	< 0.5
Fe	48.0 ± 2.6	49.1	52.1	
Mg	6.24 ± 0.15	6.30	5.02	
Mn	0.24 ± 0.03			
Ni	3.26 ± 0.07	3.28	3.06	
Pb	56.4 ± 1.8	56.9	58.4	60.0
Sn	< 4			
Sr	0.061 ± 0.01			
Ti	2.23 ± 0.05	2.52		
V	< 0.4			
Zn	20.1 ± 0.54			

^a Mean ± S.D. ($n = 6$). ^b a.c. arc emission spectrometry combined with TBP extraction chromatography. ^c Atomic absorption spectrometry combined with TBP extraction. ^d Spark-source mass spectrometry.

paring the analytical results obtained by the proposed procedure with those obtained by other techniques. The results are presented in Table 8 and show good agreement.

Conclusions

End-on viewed ICP-AES combined with TOPO–Levextrel resin chromatography was effectively applied to the determination of trace metal impurities in high-purity scandium oxide of 99.99–99.9995% purity. Extraction chromatography with the TOPO–Levextrel resin column was found, after optimizing the parameters affecting the separation process, to be simple, rapid and highly efficient for the separation of impurities from scandium oxide prior to analysis by ICP-AES. The proposed separation procedure has great advantages over ion-exchange methods because it does not require the use of specific reagents or salts for elution, and over TBP liquid–liquid extraction with respect to the acid

concentration in the separation and the speed and efficiency of the separation procedure.

The end-on viewed ICP detection technique offers advantages in analytical performance over the conventional side-on viewed ICP in optical configuration. The former technique also offers some advantages with regard to instrumental arrangement over other modern instrumental approaches with ICP sources, e.g., ICP–MS, the great expense of which has limited its use. Finally, it should be pointed out that if the end-on viewed ICP source is equipped with a modern spectrometer and photomultiplier detector, the wider calibration range, superior detection limits, higher speed and better precision should be attainable.

The authors thank Mr. X.-L. Zhang and Mr. T.-X. Zhang, Beijing Research Institute of Chemical Engineering and Metallurgy, for TBP extraction chromatography–a.c. arc emission spectrometric and TBP extraction–atomic adsorption spectrometric analyses, respectively, Professor B.-L. Li for spark-source mass spectrometric analysis, Associate Professor F.-Z. Qin for valuable discussions, Professor L.-Y. Jin, Director, for his encouragement and Professor Z.-M. Gu for language correction.

REFERENCES

- 1 J.-Y. Hwang, *Rare Earth* (in Chinese), 2 (1988) 49.
- 2 H.-P. Zhong and J.-L. Wang, *SpectroLabo*, 8 (1991) 36.
- 3 J. Sherma and F.J.V. Lenten, *Sep. Sci.*, 6 (1971) 199.
- 4 H. Hamaguchi, R. Kuroda, K. Aoki and R. Sugisita, *Talanta*, 10 (1963) 153.
- 5 M. Chakravorty and S.M. Khopkar, *Chromatographia*, 10 (1977) 100.
- 6 R.K. Winge, V.J. Peterson and V.A. Fassel, *Appl. Spectrosc.*, 33 (1979) 206.
- 7 R.L. Slyusareva, L.I. Kondrateva, A.B. Sokolov and Z.P. Maksimova, *Zh. Anal. Khim.*, 37 (1982) 237.
- 8 E. Cerrai and C. Testa, *Energ. Nucl. (Milan)*, 8 (1961) 510.
- 9 E. Cerrai and C. Testa, *J. Chromatogr.*, 9 (1962) 216.
- 10 J.W. O'Laughlin and C.V. Banks, *Anal. Chem.*, 36 (1964) 1222.
- 11 L.-Y. Li, J.-Q. Ma and G. Jin, *Fenxi Huaxue*, 16 (1988) 357.
- 12 R. Kroebel and A. Meyer, *Ger. Offen*, 2162951 (1973).
- 13 H.W. Kauczor, *Hydrometallurgy*, 3 (1978) 65.
- 14 L.-Y. Dong, *Uranium Min. Metall.*, 4 (1985) 33.

- 15 T.-B. Qian and W.-L. Liu, *Fenxi Shiyanshi*, 8 (1989) 28.
- 16 Y. Guan and X.-X. Wu, *Ion Exchange Adsorpt.*, 6 (1990) 60.
- 17 D.R. Demers, *Appl. Spectrosc.*, 33 (1979) 584.
- 18 J. Davies, J.R. Dean and R.D. Snook, *Analyst*, 110 (1985) 535.
- 19 A. Danielson, *ICP Inf. Newsl.*, 4 (1978) 147.
- 20 J.P. Rybarczyk, C.P. Jester, D.A. Yates and S.R. Koirtzohann, *Anal. Chem.*, 54 (1982) 2162.
- 21 K.W. Olson, W.J. Haas, Jr., and V.A. Fassel, *Anal. Chem.*, 49 (1977) 632.
- 22 X.-E. Shen and Q.-L. Chen, *Spectrochim. Acta, Part B*, 38 (1983) 115.
- 23 S.-C. Hung and S.C.-Liang, *Chem. Acta*, 30 (1964) 1.
- 24 M.W. Blades and G. Horlick, *Spectrochim. Acta, Part B*, 36 (1981) 861.
- 25 P.W.J.M. Boumans and F.J. DeBoer, *Spectrochim. Acta, Part B*, 27 (1972) 391.
- 26 S.P. Terblanche, K. Visser and P.B. Zeeman, *Spectrochim. Acta, Part B*, 36 (1981) 293.
- 27 S.N. Deming and S.L. Morgan, *Anal. Chem.*, 45 (1973) 278A.
- 28 T. Kato, T. Uehiro, A. Yasuhara and M. Morita, *J. Anal. At. Spectrom.*, 7 (1992) 15.
- 29 S. Vijayalakshmi, R.K. Prabhu, T.R. Mahalingam and C.K. Mathews, *J. Anal. At. Spectrom.*, 7 (1992) 565.

Wet digestion of vegetable tissue using a domestic microwave oven

Miguel-Angel Mateo and Santiago Sabaté

Departament d'Ecologia, Universitat de Barcelona, Av. Diagonal 645, 08028 Barcelona (Spain)

(Received 5th October 1992)

Abstract

A rapid, accurate, precise and inexpensive method for the wet digestion of vegetable materials is proposed. A conventional microwave oven was used as the energy source. Total phosphorus, calcium, magnesium, potassium and sulphur were determined by inductively coupled plasma atomic emission spectrometric techniques. A varied assortment of plants (algae, seagrasses, freshwater plants and terrestrial plants) and plant parts (leaves, wood, rhizomes, roots and bark) were digested to test the inter- and intra-assay method precision and the effects of the characteristics of the material on its efficiency. Three standards (NBS SRM Pine Needles and Citrus Leaves and the intercalibration sample from the Forest Research Institute of New Zealand *Pinus radiata* leaves) were also digested to test the accuracy of the method. All samples were totally digested after 20 min or less. The values found for standards coincided in all instances with the certified values. The average recovery was 97.2% and ranged from 81.3% to 114.5%. The variability of the method, in terms of the standard deviation of the mean, varied from 3.0% (Ca) to 9.72% (K). Practical considerations such as instrument availability and purchase price, operating costs, acid volume needed and especially the number of samples processed per hour were compared between the present method and classical methods using conventional heaters. Safety aspects are considered.

Keywords: Atomic emission spectrometry; Inductively coupled plasma; Sample preparation; Microwave digestion; Plant materials; Vegetable tissues; Wet digestion

Many plant ecology experiments involve total phosphorus, calcium, magnesium, potassium and sulphur determinations in different parts of the plant. Experimental designs usually require the processing of a large number of samples, which represents one of the most time-consuming steps of the whole experiment. The plant ecologist in search of a suitable digestion procedure may find a wide range of methods in the specialized literature. However, sophisticated and often complicated laboratory routines are found. Practical considerations, such as instrument availability and

purchase price, operating costs, skill or experience requirements of the analyst, number of samples processed per hour and accuracy and precision, determine the choice [1]. Hot sand-baths or metal block heaters take several hours to digest a very limited number of samples. Glass digestion vessels are expensive and fragile and acid fume evacuation is always a nuisance.

Since Gleit and Holland [2] made the first attempts to decompose organic substances using radiofrequency discharges, methods using microwave radiation have been continuously developed as an alternative to conventional heaters. Nowadays, microwave ovens are being used successfully for wet digestion purposes. Although sophisticated laboratory microwave ovens are

Correspondence to: M.-A. Mateo, Departament d' Ecologia, Universitat de Barcelona, Av. Diagonal 645, 08028 Barcelona (Spain).

available, simple domestic configurations can be designed. Barret and Davidowski [3] made some practical advances by using a Pyrex box inside a commercial microwave oven vented by a Nalgene aspirator. In this paper a new variation is proposed using a round domestic Pyrex container with a cover, and a simple system to load up to 25 samples at a time and that minimizes dead spaces. Acid fumes are aspirated by an ordinary water vacuum pump connected to the Pyrex container by Teflon tubing. Samples are digested in small resistant Teflon FEP (fluorinated ethylene propylene) bottles. Elemental analysis is performed using inductively coupled plasma atomic emission spectrometric (ICP-AES) techniques.

The NBS Standard Reference Materials (SRM) 1572 Citrus Leaves and 1575 Pine Needles and a wide range of botanical samples (see Table 3 for a list of samples) were analysed using this configuration, and satisfactory accuracy and precision levels were obtained.

EXPERIMENTAL

Apparatus

A Sanyo EM-840 domestic microwave oven with a rotary tray and a maximum power rating of 750 W (length and width 35 cm, height 25 cm) was used as energy source for the acid digestion.

Elemental analysis was performed at the Serveis Científico-Tècnics, Barcelona University, using JobinYvon JI-38 (3600 grooves mm^{-1}) and multi-channel Thermo Jarrel Ash Polyscan 61E (2400 grooves mm^{-1}) inductively coupled argon plasma emission spectrometers with special channels for K, Li and Na.

Reagents

All sample dilutions were made with deionized water of $18 \text{ M}\Omega \text{ cm}^{-1}$ resistivity obtained from a Milli-Q water purification system. HNO_3 (60%) and HClO_4 (60%) of analytical-reagent grade were used for digestion of samples.

Procedure

Samples and SRMs were oven dried at 70°C for 48 h then milled with a Tecator Cyclotec 1090

sample mill with a 0.4-mm screen and oven dried again at 70°C for 24 h. The samples were then allowed to cool to laboratory temperature in a desiccator, before weighing. About 0.1 g of sample was weighed on a Mettler AE200 analytical balance (0.1–205 g). The material was then placed in 50-ml Nalgene FEP Teflon bottles (Cent Tubes, Oak Ridge, FEP 3114-0050). Some sample particles may stick in the neck of the bottle. Nevertheless, appropriate reflux achieved during the digestion incorporates these particles with the rest in the bottom of the bottle. The bottles should be perfectly dry to minimize this.

A 1.3–2.0-ml volume of a mixed acid solution [nitric acid–perchloric acid (10 + 4)] was added to each 0.1-g sample using a Pressmatic 2000 dispenser (0.2–1.0 ml) from J. Bibby Science Products. This ratio of acid volume to sample weight coincided with the safety margin estimated by Abu-Samra et al. [4] 10 ml for every 0.5 g of sample. H_2SO_4 was not used in the solution to avoid calcium sulphate precipitation [5] and to permit sulphur determination. Three reagent blanks were included in every digestion programme. The bottles were gently agitated to obtain a homogeneous mixture between acids and materials. It is recommended that acids react with samples for several minutes before exposing them to microwave radiation in order to prevent violent exothermic reactions between perchloric acid and organic matter [6]. Insufficiently milled material may cause explosions.

The bottles were buried to about half their height in a Pyrex container (height 15 cm, diameter 25 cm) containing suitable amounts of fine sand. This procedure eliminates almost all of the dead space facilitating acid fume evacuation. Twenty-five samples were loaded each time, the limit imposed by the size of the container. The container was then closed with the bottles remaining opened inside it. No vacuum is created in the container as it is not airtight. Teflon tubing of 1.5 cm i.d. connected the container to an ordinary laboratory glass water vacuum pump for fume extraction purposes. The flux created efficiently removed fumes from the container and prevents leakage to the oven cavity. Although acid fumes are diluted in water during the aspira-

tion, the use of an acid fume scrubber containing 2 M KOH solution is recommended to avoid piping corrosion [3]. Suitable holes were drilled in the middle of the container cover and on one side of the oven. Microwave radiation leakage must be checked periodically for all parts of the configuration. A 3-cm diameter hole was reported by Barret and Davidowski [3] to show no significant radiation emissions. The 1.5-cm hole and the remainder of the system were exhaustively checked every month showing no significant leakage. Teflon angles and joints were used to assemble the configuration. Connection with the container was made in such a way that allowed it to rotate with the oven tray. This connection must be designed to be easily released from the cover.

Before starting digestion programmes, all interior surfaces of the oven, including electronics and lamps, were protected from possible acid fume leakage. For this purpose, Turbo Lube synthetic lubricant spray with Teflon particles was used. It must be totally replaced at least every week. A Pyrex vessel with deionized water must be placed in the oven to prevent it from working with little or no microwave sink. Water must be replaced every digestion programme. The last two measures will considerably increase the oven life [4].

All the configuration must be placed in a fume-hood to maximize safety conditions. In Fig. 1, a simplified scheme of the configuration is shown. Both the fume-hood extractor and water pump must be running before exposing samples to microwaves. The pump water flux and microwave power allowed a satisfactory balance to be obtained between acid evaporation and fume reflux within the bottles [4]. The digestion programmes used are shown in Table 1. Although the process requires little supervision, it needs extreme care during the first attempts. At the end of the process it is recommended to wait for several minutes to allow the system to cool, then the Teflon tubes can be safely manipulated. The content of the bottles will appear completely clear with very little acid (mainly HClO_4) remaining. Another exposure programme was used for incompletely digested samples, setting about one-third the exposure time and adding about half the

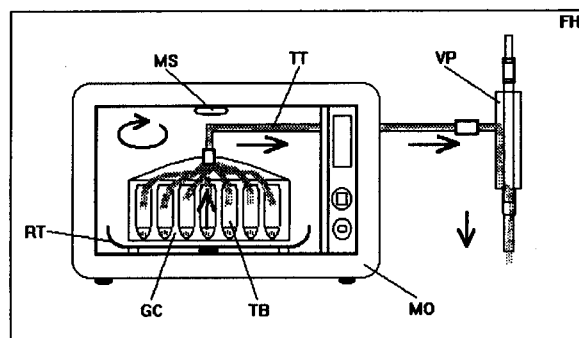


Fig. 1. Scheme of the proposed configuration. FH = fume hood; MS = microwave source; TT = Teflon tubing; VP = vacuum water pump; RT = Pyrex glass rotary tray; GC = Pyrex glass container; TF = Teflon bottles; MO = domestic microwave oven. The arrows show acid fume flux. Sand has been omitted for clarity.

volume of the mixed acid solution if necessary. It is also recommended to add 0.5–1 ml of HClO_4 or of mixed acid reagent after digestion to keep all elements in solution. The standards for elemental analysis must include the same acid proportion. Deionized water was added with a Dispensette Brand dispenser (0–10 ml) to dilute to a final volume of 20 ml, giving, for the treated samples, an appropriate elemental concentration for ICP-AES analysis. A slight green-yellow colour is accepted as a normal feature (remains of HNO_3).

Finally, the Teflon bottles were tightly closed and vigorously shaken before transferring the dilution to 50-ml polyethylene vessels for storage.

TABLE 1

Microwave digestion programmes used ^a

Sample	First		Second	
	Power (%)	Time (min)	Power (%)	Time (min)
Algae	75	15	None	None
Spermatophyta				
leaves	100	15	75	5
rest of parts	100	25	75	5

^a 100% is a power rating of 750 W. The rest of parts of the plants includes rhizomes, roots, wood and bark. The second programme is used for samples incompletely digested after the first one.

The final diluted solutions appeared to be stable for at least 1 month with no special storage conditions. The reproducibility of calcium values for ICP determination seemed to be better when the samples were stored in a refrigerator at 5°C.

No further steps were required for elemental analysis. The wide sensitivity range of the ICP-atomic emission spectrometers allowed the same dilution to be used for the five elements measured. The wavelengths used were 213.618 nm with the monochromator ICP and 178.287 nm with the polychromator for phosphorus. Both spectrometer systems were intercalibrated for phosphorus determination, giving identical results. The remaining elements were determined only with the multi-channel ICP-AES system: Ca 317.933, Mg 279.079, K 766.491 and S 182.040 nm. A high solids content nebulizer was used, making the filtration of dilutions unnecessary; a high-flow torch was selected. The output power was 1150 W; the auxiliary argon flow-rate was 0.5 l min⁻¹ and the nebulizer argon pressure was set at 30 p.s.i.

RESULTS AND DISCUSSION

All samples were digested in 20 min or less. Samples with high fibre content such as rhizomes,

roots, wood and bark, in general needed to be treated with the two exposure programmes; algae and plant leaves were totally dissolved after the first one.

The rotary configuration totally overcame hot-spot problems [7]. The use of Teflon bottles eliminated the problems of acid overheating that occur when using Pyrex glass vessels or Erlenmeyer flasks [8]. The lubricant spray with Teflon particles gave satisfactory protection against acids to all the oven parts, representing an advantageous choice when compared with expensive or complicated designs [7,9]. While classical block digestors, laboratory microwave ovens or other laboratory made configurations [5,7,8,10] are usually limited to about a dozen samples [7], with the proposed configuration 1-25 samples could be easily digested at a time, the Pyrex container size being the limit. Up to 150 samples were digested per person and per day. Never more than 4 ml of the mixed acid solution was needed to complete the digestion, representing an important reagent saving. Acid fume extraction was totally efficient with little degradation of the microwave oven parts after several months.

The values obtained for the NBS standards coincided with the certified values (table 2). A *Pinus radiata* sample was used for method intercalibration between this Department and the

TABLE 2

Method accuracy test ^a

Sample	Element	NBS value	SDM	Found value	SDM	n	White and Douthit [5]	SDM
Pine needles	P	0.12	0.02	0.120	0.002	8	0.12	0.01
	Ca	0.41	0.02	0.470	0.006	8	0.42	0.01
	Mg	-	-	0.110	0.002	8	0.12	0.01
	K	0.37	0.02	0.320	0.004	8	0.39	0.02
Citrus leaves	P	0.13	0.02	0.133	0.001	7		
		FRI value						
<i>Pinus radiata</i> leaves	P	0.15	-	0.159	0.001	5		
	Ca	0.25	-	0.227	0.005	5		
	Mg	0.16	-	0.130	0.003	5		
	K	0.85	-	0.852	0.030	5		

^a Certified and found values for the NBS standards and the Forest Research Institute intercalibration sample. Values by White and Douthit [5] were also obtained using a microwave oven and ICP-AES. SDM = standard deviation of the mean. The values are in % of element.

Forest Research Institute (FRI) of Rotorua in New Zealand. They analysed this sample using dry digestion methods [11]. The proposed method gave identical or statistically equivalent values (Table 3). Standard deviations for the FRI values are not available. The intra-assay reproducibility was tested for all the samples by digesting at least five replicates within the same digestion programme. The standard deviations ranged from

3.02% for calcium to 9.72% for potassium, depending basically on element concentration in the tissues. The errors can be considerably reduced if required by increasing the sample weight used and the final dilution volume. The results obtained are summarized in Table 3.

Three different standard markers were analyzed periodically with the proposed method during more than 1 year by different analysts to

TABLE 3
Method intra-assay precision test ^a

Sample type	Species	Part	P	SDM	Ca	SDM	Mg	SDM	K	SDM	
Seagrasses	<i>Posidonia oceanica</i>	Leaves	0.130	0.002	9.046	0.098	0.862	0.097	0.624	0.030	
		Rhizomes	0.064	0.001	6.029	0.149	0.741	0.149	0.985	0.030	
	<i>Cymodocea nodosa</i>	Leaves ^b	0.144	0.006	–	–	–	–	–	–	
		Rhizomes	0.214	0.001	–	–	–	–	–	–	
Freshwater plants	<i>Ruppia cirrhosa</i>	Leaves	0.180	0.002	2.000	0.065	1.195	0.004	0.804	0.015	
		Roots	0.117	0.006	1.226	0.020	1.235	0.011	1.368	0.020	
	<i>Ulva</i> sp.	Talus	0.062	0.001	3.408	0.029	0.948	0.009	0.478	0.019	
	<i>Oryza sativa</i>	Straw	0.097	0.002	4.948	0.084	0.413	0.013	0.822	0.044	
	<i>Isoetes lacustris</i>	Leaves	0.187	0.001	0.926	0.030	0.237	0.010	3.220	0.153	
		Corm	0.320	0.007	0.570	0.008	0.137	0.001	0.037	0.016	
		Roots	0.134	0.001	1.348	0.027	0.119	0.004	1.463	0.082	
Terrestrial plants	<i>Pinus radiata</i>	Leaves	0.159	0.001	0.227	0.005	0.130	0.003	0.852	0.030	
		<i>P. uncinata</i>	Leaves	0.069	0.001	0.364	0.010	0.090	0.001	0.386	0.058
	Bark		0.011	0.001	0.802	0.000	0.018	0.000	0.035	0.005	
	Wood		0.006	0.002	0.210	0.009	0.021	0.001	0.030	0.004	
	<i>P. nigra</i>	Leaves	0.076	0.001	0.482	0.010	0.116	0.002	0.408	0.007	
		Bark	0.013	0.002	0.818	0.006	0.021	0.001	0.020	0.004	
		Wood	0.009	0.001	0.138	0.002	0.022	0.002	0.096	0.041	
	<i>P. halepensis</i>	Leaves	0.071	0.001	0.932	0.017	0.218	0.003	0.272	0.004	
		Bark	0.011	0.002	2.333	0.097	0.047	0.001	0.053	0.006	
		Wood	0.010	0.002	0.218	0.005	0.025	0.001	0.074	0.002	
	<i>P. sylvestris</i>	Leaves	0.076	0.001	0.486	0.054	0.095	0.007	0.441	0.012	
		Bark		0.118	0.003	0.414	0.007	0.134	0.002	0.678	0.015
				0.009	0.002	0.872	0.030	0.009	0.001	0.023	0.009
				0.013	0.001	0.628	0.009	0.023	0.002	0.030	0.009
		Wood	0.011	0.001	0.120	0.009	0.021	0.001	0.066	0.004	
	<i>Quercus ilex</i>	Leaves ^b		0.011	0.002	0.140	0.006	0.023	0.001	0.060	0.004
				0.107	0.001	0.805	0.060	0.045	0.002	0.599	0.007
Bark		0.095	0.001	1.500	0.047	0.096	0.001	0.625	0.010		
Bark		0.026	0.000	6.586	0.142	0.052	0.001	0.258	0.002		
Wood		0.019	0.001	0.780	0.026	0.058	0.001	0.272	0.004		
<i>Q. cerruoides</i>	Bark	0.013	0.003	4.380	0.240	0.282	0.024	0.120	0.010		
	Wood	0.015	0.002	0.356	0.012	0.025	0.001	0.198	0.002		
	Mean % error			7.026		3.025		4.377		9.721	
% of samples with < 10% error					73.529		96.774		90.323		70.968

^a Values found for the samples used in this work. SDM = standard deviation of the mean. The values are in % of element. ^b $n = 7$; for the other samples $n = 5$.

TABLE 4

Method inter-assay precision test ^a

Standard marker	Element	Mean	SDM	n
1	P	0.025	0.001	32
2	P	0.110	0.001	54
	Ca	0.790	0.011	45
	Mg	0.054	0.004	45
	K	0.550	0.012	45
3	P	0.101	0.001	94
	Ca	0.657	0.003	94
	Mg	0.044	0.001	94
	K	0.646	0.004	94
	S	0.099	0.003	94

^a Every replicate was digested within different programmes for several months. Standard marker 1 = *Posidonia oceanica* whole rhizomes; standard marker 2 = *Pinus radiata* leaves; standard marker 3 = *Quercus ilex* leaves. SDM = standard deviation of the mean. The values are in % of element.

ensure constant accuracy and reproducibility. The results showed satisfactory inter-assay performance (Table 4).

In Fig. 2, some practical parameters of the proposed method are compared with rough averages for the classical methods. The volume of acid needed has been reduced about threefold in

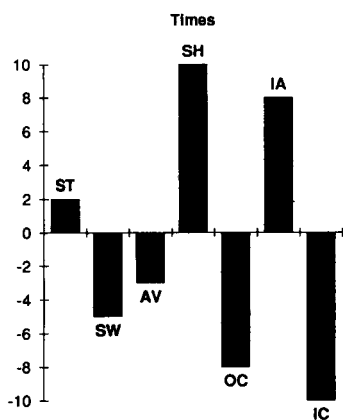


Fig. 2. Comparison between the proposed method and other methods using conventional heaters. ST = number of samples digested at a time; SW = sample weight needed; AV = acid volume needed; SH = maximum number of samples digested per hour; OC = operating costs; IA = instrument availability; IC = instrument purchase cost. Example: the number of samples digested per hour with the proposed method is roughly ten times higher than that in other methods (see text for more details).

the present method. Usually, very small amounts of sample are available. All results given here were obtained by digesting about 0.1 g of sample. However, analyses were successfully performed with half and even one quarter of this weight. The sample processing speed is increased about tenfold with respect to classical methods. Although the electric energy consumption of the oven used was higher (750 W) than that of hot-plate heaters (500 W on average), the decrease in the time required results in an eightfold decrease in overall operating costs. Instrument availability is also an important factor to be taken into account, especially when a spare may be required. Domestic apparatus have obvious advantages in this respect. The same comments can be made about instrument purchase price, this usually being a decisive point when choosing a method.

Working safety is a primary concern. After thousands of digestions no accidents or incidents have occurred. The careful observation of the safety considerations of the procedure will prevent any contingency. We recommend that the recently approved US EPA methods 3015 and 3051 regarding microwave sample preparation are consulted.

It is concluded that microwave energy-based wet digestion systems (nuclear or internal heating) show important advantages over peripheral heat conduction systems. Also, that cost reduction and design improvements of laboratory microwave ovens should extend their use for the wet digestion of all type of samples.

The authors are grateful to the Serveis Científic-Tècnics, Barcelona University, who supplied generous technical and material support in the early stages of this work, and especially to Elionor Pelfort and the other analysts in the ICP-AES Department for their kindness and the full facilities offered in elemental analysis techniques. Financial support for this work was obtained from the Comissió Interdepartamental de Recerca i Innovació Tecnològica (CIRIT) of Barcelona and from an EEC grant (STEP-0063-C).

REFERENCES

- 1 J.B. Jones, Jr., and V.W. Case, in R.L. Westerman (Ed.), *Soil Testing and Plant Analysis*, SSSA, Madison, WI, 1990, Chap. 15.
- 2 C.E. Gleit and W.D. Holland, *Anal. Chem.*, 34 (1962) 1454.
- 3 P. Barret and L.J. Davidowski, Jr., *Anal. Chem.*, 50 (1978) 1021.
- 4 A. Abu-Samra, J.S. Morris and S.R. Koirtyohann, *Anal. Chem.*, 47 (1975) 1475.
- 5 T.R. White and G.E. Douthit, *J. Assoc. Off. Anal. Chem.*, 68 (1985) 766.
- 6 M.L. Jackson, *Soil Chemical Analysis*, Prentice-Hall, Englewood Cliffs, NJ, 1958.
- 7 P.J. Lamothe, T.L. Fries and J. J. Consul, *Anal. Chem.*, 58 (1986) 1881.
- 8 M.A.E. Wandt and M.A.B. Pougnet, *Analyst*, 111 (1986) 1249.
- 9 J. Alvarado, M. Márquez and L.E. León, *Anal. Lett.* 21 (1988) 357.
- 10 H.M. Kingston and L.B. Jassie, *Anal. Chem.*, 58 (1986) 2534.
- 11 G. Nicholson, *N.Z. Forest Ser. FRI Bull.*, (1984) 70.

Comparative study of Kalman filtering, synchronous excitation and numerical derivative techniques in fluorimetry

Jingyu Zhang, Jinfu Yang, Ying Ren and Yan Zhang

Changchun Institute of Applied Chemistry, Chinese Academy of Sciences, Changchun 130022 (China)

(Received 11th November 1992; revised manuscript received 13th January 1993)

Abstract

The performance of Kalman filtering, synchronous excitation and numerical derivative techniques for the resolution of overlapping emission spectra in spectrofluorimetry was studied. The extent of spectrum overlap was quantitatively described by the separation degree D_s , defined as the ratio of the peak separation to the full width at half-maximum of the emission spectrum of the interferent. For the system of Rhodamine B and Rhodamine 6G with a large D_s of about 0.4, both Kalman filtering and synchronous techniques are able to resolve the overlapping spectra well and to give satisfactory results while the derivative spectra are still overlapped with each other. Moreover, the sensitivities are greatly decreased in derivative techniques. For more closely spaced spectra emitted by the complexes of Al and Zn with 7-iodo-8-hydroxyquinoline-5-sulphonic acid (Ferron)–hexadecyltrimethylammonium bromide, the synchronous excitation technique cannot completely separate the overlapping peaks, although it increases the separation degree from 0.25 in the conventional spectra to 0.37 in the synchronous spectra. On the other hand, Kalman filtering is capable of resolving this system. When the Al/Zn intensity ratio at the central wavelength of Al was > 1 , however, the accuracy and precision of the estimates for Zn concentration produced by the Kalman filter became worse. In this event, the combination of synchronous excitation and Kalman filtering can much improve the analytical results.

Keywords: Fluorimetry; Derivative techniques; Kalman filter; Peak resolution; Synchronous excitation

Fluorescence spectrometry with its excellent sensitivity has provided a useful tool for determining trace components. Nevertheless, despite the ability to select both excitation and emission wavelengths, conventional fluorescence methods for the analysis of mixtures with similar characteristics have limited applicability, as most spectra of complex mixtures often cannot be resolved satisfactorily. In this event, in order to obtain accurate analytical results, separation techniques are often applied, but these may be expensive or

excessively time consuming. The idea of synchronous excitation was first suggested by Lloyd in the early 1970s [1]. The advantages of synchronous techniques are mainly the band-narrowing effect and simplification of the spectral profiles [2,3]. Another method for resolving overlapping signals is the derivative technique, which has often been used in both absorption and fluorescence spectrophotometry. During the past decade, multivariate analysis techniques have been widely studied and proved to be a promising means for the resolution of overlapping signals. Among others, Kalman filtering as an effective multivariate analysis technique has been applied in a number of areas of analytical chemistry, including absorp-

Correspondence to: Jingyu Zhang, Changchun Institute of Applied Chemistry, Chinese Academy of Sciences, Changchun 130022 (China).

tion and fluorescence spectrophotometry [4–8], voltammetry [9] and inductively coupled plasma atomic emission spectrometry [10–15]. Taking two systems with large and small separation degrees, in this work synchronous excitation, Kalman filtering and derivative techniques were compared with regard to selectivity and sensitivity.

EXPERIMENTAL

Apparatus

All fluorimetric measurements were performed with a Shimadzu Model RF-5000 spectrofluorimeter fitted with 1-cm quartz cells. A 150 W xenon lamp was used for excitation. The spectral band pass was set to 3.0 nm for the system of Rhodamine B and Rhodamine 6G and 5.0 nm for the system of aluminium and zinc. For synchronous fluorescence measurements, both excitation and emission monochromators were locked together and scanned synchronously. Derivative spectra were obtained by numerically differentiating conventional spectra, which was performed by the software of the spectrometer.

Reagents

All experiments were performed with analytical-reagent grade chemicals. Doubly distilled water was used throughout.

Solutions of Rhodamine B and Rhodamine 6G ($10 \mu\text{g ml}^{-1}$) were prepared in 0.01 mol l^{-1} sodium hydroxide solution. Solutions of lower concentration were prepared by dilution with 0.01 mol l^{-1} sodium hydroxide solution.

A $5 \times 10^{-4} \text{ mol l}^{-1}$ 7-iodo-8-hydroxyquinoline-5-sulphonic acid (Ferron) solution and a $4 \times 10^{-3} \text{ mol l}^{-1}$ hexadecyltrimethylammonium bromide (HTMAB) solution were prepared in water.

Standard aluminium and zinc stock solutions with water.

A pH 5.5 buffer solution was prepared from 0.2 mol l^{-1} acetic acid–sodium acetate.

Procedures

Zinc–aluminium system. A sample solution containing 1.0–15.0 μg of aluminium and 2.5–20.0 μg of zinc was placed in a 25-ml volumetric flask,

3.0 ml of buffer solution (pH 5.5), 10 ml of $5 \times 10^{-4} \text{ mol l}^{-1}$ Ferron solution and 3 ml of $4 \times 10^{-3} \text{ mol l}^{-1}$ HTMAB solution were added and the mixture was diluted to volume with water. A reagent blank was prepared in a similar way. The fluorescence spectra were recorded 30 min after mixing the reagents. The fluorescence intensities were measured in the wavelength range 424.8–580.8 nm with excitation at 385.6 nm. Each solution was scanned eight times with a step interval of 4 nm. Synchronous fluorescence intensities were measured at a fixed wavelength difference of 80 nm in the wavelength range 428–526 nm with a step interval of 2.8 nm (also eight scans for each solution).

Rhodamine B and Rhodamine 6G system. The test solutions were prepared in such way that the concentrations of Rhodamine B and Rhodamine 6G were 0.01–0.1 $\mu\text{g ml}^{-1}$. The synchronous fluorescence intensities were measured at 570.4 and 540.0 nm for Rhodamine B and Rhodamine 6G, respectively, with a wavelength difference of 15 nm. The concentrations of these two components in a sample were directly determined according to these synchronous fluorescence intensities. Conventional fluorescence intensities were measured in the wavelength range 540–626 nm with excitation at 540 nm. Each solution was scanned eight times with a step interval of 4 nm. In order to eliminate the effect of scattered light, a Model 0-56 filter (Shimadzu) was inserted on the emission side of the filter holder.

Kalman filter

The Kalman filtering method has been described in detail elsewhere [13,14]. The essential steps of the method include filtering of spectral data, which produces the innovation sequence and the estimates for concentration, shifting of a scan along with the wavelength axis by interpolation with a cubic spline function and optimization of the peak positions of the scans according to the whiteness of the innovation sequence combined with interpolation.

For calibration, pure component solutions of appropriate concentrations were prepared and measured three times for each component, then the average intensity or sensitivity was calculated

for each point of the scan. Eight measurements were made for each sample. These data obtained by scanning were handled off-line on an NEC PC8801B computer using a Basic program.

RESULTS AND DISCUSSION

Resolution of overlapping spectra with a large peak separation

The resolution of overlapping peaks with a large peak separation will be illustrated with the binary system of Rhodamine B and Rhodamine 6G. Figure 1 shows the emission spectra of these two components with excitation at 540 nm. The peak separation was determined to be about 29 nm. A small peak due to scattered light, which

affects the measurement of the component of interest, occurs as a shoulder on the emission of Rhodamine B and coincides with the peak of Rhodamine 6G. In order to eliminate the effect of scattered light, a Model 0-56 filter was inserted on the emission side of the filter holder. The emission spectra shown in Fig. 1b were thus obtained and the peak separation became 12.4 nm. The extent of peak overlap was related not only to the peak distance but also the band width. Therefore, the separation degree D_s was defined as the ratio of the peak separation to the full width at half-maximum of the spectrum of an interferent in order to determine the extent of peak overlap. The separation degree of the spectra shown in Fig. 1b is about 0.44. Obviously, one cannot directly determine the concentrations of

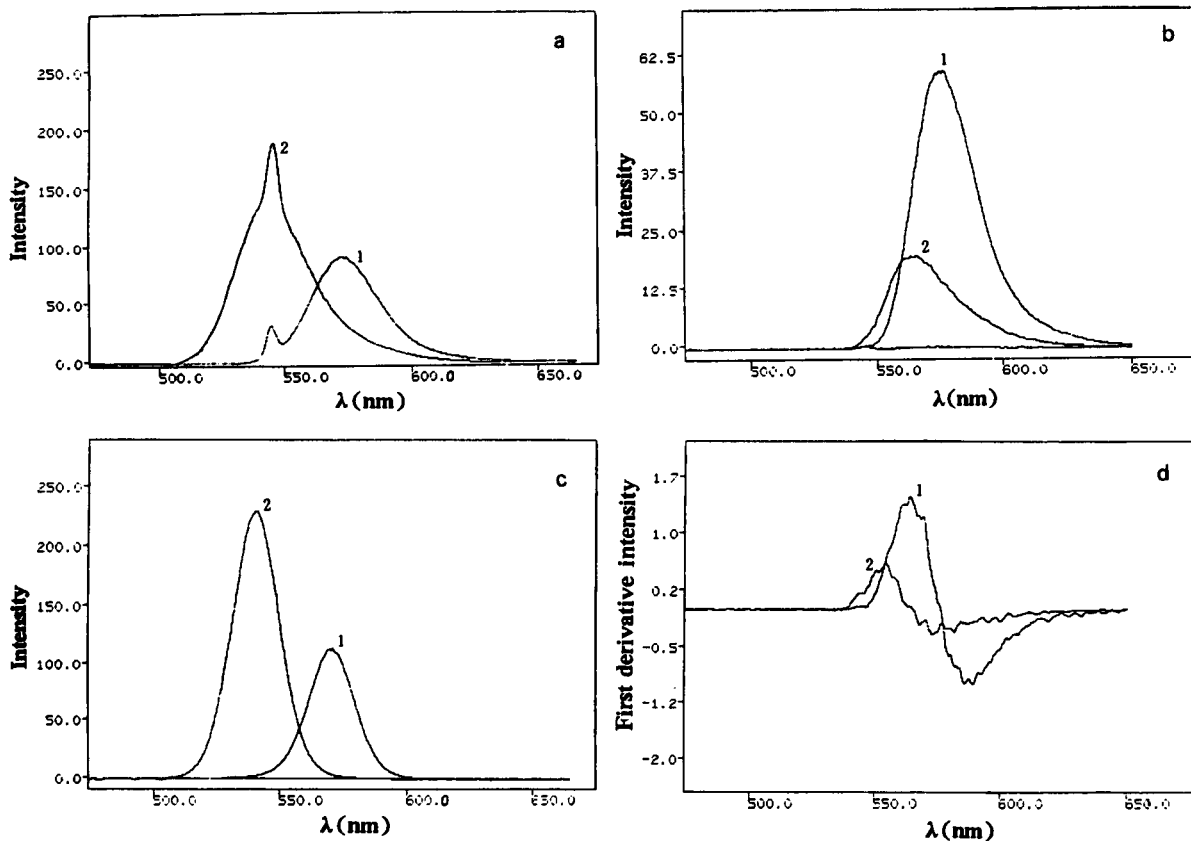


Fig. 1. Fluorescence spectra of (1) $0.1 \mu\text{g ml}^{-1}$ Rhodamine B and (2) $0.1 \mu\text{g ml}^{-1}$ Rhodamine 6G. (a) Emission spectra [$\lambda(\text{ex}) = 540$ nm]; (b) emission spectra after filtering the scattered light [$\lambda(\text{ex}) = 540$ nm]; (c) synchronous spectra with $\Delta\lambda = 15$ nm; (d) first-derivative spectra corresponding to (b).

TABLE 1

Analytical results for synthetic samples of Rhodamine B (RB) and Rhodamine 6G (R6G) (eight measurements for each sample)

No.	Sample ($\mu\text{g ml}^{-1}$)		Synchronous excitation				Kalman filtering			
	R6G	RB	Recovery (%)		R.S.D. (%)		Recovery (%)		R.S.D. (%)	
			R6G	RB	R6G	RB	R6G	RB	R6G	RB
1	0.01	0.1	120	94.8	0.0	1.3	104	94.3	35	2.5
2	0.05	0.1	93.5	92.8	1.5	1.1	109	91.4	9.5	1.9
3	0.1	0.1	100	94.4	1.1	1.2	103	92.8	3.8	2.8
4	0.05	0.01	105	117	3.6	2.8	106	96.4	3.3	2.6
5	0.05	0.05	101	100	1.0	1.7	98.2	91.7	5.3	0.70

these components by measuring their peak intensities. Fortunately, for this system with a large D_s , synchronous excitation techniques may be used for the resolution of the overlapping peaks. Fig. 1c shows the synchronous fluorescence spectra at

a fixed wavelength difference ($\Delta\lambda$) between excitation and emission of 15 nm. It is clear that the emissions are well resolved and D_s is increased to about 1.5, more than three times the D_s in the conventional spectra in Fig. 1b. The concentra-

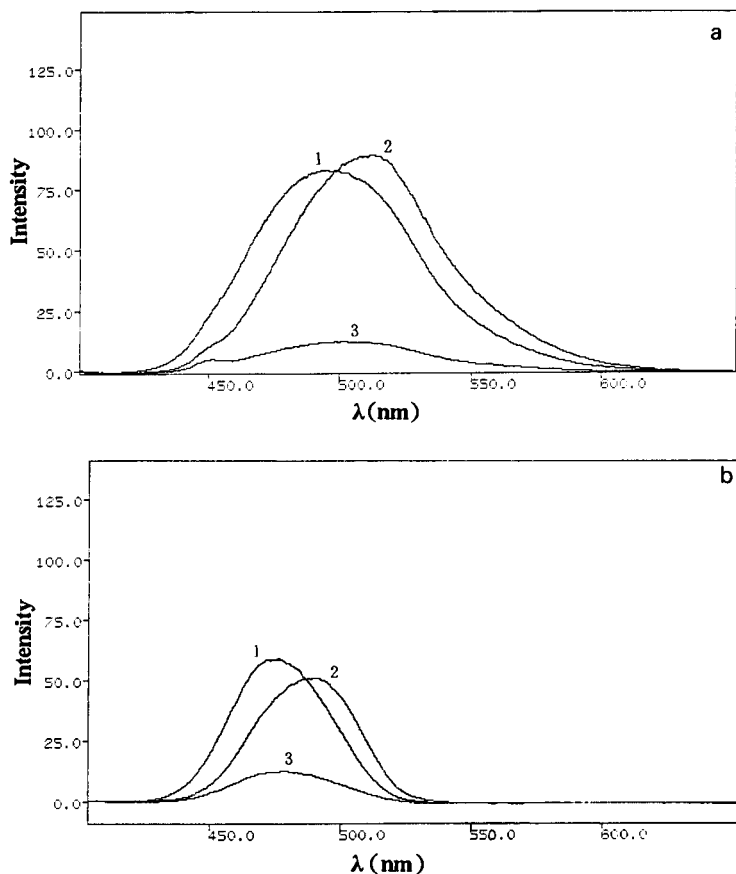


Fig. 2. Fluorescence spectra of the complexes of Al and Zn with 7-iodo-8-hydroxyquinoline-5-sulphonic acid-HTMAB. (a) Emission spectra with excitation at 385.6 nm; (b) synchronous spectra with $\Delta\lambda = 80$ nm. 1 = 5.31 μg per 25 ml of Al; 2 = 10 μg per 25 ml of Zn; 3 = reagent blank.

tions of the components can then be directly determined by measuring the signals at their own central wavelengths. Further, the synchronous spectra are free from the effect of scattered light.

Of course, resolution of the conventional spectra of these components may also be achieved by using Kalman filtering. However, the sensitivities are decreased for this particular case owing to the use of a filter, as is evident by comparing Fig. 1b, a and c.

The first-order derivative spectra are shown in Fig. 1d. It can be seen that the derivative technique is not able to separate the overlapping signals and the sensitivities are considerably reduced.

Table 1 gives the results calculated from eight measurements for synthetic samples containing Rhodamine B and Rhodamine 6G. The relative standard deviations (R.S.D.s) produced by the synchronous excitation method do not exceed 3.6% and the recoveries vary from 92.8% to 105%, with only two exceptions, samples 1, for which the recovery of Rhodamine 6G is 120%, and 4, for which the recovery of rhodamine B is 117%. The recoveries produced by the Kalman filtering method are 91.4–109% and the R.S.D.s are < 10%, the only exception being sample 1, for which the R.S.D. for Rhodamine 6G is up to 35%. It seems that results for Rhodamine 6G are systematically slightly too high and those for Rhodamine B slightly too low, probably because the filter recursively processes the spectrum from left to right, and thereby first passes the peak for Rhodamine 6G. However, in general, these filtering estimates are acceptable and there is no significant difference between the results produced by the two methods. This again implies that both techniques are able to resolve this overlapping system and give satisfactory results. From the viewpoint of sensitivity and simplicity of experiment, however, as discussed above, the synchronous technique has significant advantages over the Kalman filtering method.

Resolution of closely spaced spectra

Figure 2a shows the emission spectra of the complexes of Al and Zn with 7-iodo-8-hydroxyquinoline-5-sulphonic acid–HTMAB with excita-

TABLE 2

Separation degrees and sensitivities for complexes of Al and Zn in conventional and synchronous spectra

Parameter	Element	Conventional	Synchronous
Separation degree	Zn/Al ^a	0.26	0.37
	Al/Zn ^a	0.25	0.39
Sensitivity	Zn	8.9	4.8
	Al	16.6	11.5

^a The first component is the analyte and the second component is the interferent.

tion at 385.6 nm. The separation degree was determined to be about 0.25. Obviously, this is a more closely spaced system. As shown in Fig. 2b, the synchronous excitation technique cannot completely separate the overlapping peaks, although it does increase D_s from about 0.25 in the conventional spectra to about 0.37 in the synchronous spectra (see Table 2). Table 2 also shows that the synchronous excitation technique results in a decrease in sensitivity. On the other hand, the Kalman filtering method is capable of resolving the overlapping peaks. Table 3 lists the Kalman filtering estimates for Al and Zn concentrations. The results for Al are excellent for all the samples with an R.S.D.s within 6% and recoveries between 98.4 and 109%. The R.S.D.s for Zn are also good and all < 8%, with only one

TABLE 3

Analytical results for synthetic samples of Al and Zn obtained by Kalman filtering coupled with conventional fluorescence method (eight measurements for each sample)

No.	Sample ($\mu\text{g ml}^{-1}$)		F_A / F_{Zn}^a	Recovery (%)		R.S.D. (%)	
	Al	Zn		Al	Zn	Al	Zn
1	1.0	20.0	0.10	109	96.5	5.7	0.3
2	2.5	20.0	0.24	101	93.4	2.2	0.8
3	2.5	10.0	0.48	106	98.9	2.3	1.1
4	5.0	10.0	0.97	102	97.2	1.5	0.8
5	7.5	5.0	2.92	103	79.9	1.8	3.6
6	10.0	5.0	3.89	98.5	79.8	1.5	7.4
7	15.0	5.0	5.83	103	79.2	0.8	4.0
8	7.5	2.5	5.83	100	66.3	0.5	3.0
9	10.0	2.5	7.77	98.4	70.7	0.9	12
10	15.0	2.5	11.66	105	83.4	0.4	3.5

^a F_A / F_{Zn} is the intensity ratio of Al to Zn at the peak wavelength of Al.

TABLE 4

Analytical results obtained by Kalman filtering coupled with the synchronous excitation method for samples 5–10 in Table 3 (eight measurements for each sample)

No.	Sample ($\mu\text{g ml}^{-1}$)		$F_{\text{Al}} / F_{\text{Zn}}^a$	Recovery (%)		R.S.D. (%)	
	Al	Zn		Al	Zn	Al	Zn
5	7.5	5.0	5.21	105	100	1.2	4.8
6	10.0	5.0	6.00	104	93.6	0.7	3.8
7	15.0	5.0	10.16	97.9	113	0.7	3.5
8	7.5	2.5	10.42	105	107	0.9	6.8
9	10.0	2.5	12.0	101	84.2	2.2	10
10	15.0	2.5	20.3	100	122	0.5	6.4

^a See Table 3.

exception (sample 9). The recovery of Zn, however, is dependent on the Al/Zn intensity ratio at the peak wavelength of Al. When this ratio is < 1 (samples 1–4 in Table 3), the recoveries of Zn are 93.4–97.2%, which can be considered as excellent. For samples 5–10, however, where the intensity of Al is 2.92–11.66 times that of Zn, the recovery of Zn becomes significantly worse and is only 66.3–83.4%. In this instance the combination of the Kalman filtering and synchronous excitation techniques shows great potential. As shown in Table 4, when the Kalman filtering was used to process the synchronous fluorescence data for samples No. 5–10, although the Al/Zn intensity ratio was increased, the results for Zn were still improved; the recovery of Zn varies from 84.2 to 122%, which obviously is much better than the corresponding results in Table 3.

Conclusions

The overlap of emission spectra is a serious problem in spectrofluorimetry when a sample containing analytes with similar properties is analysed. For an overlapping system with a large separation degree, synchronous excitation may be a suitable technique because of its simplicity and

adequate resolving power. For closely spaced peaks, however, the synchronous excitation technique will not work and a multivariate analysis technique such as Kalman filtering should be used for the resolution of the overlapping signals. A combination of Kalman filtering and synchronous excitation techniques has great potential for improving results when the intensities of the overlapping components differ widely. Both techniques show significant advantages over numerical derivative techniques from the viewpoint of either selectivity or sensitivity.

This work was financially supported by the National Natural Science Foundation of China and Changchun Branch, Chinese Academy of Sciences.

REFERENCES

- 1 J.B.F. Lloyd, *Nature Phys. Sci.*, 64 (1971) 231.
- 2 J.B.F. Lloyd and I.W. Evett, *Anal. Chem.*, 49 (1977) 1710.
- 3 V.-D. Tuan, *Anal. Chem.*, 50 (1978) 396.
- 4 H.N.J. Poullisse, *Anal. Chim. Acta*, 112 (1979) 361.
- 5 C.B.M. Didden and H.N.J. Poullisse, *Anal. Lett.*, 13 (1980) 921.
- 6 Y.-M. Liu and R.-Q. Yu, *Talanta*, 35 (1988), 707.
- 7 Z.-L. Li, M.-L. Li, L.-M. Shi and R.-Q. Yu, *Chin. Rare Earth Soc.*, 7 (1989) 65.
- 8 Z.-L. Li, L.-M. Shi, M.-L. Li and R.-Q. Yu, *Chem. J. Chin. Univ.*, 11 (1990) 245.
- 9 T.F. Brown and S.D. Brown, *Anal. Chem.*, 53 (1981) 1410.
- 10 E.H. van Veen and M.T.C. de Loos-Vollebregt, *Spectrochim. Acta, Part B*, 45 (1990) 313.
- 11 E.H. van Veen, F.J. Oukes and M.T.C. de Loos-Vollebregt, *Spectrochim. Acta, Part B*, 45 (1990) 1109.
- 12 E.H. van Veen and M.T.C. de Loos-Vollebregt, *Anal. Chem.*, 63 (1991) 1441.
- 13 J.-F. Yang, Z.-X. Piao, X.-J. Zeng, Z.-Y. Zhang and X.-H. Chen, *Spectrochim. Acta, Part B*, 47 (1992) 1055.
- 14 J.-F. Yang, Z.-X. Piao, X.-J. Zeng, Z.-Y. Zhang and X.-H. Chen, *Acta Chim. Sin.*, 50 (1992) 1086.
- 15 J.-F. Yang, Z.-X. Piao, X.-J. Zeng, Z.-Y. Zhang and X.-H. Chen, *Chin. Chem. Lett.*, 3 (1992) 193.

Fluorescence-based flow-injection determination of biotin and biotinylated compounds

Truis Smith-Palmer¹, Minas S. Barbarakis², Tadeusz Cynkowski and Leonidas G. Bachas

Department of Chemistry, University of Kentucky, Lexington, KY 40506-0055 (USA)

(Received 6th November 1992; revised manuscript received 14th January 1993)

Abstract

A homogeneous fluorophore-linked binding assay for biotin and biotin-containing compounds has been used in a merging-zone flow-injection system. Analyses were first conducted by taking advantage of the enhancement in fluorescence intensity of a conjugate of avidin-fluorescein in the presence of biotin or biotin derivatives. Detection limits for biotin as low as 2×10^{-9} M could be achieved. A greater enhancement of fluorescence was found for a streptavidin-fluorescein conjugate. Calibration curves obtained by using the streptavidin conjugate are shown for the determination of various biotinylated compounds in the flow-injection system and in a batch mode.

Keywords: Flow injection; Avidin-FITC; Biotin Streptavidin-FITC

Flow-injection analysis (FIA) is gaining popularity because of its ability to provide rapid, easy to use, and reproducible analytical methods [1–3]. In this technique, a volume of sample is injected into a stream of reactants, a reaction is allowed to take place for a fixed amount of time, and the extent of the reaction is monitored by an on-line detector. The resultant signal can then be related to the analyte concentration. The type of chemical reaction used in FIA strongly influences the selectivity, sensitivity, and detection limits attainable by the method. Given the strong and selective interaction between certain biochemical reagents (e.g., antibody-antigen, binding protein-ligand, receptor-hormone, etc.), the coupling of

binding assays involving such reagents with FIA should result in the development of methods with good selectivity and detection limits.

Binding assays can be classified as either competitive or noncompetitive and involve a reaction between a biological binder (antibody, binding protein, receptor, lectin, etc.) and its respective ligand [4]. The extent of the binding reaction can be quantified by monitoring the signal from a label molecule that is chemically attached to either the binder or the ligand [4]. The sensitivity and selectivity of binding assays have been explored in flow-injection analysis and several studies on this subject have been reported based on heterogeneous binding assays of both competitive [5–7] and noncompetitive [8–10] nature. However, relatively few FIA-based homogeneous binding assays have been described [11,12], and none of these involved the determination of biotin and biotinylated compounds.

Biotin (vitamin H) is an important coenzyme in enzymatic carboxylations [13]. Deficiency of this

Correspondence to: L.G. Bachas, Department of Chemistry, University of Kentucky, Lexington, KY 40506-0055 (USA).

¹ On leave from the Department of Chemistry, Saint Francis Xavier University, Antigonish, Nova Scotia, Canada, B2G 1C0.

² Present address: Ciba Corning Diagnostics Corp., 333 Coney Street, East Walpole, MA 02032 USA.

vitamin can cause anemia, dermatitis, Leiner's disease in children, and biotin-responsive inborn errors of metabolism. In addition, the wide applicability of the avidin–biotin system in biotechnology and biomedical research has resulted in a significant number of group-specific biotin-containing reagents [14] and biotinylated biologically active molecules [15], and has further stimulated interest in the rapid and accurate determination of biotin and biotinylated compounds.

In this paper we demonstrate the feasibility of a FIA-based homogeneous fluorophore-linked binding assay for biotin and biotinylated compounds. The assay is based on the enhancement of the emission intensity of fluorescein-labeled conjugates of avidin and streptavidin by the biotin moiety. In addition, we show that the use of streptavidin rather than avidin leads to higher enhancement of fluorescence in both batch tests and in the FIA system itself. The applicability of the developed FIA system to a variety of biotinylated compounds is also demonstrated.

EXPERIMENTAL

Reagents

Biotin, fluorescein isothiocyanate (FITC) isomer I (on celite), gelatin, biotinylated bovine serum albumin (biotinylated BSA), avidin-FITC (f/p = 3.9), biotin methyl ester, biocytin, and L-thyroxine were purchased from Sigma (St. Louis, MO). The abbreviation f/p stands for fluorophore to protein ratio. Biotin hydrazide, streptavidin-FITC (f/p = 4.3 and 4.8) and the *N*-hydroxysuccinimide (NHS) ester of biotin were purchased from Pierce (Rockford, IL), while avidin (egg white) and streptavidin were purchased from Molecular Probes (Eugene, OR) and InFerGene (Oakland, CA), respectively. Anhydrous methyl sulfoxide (DMSO; Sure/Seal™), ammonium bicarbonate and sodium bicarbonate were from Aldrich (Milwaukee, WI). Sephadex G-25 (bead size medium) was obtained from Pharmacia LKB Biotechnology (Piscataway, NJ). All solutions were prepared by using deionized, distilled water obtained with a Milli-Q Water Purification System (Millipore, Bedford, MA). The buffers used

in this study were 0.0500 M sodium phosphate (pH 8.0) and 0.100 M sodium bicarbonate (pH 9.1). The sodium phosphate buffer was used to prepare a 0.10% (w/v) gelatin solution. Stock solutions (0.10 g l⁻¹) of biotin and further dilutions of the stock solution were prepared with the 0.10% (w/v) gelatin solution. In addition, all the avidin-FITC and streptavidin-FITC solutions were prepared with the 0.10% (w/v) gelatin solution.

The biotin–thyroxine conjugate was prepared as follows. The NHS ester of biotin (43.2 mg) was added to a solution of thyroxine methyl ester (100 mg; prepared by the method of Ashley and Harington [16]) in anhydrous DMSO (5 ml) under argon and stirred for 20 h protected from light. The residue was chromatographed on silica gel (CHCl₃–MeOH, 15:1) and, after evaporation of the solvent, the product was isolated as crystals (65 mg). ¹H NMR (DMSO-*d*₆, TMS) [δ 1.1–1.7 (m, 6H), 2.07 (t, 2H), 2.52 (m, 2H), 2.73–3.15 (m, 3H), 3.65 (s, 3H), 4.05–4.60 (m, 3H), 6.38 (s, 2H), 7.07 (s, 2H), 7.82 (s, 2H), 8.32 (d, 1H)].

Apparatus

The experimental setup used in this study is shown in Fig. 1A. It consisted of a Minipuls-2 variable speed peristaltic pump (Gilson; Wor-

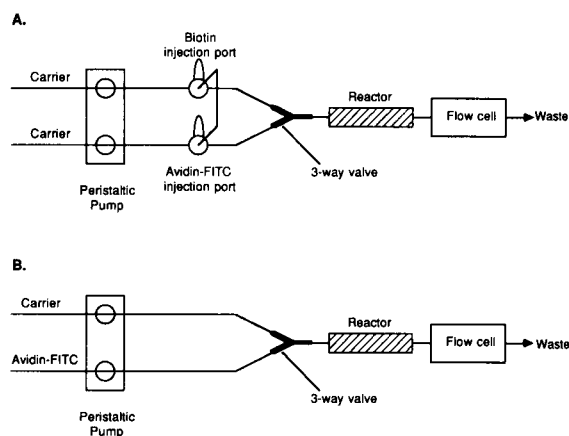


Fig. 1. Schematic diagram of the FIA system for (A) the determination of biotin using avidin- or streptavidin-FITC conjugates, (B) the determination of the maximum fluorescence signal possible for avidin-FITC passing through the flow cell.

thington, OH), a loop-injection system made from tandem Rheodyne 4-way valves, and an Omnifit 3-way flow joint. When necessary, a knitted open-tubular reactor coil (KOT2 from reference [17], helix diameter 14 mm) was placed between the mixing point and the detector. PTFE tubing (0.5 mm i.d.) was used throughout. Fluorescence detection was carried out using a Fluorolog-2 spectrofluorometer (SPEX Industries; Edison, NJ) with a μ -fluorescence flow cell (20- μ l cell volume; NSG Precision Cells; Farmingdale, NY). The excitation was at 495 nm and the emission was monitored at 518 nm. Both excitation and emission slits were set at 1 mm. Batch fluorometric measurements were carried out with the Fluorolog-2 spectrofluorometer using a standard 1 \times 1 cm quartz cuvette. A Perkin-Elmer (Norwalk, CT) (Lambda 6) UV-visible spectrophotometer was employed for all absorbance measurements.

Batch mode

Varying amounts of biotin or biotin derivative were dispensed into test tubes to a total volume of 500 μ l. A volume of 1.60 ml of avidin-FITC (or streptavidin-FITC) solution was added to each tube. After 15-min incubation, the fluorescence signal was measured. Calibration curves were constructed by plotting the percent enhancement of the fluorescence signal observed versus the biotin concentration in the assay test tube.

RESULTS AND DISCUSSION

Avidin is a naturally occurring biotin-specific binding protein. When free biotin binds to FITC-labeled avidin an enhancement of the fluorescence emission is observed, which is proportional to the concentration of free biotin present in the sample. This system was first reported by Al-Hakim et al. [18] who observed that the fluorescence of fluorescein-labeled avidin is enhanced by approximately 2-fold upon the binding of biotin, a fact that was exploited to develop a fluorometric assay for biotin. In our laboratory, it has been found that conjugates of avidin with

fluorophores other than fluorescein also show fluorescence enhancement upon biotin binding, but that this enhancement is the largest in the case of fluorescein-labeled avidin [19]. Other advantages of using fluorescein as the label include its high quantum efficiency, fluorescence emission in the visible region, and its low fluorescence temperature coefficient [20–22]. An avidin-FITC conjugate with an f/p ratio of 3.9 is commercially available and was used to develop a FIA system.

In the most common type of FIA, the reagent flows continuously through the system while samples are injected at certain time intervals. However, as avidin and its commercially available conjugates are relatively expensive, a merging-zone technique was chosen whereby reagent was injected into one buffer stream at the same time as sample was injected into a second buffer stream; the two streams were merged equidistant from the injection points. The buffer solution used in both streams was 0.050 M phosphate, pH 8.0. In these FIA systems, the choice of injection loop size influences the magnitude of the analytical signal. To help determine the best loop size, one buffer stream was replaced with an avidin-FITC solution (1 mg l⁻¹, 1.5 \times 10⁻⁸ M) as shown in Fig. 1B. This configuration gave the maximum attainable fluorescence signal, which corresponds to an infinitely large injection loop. In a separate experiment, avidin-FITC was injected into the FIA system as shown in Fig. 1A, while the biotin injection port was filled with buffer devoid of biotin. A flow-rate of 1.0 ml min⁻¹ was used. The avidin-FITC fluorescence signals obtained using varying loop sizes (30 to 70 μ l) in the presence and absence of a 2-m KOT2 reactor coil (see below) were compared. The peak heights were proportional to the loop size in all cases. Larger loop sizes would have further increased the peak height, but at the expense of using too much sample and reagent, as well as increasing the analysis time and cost per sample. A loop size of 70 μ l was thus selected, which, in conjunction with a 2-m KOT2 reactor coil, gave a peak that was 67% of the maximum attainable fluorescence signal. Without the coil a peak that was 82% of the maximum was obtained. This loop size was then used for both injection ports.

The choice of flow-rate and the size of reactor coil was a function of the concentration of biotin to be determined. As the biotin concentration was decreased, the reaction rate also decreased and a longer residence time before detection was required for the fluorescence to be enhanced. A longer residence time was given by using a reduced flow rate and, most effectively, by increasing the flow path to the detector. Use of a knitted open-tubular reactor allowed the flow path to be increased without substantial band broadening. Figure 2 illustrates how the shape of the calibration curve obtained changed as the residence time was changed. With a flow-rate of 0.47 ml min^{-1} and a 10-m KOT2 reactor coil, a detection limit of $2 \times 10^{-9} \text{ M}$ biotin was achieved. However, under these conditions the sample throughput was low and the maximum biotin concentration that could be determined was $4 \times 10^{-8} \text{ M}$. With a higher flow rate (1.0 ml min^{-1}) and a 2-m KOT2 reactor coil the throughput was substantially increased and the useful concentration range was 4×10^{-9} to $2 \times 10^{-7} \text{ M}$ biotin.

Lower detection limits can be obtained in the batch mode by reducing the avidin–FITC concentration [19], and thus the same strategy was tried in the FIA system. Figure 3 compares the results obtained using 1.0 mg l^{-1} avidin–FITC and 0.10 mg l^{-1} avidin–FITC. Use of the lower avidin concentration did lower the detection limit by a factor of two, but at the expense of range and sensitivity. In this graph we have compared percent enhancements in fluorescence intensity. If one compares absolute enhancements, the values obtained using 1.0 mg l^{-1} reagent are much greater, but are on top of a correspondingly larger background caused by the fluorescence of avidin–FITC.

Even greater enhancements were found in batch measurements involving streptavidin–FITC and biotin (Fig. 4) and, therefore, use of streptavidin–FITC for the determination of biotin by FIA was further investigated. Streptavidin is also a naturally occurring biotin-specific binding protein with a commercially available FITC-conjugate. Streptavidin is usually preferred over avidin in a variety of bioanalytical and biotechnological applications because of its low non-specific

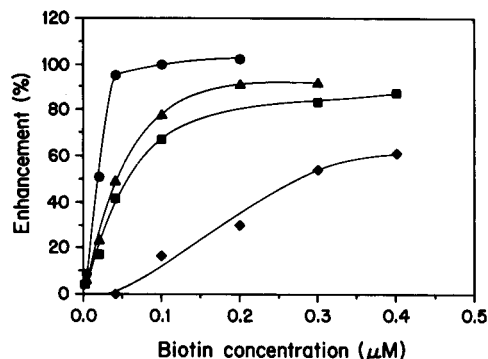


Fig. 2. Plots of percent enhancement of the fluorescence of avidin–FITC ($f/p = 3.9, 1.0 \text{ mg l}^{-1}$) as a function of biotin concentration under the following conditions: (●) 0.47 ml min^{-1} and 10-m KOT2 reactor coil, (▲) 0.75 ml min^{-1} and 10-m KOT2 reactor coil, (■) 1.0 ml min^{-1} and 2-m KOT2 reactor coil, and (◆) 0.75 ml min^{-1} and no reactor coil.

binding [23]. However, it was because of our interest in differences in reactivity between avidin and streptavidin that we initially examined whether biotin also enhanced the fluorescence of FITC–labeled streptavidin.

The fluorescence enhancement of streptavidin–FITC in FIA was found to be much superior to that of avidin–FITC. In particular under the same concentration ($1.5 \times 10^{-8} \text{ M}$) and experimental conditions, the maximum enhancement obtained with streptavidin–FITC was five-fold higher than that of avidin–FITC (data not shown). Figure 5 depicts a typical readout from

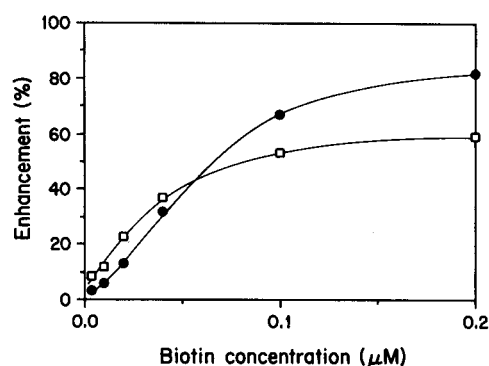


Fig. 3. Plots of percent enhancement of avidin–FITC ($f/p = 3.9$) fluorescence as a function of biotin concentration, for avidin–FITC concentrations of 1.0 mg l^{-1} (●) and 0.10 mg l^{-1} (□) at a flow-rate of 1.0 ml min^{-1} with $70\text{-}\mu\text{l}$ loops and a 2-m KOT2 reactor coil.

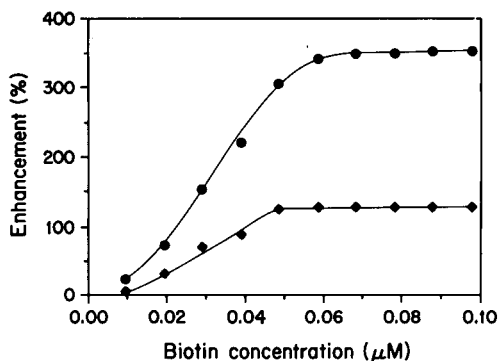


Fig. 4. Plots of percent enhancement of avidin-FITC ($f/p = 3.9$; ♦) and streptavidin-FITC ($f/p = 4.3$; ●) in the batch mode as a function of biotin concentration. The concentration of each protein in the assay cup was 0.80 mg l^{-1} .

the fluorescence detector as various biotin concentrations are reacted with 1.0 mg l^{-1} streptavidin. The detection limit of the FIA system involving streptavidin-FITC was similar to that using avidin-FITC. However, the sensitivity and dynamic range were greatly increased by using streptavidin-FITC.

To test the general applicability of the streptavidin-biotin system in fluorescence enhancement assays, we used both the batch and FIA systems to produce calibration curves for the determination of a variety of biotinylated compounds. Each curve was found to have a different slope, as illustrated in Fig. 6 for biocytin, biotin, biotin methyl ester and biotin hydrazide in the batch mode. The position of the calibration curve is consistent with protein binding theory and follows the relative binding strength of the interaction between the binding protein and the biotin derivatives [24].

Figure 7 depicts calibration curves for biocytin, biotin, biotin-thyroxine and biotinylated BSA using the FIA system. The calibration curves at relatively low concentrations were all linear, which is desirable for analytical purposes. However, the slopes varied considerably and, at high concentrations of biotinylated compound, the plots flattened out at quite different maximum percent enhancements. These data indicate that the developed system can be used for the determination of the naturally occurring biotin, and biocytin, as

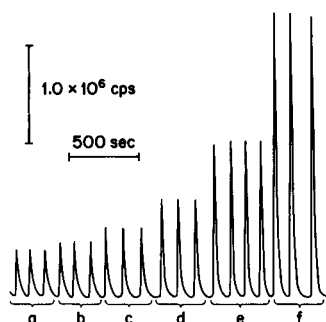


Fig. 5. Typical fluorescence signals (signal height = fluorescence intensity in counts per second) recorded using FIA with a flow-rate of 1.0 ml min^{-1} with $70\text{-}\mu\text{l}$ loops and a 2-m KOT2 reactor coil for the reaction of 1.0 mg l^{-1} streptavidin-FITC ($f/p = 4.8$) with varying concentrations of biotin as follows: (a) 0 M, (b) $2.0 \times 10^{-8} \text{ M}$, (c) $4.1 \times 10^{-8} \text{ M}$, (d) $1.0 \times 10^{-7} \text{ M}$, (e) $4.1 \times 10^{-7} \text{ M}$, and (f) $4.1 \times 10^{-6} \text{ M}$ biotin.

well as synthesized biotinylated compounds. It is also important to note that the FIA can be used for the determination of both low- and high-molecular-weight biotinylated components. Given the importance of the biotin-(strept)avidin system in bioanalysis and biotechnology, several applications of the developed system may be envisioned.

For systems containing both biotin and biocytin (or other biotin-containing compounds) separation by a method such as liquid chromatography would be necessary prior to analysis. Research along these lines is currently underway in our laboratory.

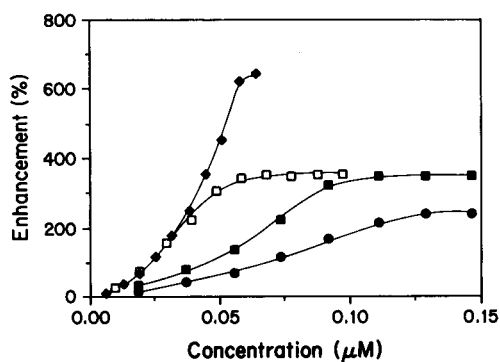


Fig. 6. Plots of percent enhancement of streptavidin-FITC ($f/p = 4.3$, 0.80 mg l^{-1}) fluorescence in the batch mode as a function of the concentration of biocytin (♦), biotin (□), biotin methyl ester (■), and biotin hydrazide (●).

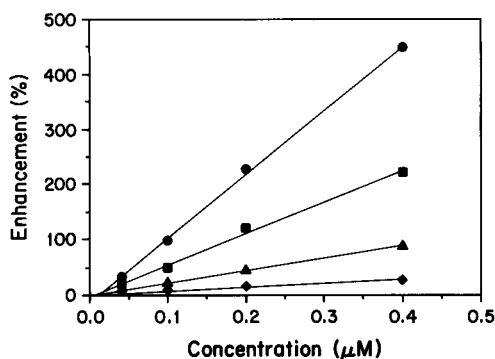


Fig. 7. Plots of percent enhancement of streptavidin-FITC ($f/p = 4.8$, 1.0 mg l^{-1}) fluorescence as a function of the concentration of biocytin (●), biotin (■), biotin-thyroxine conjugate (▲), and biotinylated BSA (◆) as measured with the FIA system with $70\text{-}\mu\text{l}$ loops, a 2-m KOT2 reactor coil and a flow rate of 1.0 ml min^{-1} .

Conclusion

It has been demonstrated that a FIA system can be used for the determination of biotin using avidin-FITC conjugates. The method is fast and reproducible, with detection limits as low as $2 \times 10^{-9} \text{ M}$. It has also been shown that the fluorescence of streptavidin-FITC conjugates is enhanced by reaction with biotin, and that substitution of streptavidin-FITC for avidin-FITC in the FIA system gives superior results in terms of range and sensitivity. The ultimate choice of FIA conditions is dictated by whether the detection limit or sample throughput is the most important consideration. The wide analytical utility of the presented procedure is illustrated by calibration curves obtained for a variety of biotinylated compounds.

This work was supported by a grant from the National Institutes of Health (Grant GM 40510) and from NSERC (TSP).

REFERENCES

- 1 J. Ruzicka and E.H. Hansen, *Flow Injection Analysis*, Wiley, New York, 1988.
- 2 M.D. Luque de Castro and M. Valcarcel, *J. Pharm. Anal.*, 7 (1989) 1291.
- 3 B. Mattiasson, P. Berden and T.G.I. Ling, *Anal. Biochem.*, 181 (1989) 379.
- 4 J.P. Gosling, *Clin. Chem.*, 36 (1990) 1408.
- 5 W.U. de Alwis and G.S. Wilson, *Anal. Chem.*, 59 (1987) 2789.
- 6 M. Nilsson, H. Hakanson and B. Mattiasson, *Anal. Chim. Acta*, 249 (1991) 163.
- 7 A.A. Arefyev, S.B. Vlasenko, S.A. Eremin, A.P. Osipov and A.M. Egorov, *Anal. Chim. Acta*, 237 (1990) 285.
- 8 W.U. de Alwis and G.S. Wilson, *Anal. Chem.*, 57 (1985) 2754.
- 9 I.H. Lee and M.E. Meyerhoff, *Anal. Chim. Acta*, 229 (1990) 47.
- 10 H. Liu, J.C. Yu, D.S. Bindra, R.S. Givens and G.S. Wilson, *Anal. Chem.*, 63 (1991) 666.
- 11 C.S. Lim, J.N. Miller and J.W. Bridges, *Anal. Chim. Acta*, 114 (1980) 183.
- 12 T.A. Kelly and G.D. Christian, *Talanta*, 29 (1982) 1009.
- 13 R.S. Harris, P. György and B.W. Langer, in W.H. Sebrell, Jr. and R.S. Harris (Eds.), *The Vitamins*, Vol. II, Academic, New York, 1968, p. 261.
- 14 M. Wilchek and E.A. Bayer, *Methods Enzymol.*, 184 (1990) 123.
- 15 E.A. Bayer and M. Wilchek, *Methods Enzymol.*, 184 (1990) 138.
- 16 J.N. Ashley and C.R. Harington, *Biochem. J.*, 22 (1928) 1436.
- 17 C.M. Selavka, K.-S. Jiao and I.S. Krull, *Anal. Chem.*, 59 (1987) 2221.
- 18 M.H.H. Al-Hakiem, J. Landon, D.S. Smith and R.D. Nargessi, *Anal. Biochem.*, 116 (1981) 264.
- 19 M.S. Barbarakis, T. Smith-Palmer, L.G. Bachas, S.-Y. Chen and B.W. Van Der Meer, *Talanta*, in press.
- 20 I. Hemmilä, *Clin. Chem.*, 31 (1985) 359.
- 21 E. Soimi and I. Hemmilä, *Clin. Chem.*, 25 (1979) 353.
- 22 D.S. Smith, M.H.H. Al-Hakiem and J. Landon, *Ann. Clin. Biochem.*, 18 (1981) 253.
- 23 M. Wilchek and E.A. Bayer, *Anal. Biochem.*, 171 (1988) 1.
- 24 M.S. Barbarakis, Ph.D. Thesis, Department of Chemistry, University of Kentucky, 1992.

Spectrofluorimetric determination of emetine by flow injection using barium peroxide and UV derivatization

C. Gómez Benito and T. García Sancho

Departament de Química Analítica, Universitat de Valencia, Valencia (Spain)

J. Martínez Calatayud

Departamento de Química, Colegio Universitario CEU, Moncada, Valencia (Spain)

(Received 17th August 1992; revised manuscript received 4th January 1993)

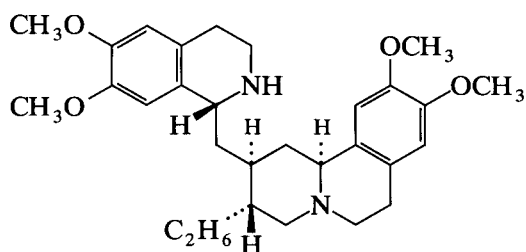
Abstract

The flow-injection spectrofluorimetric determination of emetine was carried out by photoderivatization in the presence of barium peroxide, in a flow-injection assembly in which the PTFE tubing in the injection valve is helically coiled around the lamp. The sample solution merges with a barium peroxide–phosphoric acid solution and then the resulting mixture is irradiated; pure distilled water is used as a carrier stream. The calibration graph is linear over the range 0.05–50 $\mu\text{g ml}^{-1}$ of emetine dihydrochloride. The influence of foreign compounds was studied and the method was applied to the determination of emetine in injection and human urine samples.

Keywords: Flow injection; Fluorimetry; Emetine; Pharmaceuticals; Photoderivatization

Emetine, an alkaloid in ipecacuanha, is an amoebicide acting principally in the bowel wall and in the liver. In intestinal amoebiasis emetine should be given in severe cases of acute amoebic dysentery and in acute exacerbations of chronic amoebic dysentery. Emetine hydrochloride relieves the pain of scorpion sting, it also has expectorant, diaphoretic and emetic actions. The treatment is frequently supplemented with other amoebicidal drugs. Emetine has toxic effects on all tissues and large doses, or prolonged administration of therapeutic doses, may produce degenerative changes in the heart, intestinal tract, kidney, liver and skeletal muscle. Excretion occurs mainly via the urine and is slow. Owing to its

toxic side-effects, rapid and reliable procedures for its determination are required.



Emetine can be determined by potentiometric titration with NaOH [1]. In official procedures [2], emetine is titrated in glacial acetic acid with perchloric acid using crystal violet as indicator. Most spectrophotometric methods involve its extraction from aqueous solution into an organic solution by ion pairing with a dye anion, such as bromothymol blue [3], methyl orange [4] or *p*-chloroanilic acid [5]. The yellow colour produced

Correspondence to: J. Martínez Calatayud, Departamento de Química, Colegio Universitario CEU, Moncada, Valencia (Spain).

when emetine is oxidized by cerium(IV) sulphate can be measured spectrophotometrically after stabilization with sodium acetate [6]. The condensation product of malonic acid with acetic anhydride in the presence of a tertiary amine in a heterocyclic system resulted in a highly fluorescent product [7]. Some liquid chromatographic (LC) procedures for emetine separation and determination have been published [8–10]. A flow injection (FI)–spectrophotometric procedure based on the oxidation of emetine with periodate was investigated in this laboratory [11]. Emetine shows native fluorescence with maximum emission at 318 nm, analogous of that of other compounds containing one or two *o*-dimethoxyphenyl groups; when treated with iodine in alcoholic solution emetine gave a gold-coloured fluorescence with a maximum at 570 nm [12].

Photochemical derivatization is an interesting trend in unsegmented flow methodologies such as LC and FI and it would therefore be of interest to develop methods in unsegmented continuous flow assemblies for the determination of various groups of pharmaceuticals that include light-sensitive compounds. Few papers have been published dealing with photodegradation in an FI assembly for the determination of drugs [13–15] or other compounds such as organophosphorus compounds [16] and organoarsenicals [17].

This paper describes the spectrofluorimetric determination of emetine by reaction with barium peroxide and UV irradiation. The method is suitable over the range 0.05–50 $\mu\text{g ml}^{-1}$ emetine dihydrochloride and it has been applied successfully to the determination of emetine in pharmaceutical formulations and human urine samples.

EXPERIMENTAL

Reagents

An aqueous solution of emetine (Sigma, pure), barium peroxide (Fluka, pure), sucrose (Probus, pure), lactose (Poulenc Frères, pure), glucose (Panreac, pure), ethanol (Panreac, analytical-reagent grade), resorcinol (Riedel de Haen), formaldehyde (Panreac, analytical-reagent grade) and menthol (Acofarma) were used.

Continuous-flow manifolds

The action of light was preliminarily studied by using manifolds in which the pharmaceutical solution placed in a beaker was irradiated and then it was directly transferred to the detector by means of a peristaltic pump in order to determine the influence of the irradiation time in different media and environmental conditions. In a different set of experiments, the sample was irradiated while it was circulated through a tube coiled around the lamp. However, in the proposed FI assembly (depicted in Fig. 1a), the sample solution merges with the reagent in a mixing chamber and the resulting mixture is injected by means of a Rheodyne Model 5051 valve and irradiated with a Vilber-Lurmat T-60 mercury lamp (6 W), then by means of a water stream acting as a carrier it was transferred to a Shimadzu RF-520 spectrofluorimetric detector furnished with a Hellma flow cell (20 μl inner volume). The PTFE tubing was of 0.5 mm i.d. and the peristaltic pump used was a Gilson Minipuls 2.

Procedures for sample treatment

Human urine samples were prepared by adding emetine to recently obtained human urine to give an emetine concentration of 100 $\mu\text{g ml}^{-1}$. To 25 ml of urine was added concentrated ammonia to give an ammonia concentration up to 8.6 M and extraction was effected with 25 ml of diethyl ether. The two liquid phases were shaken for 2 min and then the aqueous phase was re-extracted with 25 ml of diethyl ether. The solvent was evaporated at room temperature and the residue was dissolved in 10 ml of 4 M phosphoric acid and the solution diluted to 50 ml with distilled water; it was then diluted to about 4 $\mu\text{g ml}^{-1}$ with distilled water.

Injections were prepared according to the recommended procedure [18]: a carefully weighed amount of emetine (about 350 mg) was dissolved in 10 ml of water and the pH adjusted potentiometrically to 3.0 by adding 1.0 M HCl. Finally the resulting solution was diluted with distilled water to give emetine concentrations of up to about 4 $\mu\text{g ml}^{-1}$.

RESULTS AND DISCUSSION

Initial experiments (batch and continuous-flow) were aimed at increasing the native fluorescence of emetine by photochemical oxidation. The native fluorescence of the drug, with wavelengths of 285 and 320 nm for excitation and emission, respectively, was shifted and clearly increased by combining irradiation and the presence of dispersed solid barium peroxide into acetic acid solution; the resulting product showed high emitted fluorescence at $\lambda(\text{ex}) = 350$ nm and $\lambda(\text{em}) = 452$ nm. Irradiation alone gave the same displacement of the emission spectrum without an increase in the intensity; barium peroxide alone did not affect the native emission spectrum of the drug, even on heating the barium peroxide solution to 90°C. Only the combined action irradiation and barium peroxide resulted in an increase in emitted light.

Irradiation of the solution with continuous monitoring (see Fig. 1a) showed no differences if the solid barium peroxide was eliminated or not by filtering the solution passing through the flow cell. This set of experiments up to 32 min also showed an optimum irradiation time, producing the greatest emitted light. When the irradiation of the sample was carried out through the PTFE tubing (constant irradiation time), the contact time of barium peroxide (4 mg in 50 ml of 0.05 M acetic acid–drug solution) was studied up to 35 min; the recorded spectra remained identical. Then the length of coiled tubing around the lamp was varied and was found to be an important parameter; the irradiation time and not the barium peroxide–emetine solution contact time is the critical parameter. However, an increase in the amount of dispersed barium peroxide (tested from 38 to 199 mg in 50 ml of 0.05 M acetic acid) gave a slight increase in the emitted light up to 151 mg; higher amounts had no further effect.

Other parameters tested that were found not to be critical were the acetic acid concentration (studied range 0.3–6.9 M) or and the stirring, magnetic at different velocities or ultrasonic. The influence of the pH of different media (hydrochloric acid, acetic acid, neutral and alkaline) revealed slightly acidic media to be most suitable.

Several acidic media were tested (hydrochloric, sulphuric, nitric, acetic and phosphoric acid) the highest emitted light was obtained with acetic and phosphoric acid solutions; sulphuric acid also gave high but irreproducible results owing to the evolution of bubbles and to the instability of the pharmaceutical in sulphuric acid medium. No clear advantages were observed on heating the solution (up to 90°C) and the tedious evolution of bubbles was increased.

Optimization of the flow-injection assembly

Three different flow assemblies were tested and compared by varying the FI parameters (length of coiled tube around the lamp, flow-rate of carrier or sample and sample volume) and the chemical composition (distilled water or phosphoric acid solution) of the carrier, sample adjustment solution and the sample solution (acetic and phosphoric acid). The three studied assemblies are depicted in Fig. 1; in Fig. 1a and b a mixing chamber was used for the merging sample and adjusting media channels and in Fig. 1c a Y confluence was used. A pre-optimization was carried out with each tested manifold and the best results that could be obtained were compared; the sample aliquots contained $825 \mu\text{g ml}^{-1}$ of emetine in 1 M phosphoric acid, which merged with 1 M phosphoric acid (channel A) and pure distilled water as carrier. The best transient outputs obtained and the corresponding experimental parameters were as follows: irradiated coil length (the three manifolds), 265 cm; manifold in Fig. 1a, sample volume and irradiated coil length $733 \mu\text{l}$ and 265 cm respectively, flow-rates for S, A and C channels 2.9, 2.0 and 4.3 ml min^{-1} , respectively, and average FI signal 11.5 cm; manifold in Fig. 1b, sample volume $484 \mu\text{l}$, flow-rates 2.9, 2.0 and 4.3 ml min^{-1} and average outputs FI signal 8.5 cm; and manifold in Fig. 1c, sample volume $696 \mu\text{l}$, flow-rates 1.8, 1.2 and 1.8 ml min^{-1} and average FI signal 9.5 cm. The outputs from the manifold in Fig. 1a showed a narrower base peak than the those from the manifold depicted in Fig. 1c.

Once the assembly in Fig. 1a had been selected as a suitable manifold, a sequential optimization procedure was applied; first, and bear-

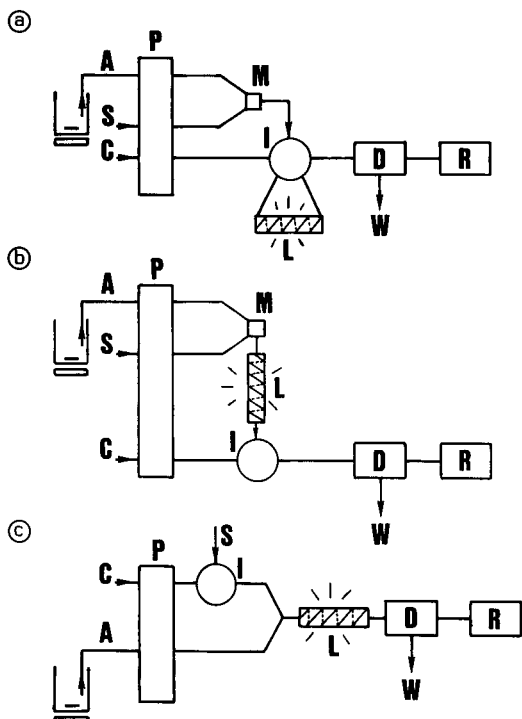


Fig. 1. FI manifolds tested for the determination of emetine. S, sample solution; A, channel with phosphoric acid for adjusting the sample acidity; I, injection valve; L, mercury lamp; C, carrier; D, detector; W, waste; R, recorder; M, mixing chamber.

ing in mind the formerly pre-optimized chemical parameters, the univariate method was applied to refining those parameters; then the optimization of FI parameters was carried out. Finally, the acidity and content of barium peroxide were also refined.

The influence of acidity was studied with phosphoric and acetic acid media. The best results were observed for acetic acid at concentrations close to 0.3 M and for phosphoric acid around 4–5 M. The emitted light was clearly greater with phosphoric acid rather than acetic acid solutions; the highest signals were 19.5 and 57 cm for concentrations of acetic acid and phosphoric acid media in the vicinity of 0.3 and 5 M, respectively. The different water–phosphoric acid combinations studied revealed higher transient outputs when the carrier was distilled water and the concentration of phosphoric acid was 4 M in both channels (sample and sample adjustment).

The influence of the barium peroxide content was studied over the range 19.1–201.8 mg in 50 ml of 4 M phosphoric acid. The results showed that an increase in peroxide content resulted in a decrease in the signal height, the highest transient signal being in the range 20–40 mg (see Fig. 2). It should be pointed out that such an amount of barium peroxide in phosphoric acid medium forms a solution, not a turbid suspension as occurs with acetic acid media; this is also in accordance with [19].

The optimization of the FI parameters, namely sample loop volume, flow-rate of sample solution, sample-to-barium peroxide flow-rate ratio, flow-rate of carrier and coil length from injection valve to detector flow cell was carried out in the reported order and by means of the univariate method. Table 1 gives the ranges studied for the tested parameters and the values selected as optimum.

The distance from the injection valve to the flow cell had no influence. The flow-rate of the carrier stream influenced the width of the base peak (influencing the sample passage). However, the other parameters tested (sample volume and flow-rate ratio) resulted in critical variations on

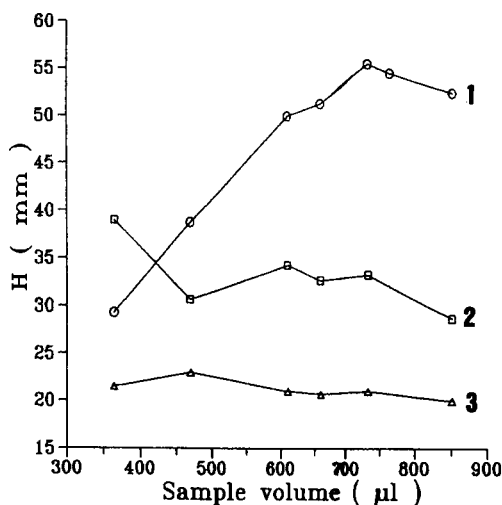


Fig. 2. Influence of sample volume and irradiation time on the degradation of emetine, as shown by the peak-height signals (H). 1, The sample is flowing through the valve loop; 2 and 3, stopped flow of the sample in the irradiated coil for 30 and 60 s, respectively.

TABLE 1

Optimization of FI parameters

Parameter	Studied range	Selected value
Sample flow-rate (ml min ⁻¹)	0.6–1.8	1.0
Flow-rate ratio ^a	0.84–1.81	1.81
Carrier flow-rate (ml min ⁻¹)	2.1–4.8	4.3
Sample volume (μl)	365–852	377
Injection valve–flow cell distance (cm)	102–358	102

^a Sample solution to barium peroxide solution.

the transient outputs. The amounts of drug and reagents resulting from merging (M in Fig. 1a), which means the flow-rates in both channels A and S were important. The reagent stream contained 40 mg of barium peroxide in 50 ml of 4 M phosphoric acid. The irradiation time of the drug (in the sample loop) is not relevant (except for small sample volumes) in this step of the optimization.

Finally, with the optimized FIA manifold, the concentrations of phosphoric acid and barium peroxide were refined and resulted in the selection of 4.0 M and 40 mg in 50 ml, respectively (see Fig. 3).

Analytical application

The analytical application of the continuous-flow procedures was studied to establish the application range, reproducibility, detection limit and sample throughput rate.

The calibration graph was linear over the range 0.05–50 μg ml⁻¹ of emetine.

The reproducibility and sample throughput were tested by injecting 34 sample aliquots of 3.5 μg ml⁻¹ emetine. The calculated R.S.D. was 0.65% and the sample throughput 67 h⁻¹.

The tolerance of the method to foreign compounds that may be found in typical pharmaceutical samples containing emetine was investigated by using solutions containing 3.5 μg ml⁻¹ of the drug and adding various concentrations of the interfering compounds up to 100 μg ml⁻¹ or when the relative error was about 3%. The results obtained were as follows (concentration of the foreign compound in μg ml⁻¹ and relative

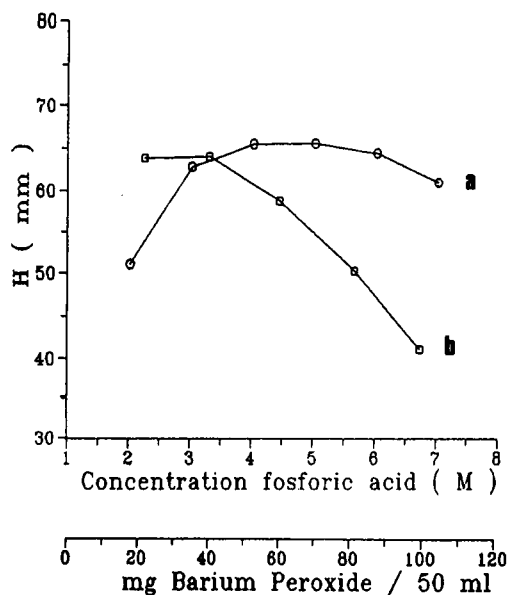


Fig. 3. Influence of (a) phosphoric acid and (b) barium peroxide concentrations on the oxidation of emetine, as shown by the peak-height signals (H).

error in %): sucrose, 100, 1.2; lactose, 90, 2.8; and formaldehyde, 16.2, 2.5; the presence of ethanol at a concentration 0.335 M reduced the signal height to about 10% of that for pure emetine; 1 ml of menthol solution in 50 ml of sample resulted in a relative error of 0.4%; the most serious interference was from resorcinol, a 3.5 μg ml⁻¹ concentration resulting in 48.5% error.

The emetine content in prepared injection and human urine samples was determined. Up to ten repetitive injections were made and at least five different preparations were analysed and the results compared with the added amount: human urine, added 4.00 and found 3.86 μg ml⁻¹ relative error 3.4%; injection, added 3.93 and found 3.94 μg ml⁻¹, relative error 0.3%.

REFERENCES

- 1 L. Saunders and R.S. Srivasta, *J. Pharm. Pharmacol.*, 3 (1951) 78.
- 2 E.E. Van Tamelen, P.E. Aldrich and J.B. Hester, *J. Am. Chem. Soc.*, 81 (1959) 6214.
- 3 V. Das Gupta and H.B. Herman, *J. Pharm. Sci.*, 62 (1973) 311.

- 4 A.K. Gabko and V.S. Konyushko, *Zh. Anal. Khim.*, 21 (1966) 486; *C.A.*, 65 (1966) 2067.
- 5 M. Abdel Salam, M. Abdel Hamid and M. Bedair, *Egypt. J. Pharm. Sci.*, 25 (1984) 303.
- 6 P.K. Seth and G.K. Ray, *Indian J. Pharm.*, 29 (1967) 203.
- 7 I.H. Refaat, M.E. El-Kommos, H.H. Farag and N.A. El-Rabat, *Bull. Pharm. Sci.*, 10 (1987) 85.
- 8 D.J. Crouch, D.M. Moran, B.S. Finkle and M.A. Michael, *J. Anal. Toxicol.* 8 (1984) 63.
- 9 M. Popl, K. Le Duy and J. Strnadova, *J. Chromatogr. Sci.*, 23 (1985) 95.
- 10 I. Jane, A. McKinnon and R.J. Flanagan, *Farm. Pol.*, 40 (1984) 593.
- 11 J. Martínez Calatayud and S. Sagrado Vives, *Pharmazie*, 44 (1989) 614.
- 12 K. Florey (Ed.), *Anal. Profiles Drug Subst.*, 10 (1981) 289.
- 13 J. Martínez Calatayud and C. Gómez Benito, *Anal. Chim. Acta*, 231 (1990) 259.
- 14 J. Martínez Calatayud and C. Gómez Benito, *Anal. Chim. Acta*, 256 (1992) 105.
- 15 A. Mellado Romero, C. Gómez Benito and J. Martínez Calatayud, *Anal. Lett.*, 25 (1992) 1289.
- 16 I.D. Mckelvie, B.T. Hart, T.J. Cardwell and R.W. Catrall, *Talanta*, 114 (1989) 1459.
- 17 R.H. Atalian and D.A. Kalman, *Talanta*, 38 (1991) 167.
- 18 Martindale, *The Extra Pharmacopoeia*, Pharmaceutical Press, London, 27th edn., 1978, p. 77.
- 19 L. Blas, *Agenda del Químico*, Aguilar, Madrid, 1973.

Polypyrrole–dodecyl sulphate electrode as a microsensor for electroinactive cations in flow-injection analysis and ion chromatography

R. Carabias Martínez *, F. Becerro Domínguez, F. Martín González and J. Hernández Méndez
Departamento de Química Analítica, Nutrición y Bromatología, Universidad de Salamanca, 37008 Salamanca (Spain)

R. Córdova Orellana

Universidad Católica de Valparaíso, Valparaíso (Chile)

(Received 6th October 1992; revised manuscript received 15th January 1993)

Abstract

An electrochemical sensor based on the incorporation of dodecyl sulphate (DDS) into polypyrrole (Ppy) by electropolymerization of pyrrole in the presence of surfactant is described. The resulting polymer film proved to be useful for the detection of non-electroactive cations (Li^+ , Na^+ and K^+ were tested). The physicochemical characteristics of the Ppy–DDS electrode and its response against the alkali metal ions in cyclic voltammetry were studied. Application of this electrode as a sensor in flow-injection analysis and in high-performance ion chromatography is demonstrated. The electrode remains stable for several weeks with no evidence of chemical or mechanical damage.

Keywords: Flow injection; Ion chromatography; Sensors; Voltammetry; Alkali metal ions; Dodecyl sulphate; Polypyrrole electrode

Since the 1970s, the development of modified electrodes has highlighted their great possibilities, especially with respect to sensitivity and selectivity [1–4]. Modification of electrodes with electrocatalytic moieties or specially functionalized polymers provides conventional electrochemical electrodes with a significant functional enhancement for analytical applications. Electrodes coated with different electrically–conductive polymers have been found to be applicable as electrochemical detectors for electroinactive anions in flow-injection analysis and liquid chromatography [5,6]. However, the determination of electroinactive cations with polymer-modified

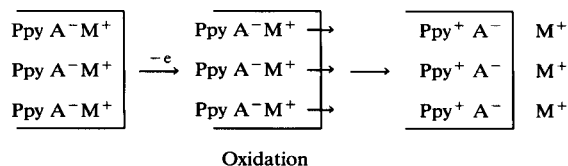
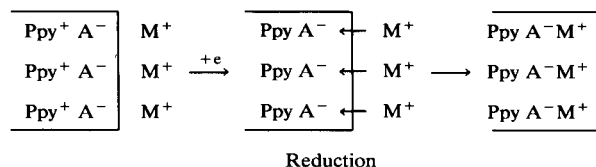
electrodes has not received as much attention [7,8].

Determinations of electroinactive anions with polymer-modified electrodes are based on the fact that oxidation of the polymer involves the incorporation of anionic species, which neutralize the positive sites generated during oxidation of the polymer. In contrast, the reduction process implies the disappearance of the positive charges from the polymer, which essentially involves the exit of the negatively charged doping ions.

This mechanism is known to be valid only in the case of hydrophilic anions, with not too high a volume. However, if the oxidation–reduction process is performed in the presence of large anions, such as dodecyl sulphate or toluenesulphonate, capture of these anions by the polymer is irreversible, because they are retained by Van der

Correspondence to: R. Carabias Martínez, Departamento de Química Analítica, Nutrición y Bromatología, Universidad de Salamanca, 37008 Salamanca (Spain).

Waals interactions between the apolar extremities of the amphiphilic surfactant anion and the neutral backbone of the polypyrrole [9–11]. In this case, during the process of reduction of the polymer, no anionic elimination occurs; rather, cations are incorporated. In turn, oxidation involves the elimination of cations and, occasionally, the incorporation of hydrophilic anions that may be present in the solution [11]. The redox process can be represented schematically as follows:



Recently, the electrochemical behaviour of a polypyrrole–dodecyl sulphate (Ppy–DDS) electrode in propylene carbonate was investigated by cyclic voltammetry and frequency response analysis using LiClO_4 or LiAsF_6 as electrolytes [12]. The results obtained showed that the presence of the surfactant anion in the polymer favours the redox processes which were faster and more reversible than those associated with the polypyrrole electrode that has a hydrophilic anion incorporated. These results have been attributed to the faster diffusion of the cation during the redox process that occurs on the Ppy–DDS electrode [12].

This paper reports on the behaviour of a modified electrode prepared by electrochemical polymerization of pyrrole in sodium dodecyl sulphate solution and its application to the detection of K^+ , Na^+ and Li^+ by cyclic voltammetry. This electrode can be used, in the amperometric mode at constant potential, as a sensor in flow injection analysis (FIA) and in ion chromatography (IC). In order to obtain reproducible responses, the procedures for the regeneration of the electrode

were optimized. The electrode is easy to prepare and its response remains stable after several weeks.

EXPERIMENTAL

Reagents

All chemicals were of analytical-reagent grade and used as received. Pyrrole was obtained from Aldrich, sodium dodecyl sulphate from Fluka, glycine from Panreac and acetonitrile from Carlo Erba. Stock solutions of the cations were prepared from potassium chloride, sodium chloride and lithium perchlorate and diluted further daily as required. Solutions of tartaric acid were prepared immediately prior to use.

Preparation of polypyrrole electrodes

In the cyclic voltammetric studies the support of the modified electrode was a Metrohm 628–50 platinum electrode with an area of about 20 mm^2 , the auxiliary electrode being made of platinum and separated from the electroanalytical cells by porous glass. The reference electrode was a saturated calomel electrode. To avoid contamination by potassium, the reference electrode was placed in a compartment separated from the cell by a narrow tube of porous glass, which was empty. On taking measurements, contact was established by aspirating the solution under study through a hypodermic needle until, by filling the auxiliary compartment, it reached the reference electrode.

In flow-injection analyses and chromatography, the polypyrrole film was formed on a Metrohm vitreous carbon electrode with an area of about 20 mm^2 . Prior to film formation, the electrode surface was polished with alumina slurries, residual polishing material being removed from the electrode surface by sonication. The auxiliary electrode was gold and the reference electrode was $\text{Ag}/\text{AgCl}/3 \text{ M KCl}$.

The polypyrrole film was formed in a 0.23 M solution of pyrrole and 0.05 M sodium dodecyl sulphate in acetonitrile–water (80 + 20, v/v). A potential of +1.400 V was applied for 5 min followed by five potential sweeps between +0.700 and –1.300 V. Film formation was completed by

applying a voltage of +0.700 V for 5 min. Immediately after the polymer had formed, the electrode was stored in a 0.01 M aqueous solution of glycine.

Apparatus

Cyclic voltammetry was performed with an AMEL system consisting of a Model 551 potentiostat, a Model 564 functions generator and a Model 862/D recorder. The following components were used in the flow-injection system: a Gilson M-3 pump, a Rheodyne Model 5021 injection valve and a Metrohm E-580 recorder. Ion chromatography was performed with a Spectra-Physics Model 8810 isocratic pump, a Rheodyne Model 7125 injection valve, an IC cation Super-Sep (Metrohm) separator and a Spectra-Physics integrator.

A Metrohm Model 656 detector coupled to a Metrohm Model 611 potentiostat was used for the FIA and chromatographic studies.

Energy-dispersive x-ray spectrometric (ED-XRS) analyses and microphotographs were obtained with a Zeiss DSM 940 scanning electron microscope.

Procedure

Voltammetric determination of lithium, sodium and potassium was carried out in a 0.01 M solution of glycine. The cyclic voltammograms were obtained by scanning between +0.650 and -1.100 V at a rate of 25 mV s⁻¹, measuring cathodic currents at -0.800 V.

FIA determinations were performed in a single-channel flow system using 0.01 M glycine as carrier. The Ppy-DDS electrode was activated for 10 min at +0.700 V while a carrier flow was passing through the detector. The injection volume was 200 μl and the flow-rate was 1.54 ml min⁻¹. The voltage used for the detection was -0.800 V and all injections were carried out in triplicate.

Chromatographic separation of lithium, sodium and potassium was performed using 1 mM tartaric acid as the mobile phase at a flow-rate of 1.00 ml min⁻¹. The modified electrode was activated by applying a potential of +0.700 V for 1 min prior to each injection, carrying out ampero-

metric detection at -0.800 V. The injection volume was 20 μl and the chromatograms were evaluated by integrating areas and measuring peak heights.

RESULTS AND DISCUSSION

Preparation and response of the Ppy-DDS electrode

The first series of experiments was carried out performing polymerization in an aqueous solution and using a layer of platinum or steel mesh as supports. Figure 1 shows a series of cyclic voltammograms obtained with the steel mesh support; it can be seen that the system becomes more irreversible as the number of cycles increases. Although from the electrochemical point of view this type of support could be useful, the mechanical behaviour of the film formed is poor because, with the passage of time, it fragments and sloughs off the support. As regards the platinum support, working in an aqueous medium the films formed on this are mechanically stable. However, the voltamperometric signals obtained, in solutions of glycine containing an alkali metal cation (potas-

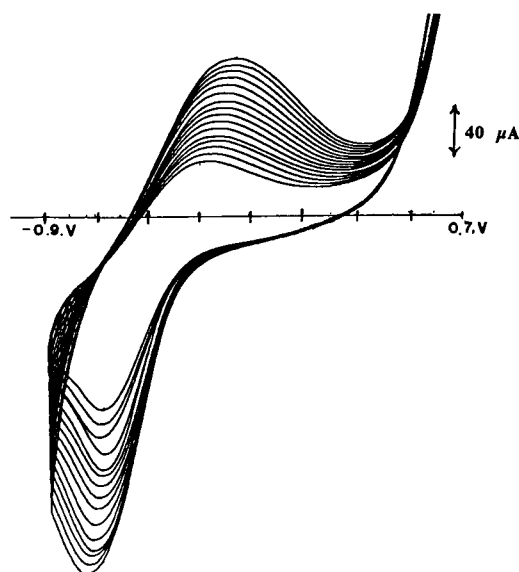


Fig. 1. Cyclic voltammograms obtained during the potentiodynamic formation of the Ppy-DDS film. Support, steel mesh. Aqueous solution of 0.112 M pyrrole and 0.05 M Na DDS.

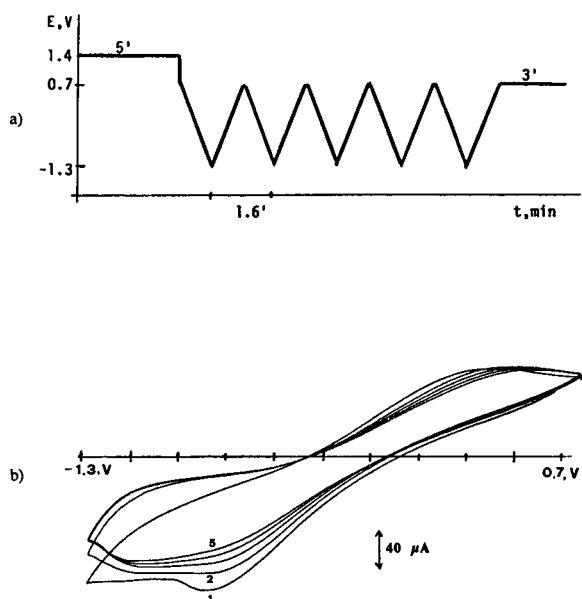


Fig. 2. (a) Potentials applied during the formation step of the Ppy-DDS electrode. (b) Cyclic voltammograms scanned between +0.700 and -1.300 V using platinum in acetonitrile-water (80 + 20, v/v), 0.23 M pyrrole and 0.05 M Na DDS. The numbers on the voltammograms represent the cycle number.

sium was used), cannot be reproduced, possibly owing to a lack of stability of the polymer.

The best results were obtained by polymerizing the pyrrole on a platinum support in acetonitrile-water (80 + 20, v/v). Figure 2 shows the cyclic voltammograms obtained on a film of polypyrrole formed in the above-mentioned medium with 0.23 M pyrrole and 0.05 M Na DDS applying the potentials indicated. After its preparation, the polypyrrole-coated electrode was stored in aque-

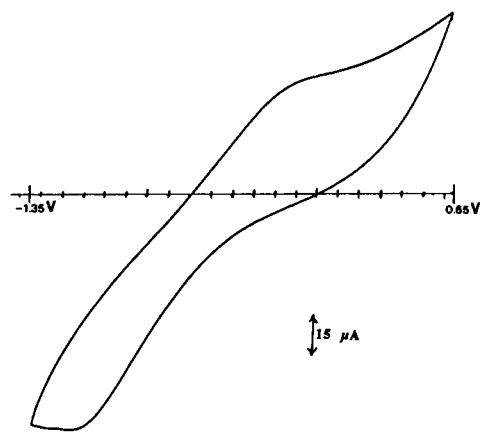


Fig. 3. Cyclic voltammetric response of a solution 0.01 M in both potassium and glycine.

ous glycine solution, avoiding exposure to air. It has been ascertained experimentally that if the film formed in acetonitrile-water (80 + 20, v/v) is exposed to air, the acetonitrile evaporates and the film degrades and sloughs off the support.

Potassium ion was chosen to study the response of the polypyrrole electrode using 0.01 M glycine as the supporting electrolyte. This response (Fig. 3) is not modified on varying the polymerization time (at +1.400 V) between 3 and 10 min, such that in later studies a time of 5 min was employed. On studying the effect of the composition of the acetonitrile-water solution used for the polymerization step, it was observed that the response of the electrode was more reproducible when polymerization is performed

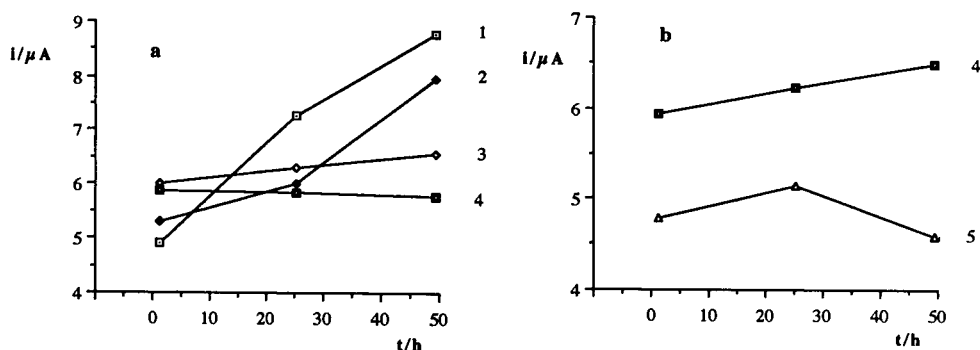


Fig. 4. Variation of the analytical signal (intensity at -0.800 V) with time. Solution containing 1×10^{-3} M potassium and 0.01 M glycine. Different Ppy-DDS electrodes: acetonitrile concentration in acetonitrile-water (a) (1) 0, (2) 50, (3) 70 and (4) 80% (v/v); (b) 80% (v/v); (4) without and (5) with N_2 .

with concentrations $> 70\%$ (Fig. 4a). Further, by carrying out polymerization with a solution containing 80% (v/v) acetonitrile without degassing either the polymerization solutions or the measuring solutions, the signals were stable, over at least 48 h, and slightly higher than those obtained when working with degassed solutions (Fig. 4b). These results show that the polymerization and the measurement can be carried out without having to degas the solutions, which is an advantage over other procedures described for the preparation of modified polypyrrole electrodes as anion sensors [5]. It was later ascertained that the re-

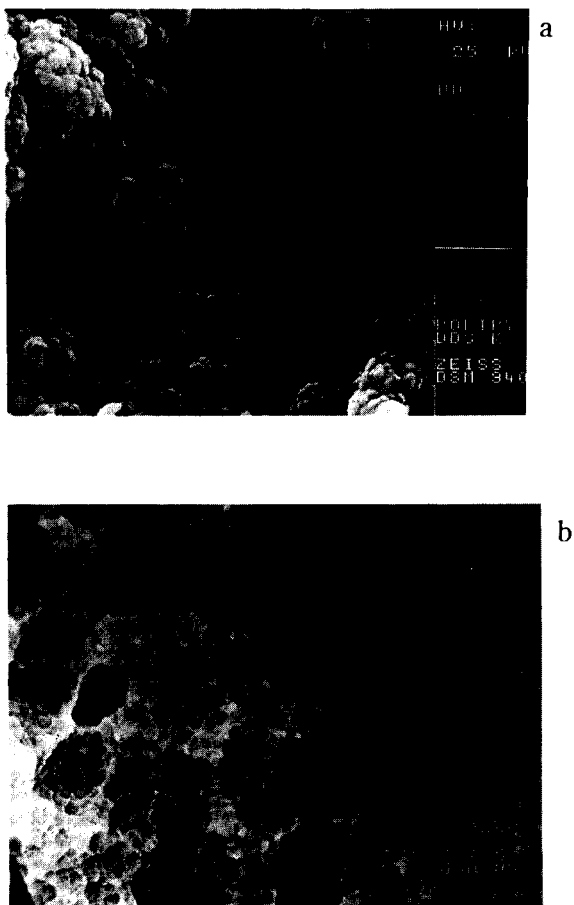


Fig. 5. Scanning electron micrographs of films of Ppy-DDS after performing several sweeps in a solution containing 1×10^{-3} M potassium in 0.01 M glycine. Final potential (a) -1.300 and (b) $+0.700$ V.

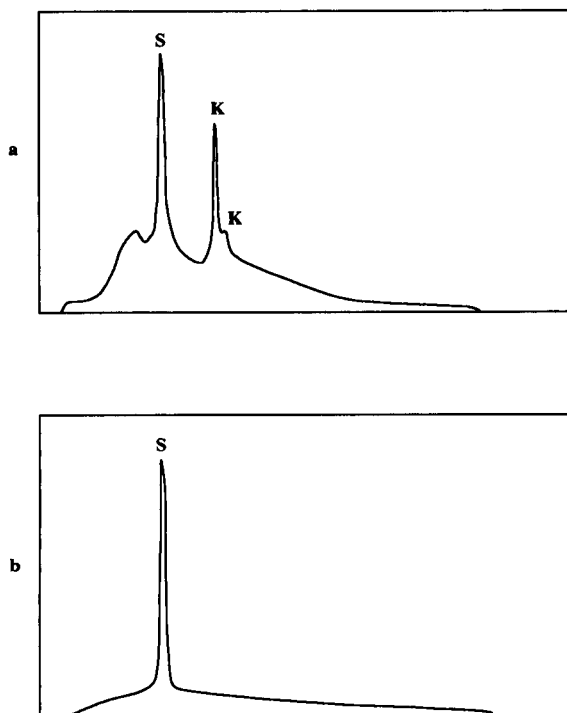


Fig. 6. EDXRS of films of Ppy-DDS after performing several sweeps in a solution of 1×10^{-3} M potassium and 0.01 M glycine. Final potential (a) -1.300 V and (b) $+0.700$ V.

sponse of the electrode is reproducible over several weeks.

Characterization of the polypyrrole film

Figure 5 shows scanning electron micrographs of the Ppy-DDS film after being introduced in a solution of potassium and glycine. In Fig. 5a, the potential scan was cut off at cathodic potentials (with potassium ions in the film) and Fig. 5b shows a micrograph of when the potential scan was cut off at anodic potentials (no potassium ions in the film).

Figure 6 shows the EDXRS of a film of Ppy-DDS film whose potential scan was cut off at either cathodic or anodic potentials. In the former instance (Fig. 6a), the signals of the $K\alpha$ lines of sulphur (2.313 keV) and those corresponding to the $K\alpha$ (3.321 KeV) and $K\beta$ (3.632 keV) lines of potassium can be seen. However, the spectrum obtained when the final potential is anodic (Fig.

6b) only shows the line corresponding to sulphur. These results show that during the reduction process potassium ions enter the film, whereas they leave it during the oxidation process. For determination of the potassium and sulphur contents in the first film, pyrite (FeS_2) and orthoclase (KAlSiO_3) were used as standards. The percentage values (by weight) in the excitation volume were 14.55% for sulphur and 17.40% for potassium. The ratio between these values (0.8362) represents a sulphur/potassium molar ratio of 1.02, such that 1 mol of potassium ions can be said to enter the film for every mole of dodecyl sulphate ions.

Electroanalytical determination of lithium, sodium and potassium

Cyclic voltammetry. Using the described Ppy-*DDS* electrode, the cyclic voltammograms of each of the species studied were recorded over concentrations ranging between 0.01 M and 1×10^{-5} M, in all cases using 0.01 M glycine as the electrolyte. The voltammograms were recorded between +0.650 and -1.100V at a scan rate of 25 mV s^{-1} , the currents being measured at -0.800 V. The relationships observed between currents and concentrations were linear for concentrations below 1×10^{-3} M. The precision of the method ($n = 10$) for concentrations close to 1×10^{-4} M ranges between 1.5% and 3.0% and the 3σ detection limits were ca. 10 μM (Table 1).

Flow-injection analysis. The response of the Ppy-*DDS* electrode was studied in a single channel manifold using 0.01 M glycine as carrier. The potential applied to the electrode was -0.800 V and on injecting different concentrations of the ions studied it was observed that it is necessary to regenerate the electrode in order to obtain stable

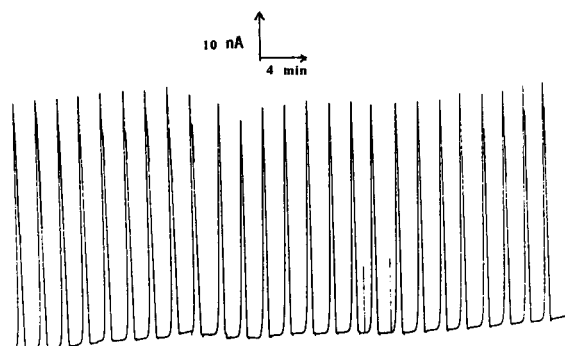


Fig. 7. Variation of the analytical signal with the number of injections (FIA). Electrode activation, 0.700 V over 10 min; carrier, 0.01 M glycine; concentration of the potassium solution injected, 1×10^{-4} M; measuring potential, -0.800 V.

signals. Other workers [6,7] applied a potential close to the formal one, where both the reduced and oxidized forms of polypyrrole co-exist. Under these conditions cations do not accumulate on the electrode but the analytical signal shows positive and negative peaks and the baseline is not so stable. In this work it was seen that electrode regeneration (exit of cations from the polymer) can be satisfactorily and easily performed by applying a potential of +0.700 V for 10 min while carrier solution is being passed through the detector. By carrying out this regeneration step after each measurement, the analytical signal remains stable and reproducible after performing 25 injections of a 1×10^{-4} M solution of potassium, ca. 1 h of work (Fig. 7). After this time, it is advisable to regenerate the electrode.

The influence of flow-rate on the response of the electrode was studied by injecting a solution of 1×10^{-4} M potassium and 0.01 M glycine as carrier. In the flow-rate range 1.30–4.40 ml min^{-1} the peak current increased as the flow-rate in-

TABLE 1

Calibration for cyclic voltammetry with concentrations between 1×10^{-5} and 1×10^{-3} M of each ion

Ion	Intercept (μA)	Slope ($\mu\text{A l mol}^{-1}$)	Correlation coefficient ^a	R.S.D. ^b (%)	Detection limit (3σ) (M)
Li^+	0.19 ± 0.06	$(4.6 \pm 0.1) \times 10^3$	0.999	1.5	1.3×10^{-5}
Na^+	0.16 ± 0.05	$(5.4 \pm 0.1) \times 10^3$	0.999	2.5	1.1×10^{-5}
K^+	0.22 ± 0.07	$(5.4 \pm 0.1) \times 10^3$	0.998	3.0	1.1×10^{-5}

^a $n = 9$, ^b $n = 10$ (sample size 1.5×10^{-4} M).

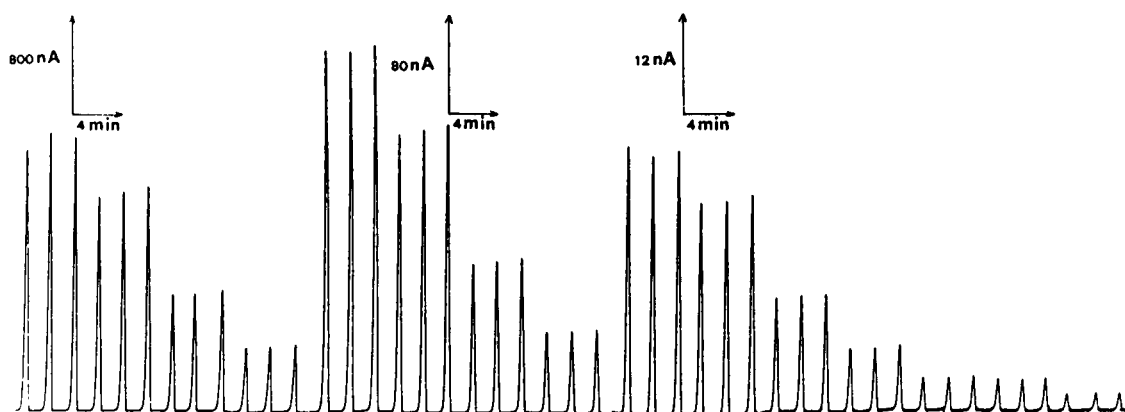


Fig. 8. Flow signals for lithium calibration graph: 6, 8, 10, 20, 40, 80 and 100 μM and 0.2, 0.4, 0.8, 1.0, 2.0, 4.0, 8.0 and 10.0 mM.

creased, its variation being relatively small; accordingly, in later experiments a flow-rate of 1.54 ml min^{-1} was used.

The flow signals obtained on injecting, in triplicate, solutions of lithium ions in the concentration range 1×10^{-6} –0.01 M are shown in Fig. 8. The relationships obtained between the currents and the concentrations of lithium, sodium and potassium are linear for concentrations lower than 0.01 M (Table 2). The reproducibility of the peak currents was satisfactory and the relative standard deviations (R.S.D.s) ranged from 4.6 to 2.7% (Table 2).

The 3σ detection limit ranged between 2.5×10^{-6} M for lithium and 1.6×10^{-6} M for potassium.

Ion chromatography. Owing to the lack of sensitivity of the Ppy–DDS electrode, its response as a detector in a chromatographic system was studied. Of the different mobile phases reported [13] as being ideal eluents (ethylenediamine, nitric

acid and tartaric acid) for separating the ions studied, tartaric acid was chosen because it gives the best background signal at the measuring potential of -0.800 V.

Chromatographic separation was optimized by varying the concentration of tartaric acid between 1×10^{-5} and 0.02 M and the flow rate of the mobile phase between 0.7 and 1.3 ml min^{-1} . The best results were found using 1.0 mM tartaric acid and a flow-rate of 1.00 ml min^{-1} . Under these conditions, the retention times for lithium, sodium and potassium are 5.22, 6.33 and 8.61 min, respectively (Fig. 9).

If a sufficiently cathodic potential is applied, in such a way that only reduction (entry of cations) occurs, the baseline obtained in the chromatograms is stable, although it is necessary to regenerate the electrode periodically in order to remove the cations accumulated in the polypyrrole film. In the light of the results obtained in the flow-injection analyses the above-described

TABLE 2

Calibration for flow-injection analysis with concentrations between 1×10^{-6} and 0.01 M of each ion

Ion	Intercept (nA)	Slope (nA l mol ⁻¹)	Correlation coefficient ^a	R.S.D. ^b (%)	Detection limit (3σ) (M)
Li ⁺	2.9 ± 1.1	$(2.97 \pm 0.03) \times 10^5$	0.999	4.2	2.5×10^{-6}
Na ⁺	3.3 ± 0.9	$(3.48 \pm 0.02) \times 10^5$	0.999	4.6	2.2×10^{-6}
K ⁺	3.1 ± 1.8	$(4.71 \pm 0.05) \times 10^5$	0.999	2.7	1.6×10^{-6}

^a $n = 13$. ^b $n = 13$ (sample size 2×10^{-4} M).

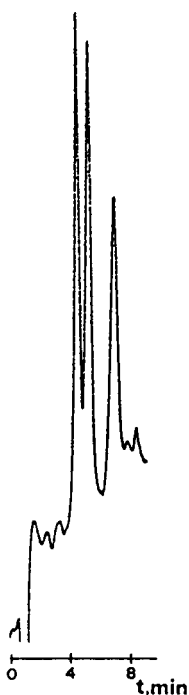


Fig. 9. Chromatograms of a solution 4×10^{-4} M lithium, sodium and potassium. Volume injected, $20 \mu\text{l}$.

pretreatment was applied, thereafter measuring the analytical signal corresponding to each of the alkali metal ions. The analytical signals obtained after ten injections are not very precise, with R.S.D.s between 7.8% for sodium and 17.3% for potassium. More precise results were obtained by regenerating (+0.700 V over 1 min) the electrode before each injection. With this kind of activation, the signals obtained are satisfactorily precise, with R.S.D.s ranging between 2.7% for sodium and 5.8% for lithium. The concentration of Li^+ , Na^+ and K^+ injected was 1×10^{-3} M.

Calibration graphs were plotted for Li^+ , Na^+ and K^+ in the 3.0×10^{-5} – 4.0×10^{-3} M range and straight lines with linear correlation coefficients better than 0.997 ($n = 9$) were obtained. The 3σ detection limits for Li^+ , Na^+ and K^+ were calculated as 2.2×10^{-5} , 1.65×10^{-5} and 2.9×10^{-5} M, respectively; similar values have been reported by Nieto and Frankenberger [14] using a $500\text{-}\mu\text{l}$ loop without a suppressor column for the determination of these ions by ion chromatography with conductimetric detection. In

contrast to the results obtained in FIA experiments, the sensitivity of the Ppy–DDS electrode to alkali metal ions was inferior in ion chromatographic determinations. This could be due to the change in the eluent and a better response of the electrode should be obtained by use of the hydrogen ion suppressor column.

Conclusions

It was found that a Ppy–DDS electrode can be constructed by electrochemical polymerization of pyrrole in the presence of dodecyl sulphate using solid materials such as platinum and vitreous carbon as substrates. Incorporation of DDS into the polymer film offers the advantage of being able to construct a novel type of polymer cation-selective electrode.

The proposed Ppy–DDS electrode can be used satisfactorily as a sensor for the detection of alkali metal ions (Li^+ , Na^+ , K^+) in cyclic voltammetry and in flow-injection analysis and ion chromatography. Compared with other detectors, it has the advantage of being easy to prepare, is inexpensive and offers the possibility of miniaturization.

Application of this electrode as a sensor in the determination of other inorganic cations such as calcium, strontium, barium, magnesium and aluminium and organic cations such as vitamin B_{12} and pyridoxal is currently being studied.

The authors thank the Dirección General de Investigación Científica y Técnica (DGICYT, Spain) for financial support of this work (project No. PB89-0397). Thanks are expressed to Dr. Juan García Julián (Servicio General de Microscopía Electrónica, Universidad de Salamanca) for his collaboration.

REFERENCES

- 1 S. Dong and Y. Wang, *Electroanalysis*, 1 (1989) 99.
- 2 E. Wang, H.Ji and W. Hou, *Electroanalysis*, 3 (1991) 1.
- 3 R.P. Baldwin and K.N. Thomsen, *Talanta*, 38 (1991) 1.
- 4 S.A. Wring and J.P. Hart, *Analyst*, 117 (1992) 1215.
- 5 Y. Ikariyama and W.R. Heineman, *Anal. Chem.*, 58 (1986) 1803.

- 6 J. Ye and R.P. Balwin, *Anal. Chem.*, 58 (1988) 1982.
- 7 J.Y. Sung and H.J. Huang, *Anal. Chim. Acta*, 246 (1991) 275.
- 8 T. Okada, H. Hayashi, K. Hiratani, H. Sugihara and N. Koshizaki, *Analyst*, 116 (1991) 923.
- 9 C. Zhong and K. Doblhofer, *Electrochim. Acta*, 35 (1990) 1971.
- 10 K. Naol, M. Lien and W.H. Smyrl, *J. Electrochem. Soc.*, 138 (1991) 440.
- 11 M.A. De Paoli, S. Panero, P. Prospero and B. Scrosati, *Electrochim. Acta*, 35 (1990) 1145.
- 12 S. Panero, P. Prospero and B. Scrosati, *Electrochim. Acta*, 37 (1992) 419.
- 13 S. Sahasranaman and N.P. Bhat, *Trans. SAEST*, 23 (1988) 13.
- 14 K.F. Nieto and W.T. Frankberger, *Soil Sci. Soc. Am. J.*, 49 (1985) 592.

Ridge regression techniques for the optimization of piecewise linear discriminants: application to Fourier transform infrared remote sensing measurements

Thomas F. Kaltenbach¹ and Gary W. Small

Center for Intelligent Chemical Instrumentation, Department of Chemistry, Clippinger Laboratories, Ohio University, Athens, OH 45701–2979 (USA)

(Received 12th November 1992; revised manuscript received 25th January 1993)

Abstract

An optimization procedure for piecewise linear discriminant analysis is described based on the application of ridge regression techniques. The method is based on the use of a matrix transformation that stabilizes data that exhibit a high degree of collinearity. Linear discriminants computed from collinear data exhibit imprecision in the estimation of the discriminant coefficients. The transform described here produces a perturbed data matrix in which the degree of collinearity has been decreased and which can be used in place of the original for subsequent discriminant calculations. The degree of stabilization provided by the transform is specified by the user in the form of a perturbation constant. The discriminant optimization procedure is demonstrated with an application in which an automated algorithm is implemented for the detection of SF₆ by Fourier transform infrared remote sensing measurements. A detailed study is described in which 96 data sets are investigated consisting of four different numbers of observations, four different dimensionalities, and six different levels of the perturbation constant. The results of this study indicate that the optimization procedure significantly improves the precision of discriminants computed with collinear data. The level of improvement is greatest in the case of greatest collinearity.

Keywords: Infrared spectrometry; Remote sensing; Ridge regression techniques; Optimization

Fourier transform infrared (FT-IR) remote sensors employ an interferometer-based optical system to collect infrared data in the outdoor environment. The collected data can be analyzed for the presence of spectral features corresponding to specific analytes. The sensor can thus be

used in a variety of applications as a dedicated monitoring device.

Recent work in this laboratory has focused on the design of algorithms that are based on the direct analysis of interferogram data collected by FT-IR remote sensors [1–3]. To simplify the complex nature of the signal, a bandpass digital filter is applied to a predetermined segment of the interferogram. The filtering step isolates those frequencies corresponding to a characteristic spectral band of a target analyte. A pattern recognition method is then used to make a yes/no decision about the presence of the analyte, given the magnitude and coherence of the filtered interferogram signal. This detection algorithm is

Correspondence to: G.W. Small, Center for Intelligent Chemical Instrumentation, Department of Chemistry, Clippinger Laboratories, Ohio University, Athens, OH 45701–2979 (USA).

¹ Present address: Analytical Technology Division, Eastman Kodak Company, Bldg. 49, Kodak Park, Rochester, NY 14652–3712 (USA).

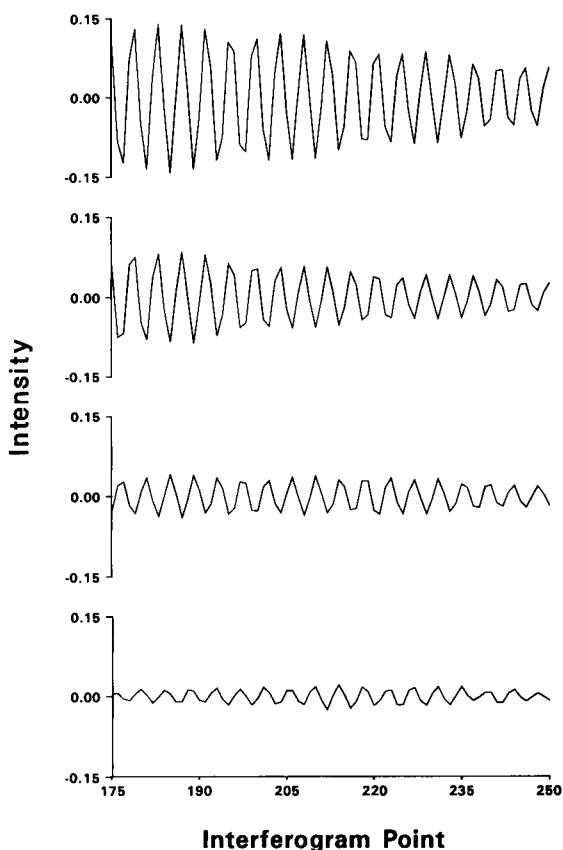


Fig. 1. Four filtered interferogram segments showing information corresponding to strong, medium, weak, and no analyte signal. The response variables are the intensities of the signal at discrete interferogram points. Collinearity among the variables is evident in the oscillating nature of the waveform.

implemented by use of piecewise linear discriminant analysis of the filtered interferogram data [1].

In this pattern recognition application, a filtered interferogram segment (i.e. a “pattern”) is classified into one of two categories. These categories correspond to one data class in which the pattern contains information indicating the presence of the target analyte, and another class in which the pattern contains no analyte information. The pattern variables are intensities at fixed interferogram points.

Figure 1 shows four interferogram segments that have been bandpass filtered to extract information about the SF_6 absorption band at 940

cm^{-1} . The strength of the analyte signal in the segments, from top to bottom in the figure, is strong, medium, weak, and none, based on an inspection of the corresponding transformed spectra. The pattern recognition method employed to classify these segments must be sensitive enough to discriminate those patterns containing a weak analyte signal from those patterns containing no analyte signal.

The oscillating nature of the waveforms depicted in Fig. 1 indicates that a high degree of collinearity exists in the interferogram data. In effect, the intensity at a given interferogram point is related to the intensities at previous and subsequent points. Collinearity among the pattern variables can have an adverse effect on numerical calculations employed with the data such as piecewise linear discriminant analysis.

In the work presented here, the effects of collinearity in the interferogram data are overcome through the development of a data stabilization procedure based on the concepts of ridge regression [4]. A matrix transformation is derived that produces a new data matrix that has been stabilized to reduce the effects of collinearity. The new data matrix can then be used in subsequent piecewise linear discriminant calculations. The method is evaluated through the investigation of 96 data sets constructed from FTIR remote sensing measurements of SF_6 .

EXPERIMENTAL

The data analysis methods described here were implemented in software using FORTRAN-77. Matrix computations were performed by use of subroutines from the LINPACK library [5]. The calculations were executed on three different computer platforms. The data transformation calculations were computed on a Prime 9955 mini-computer, while the majority of the piecewise linear discriminant calculations were performed on a Hewlett-Packard Vectra RS/20c, a 20-MHz 80386 IBM PC-compatible microcomputer with 4 Mb RAM (Hewlett Packard, Sunnyvale, CA) running the MS-DOS 3.3 operating system. The development of a five-vector piecewise linear dis-

criminant with a set of 3000 76-dimensional patterns required approximately seven hours of execution time on the microcomputer and included a total of 10 000 iterations of the Simplex optimization procedure used to position the vectors. In an effort to expedite the study of the 96 data sets, some of the discriminant calculations were performed on a Cray-2 supercomputer operating at the U.S. Army Test and Evaluation Command in Warren, MI. A study was performed to assure that the numerical results for the discriminant calculations were comparable on the two machines. The piecewise linear discriminant software has been used for previous work and is described in detail there [1].

The FT-IR data used for this research were collected with a passive FT-IR sensor built by Honeywell to the specifications of the Department of the Army. This instrument has been used for previous work, and is described there [2,3]. The data consisted of 1024-point interferograms, and were collected with the instrument mounted on moving vehicles. The target analyte employed was SF₆ (MG Industries, Jessup, MD, 97% purity), a standard test compound used in pollution monitoring. A segment of each interferogram (starting at point 175 relative to the centerburst) was used in the analysis, after digital filtering to isolate the SF₆ absorption frequencies. The length of the segment ranged from 20 to 76 points, as described below. The digital filtering techniques used in this work have been described previously [3].

DISCUSSION AND RESULTS

Linear discriminant analysis

Linear discriminant analysis (LDA) techniques have been used successfully in a variety of applications in chemistry to implement automated decision-making capabilities [6,7]. Stated simply, LDA provides a mathematical means of placing data objects (“patterns”) into pre-defined categories through the use of boundaries or separating surfaces placed in the data space. The orientation of the separating surface is computed by use of a “training set” of patterns which includes

representatives of each of the data classes. The separating surface is defined by the locus of points lying orthogonal to an ($p + 1$)-dimensional vector termed a weight vector or discriminant, where p is the dimensionality of the pattern data. The pattern data are augmented with a constant term that allows the separating surface to be offset from the origin of the data space. For the case of two data classes, the weight vector, \mathbf{w} , is calculated such that

$$\mathbf{w}^T \mathbf{x}_a > 0 \quad (1)$$

and

$$\mathbf{w}^T \mathbf{x}_n \leq 0 \quad (2)$$

where \mathbf{x}_a represents a pattern from Class 1, and \mathbf{x}_n represents a pattern from Class 2. The dot products in Eqns. 1 and 2 are termed discriminant scores. By definition, LDA methods compute the orientation of a linear separating surface. In cases in which the interface between the two data classes cannot be well characterized by a linear surface, a nonlinear surface is required. One extension of LDA which allows the computation of a nonlinear separating surface is piecewise linear discriminant analysis. The piecewise discriminant techniques use multiple linear discriminants to form a piecewise approximation of a nonlinear surface.

The algorithm employed in this work computes multiple linear discriminants that have a pure-class subset (i.e. a group of patterns of only one class) of patterns on one side of the discriminant, and a mixed-class subset on the other [1]. After each discriminant has been calculated, those patterns on the pure-class side of the discriminant are removed from the training set and the next discriminant is calculated based on the remaining patterns. In the current algorithm, each discriminant is restricted to placing the same class on its pure-class side. The result is a set of discriminants which collectively approximates a nonlinear separating surface. Each discriminant is individually optimized using Simplex optimization [8,9]. Simplex optimization is an iterative algorithm that seeks the values for a set of variables that optimize a numerical response function. Here, the variables are the elements of \mathbf{w} and the response

function is a measure of the classification performance of the discriminant. The Simplex algorithm has been applied to both single linear discriminants [10,11] and multiple discriminants [1,12].

To predict an unknown pattern with LDA techniques, the discriminant score for the unknown pattern is computed using the previously computed w . As indicated in Eqns. 1 and 2, the sign of the score determines the class assignment of the pattern. In the piecewise linear discriminant algorithm used here, discriminant scores are computed between the unknown pattern and each of the individual weight vectors comprising the piecewise linear discriminant. If any discriminant classifies the unknown pattern on the pure-class side, then that discriminant determines the predicted class. In terms of the FT-IR remote sensing application, the classification decision is a judgment of the presence or absence of the target analyte.

Effects of collinearity on LDA results

The effects of collinearity in LDA calculations are manifested in a great flexibility in the placement of the discriminant in the data space. The

undesirable nature of this flexibility can best be described by way of example. For this purpose, a two-dimensional data set was assembled, consisting of the boiling points and melting points for 31 compounds belonging to one of two data classes: ketones or carboxylic acids. The data were taken from a standard literature source [13]. Figure 2 displays the example data space. Collinearity is clearly visible in the almost linear relationship in the data.

The dashed lines in the figure indicate the broad range of discriminant orientations that are possible, within the set of orientations that completely separates the two classes. The presence of collinearity results in a reduction in the effective dimensionality of the data (i.e. the two-dimensional data space is effectively one-dimensional). This allows the discriminant to have a degree of freedom of placement that is not controlled by the separation of the data classes. Note that although this training set of data is completely separated in all cases, the orientation of the discriminant is critical to the correct classification of an unknown observation. The discriminant optimization procedure described here uses ridge regression techniques to reduce this flexibility in the positioning of computed discriminants.

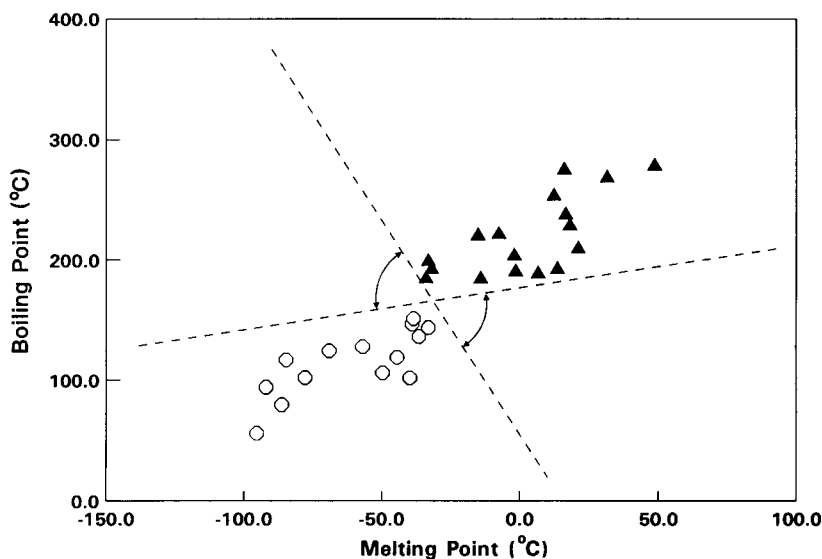


Fig. 2. A sample data space exhibiting high collinearity. The 14 circles represent carboxylic acids, while the 17 triangles represent ketones. The dashed lines indicate the range of discriminant orientations that are possible, while still separating the two classes.

Ridge regression

The ridge regression technique was first discussed in detail in 1970 [14]. The primary use of ridge regression is to reduce the effects of collinearity in linear regression when there is high correlation among the independent variables. In the general regression equation, the regression coefficients can be estimated by

$$\mathbf{b} = (\mathbf{X}^T \mathbf{X})^{-1} \mathbf{X}^T \mathbf{Y} \quad (3)$$

where \mathbf{b} represents the vector of coefficients, \mathbf{X} is the $n \times p$ data matrix of p independent variables (each having n observations), \mathbf{X}^T denotes the transpose of \mathbf{X} , and \mathbf{Y} is the $n \times 1$ matrix comprising the dependent variable for the regression. If there is high correlation among the columns of \mathbf{X} , the $\mathbf{X}^T \mathbf{X}$ matrix is said to be “ill-conditioned”,

and an accurate calculation of $(\mathbf{X}^T \mathbf{X})^{-1}$ is impossible. Consequently, the computed regression coefficients can be very inaccurate, frequently bearing the wrong sign or being too large in magnitude. Ridge regression techniques attempt to stabilize the calculation of $(\mathbf{X}^T \mathbf{X})^{-1}$ by reducing the correlation among the columns of \mathbf{X} . In ridge regression, the vector of coefficients is estimated as

$$\mathbf{b} = (\mathbf{Z}^T \mathbf{Z} + k\mathbf{I})^{-1} \mathbf{Z}^T \mathbf{Y} \quad (4)$$

where \mathbf{Z} is the data matrix \mathbf{X} where the columns (variables) have been centered and scaled to unit length, k is a perturbation constant, and \mathbf{I} is the identity matrix. The matrix $(\mathbf{Z}^T \mathbf{Z} + k\mathbf{I})$ is equivalent to the correlation matrix of \mathbf{X} with k added to each of the diagonal elements, and is termed

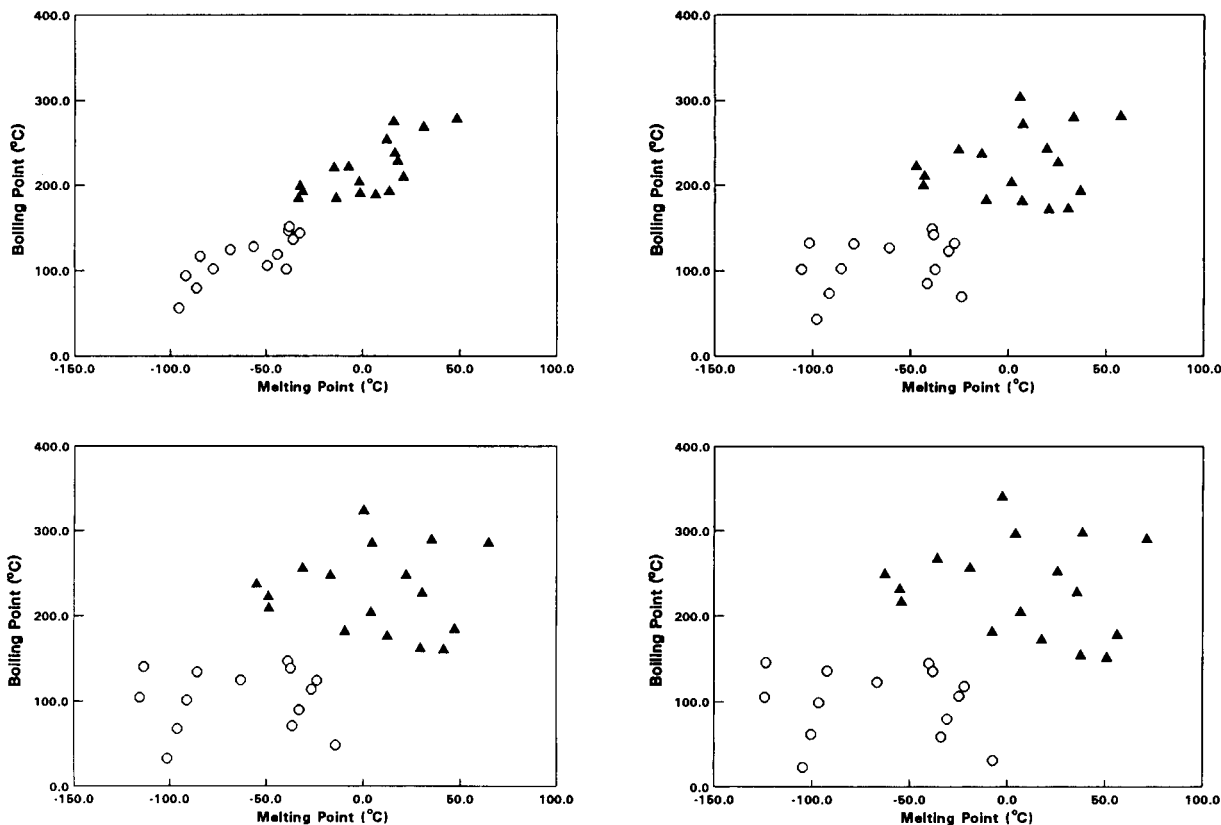


Fig. 3. Example of the effects of the ridge transform. The upper left plot represents the original data space, which is equivalent to $k = 0.0$. The upper right, lower left, and lower right plots show the data space after transformation with $k = 0.3$, 0.6 , and 0.9 , respectively. Discriminants computed with the perturbed data have significantly less flexibility in their placement in the data space. In effect, the precision of orientation of the discriminant is improved.

the perturbed correlation matrix. The value of k is the only user-defined parameter in ridge regression, and is generally chosen to be within the range of 0 to 1. The convention is to keep k as small as possible while still providing the characteristics of a near-orthogonal system. The estimation of an appropriate value for a minimal k can be aided by the diagnostic procedures discussed below. By using a minimal perturbation, the linear model is stabilized while the relationships among the data points are altered to a minimal degree. The ridge regression approach makes the assumption that increasing the orthogonality of the system will produce not only a more stable calculation but also a more ideal orientation of the regression model. This is a valid assumption in most applications.

Application of ridge regression to pattern recognition

The ridge regression technique aids in stabilizing linear models computed using $(\mathbf{Z}^T\mathbf{Z})^{-1}$, but is of no value in calculations that are not based on the direct use of $(\mathbf{Z}^T\mathbf{Z})^{-1}$. For example, the piecewise linear discriminant calculation described above is iterative in nature, operating by moving a discriminant through the data space until it reaches an optimal orientation. For the ridge regression concept to work with iterative methods, a new data matrix must be produced. This data matrix represents the data whose correlation matrix is equal to the perturbed correlation matrix described above, and is termed the perturbed data matrix.

The perturbed data matrix, \mathbf{Z}_p , is defined as

$$\mathbf{Z}_p = \mathbf{Z}\mathbf{V}\mathbf{\Lambda}\mathbf{V}^T \quad (5)$$

where \mathbf{Z} is the original scaled $n \times p$ data matrix and \mathbf{V} is the $p \times p$ orthogonal matrix of eigenvectors of $\mathbf{Z}^T\mathbf{Z}$. The entries of diagonal matrix $\mathbf{\Lambda}$ are

$$\Lambda_{ii} = [1.0 + (k/\lambda_{c,i})]^{1/2} \quad (6)$$

where k is the perturbation constant defined above and the $\lambda_{c,i}$ are the eigenvalues of $\mathbf{Z}^T\mathbf{Z}$. Thus, the eigenvectors and eigenvalues of $\mathbf{Z}^T\mathbf{Z}$ need only be computed once. Any k can then be applied to produce \mathbf{Z}_p via a simple matrix multi-

plication. The derivation of Eqns. 5 and 6 is described in detail in the Appendix.

Example of transform effects

The action of the data transform on the two-dimensional ketone-acid data set can be seen in Fig. 3. The original data space is shown in the upper left plot of the figure. This is equivalent to performing the transform with a perturbation constant of $k = 0.0$. The upper right plot shows the data space after transformation with $k = 0.3$. The lower left and right plots show the effects of $k = 0.6$ and $k = 0.9$, respectively. The action of the transform is clearly visible, increasing the variance of the data without radically altering the relationships among individual observations. By increasing the variance, a discriminant calculated on a perturbed data set is more restricted in its possible orientations, and theoretically can be positioned in a more optimal orientation. This can be observed clearly by overlaying the range of possible discriminants depicted in Fig. 2 with the new data spaces in Fig. 3. While the exact placement of the discriminant is still dependent on the success of a numerical optimization algorithm such as the Simplex procedure, a restriction in the possible orientations of the discriminant should increase the probability of finding an optimal orientation.

Evaluation of test data

To test the effects of the matrix transformation more rigorously, a test data set was generated by selecting 3000 observations from a pool of 12 141 interferograms collected during 17 different FT-IR remote sensing experiments in which SF_6 was released in the field of view of the spectrometer. Of these interferograms, 1425 were determined to contain analyte information by visual inspection of the corresponding spectra. The remaining 1575 interferograms were randomly selected from those interferograms judged to contain no analyte information. A prediction data set was also generated by combining all interferograms from three experimental runs that were not included in the 17 runs mentioned above. The prediction data set contained 2568 interferograms, corresponding to 214 analyte-containing interferograms, 2329 in-

terferograms containing no analyte information, and 25 interferograms which were judged indeterminate in terms of analyte presence. Analyte presence was again judged through visual inspections of transformed spectra.

A total of 96 different training sets were generated by varying the size and dimensionality of the training sets and the level of perturbation. Four different sizes of training sets were used, consisting of 3000, 1000, 500, and 250 patterns. The latter three sizes were chosen as random subsets of the set of 3000 patterns, and contained equal numbers of analyte-containing and non-analyte containing interferograms. Four different pattern dimensionalities were used (76, 55, 35, and 20-point patterns). Increasing the pattern dimensionality effectively increases the degree of collinearity present in the data, given the oscillating nature of the filtered interferograms. Finally, six different levels of perturbation were used, corresponding to $k = 0.0, 0.1, 0.2, 0.3, 0.4,$ and 0.5 . All possible combinations of the above factors were used to generate the 96 training sets.

For each of the training sets, a piecewise linear discriminant was calculated which consisted

of five individual linear discriminants. Each linear discriminant was optimized with 2000 iterations of the Simplex algorithm. This number of iterations was sufficient in each case for the optimization algorithm to converge. Table 1 summarizes the training statistics. The percentage of the 3000 training set patterns correctly classified is indicated for each data set. Studies in which the Simplex initialization parameters were varied confirm that the precision of these training classification percentages is approximately $\pm 1\%$ correct.

For those data sets in which the largest dimensionality was coupled with the smallest size training set, a five-vector discriminant could not be calculated, because complete separation of the classes (i.e. 100% correct classification) was obtained with three-vector or four-vector discriminants. These combinations are noted in the table. A graphical representation of the training statistics is presented in Fig. 4. The upper left, upper right, lower left and lower right plots display the statistics for the training set of 3000 patterns, 1000 patterns, 500 patterns, and 250 patterns, respectively. In training, the perturbation of the

TABLE 1

Percent correct in training set using a five-vector piecewise linear discriminant

Data set	Dim.	Perturbation level					
		0.0	0.1	0.2	0.3	0.4	0.5
3000	20	92.2	94.1	94.2	94.1	94.7	94.7
	35	94.7	95.7	95.3	96.0	96.2	96.2
	55	94.9	96.4	96.2	96.8	97.4	97.7
	76	97.8	98.0	98.1	98.0	98.1	97.4
1000	20	92.8	94.1	95.1	95.1	95.2	94.6
	35	95.9	97.1	96.2	97.5	97.2	96.6
	55	97.4	97.7	98.3	98.3	98.2	98.2
	76	98.2	98.3	98.8	98.7	99.0	99.0
500	20	90.8	92.4	92.4	94.8	92.4	92.4
	35	97.6	97.2	96.8	97.2	97.2	97.6
	55	98.4	99.2	99.6	98.8	99.2	99.2
	76	99.6	100.0	99.6	100.0	99.6	100.0
250	20	96.4	98.4	97.6	98.4	98.0	98.0
	35	100.0	100.0	100.0	100.0	100.0	99.6
	55	100.0	100.0	100.0	100.0	100.0	100.0
	76	100.0 ^a	100.0 ^a	100.0 ^b	100.0 ^b	100.0 ^b	100.0 ^b

^a Three-vector piecewise linear discriminant. ^b Four-vector piecewise linear discriminant.

data resulted in a small improvement in the number of patterns correctly classified.

In prediction, however, a significant improvement can be seen in the performance of those discriminants calculated with perturbed data. A summary of the prediction performance is provided in Table 2, and a graphical display is presented in Fig. 5. Note that the axis labeled "Pattern Dimension" in Fig. 5 has been reversed from that in Fig. 4.

In the training set of 3000 patterns, there are enough observations such that the data space is well-defined, and consequently only small improvements (0.6–1.3%) are observed in the prediction performance of discriminants computed with the transformed data. Stated differently, there are enough data points to lock the discriminant into position, despite the flexibility in the data space afforded by the presence of collinearity. With the smaller training sets, however, the discriminants computed with the transformed data clearly outperform those computed with the raw data. Here, the flexibility in discriminant placement afforded by the presence of collinearity in the raw data causes the discriminants to be

placed imprecisely. The benefit of the transform is observed to be greatest at high dimensionality, where the degree of collinearity is greatest. For example, at a dimensionality of 76 points, the raw ($k = 0.0$) data of the 500-member training set produces a discriminant that classifies only 77.8% of the prediction set patterns correctly. When the data matrix is perturbed with $k = 0.2$, the resulting stabilized discriminant classifies 94.8% of the prediction set patterns correctly. This corresponds to an absolute improvement of 17% in the classification performance.

The prediction results for the discriminants computed with the 250-member training set illustrate that substantial flexibility in discriminant placement can still be present after the data transformation. For the case of the 55 and 76-dimensional patterns, the prediction results for the discriminants computed with the perturbed data sets are significantly better than the results for discriminants computed with the unperturbed data. However, in the best cases, the percent correct in prediction is less than 80% for the 55-dimensional data and less than 60% for the 76-dimensional data. These results illustrate that

TABLE 2

Percent correct in prediction set using a five-vector piecewise linear discriminant

Data set	Dim.	Perturbation level					
		0.0	0.1	0.2	0.3	0.4	0.5
3000	20	97.2	98.1	98.3	98.2	98.3	97.8
	35	98.0	98.7	98.7	98.8	98.8	98.8
	55	97.7	99.1	99.0	99.1	99.0	99.0
	76	98.0	98.6	98.6	98.3	98.6	98.8
1000	20	96.0	98.4	98.0	98.0	97.6	97.6
	35	95.4	97.7	97.3	96.9	96.2	96.6
	55	96.6	98.4	97.8	97.5	97.2	96.7
	76	95.3	98.1	98.0	97.6	97.8	97.6
500	20	96.4	97.7	97.4	96.0	96.6	95.9
	35	93.5	95.8	95.0	94.4	93.2	92.3
	55	85.0	98.3	97.8	96.7	96.5	96.1
	76	77.8	94.5	94.8	94.1	93.0	93.0
250	20	93.6	94.5	96.5	95.1	96.3	93.6
	35	55.9	91.8	88.8	92.5	88.1	89.4
	55	55.0	76.6	77.7	76.1	73.0	75.4
	76	38.4 ^a	57.3 ^a	55.1 ^b	55.2 ^b	50.2 ^b	53.8 ^b

^a Three-vector piecewise linear discriminant. ^b Four-vector piecewise linear discriminant.

a combination of very small training set size and very high pattern dimensionality can combine to produce more flexibility in discriminant placement than can be controlled through the perturbation procedure. In effect, this example defines a limiting case for the methodology.

For the remote sensing application, the results in Table 2 indicate that excellent prediction performance can be obtained with smaller training sets, provided the flexibility in the discriminant placement is restricted through the use of the perturbation procedure. This result is potentially important in many remote sensing applications in which extensive data collection experiments are difficult to undertake or prohibitively expensive.

Diagnostics

Another means of confirming the stability provided by the data transform is to use diagnostics

typically employed in ridge regression. One measure of the stability or condition of a matrix is the condition number. This is defined as

$$c = \frac{[\lambda_{\max}]^{1/2}}{[\lambda_{\min}]^{1/2}} \tag{7}$$

where c is the condition number, and λ_{\max} and λ_{\min} are the maximum and minimum eigenvalues of $Z_p^T Z_p$. An orthogonal matrix has a condition number of one. An increase in collinearity results in an increase in the condition number. Fig. 6 is a plot of the condition number as a function of the perturbation constant for each dimensionality of the training set of 500 patterns. The condition numbers for the 76, 55, 35, and 20-dimensional data are denoted in the plot by open circles, filled circles, open boxes, and filled boxes, respectively. Plots for the other training sets were very similar.

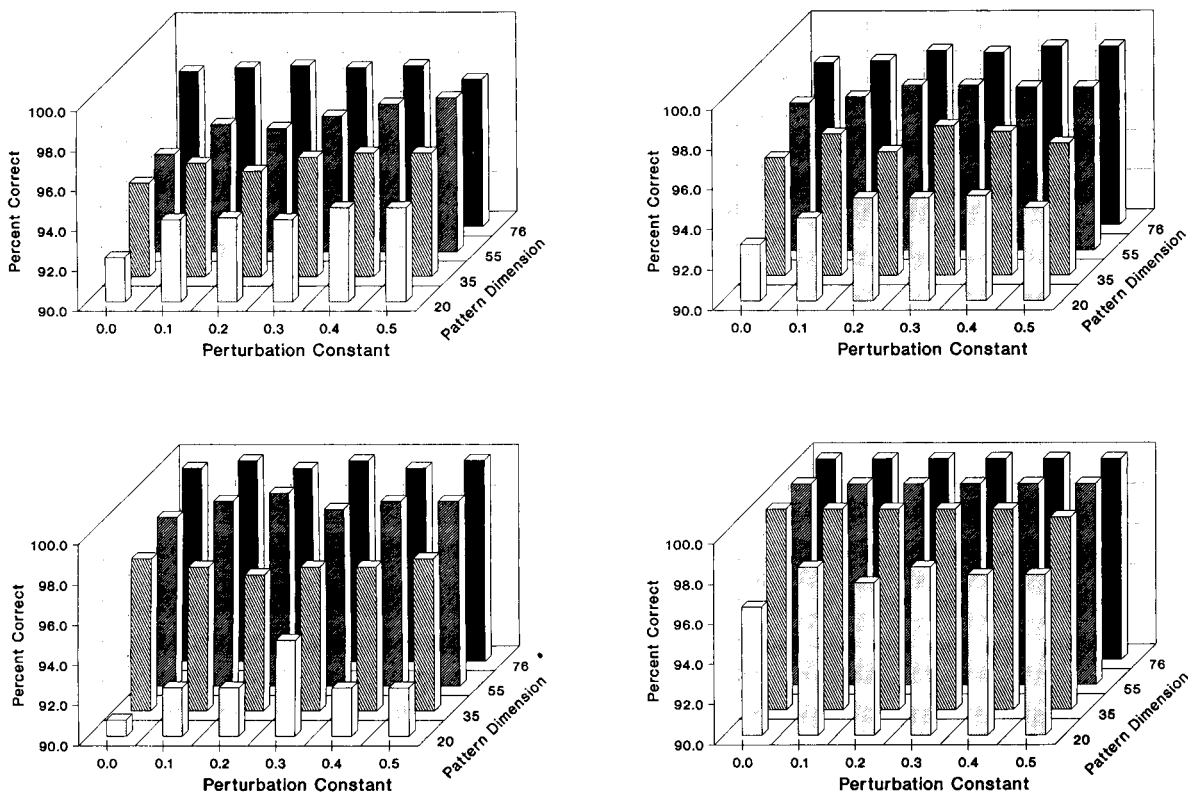


Fig. 4. Graphical representation of the number of patterns correctly classified in the training set. The upper left, upper right, lower left, and lower right plots show the results from the training sets of 3000 patterns, 1000 patterns, 500 patterns, and 250 patterns, respectively.

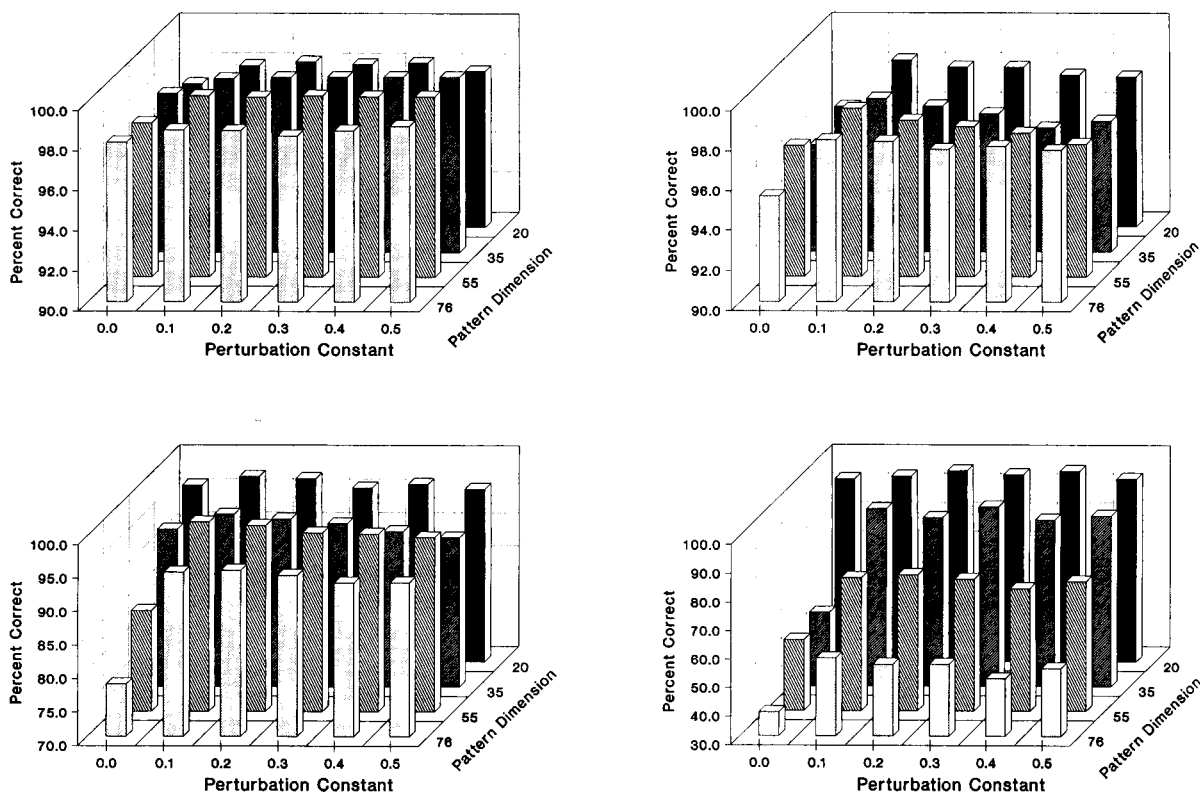


Fig. 5. Graphical representation of the number of patterns correctly classified in the prediction data. The upper left, upper right, lower left, and lower right plots show the results from the training sets of 3000 patterns, 1000 patterns, 500 patterns, and 250 patterns, respectively. To aid in interpretation, the graphs are plotted with the vertical axes on different scales.

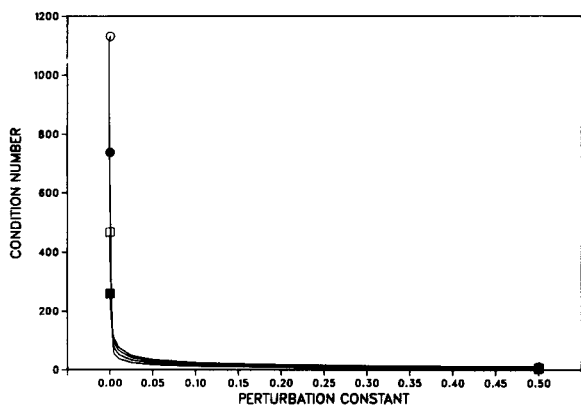


Fig. 6. Plot depicting the condition numbers corresponding to different levels of perturbation of the four data matrices based on the training set of 500 patterns. The open circles, filled circles, open boxes, and filled boxes correspond to patterns with dimensionalities of 76, 55, 35, and 20, respectively. Even with low levels of perturbation, the stability of the data matrix improves significantly.

The same six levels of perturbation described above were used. To aid in plotting the region between perturbation levels of 0.0 and 0.1, however, four additional points were calculated at perturbation levels of 0.005, 0.010, 0.025, 0.050. As expected, the condition number of the unperturbed data increases with dimensionality. The plot shows clearly that the data transformation produces data sets that quickly attain the properties of an orthogonal system.

Another measure of the effects of the data transform is termed a ridge trace, owing its name to an analogous plot used in ridge regression. This is a plot of the estimates of the coefficients of the linear model, typically the regression coefficients, as a function of the perturbation level. In the pattern recognition application described here, the linear model is embodied in the linear discriminant calculation, and the estimated coef-

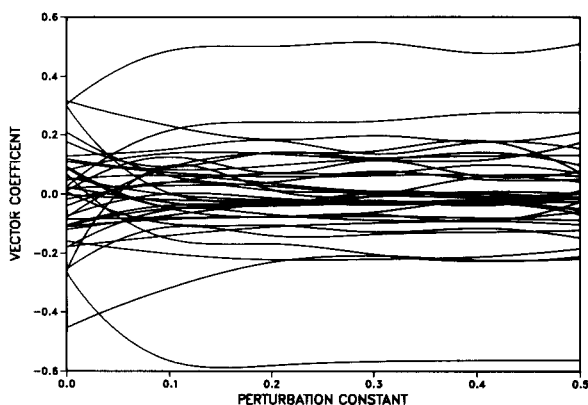


Fig. 7. Ridge trace for the first weight vector of a piecewise linear discriminant, calculated on the training set of 500 patterns with a pattern dimension of 35. With increasing levels of perturbation, the weight vector coefficients quickly approach stable values.

coefficients are therefore the weight vector coefficients. Figure 7 presents an example of a representative ridge trace. The results displayed correspond to the first vector of the five-vector discriminant computed on the training set of 500 patterns of dimension 35. Consequently, there are 36 traces in the figure, corresponding to the 36-dimensional weight vector. The figure shows that many coefficients change radically from their values prior to the transformation, and quickly stabilize with increasing perturbation. The ridge trace is an effective tool for determining the minimum perturbation constant that stabilizes the weight vector coefficients.

Conclusions

The data transformation developed in this work is a new method for stabilizing data that exhibit a high degree of collinearity. The stabilized data matrix displays the general characteristics of an orthogonal system, and can be used in place of the original data matrix with iterative calculations that are not based on a direct calculation with the $Z^T Z$ matrix. When applied to linear discriminant analysis, the work presented here suggests that the stabilization procedure may allow individual weight vectors to be more precisely positioned in the data space. The assumption inherent in ridge regression that increasing the orthogonality of the data is preferable to the existing collinearity should be acceptable for most pattern recognition

applications. The data transform should be beneficial to any iterative pattern recognition technique that is based on linear discriminant analysis.

An alternative strategy for reducing the effects of collinearity would be to employ orthogonalization transformations such as principal components analysis [15] to reduce the dimensionality of the data. The reduced data could then be used with pattern recognition methods. There are two principal drawbacks to this approach. First, an essentially subjective decision must be made regarding what level of reduction in dimensionality is appropriate. Second, the transformation matrix used to reduce the data dimensionality must be retained and used subsequently to transform unknown patterns whose classifications are being predicted. The perturbation procedure employed in our work is performed only on the training data. Predictions can be performed without any knowledge of the fact that the perturbation methodology was used as a part of the training procedure.

In recommending the discriminant stabilization procedure as a general purpose tool, it should be stressed that in only four of the 80 perturbed data sets (i.e. $k > 0.0$) did the application of the technique actually result in worse prediction results than were obtained with the discriminant computed from the unperturbed data. Of these four cases, the maximum degradation in prediction performance was 1.2%. The remaining 76 cases exhibited improved performance.

The work described in this paper represents the first generalized method for stabilizing the placement of either single linear discriminants or multiple discriminants. Wangen et al. [16] have previously reported an unrelated algorithm for increasing the precision of placement of a single linear discriminant by altering the width of the separating surface. No similar methods for the optimization of multiple discriminants have been reported, however.

While the focus of this work was the use of the data transform with filtered interferogram data from an FTIR remote sensing application, the methodology should be equally applicable to pattern recognition studies involving other types of

collinear data. For example, most data in spectroscopy and chromatography exhibit moderate collinearity due to the sampling of multiple data points across spectroscopic bands or chromatographic peaks. Furthermore, it is also quite common to be faced with a training set of limited size. In many applications, only a small set of samples is available. The results presented here indicate clearly that the flexibility in discriminant placement due to both a limited training set and to collinearity can be overcome by the data stabilization procedure.

Finally, it should be stressed that the data transform described here is a general tool that has potential use with multivariate data analysis techniques other than pattern recognition methods. For example, many other applications for numerical optimization utilize iterative techniques such as the Simplex algorithm. The data stabilization procedure may be equally useful in these cases.

APPENDIX

Derivation of data transformation

Given the original $n \times p$ data matrix \mathbf{Z} whose columns have been centered and scaled to unit length, we obtain

$$\mathbf{Z}^T \mathbf{Z} = \mathbf{C} \quad (8)$$

where \mathbf{C} is the $p \times p$ correlation matrix of the data. We want a $p \times p$ transformation matrix \mathbf{T} such that

$$\mathbf{Z}\mathbf{T} = \mathbf{Z}_p \quad (9)$$

and

$$\mathbf{Z}_p^T \mathbf{Z}_p = \mathbf{C}_p \quad (10)$$

where \mathbf{Z}_p is the new data matrix that is characterized by \mathbf{C}_p , the desired perturbed correlation matrix. The derivation of \mathbf{T} is simplified by factoring \mathbf{T} as

$$\mathbf{T} = \mathbf{T}_1 \mathbf{T}_2 \quad (11)$$

and determining \mathbf{T}_1 and \mathbf{T}_2 separately.

The derivation of \mathbf{T}_1 begins by defining

$$\mathbf{Z}' = \mathbf{Z}\mathbf{T}_1 \quad (12)$$

and

$$\mathbf{Z}'^T \mathbf{Z}' = \mathbf{I} \quad (13)$$

where \mathbf{I} is the identity matrix. \mathbf{T}_1 is a transformation matrix that orthogonalizes the columns of \mathbf{Z} to produce the new data matrix, \mathbf{Z}' . By combining Eqns. 12 and 13, we obtain

$$(\mathbf{Z}\mathbf{T}_1)^T (\mathbf{Z}\mathbf{T}_1) = \mathbf{I} \quad (14)$$

which rearranges to

$$\mathbf{Z}^T \mathbf{Z} = (\mathbf{T}_1^T)^{-1} \mathbf{T}_1^{-1} \quad (15)$$

We can factor the square matrix $\mathbf{Z}^T \mathbf{Z}$ such that

$$\mathbf{Z}^T \mathbf{Z} = \mathbf{V} \Lambda_c \mathbf{V}^T = \mathbf{V} (\Lambda_c)^{1/2} (\Lambda_c)^{1/2} \mathbf{V}^T \quad (16)$$

where \mathbf{V} is the $p \times p$ orthogonal matrix of eigenvectors of $\mathbf{Z}^T \mathbf{Z}$ and Λ_c is the corresponding $p \times p$ diagonal matrix of eigenvalues. An inspection of the right sides of Eqns. 15 and 16 reveals that

$$\mathbf{T}_1^{-1} = (\Lambda_c)^{1/2} \mathbf{V}^T \quad (17)$$

Given that the inverse of an orthogonal matrix is equal to its transpose and that the inverse of a product matrix $(\mathbf{AB})^{-1}$ is simply $\mathbf{B}^{-1} \mathbf{A}^{-1}$, Eqn. 17 simplifies to

$$\mathbf{T}_1 = [(\Lambda_c)^{1/2} \mathbf{V}^T]^{-1} = \mathbf{V} (\Lambda_c)^{-1/2} \quad (18)$$

\mathbf{T}_2 is a transformation matrix that operates on the orthogonal data in \mathbf{Z}' to produce the new data matrix, \mathbf{Z}_p , with the desired degree of orthogonality (as specified by the perturbation constant k). The derivation of \mathbf{T}_2 begins by combining Eqns. 9, 11, and 12 to yield

$$\mathbf{Z}_p = \mathbf{Z}' \mathbf{T}_2 \quad (19)$$

Substitution of Eqn. 19 into Eqn. 10 produces

$$(\mathbf{Z}' \mathbf{T}_2)^T (\mathbf{Z}' \mathbf{T}_2) = \mathbf{C}_p \quad (20)$$

Rearranging Eqn. 20 and factoring \mathbf{C}_p in a manner analogous to Eqn. 16 yields

$$\mathbf{T}_2^T (\mathbf{Z}'^T \mathbf{Z}') \mathbf{T}_2 = \mathbf{V}_p (\Lambda_p)^{1/2} (\Lambda_p)^{1/2} \mathbf{V}_p^T \quad (21)$$

where \mathbf{V}_p is the $p \times p$ orthogonal matrix of eigenvectors of \mathbf{C}_p and Λ_p is the corresponding diago-

nal matrix of eigenvalues. Given Eqn. 13, the left side of Eqn. 21 reduces to $\mathbf{T}_2^T \mathbf{T}_2$. Thus, by inspection,

$$\mathbf{T}_2 = (\Lambda_p)^{1/2} \mathbf{V}_p^T \quad (22)$$

Combining Eqns. 11, 18, and 22 yields

$$\mathbf{T} = \mathbf{V} (\Lambda_c)^{-1/2} (\Lambda_p)^{1/2} \mathbf{V}_p^T \quad (23)$$

Eqn. 23 simplifies further by exploring the relationships among \mathbf{V} , \mathbf{V}_p , Λ_c , and Λ_p . The perturbed correlation matrix, \mathbf{C}_p , can be written as

$$\mathbf{C}_p = \mathbf{C} + k\mathbf{I} \quad (24)$$

where k is the desired perturbation constant. Substitution of Eqn. 8 into Eqn. 24 and factoring in a manner analogous to Eqn. 21 produces

$$\mathbf{Z}^T \mathbf{Z} + k\mathbf{I} = \mathbf{V}_p \Lambda_p \mathbf{V}_p^T \quad (25)$$

Given that $\mathbf{V}_p^T = \mathbf{V}_p^{-1}$ for orthogonal matrix \mathbf{V}_p , rearrangement of Eqn. 25 produces

$$[\mathbf{V}_p^T (\mathbf{Z}^T \mathbf{Z}) + \mathbf{V}_p^T k\mathbf{I}] \mathbf{V}_p = \Lambda_p \quad (26)$$

and

$$\mathbf{V}_p^T (\mathbf{Z}^T \mathbf{Z}) \mathbf{V}_p + \mathbf{V}_p^T (k\mathbf{I}) \mathbf{V}_p = \Lambda_c + \Lambda_k \quad (27)$$

where Λ_k is the diagonal matrix of eigenvalues of $k\mathbf{I}$. Given that all eigenvectors diagonalize \mathbf{I} (or $k\mathbf{I}$), we see from a comparison of Eqns. 16 and 27 that

$$\mathbf{V}_p = \mathbf{V} \quad (28)$$

Further, given that the eigenvalues of the diagonal matrix $k\mathbf{I}$ are all equal to k , the right side of Eqn. 27 simplifies to

$$\Lambda_p = \Lambda_c + k\mathbf{I} \quad (29)$$

Thus, the combination of Eqns. 9, 23, 28, and 29 yields

$$\mathbf{Z}_p = \mathbf{Z} \mathbf{V} \Lambda \mathbf{V}^T \quad (30)$$

where

$$\Lambda = (\Lambda_c)^{-1/2} (\Lambda_c + k\mathbf{I})^{1/2} \quad (31)$$

The entries of diagonal matrix Λ are simply

$$\Lambda_{ii} = [(\lambda_{c,i} + k) / \lambda_{c,i}]^{1/2} = [1.0 + (k / \lambda_{c,i})]^{1/2} \quad (32)$$

Computational considerations

In order to compute the transformation in Eqn. 30 in the presence of high collinearity, care must be taken to make the computation as stable as possible. The difficulty surrounds the need for the eigenvectors and eigenvalues of the $\mathbf{Z}^T \mathbf{Z}$ matrix. This matrix is ill-conditioned due to the presence of collinearity, and consequently the calculation is potentially unstable. In order to circumvent this problem, the singular value decomposition (SVD) is used. The singular value decomposition of \mathbf{Z} is defined by

$$\mathbf{Z} = \mathbf{U} \mathbf{D} \mathbf{V}^T \quad (33)$$

where \mathbf{V} ($p \times p$) contains the eigenvectors of $\mathbf{Z}^T \mathbf{Z}$, \mathbf{U} ($n \times p$) contains the eigenvectors of $\mathbf{Z} \mathbf{Z}^T$, and \mathbf{D} ($p \times p$) is the diagonal matrix containing the singular values of \mathbf{Z} . Each singular value is the square root of the corresponding eigenvalue of $\mathbf{Z}^T \mathbf{Z}$. The SVD allows the stable computation of the eigenvectors and eigenvalues of $\mathbf{Z}^T \mathbf{Z}$ and avoids the requirement of computing the $\mathbf{Z}^T \mathbf{Z}$ matrix itself [17].

The computational speed of the SVD can be improved by first performing a QR decomposition to reduce the dimensionality of the data matrix. The QR decomposition computes the orthogonal matrix \mathbf{Q} ($n \times n$) and upper triangular matrix \mathbf{R} ($p \times p$) such that

$$\mathbf{Q} \mathbf{Z} = \begin{bmatrix} \mathbf{R} \\ \mathbf{0} \end{bmatrix} \quad (34)$$

and

$$\mathbf{Z}^T \mathbf{Z} = \mathbf{R}^T \mathbf{R} \quad (35)$$

It follows from Eqn. 35 that the eigenvalues and eigenvectors of $\mathbf{R}^T \mathbf{R}$ are equal to those of $\mathbf{Z}^T \mathbf{Z}$, and consequently the SVD can be performed on \mathbf{R} at a significant savings in the number of computations required.

The scaling of the data produces an additional computational consideration. The original data matrix is centered and scaled prior to perturbation, and the perturbed data matrix is generated within this scaled data space. The perturbed data are then scaled back into the original data space using the scaling information obtained from the original data. The result is that subsequent calcu-

lations are carried out in a space which approximates the original data space, thus eliminating the need for special scaling operations.

Robert Kroutil and co-workers of the Department of the Army are acknowledged for providing the remote sensing data and access to the Cray-2 supercomputer used in this work. This research was supported by the Department of the Army under contracts DAAA15-89-C-0010 and DAAD05-91-P-5218.

REFERENCES

- 1 T.F. Kaltenbach and G.W. Small, *Anal. Chem.*, 63 (1991) 936.
- 2 G.W. Small, R.T. Kroutil, J.T. Ditillo and W.R. Loerop, *Anal. Chem.*, 60 (1988) 264.
- 3 G.W. Small, A.C. Harms, R.T. Kroutil, J.T. Ditillo and W.R. Loerop, *Anal. Chem.*, 62 (1990) 1768.
- 4 N.R. Draper and H. Smith, *Applied Regression Analysis*, Wiley-Interscience, New York, 2nd edn., 1981, pp. 313–325.
- 5 J.J. Dongarra, J.R. Bunch, C.B. Moler and G.W. Stewart, *LINPACK User's Guide*, Society of Industrial and Applied Mathematics, Philadelphia, PA, 1979.
- 6 P.C. Jurs, *Science*, 232 (1986) 1219.
- 7 M.P. Derde and D.L. Massart, *Anal. Chim. Acta*, 191 (1986) 1.
- 8 J.A. Nelder and R. Mead, *Comput. J.*, 7 (1965) 308.
- 9 M.W. Routh, P.A. Swartz and M.B. Denton, *Anal. Chem.*, 49 (1977) 1422.
- 10 G.L. Ritter, S.R. Lowry, C.L. Wilkins and T.L. Isenhour, *Anal. Chem.*, 47 (1975) 1951.
- 11 G.F. Brissey, R.B. Spencer and C.L. Wilkins, *Anal. Chem.*, 51 (1979) 2295.
- 12 P. de B. Harrington and K.J. Voorhees, *Anal. Chem.*, 62 (1990) 729.
- 13 D.R. Lide, *CRC Handbook of Chemistry and Physics*, CRC Press, Boca Raton, FL, 71st edn., 1990.
- 14 A.E. Hoerl and R.W. Kennard, *Technometrics*, 12 (1970) 55.
- 15 D.L. Massart, B.G.M. Vandeginste, S.N. Deming, Y. Michotte and L. Kaufman, *Chemometrics: A Textbook*, Elsevier, Amsterdam, 1988, Ch. 21.
- 16 L.E. Wangen, N.M. Frew and T.L. Isenhour, *Anal. Chem.*, 43 (1971) 845.
- 17 D.A. Belsley, E. Kuh and R.E. Welsch, *Regression Diagnostics*, Wiley, New York, 1980, p. 99.

Assessment of the performance of various search systems for mass spectra files of steroids

M. Statheropoulos and C. Georgakopoulos

Department of Chemical Engineering, National Technical University of Athens, Heroon Polytechniou 5, Zografou, 15700 Athens (Greece)

(Received 24th July 1992)

Abstract

The performance of six similarity indices in combination with five encoding modes of mass spectra files of steroids, using forward searching, was tested. The evaluation was based on a number of criteria that compare the effectiveness, the resolution and the ability to retrieve structurally similar compounds. The results of searching are presented and discussed. It seems that the criteria used can differentiate sufficiently the performance of searching systems. In the particular steroid files used, it appears that search systems that use the Euclidean distance as a similarity index give a better overall performance, especially when combined with the abbreviated modes two masses every fourteen and sixteen most significant masses.

Keywords: Gas chromatography–mass spectrometry; Mass spectrometry; Euclidean distance; Similarity indices; Steroids

The rapid and accurate identification of a mass spectrum in large or dedicated mass spectra files has been the subject of a considerable number of papers in recent years [1–3]. The choice between various abbreviating and searching methods is a compromise between reliability and speed [4]. In this paper, various searching systems (abbreviating and searching methods) are evaluated in mass spectra files of steroids. Methods for evaluating the effectiveness of searching systems have been proposed [5,6]. In the following work the assessment of the searching performance of various systems is based on the ability of the system to retrieve the correct spectrum as a first selection (effectiveness), to differentiate it from other selections (resolution) and to retrieve structurally related compounds. These are implemented

through the use of four criteria that quantify the performance characteristics of the systems. The type of spectra used in the present work are mass spectra related to steroid analysis. Steroids are an important class of compounds from the analytical point of view, especially in clinical chemistry. However, this particular group of compounds was used as a case study in a broader research field, namely establishing criteria and a methodology for comparison of searching systems. This is a particularly important issue when small dedicated libraries are needed.

EXPERIMENTAL

Gas chromatographic–mass spectrometric (GC–MS) measurements

The analysis usually applied in doping control of athletes was used. The main steps of the preparation procedure for urine samples are

Correspondence to: M. Statheropoulos, Department of Chemical Engineering, National Technical University of Athens, Heroon Polytechniou 5, Zografou, GR 15700 Athens (Greece).

solid-phase extraction, hydrolysis, extraction and derivatization of *O*- and *N*-TMS derivatives. A detailed description of doping analysis can be found elsewhere [7]. The internal standard used is methyltestosterone. The instrumentation used was an HP5890 gas chromatograph and an HP5970 mass-selective detector (Hewlett-Packard) with a port temperature of 250°C, helium as carrier gas, a splitting ratio of 1:10, an Ultra 1 column (Hewlett-Packard) (25 m × 0.2 mm i.d., 0.11 μm film thickness) and an injection volume of 1 μl. The temperature programme was 180°C for 1 min, increased at 8°C/min to 220°C, then at 3°C/min to 250°C and at 14°C/min to 280°C, with a total run time of 25 min.

Mass spectra files used

Five mass spectra files were created and are described below.

STER0 consists of 93 full spectra (normalized on the base peak) of substances encountered in routine capillary GC-MS analysis for anabolic steroids at the Accredited Doping Control Laboratory, Athens. The spectra stored correspond to the average spectrum of a GC peak. An average spectrum represents the average of the spectra acquired over a time range. The time range was defined to be three scans before and three scans after the chromatographic peaks. The substances were anabolic steroids, metabolites of anabolic steroids, endogenous steroids and various artifacts or compounds of biological origin found in the analysis of anabolic steroids. The mass spectra consisted of peaks in the mass range 100–600. Masses below 100 were excluded because of the presence in the background of the strong peak of *m/z* 73 originating from the TMS group and because they are lacking structurally significant peaks. In almost all the steroid spectra the molecular ion is included.

STER1 contains the spectra of the same compounds abbreviated for the two most intense peaks every fourteen mass units [8]. STER2 contains the spectra abbreviated for the ten most intense peaks. In STER3 and STER4 the spectra were abbreviated using the ten and sixteen most significant mass peaks, respectively.

The algorithm for the ten significant masses

sorts the masses according to the product of mass and intensity. The algorithm for the sixteen most significant peaks implements the abbreviation in two steps. In the first step, each peak is viewed in a window 101 wide with the peak in question in the centre of the window. The peak will be rejected if there are 40 larger peaks in its window. The first peak in the spectrum has a mass window only 50 u wide, so it will be rejected if there are 20 larger peaks. In the second step, the largest peaks provided by the first step are selected. The method used in the first step is repeated, except that the mass window is narrowed to 15 u. A peak is rejected if there are six larger peaks in the 15-u window. After the second step, the sixteen largest peaks are added to the spectrum.

Similarity indices (SI) used

Six similarity indices were tested. These indices are a mixture of two categories: peak count indices (SI1 and SI2) and full intensity indices (SI3–SI6). All SIs except SI5 are among the most commonly used from each category of indices. SI5 was introduced in this study. The first index is

$$SI1 = \frac{N^2}{N_1 N_2} \times 100$$

where N_1 is the number of peaks for the unknown, N_2 is the number of the peaks for the reference spectrum and N is the number of common peaks. The second index is

$$SI2 = \frac{100}{R} \sum_{r=1}^R \left[\frac{1}{N^2} \sum_{k=1}^{Ar} (N - |i - j| k) \right]_r$$

where R is the number of mass intervals (14 masses), Ar is the number of the common masses in one interval r , $N = 2$ and i, j are the positions of the respective peaks for unknown and known in one interval after they have been sorted [9]. This index is applied only on the 2/14 abbreviation of the mass spectra files. The third similarity index is

Correlation coefficient:

$$SI3 = \frac{\sum_{i=1}^n (Iu_i I_l_i)}{\sqrt{\sum_{i=1}^n Iu_i^2} \sqrt{\sum_{i=1}^n I_l_i^2}} \cdot 1000$$

TABLE 1

Results of searching compounds 1–5 with the similarity index SI1 using various abbreviation modes (STER0 for full spectrum)

Compound	STER0	STER1	STER2	STER3	STER4
1	N ^a S ^b CS ^c	2 S NS	1 M NS	1 S NS D	1 S NS D
2	1 S CS	1 S CS D ^d	1 S CS D	1 M CS D	1 S CS
3	1 S CS	1 S CS D	1 S CS D	1 M CS D	1 M CS D
4	N S NS	1 S CS	N S NS	2 S NS	1 M CS D
5	6 S NS	4 S NS	1 S NS	3 M NS	1 S NS

^a The number indicates the order of the retrieval. “N” appears when the compound is not retrieved among the first ten. ^b “S” for single or “M” for more spectra as first selection with the same similarity index. ^c “CS” for chemically structurally similar compounds and “NS” for not chemically similar compounds. ^d “D” if the second selection has a similarity index 25% less than the first.

where Iu_i is the intensity of a mass i for the unknown, Il_i is the intensity for the library [10] and n is the number of masses. The fourth and the fifth indices are

Euclidean distance:

$$SI4 = \sqrt{\sum_{i=1}^n (|Iu_i^2 - Il_i^2|)} \quad [4,10]$$

$$SI5 = \sum_{i=1}^n (|Iu_i - Il_i|)$$

where Iu_i and Il_i are the intensities for the unknown and library mass i , respectively. Finally, the sixth index, a Manhattan metric index [10], is

$$SI6 = \sum_{i=1}^n \frac{|Iu_i - Il_i|}{Iu_i + Il_i}$$

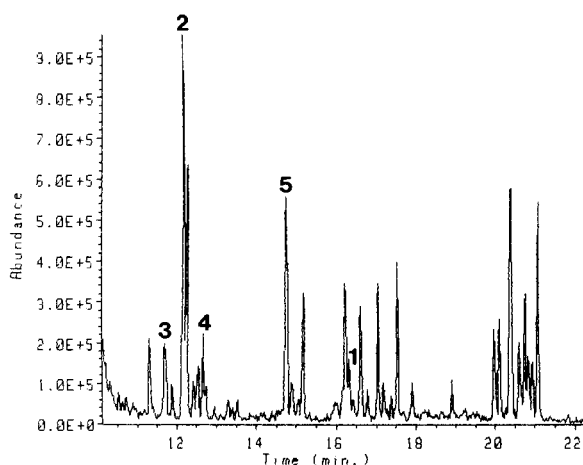


Fig. 1. Typical GC-MS trace for urine sample in steroids analysis, Compounds: 1 = methyltestosterone; 2 = androsterone; 3 = plasticizer; 4 = drostanolone main metabolite; 5 = 11 β -hydroxyandrosterone.

Software used

The programs used were written in Microsoft Quick Basic 4.0 compiler and were run on a 386 PC.

RESULTS AND DISCUSSION

The mass spectra recorded by GC-MS analysis of a urine sample were compared with those in the various files (STER0, STER1, STER2, STER3 and STER4). A typical chromatogram of the analysis is shown in Fig. 1. Tables 1–6 give the results of mass spectra matching using similarity indices SI1–SI6, respectively. Compounds 1–5 (see Fig. 1), used as unknowns, are methyltestosterone, androsterone, plasticizer, drostanolone main metabolite and 11 β -hydroxyandrosterone, respectively. Methyltestosterone was the internal standard and it was spiked. The other four compounds were encountered in an analysis of a positive (for prohibited steroids) urine sample. The spectra of these compounds were interpreted manually.

TABLE 2

Results of searching compounds 1–5 with the similarity index SI2 using the 2/14 abbreviation mode

Compound	STER1
1	1 S CS
2	2 S CS
3	1 S CS
4	1 S CS
5	3 S NS

TABLE 3

Results of searching compounds 1–5 with the similarity index SI3 using various abbreviation modes (STER0 for full spectrum)

Compound	STER0	STER1	STER2	STER3	STER4
1	1 S ND D	1 S NS D	1 S NS	1 S NS D	1 S NS D
2	1 S CS	1 S CS	1 S CS	1 S CS	1 S CS
3	1 S CS	1 S CS	1 S CS	1 S CS	1 S CS
4	1 S CS	1 S CS	2 S CS	2 S CS	1 S CS
5	2 S NS	2 S NS	2 S NS	1 S NS	2 S NS

TABLE 4

Results of searching compounds 1–5 with the similarity index SI4 using various abbreviation modes (STER0 for full spectrum)

Compound	STER0	STER1	STER2	STER3	STER4
1	1 S NS D	1 S NS D	1 S NS	1 S NS D	1 S NS
2	1 S CS D	1 S CS	1 S CS	1 S CS	1 S CS
3	1 S CS D	1 S CS D	1 S CS D	1 S CS D	1 S CS D
4	1 S CS	1 S CS	2 S CS	2 S CS	1 S CS
5	1 S NS	1 S NS	1 S NS	2 S NS	1 S NS

TABLE 5

Results of searching compounds 1–5 with the similarity index SI5 using various abbreviation modes (STER0 for full spectrum)

Compound	STER0	STER1	STER2	STER3	STER4
1	N S NS	1 S CS	1 S NS	1 S CS D	1 S NS D
2	1 S CS	1 S CS D	1 S CS D	1 S CS D	1 S CS D
3	1 S CS D	1 S CS D	1 S CS D	1 S CS D	1 S CS D
4	2 S CS	2 S CS	2 S CS	2 S CS	2 S CS
5	1 S NS	1 S NS	1 S NS	2 S NS	1 S NS D

TABLE 6

Results of searching compounds 1–5 with the similarity index SI6 using various abbreviation modes (STER0 for full spectrum)

Compound	STER0	STER1	STER2	STER3	STER4
1	N S CS	N S CS	4 S NS	1 S NS D	1 S NS D
2	1 S CS	1 S CS D	1 S CS	1 S CS	1 S CS D
3	1 S CS D	1 S CS D	1 S CS D	1 S CS	1 S CS
4	N S NS	N S NS	N S NS	2 S CS	3 S CS
5	N S NS	4 S NS	2 S NS	3 S NS	1 S NS D

The criteria used for evaluation of the performance of the various similarity indices and abbreviating schemes are the following: the first criterion (criterion 1) is a measure of the ability of the system to retrieve itself for a particular unknown. Its attributes are integers, that present the order of retrieval or “N” if the order is more than 10. The second criterion is indicative of the ability of the system to retrieve one or more spectra as a first selection. Two attributes are associated with this criterion: “S” represents a single selection and “M” more. Criterion 3 is indicative of the ability to retrieve chemically structurally similar compounds in the first four selections. Chemically structurally similar compounds are a pair of compounds where the basic structure of the molecule is the same. The compounds can be differentiated in up to two substituents. Criterion 3 has two attributes: “CS” represents chemically similar compounds and “NS” not chemically similar compounds. The last criterion (criterion 4) is a measure of the ability of the system to differentiate quantitatively the first from the second selection. It takes the attribute “D” if the second selection has a similarity index value 25% less than that of the first.

It should be emphasized that the above criteria have an empirical background that does not diminish their chemical and informational significance. In the literature there are a number of methods for the evaluation of the performance of library search systems in combination with normalization and abbreviation modes. The time of searching and the percentage of the order of the retrieval for the various examined systems have been used [9]. The order of the retrieval of the correct spectrum using four parameters has also been used [11,12]. Graphical representation of the searching results is also referred to [6,13]. The ability of the system to retrieve similar compounds has been examined using the propagation method [6]. Multivariate methods were used for the comparison of combinations of similarity indexes with normalization methods [14]. A thorough investigation of the parameters affecting the library search systems was presented by Clerc et al. [15]. It should be noted that the criteria used in this work stem from those encountered in the

literature but they are characterized by simplicity and functionality.

The construction of a library with a limited number of compounds was driven by the fact that the library was dedicated in particular to steroid analysis. The inclusion of compounds irrelevant to doping analysis in the library would have the effect of increasing the number of false interpretations.

The use of these criteria resulted in the comparative Tables 1–6. Two groups of indices can be distinguished according to their performance. The first group consists of SI2, SI3 and SI4 and presents an efficient retrieval in most instances. The correct spectrum is retrieved among the first two. SI4 gave slightly better results. Resolution according to criterion 2 was fully efficient for those indices. It should be noted that according to criterion 3 and for compound 1 for that group of indices there is a failure to retrieve structurally similar compounds. A closer examination of the respective library spectrum revealed the presence of strong background peaks, which may explain this failure. The failure to retrieve chemically similar structures in the case of compound 5 should also be noted. This can be attributed to the absence of such compounds in the files. SI4 differentiates better quantitatively between first and second selections. Two drawbacks of SI2 compared with the indices SI3, SI4 must be noted: the computation of SI2 is more complicated and it is applied only with the abbreviation procedure 2/14.

The results for the other three indices SI1, SI5 and SI6, which appear to consist of the second group (Tables 1, 5 and 6), included some failures to retrieve the correct spectrum. It must be said that SI5 fails only in the retrieval of compound 1 using the full spectrum. An explanation may be that the library spectrum of compound 1 included some small background masses above its molecular weight. SI5 attributes weighted significance in the difference of the peak intensities. Resolution according to criterion 2 for SI1 is not acceptable in particular cases (files STER2, STER3 and STER4). This is a result of the limited values that this index can take when a specific number of peaks is used in the abbreviation mode. SI5 ap-

pears to have more successes in retrieving structurally similar compounds. SI1 and SI5 seem to differentiate better between first and second selections (criterion 4).

In addition, it should be noted that from the type of abbreviation point of view, a comparison of the various abbreviated modes results in STER3 and STER4 having the advantage of being concise and at the same time carrying the most spectral and structural information. The abbreviation mode 2/14, which also has the same features, fails in some instances because it takes into consideration possible background peaks in the mass ranges where the particular spectra are "clean".

Conclusions

The use of the above four simple criteria for the assessment of the searching systems of mass spectra files appears to be a straightforward method for testing combinations of similarity indices and abbreviation modes. In the particular case of the steroid files studied, it seems that the similarity indices that have a strong geometrical background (correlation coefficient, Euclidean distance) [10,16] gave the best results. In addition, the abbreviation modes based on peak significance, as the sixteen most significant, or on 2/14 masses resulted in the best performance.

The authors thank Dr. J. Kiburis of the Doping Control Laboratory, Athens, for providing the necessary data.

REFERENCES

- 1 S.T. Brown, T.Q. Barker, R.J. Larivee, S.L. Monfre and H.R. Wilk, *Anal. Chem.*, 60 (1988) 252R; S.T. Brown, 62 (1990) 84R.
- 2 D.P. Martinsen, *Appl. Spectrosc.*, 35 (1981) 255.
- 3 J.T. Clerc, in H.L.C. Meuzelaar and T.L. Isenhour (Eds.), *Computer-Enhanced Analytical Spectroscopy*, Plenum, New York, 1987, p. 145.
- 4 J.R. Chapman, *Computers in Mass Spectrometry*, Academic, London, 1978.
- 5 D.P. Martinsen and B.H. Song, *Mass Spectrom. Rev.*, 4 (1985) 461.
- 6 G.T. Rasmussen and T.L. Isenhour, *J. Chem. Inf. Comput. Sci.*, 19 (1979) 179.
- 7 M. Donike, in G. Tosi (Ed.), *International Athletic Foundation World Symposium on Doping in Sport*, Florence,

- 1987, Official Proceedings, International Athletic Foundation, Florence, 1987, p. 53.
- 8 H.S. Hertz, R.A. Hites and K. Biemann, *Anal. Chem.*, 43 (1971) 681.
- 9 B.A. Knock, I.C. Smith, D.E. Wright, R.G. Ridley and W. Kelly, *Anal. Chem.*, 42 (1970) 1516.
- 10 P.H.A. Sneath and R.R. Sokal, *Numerical Taxonomy*, Freeman, San Francisco, 1973.
- 11 R.J. Mathews and J.D. Morrison, *Aust. J. Chem.*, 27 (1974) 2167.
- 12 R.J. Mathews and J.D. Morrison, *Aust. J. Chem.*, 29 (1976) 689.
- 13 G.T. Rasmussen, T.L. Isenhour and J.C. Marchall, *J. Chem. Inf. Comput. Sci.*, 19 (1979) 98.
- 14 F. Drablos, *Anal. Chim. Acta*, 201 (1987) 225.
- 15 J.T. Clerc, E. Pretsch and M. Zurcher, *Microchim. Acta*, II (1986) 217.
- 16 P.B. Harrington and T.L. Isenhour, *Anal. Chim. Acta*, 197 (1987) 105.

Simultaneous preconcentration of chromium(III) and chromium(VI) prior to speciation analysis

Guang-Lien Ou-Yang and Jen-Fon Jen

Department of Chemistry, National Chung-Hsing University, Taichung 40227 (Taiwan)

(Received 5th October 1992; revised manuscript received 4th January 1993)

Abstract

A method for the simultaneous preconcentration of chromium(III) and chromium(VI) in aqueous solution using an anion-exchange resin was developed. After chelating with EDTA, chromium(III) was bound to Dowex 1-X8 anion-exchange resin under the controlled conditions. Chromium(VI) was then enriched on the same resin. Factors affecting the chelate formation and optimum conditions for trapping and desorption were investigated. The proposed method provides a relatively simple and convenient procedure for the simultaneous preconcentration of chromium species by a readily available resin with the advantages of a high recovery and low operating cost.

Keywords: Liquid chromatography; Chromium; Preconcentration; Speciation

Speciation analysis of trace amounts of Cr(III) and Cr(VI) ions has become important in environmental analysis and biological studies because of their essential biochemical roles [1–3]. There is little decisive evidence on the toxic effects of Cr(III). In most instances, Cr(III) has been considered to be an essential species in nutrition [4]. In contrast, Cr(VI) has been reported as a carcinogen [5]. To obtain a better understanding of chromium toxicity, speciation analysis has been widely studied in order to differentiate Cr(III) from Cr(VI) in environmental and biological samples [1–3,6–12].

Liquid chromatography (LC) is a convenient method for separating and determining metal ions simultaneously [13–19]. Some reports have shown the practical use of LC for the determination of chromium species with conventional spectrophotometric detection, or with coupling to techniques

such as atomic absorption spectrometry and inductively coupled and d.c. plasma atomic emission spectrometry [6,8,10,20–24].

Chromium species often occur at trace levels in both environmental and biological samples, hence enrichment from aqueous solution is an important pretreatment step in analyses for chromium. Traditionally, chromium species have been enriched by different pretreatment methods on the basis of their different charge types [7,9,25–30]. De Jong and Brinkman [25] extracted Cr(III) and Cr(VI) individually by complexation with various reagents under different conditions. Subramanian [26] extracted Cr(III) or Cr(VI) selectively with isobutyl methyl ketone (IBMK)–ammonium tetramethylenedithiocarbamate [ammonium pyrrolidonedithiocarbamate (APDC)] various pH values and reaction times. Mullins [27] used $\text{Fe}(\text{OH})_3$ to coprecipitate Cr(III) and then extracted Cr(VI) with IBMK–APDC. Isshiki et al. [28] applied quinolin-8-ol to complex Cr(VI) prior to concentrating the complex on a macro-

Correspondence to: Jen-Fon Jen, Department of Chemistry, National Chung-Hsing University, Taichung 40227 (Taiwan).

porous resin. Obiols et al. [30] also used coprecipitation to enrich chromium in waters. Recently, Boussebart et al. [7] determined chromium speciation by cathodic stripping voltammetry, and Sperling et al. [9] concentrated Cr(VI) by on-line solid sorbent extraction and determined chromium speciation by two-step determination. These methods were complicated, and often caused serious losses of the interest species. Moreover, they were unable to preconcentrate Cr(III) and Cr(VI) simultaneously or to be applied in simultaneous determinations.

In this work, a simultaneous enrichment technique for Cr(III) and Cr(VI), before simultaneous determination by LC with UV detection, was investigated. Cr(III) was chelated with EDTA before being trapped on an anion-exchange resin along with Cr(VI). The optimum conditions for enrichment and elution were also studied. The performance of the proposed method was compared with that of Chelex resin.

EXPERIMENTAL

Apparatus

An LC-9A system (Shimadzu, Kyoto) was used, equipped with a Rheodyne Model 7125 injection valve (20- μ l sample loop) and a Supelcosil LC-8 reversed-phase column (25 cm \times 4.6 mm i.d., 3 μ m film thickness) (Supelco, Bellefonte, PA). A Soma Model S-3702 UV-visible detector and a Shimadzu C-R6A Chromatopac integrator were used. A Model Z-8100 polarized Zeeman-effect atomic absorption spectrometer (Hitachi, Tokyo) was used, equipped with a chromium hollow-cathode lamp at a wavelength of 359.3 nm with a slit width of 1.3 nm and a lamp current of 7.5 mA. An air-acetylene flame was used.

A Radiometer PHM82 pH meter with a glass electrode was used for pH measurements.

An ion-exchange column similar to that reported by Sturgeon et al. [31] was prepared using Dowex 1-X8 anion-exchange resin. A thick polyethylene frit of 35- μ m pore size was fitted into the columns to support the resin. All samples collected were stored in screw-capped 100-ml polypropylene bottles.

Reagents

Distilled, deionized water was used to prepare all solutions and the eluent. Stock standard solutions of 1000 μ g ml⁻¹ Cr(III) and Cr(VI) were prepared from ACS reagent grade chromium(III) chloride and potassium dichromate (RDH, Aktiengesellschaft, Germany), respectively. Fresh working standard solutions of Cr(III) and Cr(VI) (single or mixed) were prepared by appropriate dilution of the stock solutions with water. Ethylenediaminetetraacetate disodium salt (Na₂-EDTA) was obtained from Merck (Darmstadt) and tetrabutylammonium hydroxide (TBAOH) from Baker (Phillipsburg, WI). The LC eluents were prepared from LC-grade acetonitrile (Mallinckrodt, St. Louis, MO), water and TBAOH and were adjusted to the desired pH with 0.01 M sulphuric acid. All eluents were filtered through a 0.45- μ m PVDF membrane filter and degassed ultrasonically before being used. The HCl, HNO₃, H₂SO₄, NaOH, NH₃ solution, CH₃COOH and NaCl used to adjust the pH of sample and eluent solutions or as buffers were of ultra-pure grade from Aldrich (Milwaukee, WI). Dowex 1-X8 anionic-exchange resin (50–100 mesh) (Sigma, St. Louis, MO) and Chelex-100 chelating resin (100–200 mesh) (Bio-Rad, Richmond, CA) were packed in glass columns for trapping chromium ions.

Procedure

Activation of Dowex 1-X8 resin. Enrichment of Cr(III) and Cr(VI) with Dowex 1-X8 resin was performed with the aid of a burette that was slurry-loaded with 3.0 g of precleaned resin in the OH⁻ form. Before used in enrichment, the resin had to be activated. A volume of 30 ml of 1.0 M NaOH solution was passed through the enrichment column, followed by 10 ml of water to remove excess of NaOH, and then 30 ml of 1.0 M HCl were passed through the column to convert the resin into the Cl⁻ form, followed by 10 ml of water to remove excess of HCl.

Preparation of standard sample solution. Standard sample solutions containing 100 μ g of Cr(III) or Cr(VI) in 2.0 l was prepared. Before enrichment, an appropriate amount of EDTA was added to the sample solution and the pH of the solution

was adjusted to 6.0 with 5.0 ml of 0.5 M ammonium acetate solution, which was prepared from 1.0 M acetic acid and 1.0 M ammonia solution.

Simultaneous concentration of Cr(III) and Cr(VI) on Dowex 1-X8 anion-exchange resin. Before performing the enrichment step, 50 ml of 1.0 M NaOH were passed through the resin bed to convert the resin into the OH⁻ form, was followed by 50 ml of water to remove excess of NaOH. For controlling the pH in the resin bed, 30 ml of 0.5 M ammonium acetate buffer (pH 6.0) were passed through the enrichment column. Then the sample solution was loaded on the column under an effluent flow-rate of 0.5–0.6 ml min⁻¹. After passage of the sample, the column was washed with 10 ml of 0.5 M ammonium acetate buffer solution to rinse the sample adhering to the wall of column and remove the unabsorbed ions.

Recovery of Cr(III) and Cr(VI) by elution with NaOH–NaCl. The NaOH–NaCl elution system was applied by first weakening the absorption tendency of the trapped Cr(III) and Cr(VI) on the resin bed with 15 ml of 0.5 M NaOH, then rinsing with water to remove excess of NaOH and finally eluting with 1.0 M NaCl. The eluate from the passage of 1.0 M NaCl was collected for analysis.

Concentration with Chelex-100 resin. A column was slurry-loaded with 3.0 g of Chelex-100 resin. Before being used in the concentration step, the resin had to be activated. A volume of 30 ml of 5.0 M HNO₃ was passed through the resin bed, followed by 10 ml of water to remove excess of HNO₃, and then 30 ml of 1.0 M ammonia solution were passed through column to convert the resin into the NH₄⁺ form followed by 10 ml of water to remove excess of ammonia. Subsequently, 15 ml of 1.0 M ammonium acetate buffer solution (pH 4.0) were passed through the resin to keep the pH in the column at 4.0. Then the pH of sample solution was adjusted to 4.0 by adding 5.0 ml of 1.0 M ammonium acetate buffer and 1.0 M acetic acid or ammonia solution. The prepared sample solution was loaded on the column under an effluent flow-rate at 0.8–1.0 ml min⁻¹. After passage of the sample, the column was washed with 10 ml of 1.0 M ammonium acetate buffer

solution to rinse the sample adhering to the wall of the burette and remove the unabsorbed ions. The trapped Cr(III) was eluted with 50.0 ml of 5.0 M HNO₃ to recover completely the Cr(III).

RESULTS AND DISCUSSION

To establish the optimum conditions for the simultaneous preconcentration of Cr(III) and Cr(VI), factors affecting the formation of chelates and the retention behaviour, such as the pH of the sample medium and of the eluate, concentrations of EDTA and buffer solutions and the desorption procedure, were studied in detail. The results achieved with the proposed method were compared with those obtained with Chelex-100 resin.

Cr(III) chelate formation

Conversion of both chromium ions into species with similar charge is necessary for them to be retained simultaneously in an ionic concentration column. Cr(III) exists in the form of Cr(H₂O)₆³⁺ in aqueous solution, hence a complexation reagent with higher chelating ability than water is required to complex Cr(III). EDTA is known to complex with metal ions in a 1:1 ratio, and the chelates are always negatively charged whatever the charge on the cations [9]. Being chelated with EDTA, as CrY⁻ (where Y⁴⁻ represents the completely deprotonated EDTA species), Cr(III) will possibly be retained simultaneously with chromates on an anion-exchange resin.

As Cr(III) was precolumn chelated with EDTA, the enrichment would depend on the extent of chelation. Chelation between metal ions and EDTA has been discussed elsewhere [32]. Both solution pH and EDTA concentration are important factors in the chelation. Higher pH favours complex (CrY⁻) formation, but there is a risk of chromium(III) hydroxide [Cr(OH)₃] precipitation. Equilibria among Cr(VI) species also depend on the pH of the solution [33]. Although Cr(VI) species are still in anionic form at very low pH, Cr(III) chelation is difficult owing to the lack of Y⁴⁻. Therefore, controlling the pH of sample solution in the range 3.0–6.5 gave better results than other pH values.

The reaction rate of Cr(III) with EDTA is slow at a 1:1 ratio at the room temperature. This could be improved by increasing the pH of chelation and temperature and addition of EDTA. As verified in this work, it was advantageous to chelate at high temperature and high pH, and it was unnecessary to consider the oxidation ability of chromate at the controlled pH. Thus, the ratio of the Cr(III) to Cr(VI) was not changed during the sample pretreatment. On increasing the EDTA concentration to a 30:1 molar proportion of Cr(III), it took 15 min to complete the chelation at pH 6.0 at room temperature; if the sample was heated to 40°C at pH 6.0, only 5 min were required for chelation.

Simultaneous concentration of Cr(III) and Cr(VI) on Dowex 1-X8 anion-exchange resin

Dowex 1-X8 is a strongly basic anion-exchange resin that was obtained in the Cl⁻ form. Before performing the enrichment, the resin was converted into the OH⁻ form by passing NaOH through the enrichment column to increase the distribution coefficients of chromium species on the anion-exchange resin. However, the high pH of the OH⁻ form of the resin was not suitable for the adsorption of metal species. In order to improve the applicability of the anion-exchange resin in chromium species enrichment, 50 ml of water were passed through the resin to remove excess of NaOH, followed by 30 ml of ammonium acetate buffer to maintain the pH of resin bed at pH 6.0, prior to the elution of sample solution, which was adjusted to the same pH.

Table 1 gives the recoveries of Cr(III) and Cr(VI) obtained at various pH values with Dowex 1-X8 anion-exchange resin. It indicates that almost all of the Cr(III) was recovered by the Dowex 1-X8 if it was enriched at pH 4–6 under a flow-rate of 0.6 ml min⁻¹ and rinsed with 15 ml of 0.5 M NaOH and 5 ml of water before elution with 25 ml of 1.0 M NaCl; 97–104% of Cr(VI) was recovered with enrichment at pH 3–7 with the same flow-rate and the same elution conditions as for Cr(III). These results are consistent with the fact that the Cr(III) was chelated with low efficiency at low pH and was lost as Cr(OH)₃ at a higher pH, whereas the Cr(VI) was stable

TABLE 1

Recovery of Cr(III) and Cr(VI) at various sample pH values^a

pH (± 0.01)	Recovery (%)	
	Cr(III)	Cr(VI)
2.00	BDL ^b	91.0
3.00	21.8	98.0
4.00	99.8	104.0
5.00	99.5	102.7
6.00	101.1	103.6
7.00	54.0	97.3

^a Enrichment: Dowex 1-X8 resin at a flow-rate of 0.6 ml min⁻¹ with pH controlled by ammonium acetate buffer. Species content: 100.0 µg of Cr(III) and Cr(VI) each in 2.0 l of water. Elution: 15 ml of 0.5 M NaOH first, then 5 ml of water and finally 25 ml of 1.0 M NaCl. ^b Below detection limit.

over the pH range 3–6. Therefore, the optimum pH for the simultaneous enrichment of Cr(III) and Cr(VI) was in the range 4–6.

Effect of NaOH–NaCl eluent system on recovery

According to the equilibrium calculation related to the conditional formation constant, the Cr–EDTA complex would dissociate with a low-pH eluent, and Cr(III) (with positive charge) would be repelled from the positive sites of the anion-exchange resin. Hence Cr(III) could be eluted easily with a low-pH eluent. However, an acidic eluent was unable to elute Cr(VI) completely from the anion-exchange resin. On eluting the enrichment column with 1.0 M NaCl, only 90% of Cr(VI) and 75% of Cr(III) were recovered. It was found that rinsing the enrichment column with appropriate amounts of NaOH before the elution with NaCl increased the recoveries of both chromium species. A consecutive NaOH–NaCl elution system was therefore adopted. After the enrichment of Cr(III) and Cr(VI) on Dowex 1-X8 resin, several millilitres of dilute NaOH solution were first passed through the enrichment column to weaken the adsorption tendency of the trapped Cr(III) and Cr(VI) on the Dowex resin, then water was used to remove the excess of NaOH and finally 1.0 M NaCl solution was used for elution.

TABLE 2

Effect of NaOH addition on Cr(III) recovery ^a

NaOH added	Cr(III) recovery (%)
None	74.8
0.3 M NaOH, 10 ml	84.5
0.4 M NaOH, 20 ml	90.3
0.5 M NaOH, 15 ml	101.1
1.0 M NaOH, 15 ml	91.5

^a Enrichment: as described at pH 6.0. Species content: 100.0 μg of Cr(III) in 2.0 l of water. Elution: y ml of x M NaOH as indicated first, then 5 ml of water and finally 25 ml of 1.0 M NaCl.

Table 2 shows the effect of NaOH addition on the Cr(III) recovery. Rinsing with 15 ml of 0.5 M NaOH gave the best recovery. Hence the NaOH–NaCl elution system is recommended for the simultaneous preconcentration of Cr(III) and Cr(VI) with the Dowex 1-X8 anion-exchange resin.

Effect of flow-rate on enrichment efficiency

The degree of enrichment of Cr(III) and Cr(VI) on the Dowex 1-X8 anion-exchange resin is based on the charge interaction law, that is, the higher the charge on the ion, the greater is the interaction between the ion and the bed. It also depends on the flow-rate of sample passing through the enrichment column. The longer the sample species remain in the enrichment column, the better are the adsorption results. Table 3 shows that the recovery of Cr(VI) is up to 100% if the

TABLE 3

Effect of retention time on recoveries of Cr(III) and Cr(VI) ^a

Retention time (min)	Flow-rate (ml min^{-1})	Recovery (%)	
		Cr(III)	Cr(VI)
20.0	0.20	101.1	103.6
12.0	0.33	94.9	100.5
6.0	0.67	92.1	100.1
3.0	1.33	87.2	101.5
2.4	1.67	74.8	94.7

^a Enrichment: Dowex 1-X8 resin at a flow-rate of x ml min^{-1} as indicated at pH 6.0 controlled by ammonium acetate buffer. Species content: 100.0 μg of Cr(III) and Cr(VI) each in 2.0 l of water. Elution: 15 ml of 0.5 M NaOH first, 5 ml of water and finally 25 ml of 1.0 M NaCl.

retention time is above 3.0 min; a retention time of 20 min is required for 100% enrichment and complete recovery of Cr(III). The preconcentration factor under these conditions was 80 (26.67 per g of Dowex 1-X8 resin). Therefore, 20 min of sample retention in the Dowex 1-X8 enrichment column is recommended for the simultaneous enrichment of Cr(III) and Cr(VI) at pH 4–6.

Comparison with Chelex-100 resin

Chelex 100 is widely used for the enrichment of metal ions. Owing to the different charges of Cr(III) and Cr(VI), they cannot be enriched simultaneously on Chelex-100 resin. Two-step enrichment and determination for Cr(III) and Cr(VI) were required if Chelex-100 was used. Pre-reduction of Cr(VI) to Cr(III) is necessary to enrich the chromate. These procedures take a long time to achieve effective enrichment. It was found that elution of Cr(III) with a high recovery could not be achieved with HCl, even though different amounts of HCl were tried. Also, 5.0 M HNO₃ was required to recover 99% of Cr(III) from Chelex-100 resin (Table 4), which would cause environmental pollution. Based on the above performances, Dowex 1-X8 resin is to be preferred to Chelex-100 resin for the simultaneous preconcentration of Cr(III) and Cr(VI).

Conclusion

The simultaneous preconcentration of Cr(III) and Cr(VI) can be achieved by chelating Cr(III) ion with EDTA, followed by trapping the anionic Cr–EDTA chelate and chromates on an enrich-

TABLE 4

Effect of HNO₃ concentration on Cr(III) recovery ^a

HNO ₃ concentration (M)	Cr(III) recovery (%)
0.5	69.8
1.0	79.3
2.0	82.2
3.0	86.9
4.0	91.0
5.0	99.2

^a Enrichment: Chelex-100 resin at pH 4.0, retention time 12.0 min, flow-rate 0.33 ml min^{-1} . Species content: 100.0 μg of Cr(III) in 2.0 l of water. Eluent: x M HNO₃ as indicated.

ment column packed with Dowex 1-X8 anion-exchange resin. Almost all of the Cr(III) and Cr(VI) can be enriched simultaneously in the pH range 4.0–6.0 with a 20 min retention time. By using the consecutive NaOH–NaCl elution system, all of the trapped chromium species can be recovered simultaneously. The proposed procedure can be employed to preconcentrate chromium ions prior to simultaneous determination of Cr(III) and Cr(VI) by LC or other methods. It has the advantages of quantitative recovery, low operating cost and a simple procedure.

The authors thank the National Science Council of the Republic of China for financial support under grant contract Number NSC 80–0208-M-005–29.

REFERENCES

- 1 F. Borguet, R. Cornelis and N. Lameire, *Biol. Trace Elem. Res.*, 26 (1990) 449.
- 2 H. Salem and S.A. Katz, *Sci. Total Environ.*, 86 (1989) 59.
- 3 K.M. Jop, K.L. Dickson, P.B. Dorn, T.F. Parkerton and J.H. Rodgers, *Environ. Toxicol. Chem.*, 6 (1987) 697.
- 4 K. Schwartz and W. Mertz, *Arch. Biochem. Biophys.*, 85 (1959) 292.
- 5 Chromium – Health and Safety Precautions. Guidance Note EH₂, Health and Safety Executive, London, 1977.
- 6 M. Trojanowicz, E. Pobozy and P.J. Worsfold, *Anal. Lett.*, 25 (1992) 1373.
- 7 M. Boussemart, C.M.G. Vandenberg and M. Ghaddaf, *Anal. Chim. Acta*, 262 (1992) 103.
- 8 B. Gammelgaard, O. Jons and B. Nielsen, *Analyst*, 117 (1992) 637.
- 9 M. Sperling, X.F. Yin and B. Welz, *Analyst*, 117 (1992) 629.
- 10 I.H. Elsokkary and G. Muller, *Sci. Total Environ.*, 97 (1990) 455.
- 11 M. Pettine and F.J. Millero, *Limnol. Oceanogr.*, 35 (1990) 730.
- 12 E. Otabbong, *Acta Agric. Scand.*, 39 (1989) 119.
- 13 J.N. King and J.S. Fritz, *Anal. Chem.*, 59 (1987) 703.
- 14 C.-W. Whang, L.-C. Wu and L.-C. Chou, *Proc. Natl. Sci. Counc. ROC (A)*, 11 (1987) 363.
- 15 K. Ito, Y. Ariyoshi, F. Tanabiki and H. Sunahara, *Anal. Chem.*, 63 (1991) 273.
- 16 T. Okada, *Anal. Chem.*, 60 (1988) 1511.
- 17 B.A. Bidlingmeyer, C.T. Santasania and F.V. Warren, *Anal. Chem.*, 59 (1987) 1843.
- 18 J. Dai and G.R. Hilz, *Anal. Chem.*, 60 (1988) 301.
- 19 R. Milacic, J. Stupar, N. Kozuh and J. Korosin, *Analyst*, 117 (1992) 125.
- 20 J.-F. Jen and C.-S. Chen, *Anal. Chim. Acta*, 270 (1992) 55.
- 21 W.-L. Fong, and J.-C. Wu, *Spectrosc. Lett.*, 24 (1991) 931.
- 22 S. Ahmad, R.C. Murthy and S.V. Chandra, *Analyst*, 115 (1990) 287.
- 23 K.E. Collins, C.H. Collins and M.E. Dequeiroz, P.S. Bonato, C. Archundia, *Chromatographia*, 26 (1988) 160.
- 24 A.G. Cox, I.G. Cook and C.W. McLeod, *Analyst*, 110 (1985) 331.
- 25 G.J. De Jong and U.A.Th. Brinkman, *Anal. Chim. Acta*, 98 (1978) 243.
- 26 K.S. Subramanian, *Anal. Chem.*, 60 (1988) 11.
- 27 T.L. Mullins, *Anal. Chim. Acta*, 165 (1984) 97.
- 28 K. Isshiki, Y. Sohrin, H. Karatani and E. Nakayama, *Anal. Chim. Acta*, 224 (1989) 55.
- 29 F. Ahern, J.M. Eckert, N.C. Payne and K.L. Williams, *Anal. Chim. Acta*, 175 (1985) 147.
- 30 J. Obiols, R. Devesa, J. Garciaberro and J. Serra, *Int. J. Environ. Anal. Chem.*, 30 (1987) 197.
- 31 R.E. Sturgeon, S.S. Berman, A. Desaulniers and D.S. Russell, *Talanta*, 27 (1980) 85.
- 32 D.A. Skoog, D.M. West and F.J. Holler, *Fundamentals of Analytical Chemistry*, Saunders, New York, 1992, 6th edn., pp. 286–294.
- 33 R.K. Tandon, P.T. Crisp, J. Ellis and R.S. Baker, *Talanta*, 31 (1984) 227.

Effect of pH on the redox equilibria of immobilised 2,6-dichloroindophenol

G. Goodlet and R. Narayanaswamy

*Department of Instrumentation and Analytical Science, University of Manchester,
Institute of Science and Technology, P.O. Box 88, Manchester M60 1QD (UK)*

(Received 20th November 1992; revised manuscript received 15th January 1993)

Abstract

The effects of immobilisation on the oxidation–reduction equilibria of 2,6-dichloroindophenol (DIP) between pH 2 and 6 have been studied. The formal potentials of the indicator in solution and in the immobilised form were obtained using absorbance and reflectance techniques, respectively, and were deduced from percentage reduction versus redox potential plots. The redox potential of the solution was altered using potentiopoised solutions containing different ratios of potassium hexacyanoferrate(II) and hexacyanoferrate(III). The formal potentials were found to be lowered when DIP was immobilised on XAD-4 resin. This and other observations described in this paper would be useful in the development of optical redox sensors.

Keywords: Reflectance spectrometry; UV–Visible spectrophotometry; 2,6-Dichloroindophenol; Fibre-optic sensors; Formal potential; Immobilization; pH; Redox equilibria

Reagents used in fibre-optic sensing probes are often immobilised at the distal end of the fibre optics. Chemical species can interact with the immobilised reagent causing optical changes which can be monitored via the fibre optics. Upon immobilisation the properties of the reagent have been observed to change. Previously [1] the acid–base properties of 2,6-dichloroindophenol (DIP) have been observed to alter when the reagent was immobilised on a polymeric resin (Amberlite XAD-2).

This paper reports changes observed in the redox equilibria of DIP with varying pH. DIP is an example of a well known redox indicator and the effect of pH on the properties of such indica-

tors in solution is well documented [2]. The properties of this indicator in solution are compared to its properties when immobilised on XAD-4 resin by adsorption. The redox equilibria were examined using potentiopoised solutions [3]. A potentiopoised solution is a solution which is buffered by control of redox reactions such that the redox potential of the solution remains constant. This paper reports new investigations on the use of potentiopoised solutions which have only been used previously in highly acidic conditions. Also, the immobilised redox chemistry of DIP has only previously been investigated at pH 0 [4]. The studies include the use of solutions of varying pH, and a mechanism has been proposed which incorporates associated chemical equilibria which contribute to the redox response of the immobilised indicator. The results will be useful in the development of optical redox probes using immobilised DIP.

Correspondence to: R. Narayanaswamy, Department of Instrumentation and Analytical Science, University of Manchester, Institute of Science and Technology, P.O. Box 88, Manchester M60 1QD (UK).

EXPERIMENTAL

Instrumentation

All redox potential measurements were made using a platinum electrode (fabricated by the recommended procedure [5]), an EIL reference electrode and an EDT research pH/ion meter (ECM 201). The potentioposed solutions were not stirred because equilibrium potentials were recorded.

The absorbance measurements of indicator solutions were measured using a Perkin-Elmer Lambda 5 UV-visible spectrophotometer. Reflectance measurements were made on the immobilised indicator using a system which featured a bifurcated optical fibre and a flow cell arrangement [4]. The immobilised DIP was contained in the flow cell through which the potentioposed solution was continuously circulated. The response of the resin was recorded using a chart recorder (Servo Scribe RE111).

Reagents

2,6-Dichloroindophenol indicator was supplied by Aldrich. All other reagents used were of analytical-reagent grade.

Potentioposed solutions were prepared by taking a 0.1 M potassium orthophosphate buffer solution and adjusting the pH using sodium hydroxide (5 M) or sulphuric acid (0.5 M). The ionic strength of the solution was maintained at 0.2 M (NaOH–NaCl) by adding sodium chloride. The redox potential of the solution was adjusted by mixing different ratios and concentrations of potassium hexacyanoferrate(II) and potassium hexacyanoferrate(III). The buffer solution was deaerated (using nitrogen) before the potentioposed solutions were prepared. The potentioposed solutions were also deaerated continuously after preparation.

The indicator was immobilised on Amberlite XAD-4 resin (particle sizes 71–90 μm) by equilibrating 2.0 g of the copolymer with 50 ml of a 1 mg ml^{-1} aqueous solution of the indicator for 24 h. Before use, the copolymer was soaked in methanol and then washed well with water to displace the methanol. The resulting reagent phase was then washed thoroughly with distilled

water until the washings were colourless. The immobilised indicator was kept at pH 6 due to previous observations [6] that at above pH 7 the indicator was noted to gradually desorb from the resin.

Procedure

The redox equilibria of the indicator in solution were examined by observing the change in the absorbance of the indicator with corresponding changes in its redox potential. To 15 ml of a DIP solution (2.115×10^{-4} M), 10 ml of the potentioposed solution were added. The potential of the solution and the absorbance spectrum of the solution (between 350 and 750 nm) were recorded. This was repeated at a series of potentials. The procedure was carried out with solutions with pH values of exactly 4, 5 and 6. Below pH 4 the indicator precipitated and above pH 6 the indicator could not be fully reduced because the redox potential of the solution could not be lowered sufficiently because the hexacyanoferrate(II) became insoluble, so more concentrated solutions could not be prepared. The absorbance values were measured at the peak maximum for each solution.

The redox equilibria of the immobilised indicator were examined by observing the change in reflectance of the indicator with corresponding changes in its redox potential. A potentioposed solution was passed over the immobilised indicator in a flow cell until a constant reflectance value was recorded indicating the attainment of equilibrium. This was repeated at a series of potentials. Equilibration took 5–10 min depending on the pH of the solution. The procedure was carried out at pH values of exactly 2, 3, 4, 5 and 6. All reflectance measurements were recorded at 545 nm; preliminary studies indicated that the greatest reflectance change occurred at this wavelength on oxidation or reduction. Three sets of measurements were made at each pH. Each set of measurements involved a fresh indicator solution or a fresh batch of the immobilised indicator; in both cases the indicator was initially in the oxidised form.

The results of the measurements were expressed as absorbance or relative reflectance vs.

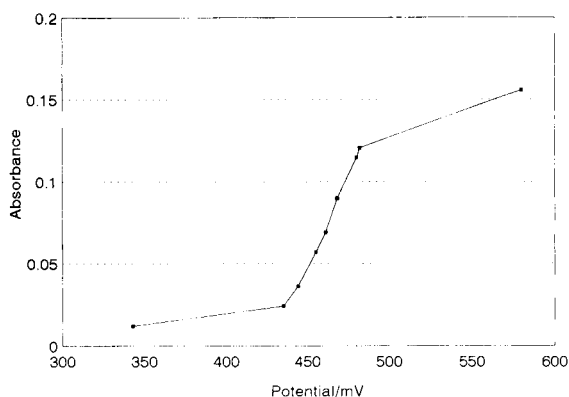


Fig. 1. Variation in the absorbance of DIP with redox potential in solution at pH 4.0.

potential (mV). These were both converted to % reduction vs. potential (mV) plots.

RESULTS AND DISCUSSION

Variations of absorbance and reflectance with potential

Figures 1 and 2 respectively show the variation of absorbance and reflectance with potential at pH 4. The sigmoid curves resemble titration curves and can be correlated with changes in the relative amounts of the oxidised and reduced forms of the indicator. At lower potentials the reduced form predominates, which is colourless. Therefore the indicator exhibits a low absorbance

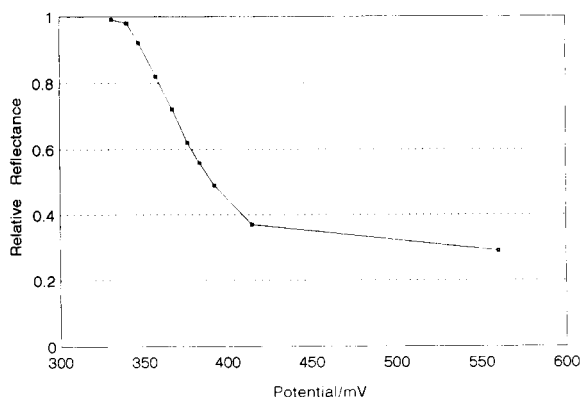
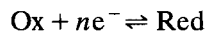


Fig. 2. Variation in the relative reflectance of immobilised DIP with redox potential at pH 4.0.

or a high reflectance. At higher potentials the major species is the oxidised form which is intensely coloured and consequently the indicator exhibits a high absorbance or a low reflectance.

Evaluation of the formal potential

If a redox half-reaction is represented by



where Ox represents the oxidised species and Red the reduced species, and n is the number of electrons (e^-) transferred, then the electrode potential of the redox couple will be given by the Nernst equation:

$$E_n = E_o + \frac{RT}{nF} \ln \left(\frac{[\text{Ox}]}{[\text{Red}]} \right)$$

where E_o is the value of the potential at unit molar concentrations of the oxidised and reduced species (i.e. $[\text{Ox}]$ and $[\text{Red}]$) and is called the normal potential of the redox couple. When $[\text{Ox}] = [\text{Red}] = 1$ then $E_n = E_o$. However, the normal potential, E_o , will vary with the activity coefficients of the oxidised and reduced species and hence with the ionic strength of the solution, and therefore, with the nature and concentration of any electrolytes present. To allow for these variations the term E'_o , the formal potential, will be used. This is the potential of the solution containing equal concentrations of the oxidised and reduced species, under the conditions specified in terms of other electrolytes. The formal potential,

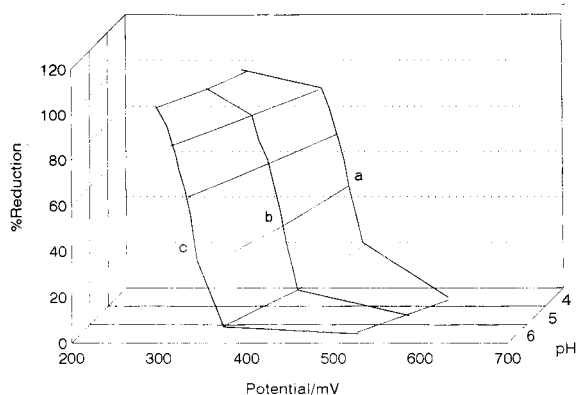


Fig. 3. A three-dimensional plot of % reduction vs. potential at different pH values for DIP in aqueous solution; (a) pH 4.0; (b) pH 5.0; (c) pH 6.0.

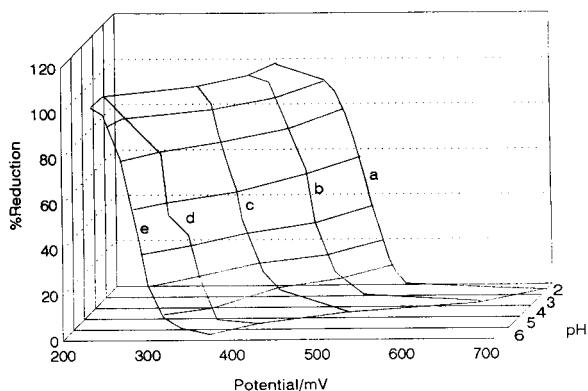


Fig. 4. A three-dimensional plot of % reduction vs. potential at pH: (a) 2.0; (b) 3.0; (c) 4.0; (d) 5.0; (e) 6.0 for DIP immobilised on XAD-4 resin.

E'_0 , varies with pH in the majority of systems. Both E_0 and E'_0 apply to pH 0. For values of E'_0 at other pH values the term E_m will be used (for example, E_m^6 means the value of the formal potential at pH 6). The distinction between E'_0 and E_m is very important in the consideration of redox indicators as their formal potentials are dependent on the pH of the solution.

The formal potential of DIP in solution or in the immobilised form was deduced from the percentage reduction vs. potential plots (see Fig. 3 and 4). At 50% reduction, $[\text{Red}] = [\text{Ox}] = 50\%$. Thus the potential at which the 50% reduction occurred was recorded as the formal potential.

Comparison of the formal potentials

Table 1 displays the formal potentials of DIP in aqueous solution and in the immobilised form at various pH values, from which it can be seen that immobilisation lowers the formal potential of

TABLE 1

Formal potentials (E_m , mV) of DIP in aqueous solution and in the immobilised form at various pH values

	pH				
	2	3	4	5	6
Aqueous solution ^a	—	—	462.3 ± 7.2	392.0 ± 2.0	326.3 ± 4.0
Immobilised ^a	497.0 ± 6.9	428.7 ± 2.5	372.7 ± 5.9	329.7 ± 8.1	271.7 ± 5.0

^a Mean ± S.D. ($n = 3$).

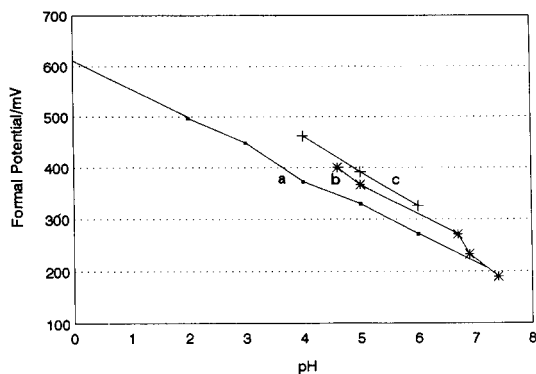
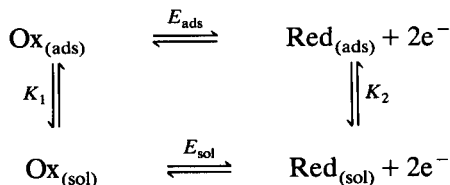


Fig. 5. A comparison of formal potential vs. pH for: (a) immobilised DIP; (b) DIP in solution, (c) plot for DIP in solution obtained by Gibbs et al. [7].

the indicator. The magnitude of the decrease appears to increase as the pH is decreased. Previously it has been proposed [4] that this decrease was due to the existence of simultaneous redox and adsorption–desorption equilibria which altered the properties of the immobilised indicator. Figure 5 compares the results obtained in this investigation with solution studies carried out by Gibbs et al. [7]. It also shows that the plot for the immobilised reagent when extrapolated to pH 0 gives an E'_0 value (605 mV) which is similar to that reported previously [4]. The results obtained in the solution studies in this investigation compare favourably with those obtained by Gibbs et al. Both sets of results yield approximately the same formal potential vs. pH plot (although the plot in this investigation is slightly different, possibly due to the higher ionic strength of the solution).

The results for the immobilised studies gave a plot with a lower gradient than those obtained from the solution studies. The plot converges with the plot at pH 7 obtained by Gibbs et al. [7]. This observation can be explained by consideration of a set of equilibria as follows:



where

$$E_{\text{ads}} = E_{m,\text{ads}} + \frac{RT}{2F} \ln \left(\frac{[\text{Ox}]_{\text{ads}}}{[\text{Red}]_{\text{ads}}} \right)$$

$$E_{\text{sol}} = E_{m,\text{sol}} + \frac{RT}{2F} \ln \left(\frac{[\text{Ox}]_{\text{sol}}}{[\text{Red}]_{\text{sol}}} \right)$$

$$K_1 = \frac{[\text{Ox}]_{\text{ads}}}{[\text{Ox}]_{\text{sol}}} \quad K_2 = \frac{[\text{Red}]_{\text{ads}}}{[\text{Red}]_{\text{sol}}}$$

where, e.g. $[\text{Ox}]_{\text{ads}}$ and $[\text{Ox}]_{\text{sol}}$ are the concentrations of the oxidised species adsorbed onto the resin and in solution, respectively (in mol l⁻¹).

Since the potential in the adsorbed and solution phases must be equal, i.e. $E_{\text{sol}} = E_{\text{ads}}$, it follows that:

$$E_{m,\text{ads}} - E_{m,\text{sol}} = \frac{RT}{2F} \ln \left(\frac{K_2}{K_1} \right)$$

At low pH the keto, oxidised form is found to possess a greater distribution coefficient than the phenolic reduced form (observed for XAD-2, a similar resin) [8]. Therefore $K_1 > K_2$, thus $E_{m,\text{ads}} < E_{m,\text{sol}}$. As the pH increases the value of $E_{m,\text{ads}}$ gradually approaches that of $E_{m,\text{sol}}$ suggesting that the value for K_2 approaches the value for K_1

TABLE 2

Response times of the immobilised indicator at various pH values

pH	Response time (min)
6.0	5.0
5.0	6.2
4.0	5.5
3.0	3.0
2.0	3.0

or vice versa. The former case is thought to occur owing to the increased desorption of the reduced form of the indicator. The reduced form is not resonance stabilised (unlike the oxidised form), and it becomes more solvated. Therefore its tendency to desorb increases. Figure 6 summarises this explanation.

Comparison of the response times of the immobilised indicator

Table 2 displays the response times, which are the values for which 90% response was achieved. It can be seen that the response times were significantly less at pH 2 and 3. This difference in the response time may be due to a more rapid pathway being followed by the reaction at pH < 4.

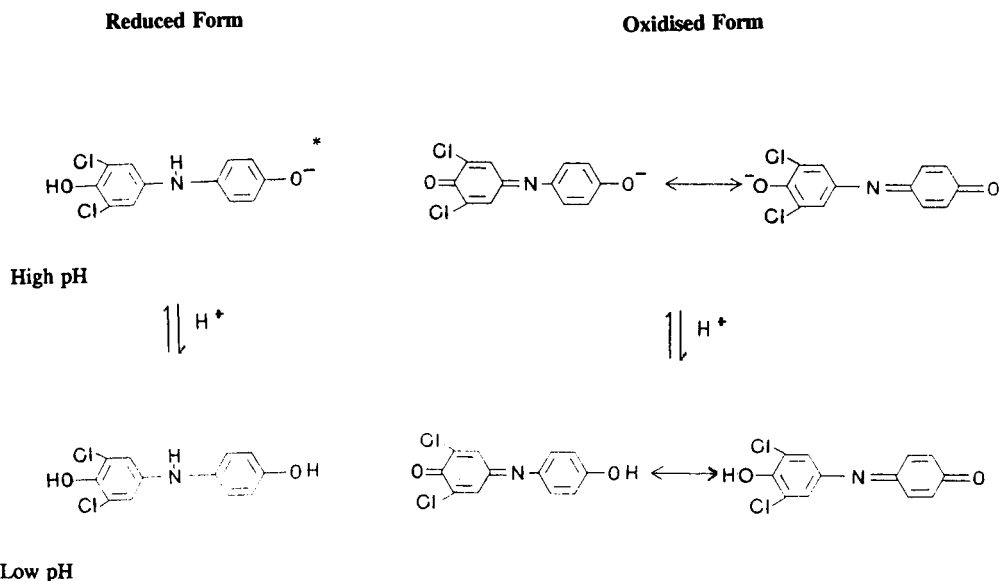


Fig. 6. Equilibria involving the reduced and oxidised forms of DIP at higher and low pH. * indicates more solvated species which is more readily desorbed.

A model is currently being pursued in order to explain the mechanisms of DIP at various pH values.

REFERENCES

- 1 R. Narayanaswamy and F. Sevilla III, *Anal. Chim. Acta*, 189 (1986) 365.
- 2 E. Bishop, *Indicators*, Pergamon, Oxford, 1972, Chap. 8.
- 3 W.M. Banick and G.F. Smith, *Talanta*, 2 (1959) 348.
- 4 R. Narayanaswamy and F. Sevilla III, *Mikrochim. Acta*, I (1989) 293.
- 5 D. Brennan and C.F.H. Tipper, *A Laboratory Manual of Experiments in Physical Chemistry*, McGraw-Hill, London, 1967, Expt. 35, p. 128.
- 6 R. Narayanaswamy and F. Sevilla III, *J. Opt. Sensors*, 1 (1986) 403.
- 7 H.D. Gibbs, B. Cohen and R.K. Cannon, *Hyg. Lab. Rep. (U.S.)*, 151 (1927–28) 150.
- 8 M.D. Grieser and D.J. Pietrzyk, *Anal. Chem.*, 45 (1973) 1348.

BOOK REVIEWS

Andrew van Es, *High Speed Narrow Bore Capillary Gas Chromatography*, Hüthig Verlag, Heidelberg, 1992 (ISBN 3-7785-2027-X). vi + 158 pp. Price DM 88.00.

High speed gas chromatography employing narrow bore open tubular columns with internal diameters $< 100 \mu\text{m}$ is not employed in my laboratories at present. Suitable columns have been available for a number of years but a lack of commercial instrumentation to fully exploit the properties of these columns was and still is the major impediment to their acceptance by most chromatographers. The major instrumental problems are a lack of suitable inlets, peak broadening caused by detector dead volumes, and inadequate data acquisition rates of detectors and integrators, combined with the low sample capacity of narrow bore columns. The author's stated objective is to find technological solutions to the above problems as well as presenting a theoretical framework for an understanding of the properties of narrow bore columns and their operation.

The author succeeds in summarizing the relevant theory of narrow bore columns. The book contains several sections in which the space occupied by equations exceeds that devoted to text. Throughout the book, in fact, the author uses words sparsely and there are many short paragraphs in which facts are presented without description or explanation. Likewise, equations are not derived and, therefore, there is little opportunity to understand the limitations and/or approximations in the theoretical aspects presented.

In terms of the practice of narrow bore gas chromatography the author describes a number of experiments in a format similar to a regular scientific paper or doctoral thesis (introduction, experimental, results and discussion). This is not always a useful format for comparison and consolidation of knowledge. Rather than demonstrate solutions to problems, as promised, there is no integration to the problems presented and one

is left wondering whether high speed gas chromatography is practically useful or not. There is not one single practical application presented in the book which would tend to support the latter conclusion.

The information provided may invoke fruitful thought but is unlikely to inspire the majority of analytical chemists not already involved in high speed GC to become so in the near future. Also, the referenced work in the book seems to be unusually dated for a 1992 publication. There are a few scattered references to work performed in 1989 but a comprehensive review of the literature seems to have stopped with 1988. There are also short sections on correlation chromatography and turbulent flow GC at the end of the book. These are only loosely related to the main theme of the book and too short to be generally useful.

Overall, the book is aimed at a very specialized audience and has little general appeal to those not attracted to the book by its title. It is the only comprehensive account of high speed GC with narrow bore columns I am aware of. Thus, it may find its way into some professional libraries but this is not a book likely to spur on research work in this area and could have offered the reader a more thorough and insightful approach to the topic.

Colin F. Poole

Wilfried Niessen and Jan van der Greef, *Liquid Chromatography–Mass Spectrometry*, Marcel Dekker, New York, 1992 (ISBN 0-8247-8635-1). vi + 479 pp. Price US\$165.00 (USA and Canada), US\$189.75 (other countries).

This text is Volume 58 in the Chromatographic Science Series. It deals primarily with the true hybrid nature of liquid chromatography–mass spectrometry (LC–MS), and has a satisfying feeling of completeness about it. The reader is presented with three introductory chapters covering

the topics of liquid chromatography, mass spectrometry and the interfacing of chromatography with mass spectrometry.

The longest section (nine chapters) relates to interface technology as applied to LC-MS. This includes an overview of the large number of different types of interface available followed by a more detailed discussion of the most commonly used types. The newer topics of coupling supercritical fluid chromatography and capillary electrophoresis to mass spectrometry are dealt with in the concluding two chapters of this section.

No book on mass spectrometry would be complete without some discussion of the ionisation techniques used and five chapters are devoted to these topics. As well as a detailed discussion of the commonly used ionisation methods alternative means of inducing useful addition fragmentation in the soft ionisation techniques are reviewed at the end of this section.

The short applications section is appropriate for a book of this nature.

The book is well referenced and particularly well cross-referenced between the individual chapters and sections. The excellent illustrations enhance the text and clarify the understanding promoted by the book.

This is a book for the practising mass spectroscopist and chromatographer, but is also a text that could provide advanced students with a comprehensive insight into the subject of LC-MS. It can be recommended as a valuable contribution to study and reference in an area of developing technology and applications.

John D. Green

Otto S. Wolfbeis (Ed.), *Fluorescence Spectroscopy, New Methods and Applications*, Springer, Berlin, 1993 (ISBN 3-540-55281-2). xx + 310 pp. price DM 168.00.

Fluorimetry has developed rapidly over the last decade, and the rate of advance is unlikely to decrease in the near future. This book, which is based on the plenary lectures presented at a 3-day conference on "Methods and Applications of Fluorescence Spectroscopy" held in Graz,

Austria, in October 1991, provides analytical chemists and biomedical scientists with an excellent summary of progress in areas of the subject that are developing most rapidly. Each chapter is written by a well-known expert, and the total of 21 contributions is arranged into five sections, viz. new methods in fluorescence spectroscopy, new applications, fluorimetric analysis, fluorescence immunoassay and fluorescence in biomedical sciences. The chapters are well focussed, and cover such topics as fluorescence correlation spectroscopy of single molecule events, fluorescence quenching sensors, applications in forest decline studies, investigation of structure formation in surfactant monolayers, fluorescent lifetime imaging, fluorescent probes on biomembranes, near-IR fluorimetry, applications in environmental studies, and studies of fluorescent transients in neurobiology. There is also an article on chemiluminescence detection in immunoassay, which is valuable, but strictly is outside the scope of the book. This is a book that can be recommended to all analytical scientists interested in fluorimetry.

Alan Townshend

W.A. Steger, K. Dathe, R. Herzschuh, A. Mehlhorn, B. Müller and E. Müller, *Strukturanalytik*, Deutscher Verlag für Grundstoffindustrie GmbH, Leipzig, 1992 (ISBN 3-342-00044-9). Soft cover, 340 pp.

This book gives a truly excellent introduction to the various instrumental methods for the structure elucidation of organic compounds. After a short introduction to introduce a consistent terminology and an overview of the basic philosophy there are chapters on mass spectrometry, vibrational spectroscopy, electron spectroscopy, nuclear magnetic resonance methods and electron spin resonance, and diffraction methods. This part is followed by a discussion of the synergistic effects of the combined application of spectroscopic methods, and a short discussion of computer-aided methods in structure analysis, ranging from capturing raw data to quantum chemical calculations. The final chapter gives a limited but quite useful compilation of relevant spectroscopic

data for more common compound classes. Despite the fact that the book is written by a collective of 6 authors, the presentation style, the terminology, the logical skeleton, and the depth of presentation are perfectly homogeneous. This makes it easy to read across the method boundaries and helps to realize and understand the synergistics between the different methods. Furthermore, style and presentation of the contents are selected so as to make it fairly easily accessible to interested non-chemists, e.g. engineers, geologists, or medical doctors. The respective selection criteria have also been applied to the many examples and exercises given. In summary, this is an excellent book which can be recommended without any reservation. It has but one drawback. As the book is written in German, a working knowledge of that language is required.

J.T. Clerc

C.N. Hewitt (Ed.), *Methods of Environmental Data Analysis*, Elsevier Applied Science, London, 1992 (ISBN 1-851-66735-0). xii + 309 pp., Price £75.00.

The Environmental Management series from Elsevier provides a medium for the coverage of particular scientific topics within a multi-disciplinary, environmental problem-solving context. This particular volume is a multi-author collection of seven chapters dealing with the treatment of environmental data. It is a particularly important area of environmental science due to the exponentially increasing volume of analytical data that is being collated. This is due to the greater public interest in environmental matters, an increased automation of both the sampling and measurement stages of the analytical process and, more recently, the adoption of remote sensing techniques.

The major attraction of the book is that all of the chapters make extensive use of real environmental analytical data in order to illustrate the text. This obviously makes it more relevant to the intended readership of undergraduates, researchers, policy makers and administrators. The material covered ranges from an introduction to

descriptive statistical techniques (e.g., mean, median, standard deviation), through regression and correlation, errors and detection limits and quality assurance (an important and often overlooked issue) to the visual representation of data, univariate methods for nonstationary time-series analysis (which is of particular significance to environmental scientists) and factor and correlation analysis of multivariate data.

It is therefore a wide ranging treatment, some of which will be beyond the scope of many undergraduates, but nonetheless it is a useful and generally readable contribution that will help environmental scientists to "produce information, not just numbers". One minor criticism is that the individual chapters could have been arranged more logically and, consequently, that an overview of each chapter and their inter-relationships would be helpful. However, it is a positive contribution to the environmental science literature.

P.J. Worsfold

William C. Golton (Ed.), *Analysis of Paints and Related Materials: Current Techniques for Solving Coatings Problems*, ASTM, Philadelphia, 1992 (ISBN 0-8031-1465-6). vii + 202 pp. Price US\$51.00.

This is a collection of papers presented at a symposium, sponsored by ASTM, of the same title as the book, held in Pittsburgh, PA, May 1990. Its four sections of 11 contributions encompass the analysis and characterisation of whole paint, and of paint components, cure characterisation etc., and paint failure and defects. A wide range of modern instrumentation is discussed, well supported by illustrations and references. The text shows that, like most other fields, paint analysis has advanced rapidly, in step with the development of instrumental techniques. The lack of a subject index spoils what is otherwise a very useful and informative monograph.

P.J. Kistemaker and N.M.M. Nibbering (Eds.), *Advances in Mass Spectrometry*, Vol. 12, Elsevier, Amsterdam, 1992 (ISBN 0-444-88871-3). xxii + 951 pp. Price US\$281.50/Dfl. 450.00.

These are the Proceedings of the *12th International Mass Spectrometry Conference, Amsterdam, 26–30 August, 1991*. The papers are reprinted from the *International Journal of Mass Spectrometry and Ion Processes*, Vols. 118 and 119. This large text is devoted to 31 major presentations, by the top “names”, covering a wide variety of aspects of mass spectrometry and ion processes. Unlike many conference proceedings, therefore, this is a comprehensive review of the state of mass spectrometry, and contain a tremendous collection of information of current interest. These papers are supplemented by lists of hundreds of poster titles and authors, and an index of authors.

Heinz-Helmut Perkampus, *UV–VIS Atlas of Organic Compounds*, 2nd edn., VCH, Weinheim, 1992 (ISBN 3-527-28510-5). iv + 336 pp. (Part 1), iii + 1189 pp. (Part 2). Price DM 750.00.

This is the Second Edition of the original collection which appeared as five loose-leaf volumes about 20 years ago, but is now available as two hard-back volumes of A4 pages, the second of which has three times the number of pages of the first. There are about 1170 spectra, recorded from 180 to 500 nm, over a molar absorptivity scale usually of $0\text{--}10^5 \text{ l mol}^{-1} \text{ cm}^{-1}$ plotted logarithmically. In addition, there are tabulated data of peak wavelengths and molar absorptivities for similar derivatives of particular molecules (e.g., substituted fluorenones). The information

(from spectra and tables) can be retrieved by referring to indexes of compound group (based on chromophores or use (e.g., solvents, compounds of biochemical and clinical interest)), formula, name (in alphabetical order) and number of rings. There is also introductory material, mainly contributions from a range of authors on the spectra of each compound group. The collection is beautifully produced, and will be of considerable value to analytical scientists.

Stephen R. Cooper (Ed.), *Crown Compounds: Toward Future Applications*, VCH, New York, 1992 (ISBN-1-56081-024-6). x + 325 pp. Price DM 218.00/£89.00.

This book is an interesting “experiment”. It attempts to project forward thoughts about the future uses of the various classes of macrocyclic ligands. In sixteen chapters, numerous authors cover such diverse areas of application as metal ion isotope separations, control of redox properties of metal ions, molecular and enantiomeric recognition and biomedical applications. Macrocyclic sulphides, torands and tetraazamacrocycles are some of the less usual structures considered. The design of cavities with particular properties is a topic that receives particular attention. This is altogether a most valuable collection of information that deserves to stimulate many further advances in what is a most fascinating area of chemistry.

ANALYTICA CHIMICA ACTA, VOL. 279 (1993)

AUTHOR INDEX

- Anis, N., see Wong, R.B. 141
- Bachas, L.G., see Smith-Palmer, T. 287
- Bai, M., see Pan, S. 195
- Barbarakis, M.S., see Smith-Palmer, T. 287
- Becerro Domínguez, F., see Carabias Martínez, R. 299
- Bode, J., see Schügerl, K. 3
- Boers, G.W.
—, Kettenes-van den Bosch, J.J. and Bult, A.
Applications of HY-APATITE in liquid chromatography 89
- Bordás, B., see Forgács, E. 115
- Brandes, L., see Schügerl, K. 3
- Brandt, J., see Schügerl, K. 3
- Brinkman, U.A.Th., see Van de Merbel, N.C. 39
- Bult, A., see Boers, G.W. 89
- Burewicz, A., see Malinski, T. 135
- Buttler, T.
—, Gorton, L. and Marko-Varga, G.
Characterization of a sampling unit based on tangential flow filtration for on-line bioprocess monitoring 27
- Carabias Martínez, R.
—, Becerro Domínguez, F., Martín González, F., Hernández Méndez, J. and Córdova Orellana, R.
Polypyrrole-dodecyl sulphate electrode as a microsensor for electroinactive cations in flow-injection analysis and ion chromatography 299
- Carlsen, M.
—, Johansen, C., Min, R.W., Nielsen, J., Meier, H. and Lantreibecq, F.
On-line monitoring of penicillin V during penicillin fermentations: a comparison of two different methods based on flow-injection analysis 51
- Cheng, G., see Dong, S. 235
- Conway, V., see Pan, S. 195
- Córdova Orellana, R., see Carabias Martínez, R. 299
- Corrieu, G., see Picque, D. 67
- Cserhádi, T.
—, Forgács, E. and Ujházy, A.
Retention characteristics of a β -cyclodextrin polymer-coated liquid chromatographic column 107
- Cserhádi, T., see Forgács, E. 115
- Cynkowski, T., see Smith-Palmer, T. 287
- Davey, C.L.
—, Davey, H.M., Kell, D.B. and Todd, R.W.
Introduction to the dielectric estimation of cellular biomass in real time, with special emphasis on measurements at high volume fractions 155
- Davey, H.M., see Davey, C.L. 155
- Dekeyser, P.M.
—, De Smedt, S., Vercruyse, K., Demeester, J. and Lauwers, A.
High-performance size-exclusion chromatography of proteoglycans extracted from bovine articular cartilage 123
- De Kock, S.S., see Fourie, L. 163
- Demeester, J., see Dekeyser, P.M. 123
- Dempsey, E., see Wang, J. 203
- Deng, Q., see Dong, S. 235
- De Rijke, L.C., see Van de Merbel, N.C. 39
- De Smedt, S., see Dekeyser, P.M. 123
- Docekal, B.
— and Krivan, V.
Halogen-assisted cleaning after-treatment in graphite furnace atomic absorption spectrometry for analysis of molybdenum-based materials 253
- Dong, S.
—, Deng, Q. and Cheng, G.
Cholesterol sensor based on electrodeposition of catalytic palladium particles 235
- Eisenthal, R., see Hubble, J. 167
- Ekroth, R., see Kyröläinen, M. 149
- Eldefrawi, M.E., see Wong, R.B. 141
- Emerson, S., see Pan, S. 195
- Engasser, J.M., see Mathis, C. 59
- Eremenko, A., see Wang, J. 203
- Feola, M., see Simoni, J. 73
- Forgács, E.
—, Cserhádi, T. and Bordás, B.
Application of multivariate mathematical-statistical methods for the comparison of the retention behaviour of porous graphitized carbon and octadecylsilica columns 115
- Forgács, E., see Cserhádi, T. 107
- Fourie, L.
—, Van der Merwe, K.J., Swart, P. and De Kock, S.S.
Application of fast atom bombardment mass spectrometry for the analysis of biologically active compounds 163






- García Sancho, T., see Gómez Benito, C. 293
 Georgakopoulos, C., see Statheropoulos, M. 323
 Gibson, T.D.
 —, Hulbert, J.N. and Woodward, J.R.
 Preservation of shelf life of enzyme based analytical systems using a combination of sugars, sugar alcohols and cationic polymers or zinc ions 185
 Gómez Benito, C.
 —, García Sancho, T. and Martínez Calatayud, J.
 Spectrofluorimetric determination of emetine by flow injection using barium peroxide and UV derivatization 293
 Goodacre, R.
 — and Kell, D.B.
 Rapid and quantitative analysis of bioprocesses using pyrolysis mass spectrometry and neural networks: application to indole production 17
 Goodlet, G.
 — and Narayanaswamy, R.
 Effect of pH on the redox equilibria of immobilised 2,6-dichloroindophenol 335
 Gorton, L., see Buttler, T. 27
 Grappin, R., see Picque, D. 67
 Grunfeld, S., see Malinski, T. 135
 Guan, J.-S., see Yang, X.-J. 261
- Håkanson, H., see Kyröläinen, M. 149
 Hernández Méndez, J., see Carabias Martínez, R. 299
 Hilhorst, R.
 Catalytic antibodies: new developments 129
 Hitzmann, B., see Schügerl, K. 3
 Hubble, J.
 —, Mayes, A.G. and Eisenthal, R.
 Spectral analysis of interactions between proteins and dye ligands 167
 Hubble, J., see Meng-Yang, Y. 95
 Hulbert, J.N., see Gibson, T.D. 185
- Il Ree, J., see Schügerl, K. 3
- Janssen, L.J.J., see Van Stroe, A.J. 213
 Jen, J.-F., see Ou-Yang, G.-L. 329
 Johansen, C., see Carlsen, M. 51
- Kaltenbach, T.F.
 — and Small, G.W.
 Ridge regression techniques for the optimization of piecewise linear discriminants: application to Fourier transform infrared remote sensing measurements 309
 Kell, D.B., see Davey, C.L. 155
 Kell, D.B., see Goodacre, R. 17
 Kettenes-van den Bosch, J.J., see Boers, G.W. 89
 Kiechle, F., see Malinski, T. 135
 Klenke, T., see Sachsenberg, S. 241
 Kolhorn, A., see Van de Merbel, N.C. 39
 Kopelyan, E.A., see Oshtrakh, M.I. 179
 Krivan, V., see Docekal, B. 253
 Krumbein, W.E., see Sachsenberg, S. 241
- Kyröläinen, M.
 —, Håkanson, H., Ekroth, R. and Mattiasson, B.
 Biosensor monitoring of blood lactate during open-heart surgery 149
- Lantreibeccq, F., see Carlsen, M. 51
 Lauwers, A., see Dekeyser, P.M. 123
 Lefier, D., see Picque, D. 67
 Legg, K.D., see Pan, S. 195
 Lenoel, M., see Mathis, C. 59
 Lingeman, H., see Van de Merbel, N.C. 39
 Lockett, A.D., see Meng-Yang, Y. 95
- Malinski, T.
 —, Taha, Z., Grunfeld, S., Burewicz, A., Tomboulian, P. and Kiechle, F.
 Measurements of nitric oxide in biological materials using a porphyrinic microsensor 135
 Marko-Varga, G., see Buttler, T. 27
 Martínez Calatayud, J., see Gómez Benito, C. 293
 Martín González, F., see Carabias Martínez, R. 299
 Mateo, M.-A.
 — and Sabaté, S.
 Wet digestion of vegetable tissue using a domestic microwave oven 273
 Mathis, C.
 —, Pons, M.N., Engasser, J.M. and Lenoel, M.
 Development of an on-line method for the monitoring of vicinal diketones and their precursors in beer fermentation 59
 Mattiasson, B., see Kyröläinen, M. 149
 Mayes, A.G., see Hubble, J. 167
 Meier, H., see Carlsen, M. 51
 Meng-Yang, Y.
 —, Rathbone, R.R., Hubble, J. and Lockett, A.D.
 In situ thermal monitoring of adsorption column performance 95
 Min, R.W., see Carlsen, M. 51
- Narayanaswamy, R., see Goodlet, G. 335
 Nielsen, J., see Carlsen, M. 51
- Oshtrakh, M.I.
 —, Kopelyan, E.A. and Semionkin, V.A.
 Oxyhaemoglobin degradation and radiolysis analysed by Mössbauer and positron annihilation techniques 179
 Ou-Yang, G.-L.
 — and Jen, J.-F.
 Simultaneous preconcentration of chromium(III) and chromium(VI) prior to speciation analysis 329
- Pan, S.
 —, Conway, V., Shakhsher, Z., Emerson, S., Bai, M., Seitz, W.R. and Legg, K.D.
 Mechanically robust amine derivatized polystyrene for pH sensing based on polymer swelling 195

- Picque, D.
—, Lefier, D., Grappin, R. and Corrieu, G.
Monitoring of fermentation by infrared spectrometry. Alcoholic and lactic fermentations 67
- Pons, M.N., see Mathis, C. 59
- Powell, H.K.J., see Town, R.M. 221
- Rathbone, R.R., see Meng-Yang, Y. 95
- Ren, Y., see Zhang, J. 281
- Sabaté, S., see Mateo, M.-A. 273
- Sachsenberg, S.
—, Klenke, T., Krumbein, W.E., Schellnhuber, H.J. and Zeeck, E.
Direct graphite furnace atomic absorption spectrometric determination of metals in sea water: application of palladium modifiers and a fractal approach to their analytical support 241
- Sadik, O.A.
— and Wallace, G.G.
Pulsed amperometric detection of proteins using antibody containing conducting polymers 209
- Schellnhuber, H.J., see Sachsenberg, S. 241
- Schügerl, K.
—, Brandes, L., Wu, X., Bode, J., Il Ree, J., Brandt, J. and Hitzmann, B.
Monitoring and control of recombinant protein production 3
- Seitz, W.R., see Pan, S. 195
- Semionkin, V.A., see Oshtrakh, M.I. 179
- Shakhsher, Z., see Pan, S. 195
- Simoni, G., see Simoni, J. 73
- Simoni, J.
—, Simoni, G. and Feola, M.
Chromatographic analysis of biopolymers distribution in "poly-hemoglobin", an intermolecularly crosslinked hemoglobin solution 73
- Small, G.W., see Kaltenbach, T.F. 309
- Smith-Palmer, T.
—, Barbarakis, M.S., Cynkowski, T. and Bachas, L.G.
Fluorescence-based flow-injection determination of biotin and biotinylated compounds 287
- Smyth, M.R., see Wang, J. 203
- Statheropoulos, M.
— and Georgakopoulos, C.
Assessment of the performance of various search systems for mass spectra files of steroids 323
- Swart, P., see Fourie, L. 163
- Taha, Z., see Malinski, T. 135
- Todd, R.W., see Davey, C.L. 155
- Tombouliau, P., see Malinski, T. 135
- Town, R.M.
— and Powell, H.K.J.
Ion-selective electrode potentiometric studies on the complexation of copper(II) by soil-derived humic and fulvic acids 221
- Ujházy, A., see Cserháti, T. 107
- Van de Merbel, N.C.
—, Lingeman, H., Brinkman, U.A.Th., Kolhorn, A. and De Rijke, L.C.
Automated monitoring of biotechnological processes using on-line ultrafiltration and column liquid chromatography 39
- Van der Merwe, K.J., see Fourie, L. 163
- Van Stroe, A.J.
— and Janssen, L.J.J.
Determination of the diffusion coefficient of oxygen in sodium chloride solutions with a transient pulse technique 213
- Vercruyssen, K., see Dekeyser, P.M. 123
- Wallace, G.G., see Sadik, O.A. 209
- Wang, J.
—, Dempsey, E., Eremenko, A. and Smyth, M.R.
Organic-phase biosensing of enzyme inhibitors 203
- Wong, R.B.
—, Anis, N. and Eldefrawi, M.E.
Reusable fiber-optic-based immunosensor for rapid detection of imazethapyr herbicide 141
- Woodward, J.R., see Gibson, T.D. 185
- Wu, X., see Schügerl, K. 3
- Yang, J., see Zhang, J. 281
- Yang, X.-J.
— and Guan, J.-S.
End-on viewed inductively coupled plasma for the determination of trace impurities in high-purity scandium oxide by extraction chromatography 261
- Zeeck, E., see Sachsenberg, S. 241
- Zhang, J.
—, Yang, J., Ren, Y. and Zhang, Y.
Comparative study of Kalman filtering, synchronous excitation and numerical derivative techniques in fluorimetry 281
- Zhang, Y., see Zhang, J. 281

Announcement from the Publisher

Elsevier Science Publishers encourages submission of articles on floppy disk.

All manuscripts may now be submitted on computer disk, with the eventual aim of reducing production times still further.

-  The preferred storage medium is a 5¼ or 3½ inch disk in MS-DOS format, although other systems are welcome, e.g. Macintosh.
-  After final acceptance, your disk plus one final, printed and exactly matching version (as a printout) should be submitted together to the editor. **It is important that the file on disk and the printout are identical.** Both will then be forwarded by the editor to Elsevier.
-  Illustrations should be provided in the usual manner.
-  Please follow the general instructions on style/arrangement and, in particular, the reference style of this journal as given in 'Instructions to Authors'.
-  Please label the disk with your name, the software & hardware used and the name of the file to be processed.

Contact the Publisher for further information:

Elsevier Science Publishers
Analytica Chimica Acta
P.O. Box 330
1000 AH Amsterdam, The Netherlands
Phone: (+31-20) 5862 791 Fax: (+31-20) 5862 459

ELSEVIER SCIENCE PUBLISHERS



TrAC - Trends in Analytical Chemistry: Reference Edition

- A compilation of the material published from the regular issues of the journal in the previous year, *TrAC* reference edition provides a topical digest of current developments and new ideas in the analytical sciences, in the form of broadly-based, easy-to-read scientific reviews, backed up by news and other features of interest.
- They provide informative and stimulating reading for all those who use analytical methods.
- For subscribers to the library edition of *TrAC*, the reference editions form an integral part of the annual subscription, but for others these indispensable sources of information can be purchased individually.

"I believe that the annual Reference Edition of Trends in Analytical Chemistry (TrAC) now provides one of the clearest and most wide ranging accounts of what is happening in Analytical Science. It provides invaluable information to researchers, students and teachers, and is strongly recommended for library purchase."

Analytica Chimica Acta

Volume 3: 1984

© 1984 viii + 284 pages

Price: US \$ 176.50 / Dfl. 309.00

ISBN 0-444-42458-X

Volume 4: 1985

© 1986 viii + 280 pages

Price: US \$ 186.25 / Dfl. 326.00

ISBN 0-444-42635-3

Volume 5: 1986

© 1987 viii + 292 pages

Price: US \$ 186.25 / Dfl. 326.00

ISBN 0-444-42772-4

Volume 6: 1987

© 1988 viii + 282 pages

Price: US \$ 192.00 / Dfl. 336.00

ISBN 0-444-42941-7

Volume 7: 1988

© 1989 x + 404 pages

Price: US \$ 239.50 / Dfl. 419.00

ISBN 0-444-87323-6

Volume 8: 1989

© 1990 404 pages

Price: US \$ 270.25 / Dfl. 473.00

ISBN 0-444-88640-0

Volume 10: 1991

© 1991 viii + 372 pages

Price: US \$ 311.50 / Dfl. 545.00

ISBN 0-444-89503-5

Volume 11: 1992

© 1992 viii + 402 pages

Price: US \$ 354.25 / Dfl. 620.00

ISBN 0-444-89926-X

Full contents for all volumes are available on request from the Publisher.

Volumes 1, 2 and 9 are Out of Print but are still available through Swets & Zeitlinger
P.O. Box 810
2160 SZ Lisse
The Netherlands

ORDER INFORMATION

For further information contact your regular supplier or in the USA and Canada

ELSEVIER SCIENCE PUBLISHERS

Fax: (212) 633 3880

In all other countries
ELSEVIER SCIENCE PUBLISHERS

Fax: (+31-20) 5803 705

US\$ prices are valid only for the USA & Canada and are subject to exchange rate fluctuations; in all other countries the Dutch guilder price (Dfl.) is definitive. Customers in the European Community should add the appropriate VAT rate applicable in their country to the price(s). Books are sent postfree if prepaid.



ELSEVIER
SCIENCE PUBLISHERS

PUBLICATION SCHEDULE FOR 1993

	S'92	O'92	N'92	D'92	J	F	M	A	M	J	J	A
Analytica Chimica Acta	267/1 267/2	268/1 268/2	269/1 269/2	270/1 270/2	271/1 271/2	272/1 272/2 273/1-2	274/1 274/2	275/1-2 276/1 276/2	277/1 277/2	278/1 278/2	279/1 279/2	280/1 280/2
Vibrational Spectroscopy		4/1			4/2		4/3	5/1		5/2		5/3

INFORMATION FOR AUTHORS

Manuscripts. The language of the journal is English. English linguistic improvement is provided as part of the normal editorial processing. Authors should submit three copies of the manuscript in clear double-spaced typing on one side of the paper only. *Vibrational Spectroscopy* also accepts papers in English only.

Abstract. All papers and reviews begin with an Abstract (50–250 words) which should comprise a factual account of the contents of the paper, with emphasis on new information.

Figures. Figures should be prepared in black waterproof drawing ink on drawing or tracing paper of the same size as that on which the manuscript is typed. One original (or sharp glossy print) and two photostat (or other) copies are required. Attention should be given to line thickness, lettering (which should be kept to a minimum) and spacing on axes of graphs, to ensure suitability for reduction in size on printing. Axes of a graph should be clearly labelled, along the axes, outside the graph itself. All figures should be numbered with Arabic numerals, and require descriptive legends which should be typed on a separate sheet of paper. Simple straight-line graphs are not acceptable, because they can readily be described in the text by means of an equation or a sentence. Claims of linearity should be supported by regression data that include slope, intercept, standard deviations of the slope and intercept, standard error and the number of data points; correlation coefficients are optional.

Photographs should be glossy prints and be as rich in contrast as possible; colour photographs cannot be accepted. Line diagrams are generally preferred to photographs of equipment.

Computer outputs for reproduction as figures must be good quality on blank paper, and should preferably be submitted as glossy prints.

Nomenclature, abbreviations and symbols. In general, the recommendations of the International Union of Pure and Applied Chemistry (IUPAC) should be followed, and attention should be given to the recommendations of the Analytical Chemistry Division in the journal *Pure and Applied Chemistry* (see also *IUPAC Compendium of Analytical Nomenclature, Definitive Rules, 1987*).

References. The references should be collected at the end of the paper, numbered in the order of their appearance in the text (*not* alphabetically) and typed on a separate sheet.

Reprints. Fifty reprints will be supplied free of charge. Additional reprints (minimum 100) can be ordered. An order form containing price quotations will be sent to the authors together with the proofs of their article.

Papers dealing with vibrational spectroscopy should be sent to: Dr J.G. Grasselli, 150 Greentree Road, Chagrin Falls, OH 44022, U.S.A. Telefax: (+1-216) 2473360 (Americas, Canada, Australia and New Zealand) or Dr J.H. van der Maas, Department of Analytical Molecule Spectrometry, Faculty of Chemistry, University of Utrecht, P.O. Box 80083, 3508 TB Utrecht, The Netherlands. Telefax: (+31-30) 518219 (all other countries).

© 1993, ELSEVIER SCIENCE PUBLISHERS B.V. All rights reserved.

0003-2670/93/\$06.00

No part of this publication may be reproduced, stored in a retrieval system or transmitted in any form or by any means, electronic, mechanical, photocopying, recording or otherwise, without the prior written permission of the publisher, Elsevier Science Publishers B.V., Copyright and Permissions Dept., P.O. Box 521, 1000 AM Amsterdam, The Netherlands.

Upon acceptance of an article by the journal, the author(s) will be asked to transfer copyright of the article to the publisher. The transfer will ensure the widest possible dissemination of information.

Special regulations for readers in the U.S.A.—This journal has been registered with the Copyright Clearance Center, Inc. Consent is given for copying of articles for personal or internal use, or for the personal use of specific clients. This consent is given on the condition that the copier pays through the Center the per-copy fee for copying beyond that permitted by Sections 107 or 108 of the U.S. Copyright Law. The per-copy fee is stated in the code-line at the bottom of the first page of each article. The appropriate fee, together with a copy of the first page of the article, should be forwarded to the Copyright Clearance Center, Inc., 27 Congress Street, Salem, MA 01970, U.S.A. If no code-line appears, broad consent to copy has not been given and permission to copy must be obtained directly from the author(s). All articles published prior to 1980 may be copied for a per-copy fee of US \$2.25, also payable through the Center. This consent does not extend to other kinds of copying, such as for general distribution, resale, advertising and promotion purposes, or for creating new collective works. Special written permission must be obtained from the publisher for such copying.

No responsibility is assumed by the publisher for any injury and/or damage to persons or property as a matter of products liability, negligence or otherwise, or from any use or operation of any methods, products, instructions or ideas contained in the material herein.

Although all advertising material is expected to conform to ethical (medical) standards, inclusion in this publication does not constitute a guarantee or endorsement of the quality or value of such product or of the claims made of it by its manufacturer.

This issue is printed on acid-free paper.

PRINTED IN THE NETHERLANDS

Capillary Electrophoresis

Principles, Practice and Applications

by S.F.Y. LI, National University of Singapore, Singapore

Journal of Chromatography Library Volume 52

NOW ALSO
IN PAPERBACK

Capillary Electrophoresis (CE) has had a very significant impact on the field of analytical chemistry in recent years as the technique is capable of very high resolution separations, requiring only small amounts of samples and reagents. Furthermore, it can be readily adapted to automatic sample handling and real time data processing. Many new methodologies based on CE have been reported. Rapid, reproducible separations of extremely small amounts of chemicals and biochemicals, including peptides, proteins, nucleotides, DNA, enantiomers, carbohydrates, vitamins, inorganic ions, pharmaceuticals and environmental pollutants have been demonstrated. A wide range of applications have been developed in greatly diverse fields, such as chemical, biotechnological, environmental and pharmaceutical analysis.

This book covers all aspects of CE, from the principles and technical aspects to the most important applications. It is intended to meet the growing need for a thorough and balanced treatment of CE. The book will serve as a comprehensive reference work and can also be used as a textbook for advanced undergraduate and graduate courses. Both the experienced analyst and the newcomer will find the text useful.

Contents:

- 1. Introduction.** Historical Background. Overview of High Performance CE. Principles of Separations. Comparison with Other Separation Techniques.
- 2. Sample Injection Methods.** Introduction. Electrokinetic

Injection. Hydrodynamic Injection. Electric Sample Splitter. Split Flow Syringe Injection System. Rotary Type Injector. Freeze Plug Injection. Sampling Device with Feeder. Microinjectors. Optical Gating. **3. Detection Techniques.** Introduction. UV-Visible Absorbance Detectors. Photodiode Array Detectors. Fluorescence Detectors. Laser-based Thermo-optical and Refractive Index Detectors. Indirect Detection. Conductivity Detection. Electrochemical Detection. Mass Spectrometric Detection. **4. Column Technology.** Uncoated Capillary Columns. Coated Columns. Gel-filled Columns. Packed Columns. Combining Packed and Open-Tubular Column. **5. Electrophoretic Media.** Electrophoretic Buffer Systems. Micellar Electrokinetic Capillary Chromatography. Inclusion Pseudophases. Metal-complexing Pseudophases. Other Types of Electrophoretic Media. **6. Special Systems and Methods.** Buffer Programming. Fraction Collection. Hyphenated Techniques. Field Effect Electroosmosis. Systematic Optimization of Separation. **7. Applications of CE.** Biomolecules. Pharmaceutical and Clinical Analysis. Inorganic Ions. Hydrocarbons. Foods and Drinks. Environmental Pollutants. Carbohydrates. Toxins. Polymers and Particles. Natural Products.

Fuel. Metal Chelates. Industrial Waste Water. Explosives. Miscellaneous Applications. **8. Recent Advances and Prospect for Growth.** Recent Reviews in CE. Advances in Injection Techniques. Novel Detection Techniques. Advances in Column Technology. Progress on Electrolyte Systems. New Systems and Methods. Additional Applications Based on CE. Future Trends.

References. Index.

1992 608 pages Hardbound
US\$ 225.75 / Dfl. 395.00

ISBN 0-444-89433-0

1993 608 pages Paperback

Price: US\$ 114.25 / Dfl. 200.00

ISBN 0-444-81590-2

"Everything seems to be there, any detection system you have ever dreamed of, any capillary coating, enough electrolyte systems to saturate your wits, and more..."

"...by far the most thorough and comprehensive book in the field yet to appear."

P.G. Righetti, Milan

ORDER INFORMATION

For USA and Canada
ELSEVIER SCIENCE PUBLISHERS

Judy Weislogel,

P.O. Box 945

Madison Square Station,

New York, NY 10160-0757

Fax: (212) 633 3880

In all other countries

ELSEVIER SCIENCE PUBLISHERS

P.O. Box 211,

1000 AE Amsterdam

The Netherlands

Fax: (+31-20) 5803 705

US\$ prices are valid only for the USA & Canada and are subject to exchange rate fluctuations; in all other countries the Dutch guilder price (Dfl.) is definitive. Customers in the European Community should add the appropriate VAT rate applicable in their country to the price(s). Books are sent postfree if prepaid.



ELSEVIER
SCIENCE PUBLISHERS



0003-2670(19930715)279:2;1-5

711/414/143/LI

29 N.A. 2536